SPECIAL REPORT 93-17

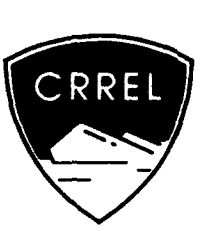

2

First International Conference on Winter Vehicle Mobility

Santa Barbara, California, June 1991

George L. Blaisdell, Editor

July 1993

Abstract

The First International Conference on Winter Vehicle Mobility was the first international meeting entirely devoted to the subject of vehicle travel in cold regions. The technical sessions focused on prediction and testing methods, general vehicle mobility, mobility enhancement, cold regions materials properties, and novel designs for winter mobility. This report includes 21 papers presented at the conference.

For conversion of SI metric units to U.S./British customary units of measurement consult ASTM Standard E380-89a, *Standard Practice for Use of the International System of Units*, published by the American Society for Testing and Materials, 1916 Race St., Philadelphia, Pa. 19103.

Special Report 93-17

U.S. Army Corps of Engineers
Cold Regions Research & Engineering Laboratory

First International Conference on Winter Vehicle Mobility

Santa Barbara, California, June 1991

George L. Blaisdell, Editor

July 1993

FOREWORD

Over the past several years, various researchers and practitioners of winter mobility have gotten together in small groups in an attempt to solve mutual problems and share information. No standard forum has been available for this unique topic, however, so each meeting has been somewhat ad hoc in nature and often occurs as a small part of another larger meeting.

The Engineering Foundation recognized the need for a conference, perhaps leading to a regularly occurring meeting, devoted entirely to the subject of vehicle travel in cold regions. Thus they encouraged and sponsored this international conference. Funding was provided by the Engineering Foundation and the National Science Foundation. Support for conference organizers was provided by the Civil and Agricultural Engineering Department of Montana State University and the Keweenaw Research Center. The Cold Regions Research and Engineering Laboratory sponsored the conference chairperson and edited and produced the conference proceedings.

Technical sessions for the conference focused on:

1) Prediction and testing methods,
2) General vehicle mobility,
3) Mobility enhancement,
4) Cold regions materials properties,
5) Novel designs for winter mobility.

A final discussion about the remaining needs of the mobility community and means of addressing these needs concluded that regular (probably annual) meetings that include field demonstrations and exercises are very much desired. While no single group or organization felt compelled to take a lead in organizing future meetings, all attendees seemed eager and available to help in producing follow-on conferences. Clearly, continued involvement by the Engineering Foundation, especially in instigating future Winter Mobility conferences, would be very beneficial.

GEORGE L. BLAISDELL
Chairperson

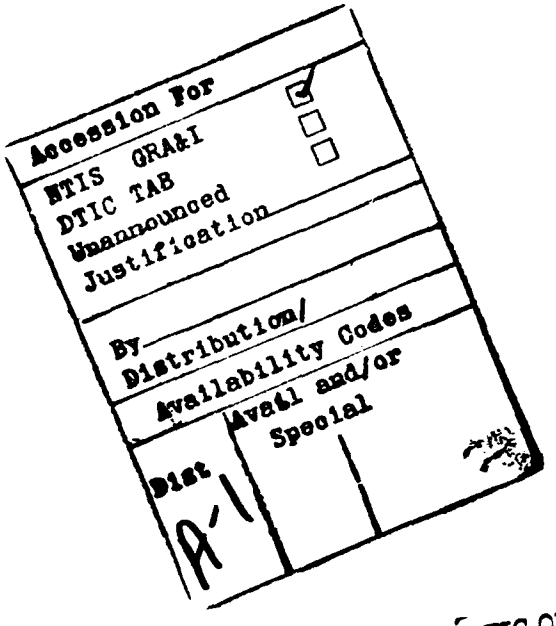

FIRST INTERNATIONAL CONFERENCE ON WINTER VEHICLE MOBILITY

Chairperson
George L. Blaisdell
Experimental Engineering Division
Cold Regions Research and Engineering Laboratory
Hanover, New Hampshire

Co-Chairpersons
Robert Brown
Department of Civil and Agricultural Engineering
Montana State University
Bozeman, Montana

Russell Alger
Institute of Snow Science
Keweenaw Research Center
Michigan Technological University
Houghton, Michigan

Engineering Foundation
Charles Freiman, Director
Gordon Fisher, Conference Committee Representative

Proceedings Editor
George L. Blaisdell

To obtain a copy of these proceedings write to
CRREL-TL, 72 Lyme Road, Hanover,
New Hampshire 03755-1290, USA.

ATTENDEES

Russ Alger
Keweenaw Research Center
Michigan Technological University
Houghton, MI 49931

Michael Barber
Department of Civil and Agricultural Engineering
Montana State University
Bozeman, MT 59717

Joseph Barthelemy
Naval Civil Engineering Laboratory
Code L66
Port Hueneme, CA 93043-5003

Sture Bernhardsson
Defense Materiel Administration
Mobility Directorate
Transport Vehicles Division
Test Center
S-645 83 Strangnas
SWEDEN

George L. Blaisdell
Applied Research Branch
Cold Regions Research and Engineering Laboratory
72 Lyme Road
Hanover, NH 03755

Robert Brown
Department of Civil and Agricultural Engineering
Montana State University
Bozeman, MT 59767

Leonard Della-Moretta
1796 Russell Place
Pomona, CA 91767

Michael Edens
Department of Civil and Agricultural Engineering
Montana State University
Bozeman, MT 59717

Michael A. Gillis
Navy Support Force Antarctica
Box 100, Code 50
FPO San Francisco, CA 96601-6010

Keafur Grimes
Waterways Experiment Station
WES GM-IE
P.O. Box 631
Vicksburg, MS 39180-0631

Bill Grusonik
FMC Corp.
2890 Della Cruz
Box 58123 (MD-P73)
Santa Clara, CA 95052

Doug Hanna
DOD Canada
P.O. Box 4000
Medicine Hat
Alberta, CANADA T1A 8K6

Andrew Hansen
Mechanical Engineering Department
University of Wyoming
Box 3295, University Street
Laramie, WY 82071

Henry Hodges
Nevada Automotive Test Center
P.O. Box 234
Carson City, NV 89701

Glen Isnor
Lete
National Defense Department
Ottawa, Ontario, CANADA K1A 0K2

Roger Jacobson
Imagineering
3236 16th Avenue, SW
Seattle, WA 98134

Michael Kriz
Tank-Automotive Command
AMSTA-ZDM
Warren, MI 48397-5000

Ronald Liston
Applied Research Branch
Cold Regions Research and Engineering Lalboratory
72 Lyme Road
Hanover, NH 03755

Urban Lundberg
Hagglunds
35414 Mound Road
Sterling Heights, MI 48310

Michael Moggridge
Canadian Armed Forces
MRCV Project
NDHQ/CLDO/DLR
G. Pearkes Bldg.
Ottawa, Ontario, CANADA K1A 0K2
Marc Moosang

Northern Terrain Vehicles
CLDO Branch/PD-NTV, NDHQ
G. Pearkes Bldg.
Ottawa, Ontario, CANADA K1A 0K2

Mark Osborne
Keweenaw Research Center
Michigan Technological University
Houghton, MI 49931

James Poplin
Esso Resources Canada, Ltd
3535 Research Road,NW
Calgary, Alberta, CANADA T2L 2K8

Rick Schenck
Tank-Automotive Command
AMSTA-WS
Warren, MI 48397-5000

Tom Schmidt
Navy Support Force Antarctica
Box 100, Code 50
FPO San Francisco, CA 96601-6010

Sally Shoop
Applied Research Branch
Cold Regions Research and Engineering Laboratory
72 Lyme Road
Hanover, NH 03755

Dale Steinke
Defense Products, JB7
Caterpillar, Inc.
Peoria, IL 61629

M. R. Surendran
U.S. Army Tank Automotive Command
AMSTA-WS
Warren, MI 48397-5000

Calude Thomas
Naval Civil Engineering Laboratory
Code L66
Port Hueneme, CA 93043-5003

Jeffrey Weaver
Esso Resources Canada, Ltd
3535 Research Road, NW
Calgary, Alberta, CANADA T2L 2K8

CONTENTS

1. INTRODUCTION

Mobility Research: Where We Have Been and Where We Are Going

RONALD A. LISTON
U.S. Army Cold Regions Research and Engineering Laboratory
Hanover, New Hampshire 03755-1290

The request to give an hour's talk on mobility research seemed an innocuous one when it was made to me. But as I began to think about how I would cover the topic, things became more and more complicated. My first thought was to prepare a list of the people whose contributions should be highlighted and I was inundated with a flood of names: Uffelmann, Janosi, Micklethwaite, Bekker, Van Duesen, Knight, Turnbull, Grabau, Murphy, Green, Shockely, Ehrlich, Nuttall, the Hodges clan, Reece, Leger, Dixon, Sela, Soehne, Areskoug, Kitano, and on and on until I realized that I was going to have to cover the complete roster of the ISTVS and all of its associates—an impossible task for 60 minutes.

My next thought was to cover the major groups of research organizations that have been active over the past half century. The list quickly became unmanageable: Valcartier, TACOM and all its variants, WES, SIPRE, CRREL, NIAE, FVRE, Stevens, U. of M., Michigan Tech., U. Cal. Davis, Tulane, McGill, Carlton, U. of Miss., DRES, NATC, and this list also went on and on.

My conclusion was that I would be lucky in one hour to cover what has happened in the U.S. Government-supported mobility research program during its lifetime (which happens to fit nicely into the half century mentioned above). I proposed that my historical review be anecdotal in nature, so that what is presented is not supported by references, making some details open to challenge. I hope that, in general, my review captures the essence of what has transpired.

Before discussing the mobility programs and various approaches taken to studying vehicle/terrain interactions, let us take a quick look at what our research efforts have produced. Unhappily we have worked diligently and, usually, well but have had little impact on the performance of machines in use, whether they be military, agricultural, forestry, construction or highway. One is forced to wonder why the significant body of knowledge that we have developed about vehicles has not resulted in dramatic changes in form and performance.

The first reason that comes to mind is that dramatic improvements do not come from modest changes. For example, the difference between a high-speed catamaran and a conventional sailboat is clearly major. The more than doubling in speed of wind-powered craft could only be achieved by making a clear departure from conventional designs. In general, I think that a drive created by competition between teams of men and their machines creates an attitude that anything new and different will not only be accepted but sought out if there is the possibility of gaining a slight advantage. Innovation is vital to competition. The users of automotive equipment simply will not accept radical changes required to give them vehicles that can operate either at high speed off the road or in terrain conditions that prevent operation of conventional vehicles because their agendas, for reasons that aren't immediately clear, don't have an element of desperately seeking for the competitive edge. For example, the Twister (Fig. 1), developed by Steve Hodges at Lockheed, was an amazing machine that allowed highway speeds to be achieved in rough terrain that would normally limit vehicles to four or five miles per hour. It was offered in a variety of configurations that ranged from an ambulance to a full-fledged fighting vehicle. The concept was discarded partly because its form was as unconventional as was its performance: two engines, multiple walking beam suspension, articulation with three degrees of freedom. Except for a handful of people who become overwhelmed by radically new off-road machines, the revolutionary potential of this machine was overlooked because it was so different that it demanded rejection.

A second example is the series of vehicles developed in response to Bob Phillipe's desire to show that highly mobile vehicles designed to operate in very weak soils

Figure 1. Prototype of the Lockheed "Twister"

could operate equally well on the road as off the road. One tracked version (Fig. 2) and two wheeled versions (Fig. 3 and 4) were designed to operate in soil conditions so weak that only the lightest vehicles available at the time would remain mobile. The vehicles were designed to operate in soils with a VCI of 7; their impact on the world of off-road machinery was nil. A very senior TACOM manager's response was "What in the world are you going to do with those monstrosities?" It is a sad observation that the automotive design community and the user community seem to have the impression that if you use the right tire or track you can go almost anywhere, or maybe that there is a magical transmission that will let you drive on water. We in the mobility community have demonstrated the value of articulation, of a super-flexible frame, of highly compliant

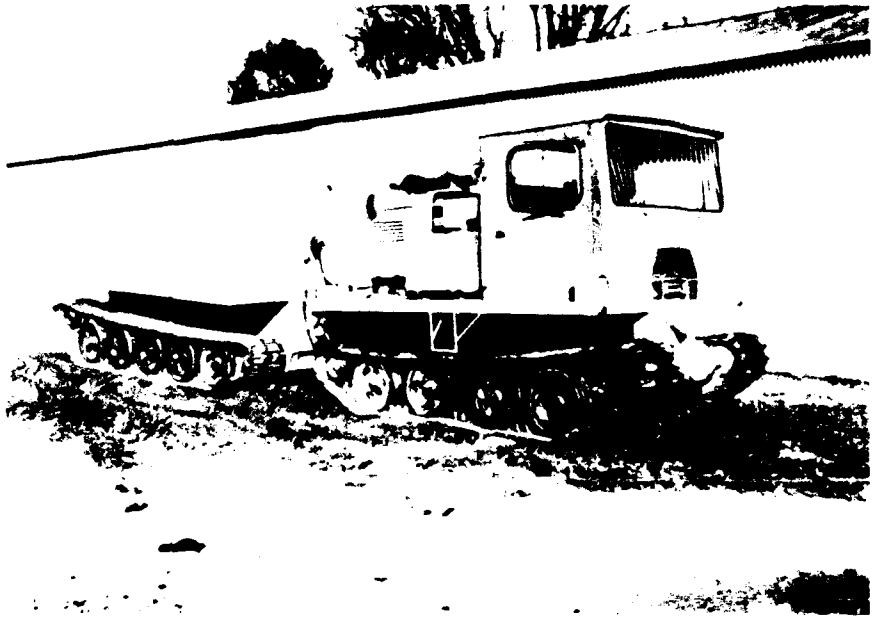

Figure 2. Tracked version of the MEXA vehicles.

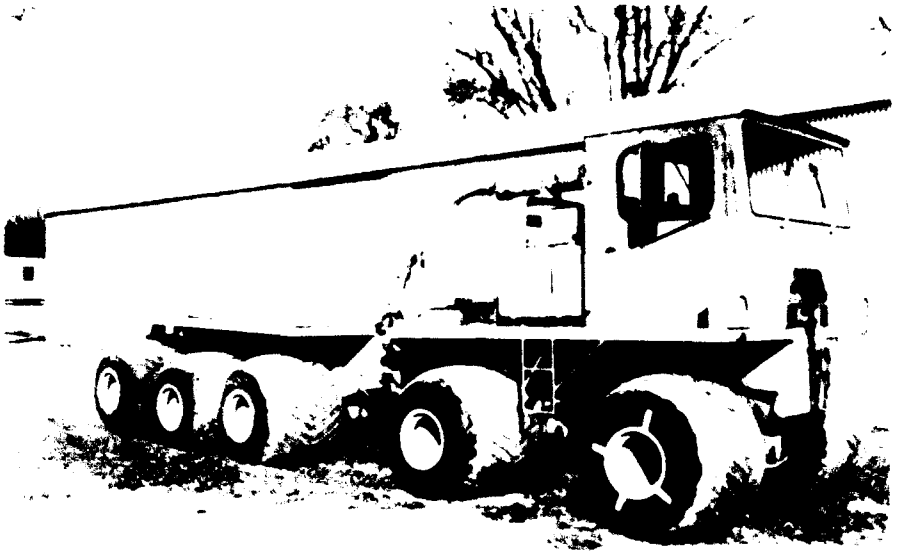

Figure 3. 10×10 version of the MEXA vehicles.

suspensions, of controllable pitch joints, and of a wide collection of things that can be done to provide machines that are at ease in the off-road environment. But it has taken us 50 years to convince the Army customer that radial tires in the single configuration, locking differentials and central inflation systems are reliable, inexpensive, not really exotic and can provide significant, if not dramatic, improvements in performance. As I will point out later, the mobility community may be more at fault than the user community because we probably tried to solve the wrong problem with most of the new vehicle concepts that were proposed. With that happy note, I will turn to who did what to whom.

In the beginning, God created mud, and the Bureaucracy created the Mud Mobility Committee. The formation of the committee formalized mobility as a problem

Figure 4. 8×8 version of the MEXA vehicles.

and eventually led to mobility research efforts and organizations having the goal of solving the Army's mobility problems.

The period between the two World Wars saw virtually no research or development of military vehicles. The Quartermaster Corps had responsibility for the development, procurement and maintenance of the modest collection of vehicles that the Army had. Probably the most ambitious piece of vehicle development was done by Walter Christie, who thought that he had a contract with the War Department to build a new tank. He devised a highly efficient suspension system that relied on large-diameter road wheels that provided a ground pressure that was fairly uniform and resulted in a low rolling resistance. The vehicle was capable of very high speeds but was rejected, partly because of the battle between Christie and the War Department (which allegedly included a dramatic trip up the stairs of the Treasury Department with an angry Christie dismounting the vehicle and storming away) and partly because there was not a clearly stated need for new vehicles and no money to buy them even if there were a need. Mr. Christie took his suspension to Europe, where it became the mainstay of the German Panzer fleet.

With the entry of the U.S. into WWII, responsibility for automotive equipment was transferred to the Ordnance Corps, and their frantic activities to get an adequate vehicle inventory produced some very good vehicles: the jeep (Fig. 5) (or peep, if your memory goes back farther than you like to admit); the 2-1/2 ton Jimmie; the Weasel (Fig. 6) and the M4 tank series. The development of the Weasel was remarkable in that it was designed at the newly formed Detroit Arsenal in a period of six weeks; compare this to the 14 years expended on the disastrous M114 personnel carrier.

It is difficult to be precise in tracking the dates at which various people began their work; most of the early researchers are dead and those who aren't have flexible memories. The Mud Mobility Committee had joint U.S./U.K. membership, and its name implied that mud was the primary problem to be addressed. The Committee advised Board #2 at Ft. Knox relative to their test procedures, and a reference mud course was established there. The board, which later became the Armor Board, was responsible for all tire, track and tire chain testing for the Army but had no research role. However, the earliest studies seemed more heavily involved with sand than mud. Colonel Karl Eklund, who was responsible for an Engineer Research and Development Laboratory study, was one of the first investigators to attempt to develop an understanding of the interaction between tires and soil. He conducted a series of tests in the Mojave desert in the 1943-44 time frame, and the analysis of the results of these tests produced an equation that was known widely as the Eklund formula, which related tire pressure and several other tire parameters to performance. The formula was elegant in its simplicity; only a piece of paper and pencil or a slide rule was needed to estimate vehicle performance. Whenever mobility grey heads meet, Karl's name is sure to come up with a certain air of nostalgia: "If good old Karl were still around, life would surely be

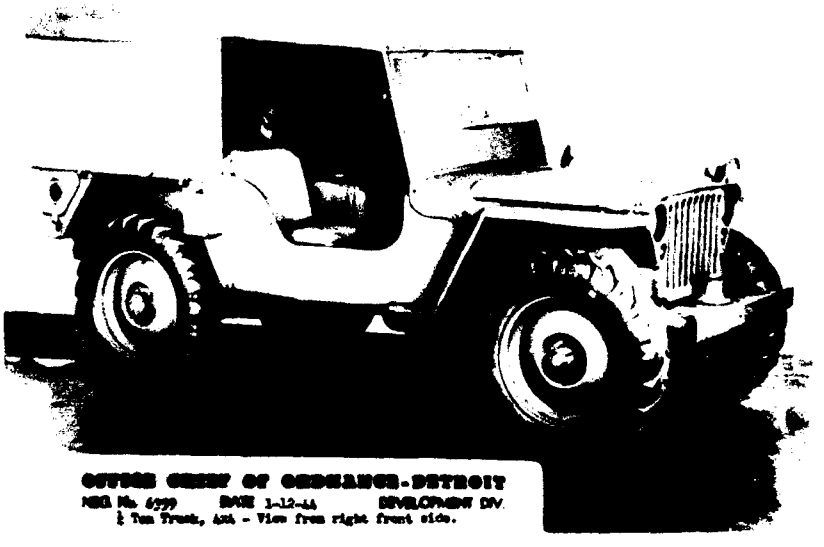

Figure 5. The original "Jeep."

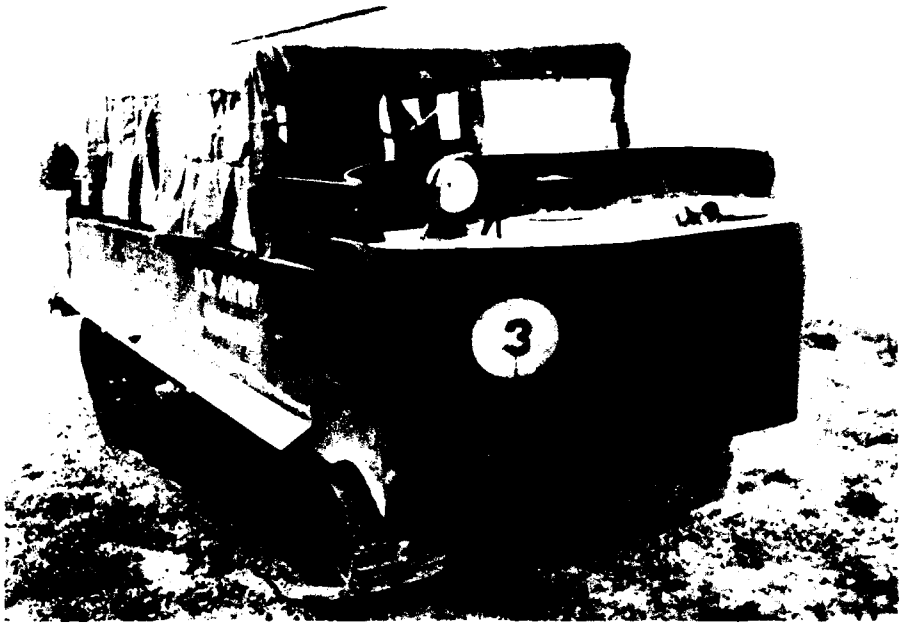

Figure 6. The WWII "Weasel," the miracle machine.

simpler without all this computer nonsense."

At about the same time that Eklund was working in the Mojave, Dick Kerr, Bill England and J.W. Shields were conducting an extensive series of tests with the objective of selecting a tread for the tires to be used on all wheeled vehicles. If tenacity is a virtue, the length of time that the selected treads stayed around would imply that the series of tires was faultless. There were four NDCC treads that were agreed upon. As time passed, the identity of the different treads seemed to disappear, but the sand version, if findable, is still considered to be as good in sand as any of the current tires. The tests by Kerr and company reflected the early wartime approach to R&D: get out in the field and test everything that you can find and come up with the best that is available. There simply wasn't time to study why the best was best; results were needed immediately and work was a seven-day-a-week routine. In later years Dick Kerr joined ARAMCO in Saudi Arabia and trained operators for heavy, expensive equipment to solve transportation problems in the desert. He solved both people and vehicle problems so well that his name was known throughout the truck/trailer world. After solving ARAMCO's problems, Dick became the Chief Scientist of the Transportation Corps. Bill England took over the tire group at TACOM and defended the NDCC until his retirement. One of his arguments for the NDCC tire was that it developed the same traction whether going forward or backward: if forward traction was better than rearward traction, he reasoned that in marginal conditions a vehicle could become immobilized if an attempt was made to back up when forward motion had been lost. The key point to the careers of Kerr and England was that they had an in-depth understanding of how tires behaved; this understanding was gained by years of observing vehicles in the field rather than by research in the laboratory that could provide an understanding of the fundamentals of tire performance.

Camp Bullis became the first "center" for tire testing. It was first operated by the Copolymer Company, which was tasked with determining the performance of tires using the new synthetic rubbers. Bullis operations began in 1942, and Copolymer was replaced by Hodges Transportation in 1951, who ran the operation until 1957 when it was closed down.

The first real Army mobility research began in 1944 at the Waterways Experiment Station in preparation for the invasion of Japan. The landing at Iwo Jima was a disaster, when most of the automotive equipment got stuck on the beach, which consisted of powdered coral rather than sand as assumed, and the vehicles were easy prey for the Japanese defenders. WES began what was a long series of studies that relied on the cone penetrometer in order to assure that the Iwo Jima disaster would not be repeated. Keith Boyd, Chief of the Flexible Pavements Branch, selected 14 vehicles that represented the Army vehicle fleet and began a series of tests to relate soil strength as measured by the cone penetrometer to the ability of a vehicle to negotiate a given area. They ran tests both at WES and at Yuma Proving Ground; these tests consisted of progressively weakening the soil by adding water until the test vehicle became

immobilized. The soil strength, or lack of it, that produced immobilization became the vehicle cone index. The concept was that when Japan was invaded, scouts would be sent forward to measure the soil strength of the rice paddies to determine which vehicles could be moved off-road.

The idea was interesting, but studies conducted many years later showed that weak soil was not a rice paddy problem: to have a rice paddy it is necessary to have an impervious base or else the water will drain out. The problem posed by rice paddies to vehicles is one of geometry, because there must be berms to keep the water in the paddy and the berms are severe obstacles to any wheeled vehicle and to many tracked vehicles. One outcome of the initial WES study was the development of two concepts that plagued the mobility research community and was the source of confusion and bickering. These two concepts were trafficability and mobility: trafficability referred to the ability of soil to support traffic and was a function of soil strength; mobility, on the other hand, was the ability of a vehicle to operate on soft soil and was a function of soil strength plus some vehicle characteristics. Although the distinction between the roles of these two ideas seems modest, many of the discussions of these concepts were conducted with the dignity of a hair pulling contest and created much heat but little light and absolutely no mutual understanding.

Prior to 1962 the majority of mobility research was done for the Army at three facilities: the Transportation Corps' Transportation Research Engineering Command (TRECOM), WES and the Ordnance Tank Automotive Command, the predecessor of TACOM. The Snow, Ice and Permafrost Research Establishment, later CRREL, concentrated on oversnow mobility, but they tended to be more concerned with evaluating and developing equipment for operations in deep snow that could be used to support their science programs. Because each technical service was a completely separate agency, the programs of the three major groups went their individual ways, since there was no strong hand monitoring what was going on. I will cover their approaches and histories reasonably briefly.

WES: The WES approach essentially followed the lead established by Keith Boyd (who later became the Chief Engineer of CRREL) and was based on the cone penetrometer. They conducted a great many tests and gradually developed empirical relationships that related the vehicle cone index to such things as transmission type, number of wheels, wheel size, engine power, number of powered wheels, track contact area, nominal contact pressure and any parameter that appeared to have a critical role in how well a vehicle performed. One problem with the "how well a vehicle performed" approach is that it was assumed that to be able to operate in very soft soil was a virtue, and that was the controlling criterion for "good." The concentration on soft soil as the primary vehicle problem is fully understandable in light of the horror stories about seas of mud that came out of WWII from Europe and the Pacific theaters, and it took many years for the development of a realization that soft soil operations play a very small role in the life of a vehicle. When soft soil is a problem, it may well be critical, as demonstrated in Figure 7, but soft soil performance must be viewed as one of many criteria used to evaluate a vehicle. The WES studies concentrating on granular and fine-grained soils were designed to establish the one-pass cone index and the fifty-pass cone index. Essentially these numbers were taken as a measure of quality: if one vehicle had lower indexes, it was better than the other vehicle. They also did some work in snow in Greenland and at Ft. Churchill and Kapuskasing in Canada. They made the same error in approaching snow that TACOM did in its snow studies and as did CRREL, which had little excuse for sharing their sister lab's views that snow is similar to soil and that soil mechanics and snow mechanics are closely enough related that what works for soil should work for snow and that therefore the equations relating vehicle/soil interactions can be applied freely to either snow or soil.

The WES approach for the description of soil/vehicle interactions worked well and still does in most situations because their equations are based on an incredible number of tests and those equations are almost exclusively applied to the kinds of vehicles used to establish the equations. The truck/tank of WWII is hardly distinguishable from the vehicles of today; the wheeled vehicles are conventional, and the tracked vehicles are conventional so that the equations used to predict vehicle performance, which are based on data gathered on conventional vehicles for decades, should work nicely.

When WES established the Mobility Systems Division in the early sixties, Warren Grabau began forcing a change in their conception of off-road mobility by including many other parameters in the analysis of the vehicle/terrain problem. Such things as vegetation, tree spacing and the use of terrain analysis to prepare going maps based on the total terrain environment began to be introduced, and a more sophisticated outlook developed. In addition, Grabau proposed the concept of linear obstacles, such as rivers, streams or cliffs, to highlight the fact that some obstacles extend well to the right and left of a vehicle's path.

Although much of WES's work involved field operations, they developed laboratory facilities consisting primarily of a series of truly impressive soil bins that were mounted on rails so that they could be moved from

Figure 7. A 1/4 ton with little immediate future.

the test location to the soil processing station. The sophisticated wheel carriage drive permitted high-speed tests of single wheels and also allowed the introduction of limited steering angles. The automatic readout, storage and processing of performance data was high tech for the time. The system included a very accurate apparatus for soil processing, a problem that slowed the tests conducted at many soil bin facilities. These bins were used to evaluate several wheel concepts proposed for the lunar roving vehicle; because of the critical importance of making the proper wheel selection, their ability to maintain tight control of soil conditions assured that the selection was reliable. The laboratory had a well-equipped soils laboratory that supported their soils studies. If an oversimplified characterization of the WES approach can be accepted, it would be that most of their early mobility studies, clearly not all, were experimental, but that the results remain successful partly because there has been little change in the principal object of their studies: the conventional vehicle.

TACOM: The TACOM facility was established as the Land Locomotion Laboratory in the mid-fifties when Greg Bekker was enticed away from Canada with the promise of dollars, of equipment, of freedom to develop an Ordnance mobility research program and of all kinds of tender loving care. The birth of the laboratory was also the birth of a decade of fierce animosity between the Bekker camp and what had become the Turnbull camp of WES. The whole misunderstanding could likely have been avoided if the Ordnance program had not become touted as the "rational approach to terrain/vehicle mechanics." Not too many people appreciate being called irrational, and Bill Turnbull and his team were no exception. More about this later.

The basis of what I will call the Bekker approach was, at the outset, the development of equations that described wheel/soil and track/soil interactions based on classical soil mechanics. Everyone in the laboratory, including the secretary, had a copy of Terzaghi on their desk that was expected to be dog-eared. Greg developed the Bevameter, which had two parts: a shear annulus used to establish the Mohr/Coulomb soil parameters and several plates that were pushed into the soil to allow calculation of an equation that produced three parameters that were related to the bearing strength of the soil. It was assumed that traction could be calculated on the basis of the Mohr/Coulomb parameters and sinkage, and hence motion resistance could be calculated from the bearing strength parameters. The fact that the two things, sinkage and traction, were far from independent was accepted as being relatively irrelevant. The output from the equations was the drawbar-pull-to-weight ratio, and TACOM fell into the same trap as WES by assuming that a better ratio meant a better vehicle. The clash between the Bevameter users and the cone penetrometer users probably clouded the whole issue of vehicle mobility and delayed recognition of the total vehicle/terrain interaction problem by a decade. Bekker left TACOM in 1962, but, unfortunately, even today there is an undercurrent at mobility conferences of the earlier clashes over the two approaches, which may well have been equally flawed.

Bekker shared Grabau's view that mobility was more than soft soil and early on began a series of studies to relate ground roughness to vehicle speed. This work, by Bogdanoff and Kozin at Purdue, was groundbreaking in the sense that their use of stochastic methods applied to describing vehicle ride represented a new level of sophistication in terramechanics. It stirred up a great amount of interest both in academia and industry, and mobility researchers started going around talking like aeronautical engineers, saying things like deviatoric, constitutive or algorithmic. In a more serious vein, one of the major impacts of the work that was developing at the Land Locomotion Laboratory (LLL) was the recognition that the computer age was around the corner and that we could look forward to solving problems that we could only think about at the time. There was a movement to bring in the best brains that could be found in the universities to begin to attack the difficult problems of soil mechanics, vehicle ride, vehicle stability and a new range of topics. This movement spread throughout the Army Mobility Labs.

Because of the approach of the LLL, there was an orientation toward laboratory studies supported by field studies. The laboratory had one small soil bin, two very large soil bins, a vehicle ride facility (consisting of a track that had a profile whose power spectral density function was representative of reasonably rough terrain), a four-wheeled vehicle model whose characteristics could be changed to match those selected for any particular analytical analysis, and a water basin for the study of amphibious vehicles. The basin had a test section large enough to allow the testing of 1/4-scale models in water moving at speeds up to 2-1/2 miles per hour. There was a machine shop and a soils laboratory to provide in-house independence.

Most of the field studies were conducted at SIPRE's Keweenaw Field Station located near the campus of the Michigan Technological University. When SIPRE was integrated into CRREL, the station became TACOM property. Field testing was concentrated in the winter and mid-summer; to keep the station from being greatly underused, TACOM wrote a contract with Michigan Tech stating that they could use the facilities to conduct any research that they were able to find support for. TACOM's program considered four topical areas: soft soil, muskeg, trails and unprepared off-road terrain and snow. The soft soil testing had the objective of improving the equations used to predict traction and motion resistance by identifying differences in laboratory and field conditions. Muskeg testing had the objective of trying to find a useful way to measure the strength of the vegetative mat; unhappily the attempt began with the idea that a modified Bevameter could do the trick and ended with the conclusion that muskeg terrain was off limits to all military vehicles except in the winter when the bogs were frozen and were no longer barriers. The studies of vehicles operating in trails and unprepared terrain began as being observational in nature and gradually changed in complexion to be fairly carefully instrumented and documented. The change was a result of the gradual realization that understanding vehicle/terrain interactions was hugely more complicated than originally thought. Because the change in perspective was so important, I will take a few minutes of your time to relate the change: based on ideas about terrain features being advanced by Grabau, it was decided that a team of researchers would look at a series of soils having the same pedological identification but separated by as large distances as possible. The proposition was that if two soils are so similar that they have the same series name, then they should have the same strength properties given the same moisture contents or, at least, similar contents. The test was totally inconclusive because in every test site selected, the soil was so strong that our vehicularly mounted Bevameter could barely measure shear strength and was totally unable to penetrate the soil to establish bearing strength parameters.

These results led to a test at the field station to relate performance to drawbar pull. The measure of performance was average speed achieved on a test course that included trails, steep slopes, rough surfaces, stream crossings and wooded areas. The drawbar-pull ratios of a group of vehicles, including the D7 tractor (Fig. 8), a Weasel and a Polecat (two Weasels joined with an articulation joint, Fig. 9) were the most significant in the test. The D7 had the best pull-to-weight ratio, followed by the Polecat, which was followed by the Weasel. The results were revealing in that the order of performance was the reverse of the ratios because the D7 can't go very fast and the Polecat is twice as long as the Weasel and is at a disadvantage in conditions requiring agility. Attitudes and opinions didn't come crashing down, but doubts began to creep in.

Because LLL was a part of the organization responsible for automotive development, it had, if not a charter, an opportunity to indulge in the investigation of new concepts for vehicles and vehicle components. Thus, in addition to the study of terrain/vehicle interaction, a significant amount of energy was expended on the development or evaluation of new ideas. The list of ideas and concepts is fairly lengthy: the spaced link track (Fig. 10); the hubless wheel (later dubbed the hopeless wheel when it didn't live up to expectations); several varieties of elliptical wheels; a stream of articulated vehicles, each of which had some new idea such as a controllable pitch joint or a capability to inch forward when immobilized; walking machines; force feedback

Figure 8. The venerable D-7 "Cat."

control systems; flexible frames to permit negotiation of severe geometric obstacles; wheels for amphibious vehicles that acted as propulsion pumps; wheel shrouds to increase the efficiency of wheeled vehicles operating in water; flotation bags to convert conventional wheeled vehicles into amphibians; and the list could go on.

TRECOM: The Transportation Corps' program was largely conducted out of house, with Nuttall playing a major role in conducting their research studies of soil and in the construction of vehicle concepts that were aimed at the light-weight end of the scale of TRECOM's interests. The TRECOM program was initiated in 1951 with a study of the changes in vehicle requirements that had occurred in the post-WWII period. This study identified two primary needs: to increase the understanding of how soil behaves and how to relate that

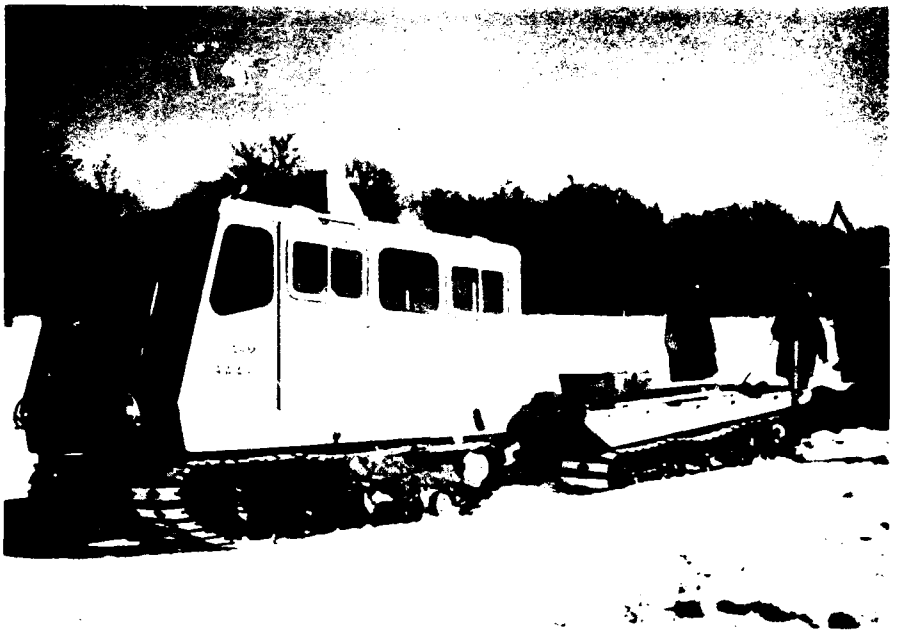

Figure 9. The Polecat; an articulated version of the Weasel.

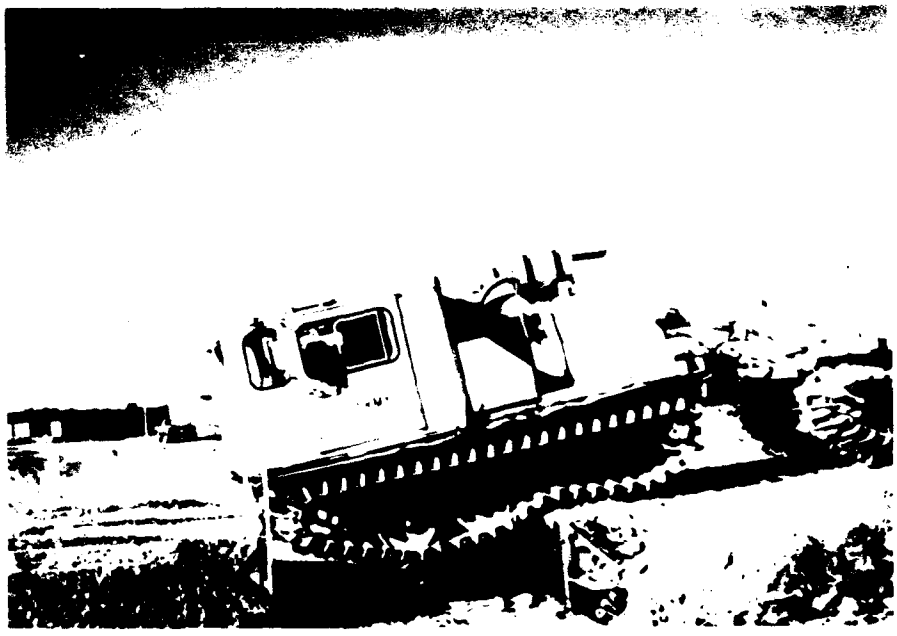

Figure 10. The Cobra with a spaced-link track.

behavior to vehicle operations; and to develop high-mobility, high-cargo-capacity equipment for negotiating desert, arctic and marshy terrains. An initial reaction to the selection of this terrain set might be one of surprise: in 1951 the Korean War was in progress, so that the challenges of hilly terrain, rice paddies and poor roads would seem to be paramount. Evidently the study was directed to future needs rather than current needs, which were not likely to benefit from research efforts in the near and long terms. That Dick Kerr was a consultant to the Transportation Corps can explain the interest in moving heavy loads over deserts. The importance of the DEW Line and the need to resupply the DEW sites by ground transport could explain the need to develop an arctic heavy-load capability. It is difficult to find marshy terrain as being of vital interest as a transportation problem simply because major military operations are not conducted in marshes. In the mid-Vietnam war, there were operations in the Rung Sat and in the Plain of Reeds, both of which qualify as marshy terrain, but these operations were at the squad, platoon or company level and did not involve extensive logistical support. One explanation is that the 1951 study found that the mainstream development activities ignored marshes and that the problem should at least be studied. This position was reflected by the two major exercises that TRECOM conducted in the jungles of Panama. The first, Swamp Fox, was almost an exercise in futility in that it consisted of driving a fleet of military vehicles through an untamed, unmodified jungle, relying solely on on-board equipment to recover vehicles when they became stuck. Become stuck they did, with bone-crushing regularity that slowed progress to several miles per day. The results of this remarkable effort demonstrated that given enough time, enough energy and enough will power a team of men can negotiate jungle terrain. Swamp Fox II was considerably more "tester friendly" in that the tests were of an engineering, rather than operational, nature so that machines, not men, were stressed to the utmost.

The criterion that TRECOM selected to evaluate performance differed from the WES and TACOM criteria in that it was tons of cargo moved per hour. The use of this criterion had a major impact on the kinds of automotive equipment that they considered because speed became secondary to load, making it possibly better to move a large load slowly than a light load quickly.

In developing their research program, the TRECOM people decided that the first priority was to develop an analytical basis to guide the conduct of scale model studies. If very large concepts were to be evaluated, it would be cost-effective to deal with scale models that could demonstrate concept feasibility without breaking the bank. Nuttall (of Wilson, Nuttall and Raimond) and Finelli (of Stevens Institute) were contracted to develop the critical scaling laws and soil parameters required to assure the credibility of scale model test results. Included with the identification of critical soil parameters was a need to develop apparatus to measure the parameters and methods to extract the data needed. Nuttall and Finelli developed the scaling laws successfully but

found dealing with the critical soil parameters a difficult chore, as did virtually every other research team who followed them in attempting to conduct model tests in soil. The Nuttall/Finelli work served as a valuable starting point for many subsequent studies, so their efforts can certainly claim success.

The TRECOM vehicle developmental concepts were interesting both in their individual originality and in their variety of application. The decision to develop heavy load movers in desert, arctic and marshy terrains demanded variety at the outset, since each terrain type had its peculiar characteristics (although a good solution for the Arctic might work well in desert terrains). Because of Kerr's remarkable success in solving the heavy load movements of ARAMCO, it is evident that it was determined that the technology, equipment and operational doctrine were on hand that could be quickly exploited if desert operations became a fact; this took about 40 years to occur, and re-supply by land transport was hardly a factor in Desert Shield or Desert Storm. Thus, the emphasis of the TRECOM vehicle studies was on marsh and arctic operations.

The development of the Marsh Buggy was an interesting program because of its dual function. First, a full-scale version of the four-by-four vehicle, which had 120-inch-diameter tires, was purchased, and a 1/4-scale model was constructed. The pair, which eventually became affectionately known as Mutt and Jeff, was used to evaluate the validity of the scaling factors and was likely one of the first opportunities to conduct tests with a not-very-small model and a very large prototype. The second purpose of obtaining the Marsh Buggy was to evaluate its potential as a heavy load carrier for marsh operations. It is not clear that it served its second role as well as its first.

The arctic areas selected to serve as a development laboratory were the ice cap regions that required movement over great distances and that placed a premium on moving a lot of stuff with a high degree of reliability. The approach settled upon was the concept of a land train; so firm was the train concept that the first unit was called a locomotive to emphasize the fact that its sole function was to provide power to the three trailer units. The locomotive and all trailers were powered; the design payload was 90,000 pounds to be moved at a maximum speed of twenty miles per hour. Two models of the train were constructed, one of which was tested in Greenland (Fig. 11). Stability problems were encountered at about fifteen miles per hour, and later Nuttall was approached to provide a solution. He constructed a four-unit train using quarter-ton vehicles and looked at power control stability and steering stability, but the passage of time had made the study obsolete.

The development of the PoleCat II by TRECOM was a reflection of their pursuit of heavy load movement capabilities. The PoleCat had been developed for SIPRE to support their snow studies. As mentioned earlier, this vehicle consisted of two Weasel chassis connected with a joint that transferred power from the front unit to the rear unit and also provided steering. The vehicle was a

Figure 11. The Letourneau Land Train.

great success and was used extensively in support of SIPRE's and CRREL's work in Greenland. TACOM used several Polecats as workhorses to support the winter and summer tests in northern Michigan and in Greenland. The success of the PoleCat prompted TRECOM to consider a much larger version, having the potential of tripling or quadrupling the load-carrying capability of the original machine. The vehicle was built by Nuttall and performed well enough that it was decided to build an amphibious version, the Terrapin, named after the large turtle that inhabits the salt marshes in coastal areas. The Terrapin was a success, but time had also passed it by.

In 1962 an event occurred that would have a profound effect on the Army's mobility research program, along with virtually every aspect of the Army. The Army Materiel Command was formed, and the R&D responsibilities of the technical services were handed over to the direct control of the new command, with the exception of the Corps of Engineers, which had major research duties but was responsible for almost no development programs. The impact on mobility research was that one man now monitored all research in progress, including WES's because their mobility research applied to AMC and not to the Corps. The one man, Robert Phillipe, was disturbed with what he found and eventually formed a committee, chaired by Dick Kerr, to survey the research and development in progress and assess its value to AMC and the Army. The Kerr Committee spent several weeks visiting the three main players, receiving in-depth briefings and tours and being dragged to desperate lunches, cocktail hours and dinners. The group prepared its report, which was not very flattering to any of the labs involved, and it recommended that the WES and TACOM programs continue with the understanding that programs would be coordinated. Because CRREL's program was low key, they weren't taken behind the barn, but the message was clear that business was not to continue in the future as in the past and that the Army's program would be subjected to frequent scrutiny.

A day of reckoning occurred in the mid-sixties when it was agreed that TACOM and WES would either have a coordinated program or there would be no program. A series of meetings produced the AMC Five Year Mobility Plan. The goal of the plan was a verified mobility model whose primary functions were to develop vehicle concepts to meet a given set of environmental conditions and to evaluate concepts proposed by other people to meet the stated conditions. A secondary objective was to assess the potential of the model produced by the WES/TACOM team, later expanded to include CRREL, to be used by field commanders to assist in making decisions relative to route selection and to identify the potential performance capabilities of both their own vehicle fleet and the threats'. The outline of the model was agreed upon, and the next several years were devoted to developing, collecting and providing input to the model. The deficiencies of the model have been the driving force for most of the studies that have been initiated since the introduction of the model into the vehicle procurement process and by its acceptance as the NATO mobility model.

The CRREL mobility research program for the past 20 years or so is a demonstration of the dominance of the needs of the model. Emphasis was transferred from the interaction between vehicles and deep snow to shallow snow. Reason: except for the BV206 (Fig. 12), there are no vehicles in the inventory that can operate in deep snow; hence we have no need to develop a deep snow model. In addition, the Canadian mobility research program is directed to the deep snow problem so that a parallel U.S. study would be superfluous. The primary soft soil problem facing military operations is the classic mud season when we have to attempt to operate in thawing soils; thawing soils were never included in the model because no work had been done to study the problem. Therefore, CRREL developed a program to study this particularly difficult analytical and operational problem in order to expand the capabilities of the model.

Contributions of the mobility research community: There have been literally millions of dollars spent over the past 40 years on mobility research, learning about vehicles, about vehicle components, about terrain, about the fundamental behavior of soil and snow, about the interaction of vehicles with terrain and the components of the terrain, so that it is reasonable to ask what all this effort has produced. Frankly, it is hard to answer the question, partly because one of the contributions of the mobility community was negative, because it could recommend to not do something and back up that recommendation with fact. An example from the past that would not happen today because of the knowledge that we have gained over the years was the Snow Cruiser (Fig 13), designed and constructed to support a Byrd expedition to the Antarctic. The design was given careful attention, and all details appeared to be addressed. Unfortunately Dr. Thomas Poulter, the engineer/scientist responsible for the vehicle development, assumed that since snow was granular and sand was granular, it would be valid to test the vehicle in sand and infer the over-snow performance from the sand tests. That nothing could be further from the truth was demonstrated by the performance of the Snow Cruiser when it arrived at Antarctica. It was able to debark from the ship that delivered it but was able after much effort to move only about a hundred yards in the snow. Thus, for

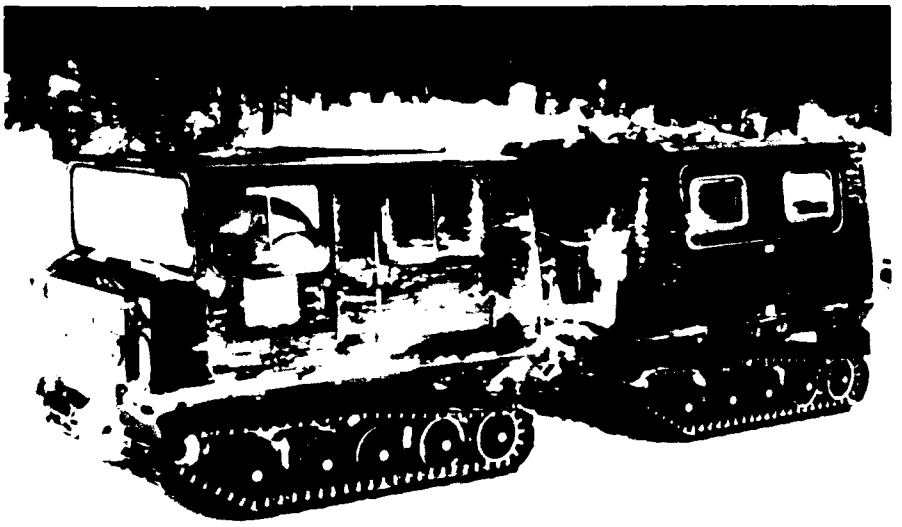

Figure 12. The BV206: master of snow country.

the lack of a little knowledge, the Snow Cruiser was downgraded from the primary science support vehicle to a stationary office and laboratory. Eventually the Snow Cruiser became a component of an iceberg and sank to a watery grave somewhere near the Antarctic continent.

Before addressing contributions that can be considered significant, I think that it is important to examine the majority of the mostly unsuccessful attempts that have been made to provide new levels of off-road vehicle performance. Virtually all of the prototypes of high mobility concepts that have been constructed have involved the goal of providing devices and vehicles that can operate in extremely soft soil. The number of wheel concepts, of track concepts, of hybrid suspension concepts, of hybrid vehicle concepts that have been pro-

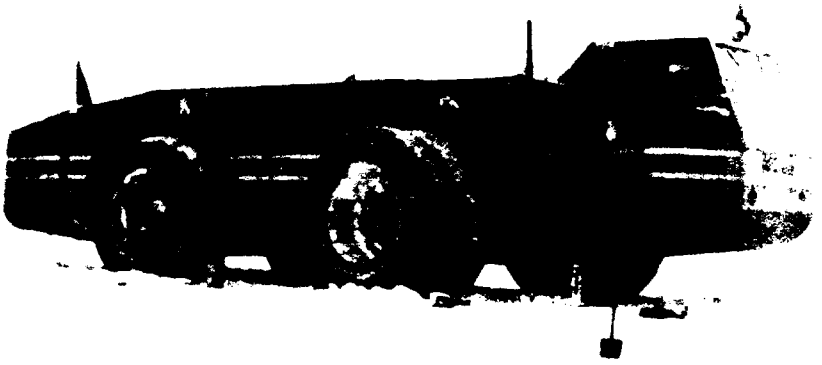

Figure 13. The Sno-Cruiser.

posed to conquer demon mud would take weeks, perhaps months, to catalog. Sadly, the expert has been as guilty of misreading the mobility problem as the amateur, but he has been more often able to get his ideas into hardware because of having expert status and thus capable of inflicting more damage than his idea deserved.

In defense of the mobility expert, I offer a purely random chance event that occurred in my attic in the very recent past. While looking for a door handle, I saw that the shelving holding our *National Geographic* collection had failed. I walked over to the stack, and the topmost issue had on its cover as its first article "The Coming Revolution in Transportation"; the issue date was September 1969. What things did I find that were to be responsible for that revolution? The air cushion vehicle wafting us across heavy seas with barely a bump. The Concorde soaring into a new age. The people capsule eliminating the need for your car in the urban environment: dial your destination and sit back in peace and comfort. VERTOL aircraft solving airport congestion. Trains, trains: single rail, push-pull with a gas turbine at either end; "Bullet" trains in Japan operating at 130 miles per hour and so smooth that you can drink your tea without fear of spillage. The Boeing 747 has lived up to and far exceeded all of the predictions made in the *Geographic* article, but all of the other problems that the revolution was going to solve are still with us and, in most cases, are more intense. The point of this defense is that good solutions to problems may not be useful solutions because the cost of implementing them may be greater than the cost of living with the problem. This situation may well explain why what appear to be good solutions to proposers are viewed as being bad solutions to potential users.

One of the contributions that can be attributed to Army mobility research is the articulated, over-the-snow vehicle: the BV206 produced by Hagglunds in Sweden (Fig. 12). Curiously, perhaps, the articulated form was conceived of early in this century to provide a long, narrow track that would reduce motion resistance in soft soil and thereby increase net traction. Mr. Diblock, in submitting his 1918 patent application, did not, I am sure, describe his invention in those terms, but that is what he achieved. SIPRE, TACOM and TRECOM were all involved with the exploitation of the articulated vehicle concept and rushed forward with an articulated vehicle solution for any new vehicle requirement that appeared on the scene. The introduction of a successful articulated vehicle was delayed by attempts to militarize either successful civilian prototypes such as the Gama Goat or vehicles such as the Letourneau scraper, which performed exceptionally well in roles not really compatible with the military heavy transport scenario. The militarization of Gama Goat involved a process of increasing weight while decreasing wheel diameter with the mobility community attempting to set things right. The scraper was not intended to be a highway vehicle and therefore no suspension was provided. Large, low-inflation tires worked well in the scraper role, but when placed on the highway the vehicle bounced so badly that 15 miles per hour was about tops. The articulated vehicle concept was not at fault; the application of the concept was at fault. When the requirements for the Small Unit Support Vehicle (SUSV) were published, it was clear that the requirement could only be met with an articulated concept. When hands-on evaluations of available vehicles were completed, the BV206 was the clear winner. However, the Swedish Army would never have selected an articulated vehicle concept as their mainstay if U.S. Army mobility research had not established, analytically and experimentally, the remarkable advantages of this vehicle form for some terrain/operational environments.

Probably the contribution that has brought more satisfaction to more people in the mobility community is the user recognition, after years of cajoling, that it is possible to make gains in wheeled-vehicle off-road performance and save money at the same time. Save money first: although it was difficult to establish exact figures, the best data that could be found stated that the average life of the NDCC tire, regardless of manufacturer, was of the order of 7000 miles. It had also been established by tests that the NDCC tread on a bias-ply carcass was the worst performer of any currently available tires except on ice, where it was as good as any other tire. By switching to all-season tires with radial-ply construction, performance could be increased, but, more important to the user who buys the tires, life could be dramatically extended. Performance next: the coupling of radial tires with a central tire inflation system and locking differentials can provide a major performance increase. The radial tire can be deflated to very low pressures, which increases contact area with a minor increase in contact width, resulting in an increase in net traction. The central tire inflation system allows tires to be deflated rapidly, on the order of 5 minutes for a five-ton truck as compared to 50 minutes when done manually. After moving back on the road, the tires can be re-inflated while on the move. The locking differential is a device that extracts the maximum traction available from a soil/wheel system: with a standard differential, what is called a 2×4 is actually a 1×4 when soil surface strength is low. A differential is a torque-splitting device so that all of the driving torque is developed by the wheel operating in the weakest soil. Similarly, a 4×4 is a 2×4 and a 6×6, a 3×6. Point made. By activating locking differentials when the going gets

tough, the operator, regardless of the configuration of his vehicle, at least doubles available traction. The new five-ton trucks and HMMWVs coming off the assembly line have radial tires and central tire inflation systems; at least we got two out of three. The acceptance of these new (old) ideas is based on the fact that the user could be shown that he could have an increase in performance without paying an unacceptable penalty.

The switch from rear dual wheels to rear singles also represents a major victory for the mobility research community. It had been established both by theory and by experiment that a properly selected single tire can provide better performance than a set of duals. The reason is straightforward: traction is a function of contact area; motion resistance is a function of both contact area and its orientation. A wide tire produces more resistance than a narrow tire, as any Model T Ford owner would tell you. However, to produce the same contact area with a narrow tire as that produced by a wide tire, it is necessary that the diameter of the narrow tire be greater than that of the wide tire. The large-diameter tire was slow to receive acceptance because it made cargo loading a bit more difficult, and the idea didn't seem to make good intuitive sense to the user. The combination of nagging by the mobility research community and the rejection of the dual tire configuration by almost every army in the world convinced the user to cave in to the forces of progress. An important point is that the change could be accepted because it could be shown that a performance improvement would be obtained accompanied with a cost saving. A 6×6 now had six tires instead ten tires and six wheels instead of ten wheels, clearly a cost saving. It is apparent that the overwhelming criterion for acceptance of change is at least a dollar return for every dollar invested.

One of our contributions has been elusive in its implementation. This is the development of a new way to specify tire requirements, in which the automotive industry would be given a level of performance that had to be achieved and it would be the responsibility of industry to meet the performance specifications in any way that it chose. The tire selection would not have to be radial ply or bias ply because the sole criterion is delivery of the required performance. There has been considerable user happiness with the concept, but the procurement people balk because they worry that the supply system will be flooded with a mishmash of oddball tires, with the result that the system would become over-burdened.

The most important contribution of the Army mobility community is the mobility model that contains the results of the efforts several hundred people over several decades. It is comprehensive in that it includes all of the critical elements of the highway and off-highway environments; it includes the constraints imposed by the vehicle and by the operator. Currently the operator only enters the analysis as a limit to speed in rough terrain because there is a well-identified limit to the vibration input that operators will accept. An expanded operator module is appropriate but has not been developed to date because of concern over stepping on the human engineering turf. The model is still far from perfect, but it is gradually reaching the point where changes will be less and less significant.

Given this circumstance, where do we go from here? I'm sure that there will always be fundamental questions that will excite our imagination and when answered will improve the model, but I wonder whether serving the model will use our talents most effectively. The search for a better understanding of all elements of the terrain-vehicle system is a worthy end itself and hardly needs defense. But what of the rest of our energy? I see a body of knowledge that has been developed and that continues to grow, and it is our job to seek out the problems facing the users of automotive equipment and develop appropriate solutions. If the mobility research community has done nothing else, it has generated a perspective of what is really important and has achieved a maturity of viewpoint that can provide a dispassionate assessment of the worth of a new idea or of a solution to a problem and then act on that assessment to produce a positive change.

Perhaps during this workshop, while you are discussing our current approaches to the analysis and evaluation of off-road vehicle performance, you can be formulating in your mind what you view as the most important future needs that we should be addressing. It should be possible for us to take a few minutes near the end of the week to examine your collective thoughts.

Examples of vehicles developed to operate in extremely soft soil that range from the almost practical to the bizarre are shown in Figures 14–17.

Figure 14. The Rolligon: successful on the Alaskan North Slope.

Figure 15. The Terra-Star designed for operation in deep mud.

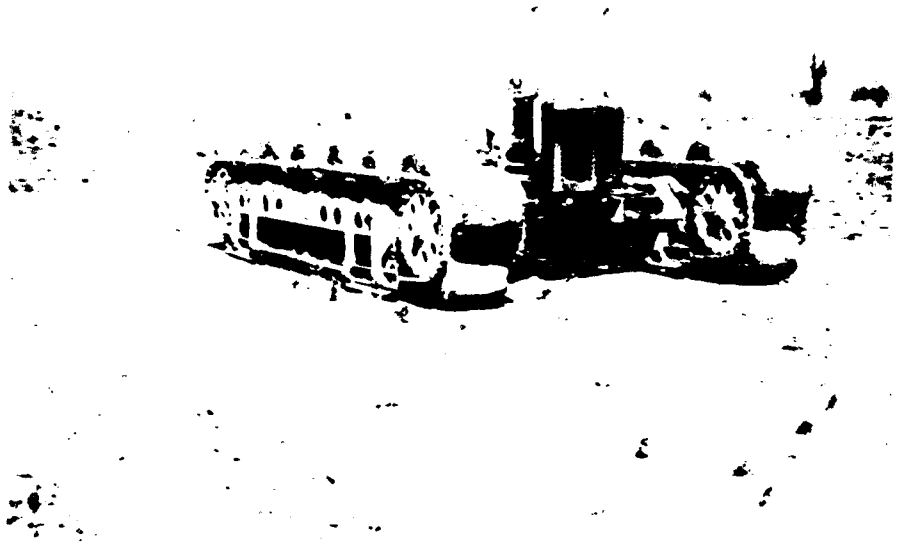

Figure 16. The Air-roll, fine for level sand or mud.

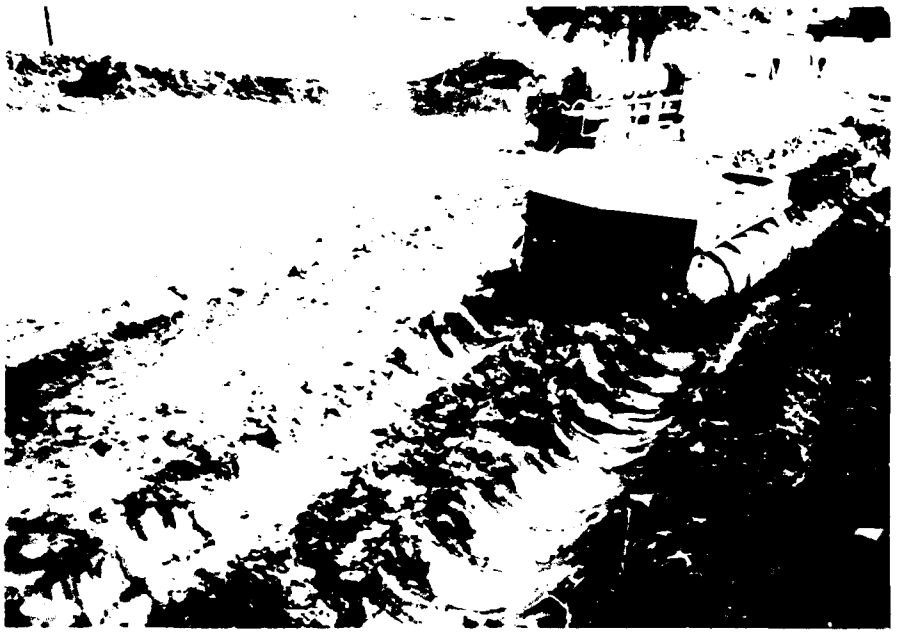

Figure 17. A version of the Archimedes screw vehicle.

2. PREDICTION AND TESTING METHODS

Predicting Vehicle Mobility On Snow-Covered Slopes

PAUL W. RICHMOND
U.S. Army Cold Regions Research and Engineering Laboratory
Hanover, New Hampshire 03755-1290

ABSTRACT

Recently, a semi-empirical model for shallow snow mobility predictions was developed at CRREL in support of an evaluation of wheeled and tracked vehicles. These equations were developed from a large data base of traction and resistance data obtained on level, snow-covered terrain using current U.S. Army military vehicles. Winter military operations will not be limited to level terrain; thus, it is important to be able to predict mobility characteristics on snow-covered, sloped terrain as well. This paper describes a simple modification to the CRREL shallow snow mobility model to account for sloped terrain and compares mobility predictions to go–no-go mobility tests on snow-covered slopes. Go–no-go data were available for nine vehicles (both wheeled and tracked), all obtained at the Keweenaw Research Center, Michigan, using their test slopes. Snow conditions ranged from a thin layer of hard packed snow to 60 cm of 150-kg/m^3 density snow. Go–no-go predictions using the model were correct for about 70% of the test data available. It was found that the surface underlying the snow may have more effect on traction on slopes than it does on level terrain, at least for shallow, low-density snow layers.

INTRODUCTION

Recently, researchers at CRREL presented and verified an oversnow mobility model (Blaisdell et al. 1990, Richmond et al. 1990). This model was developed from traction or drawbar and resistance tests on level or nearly level, snow-covered terrain using a variety of current military vehicles. Since these vehicles are also expected to be able to travel over sloping terrain, it is also important to know their limitations on snow-covered slopes. Measurements of traction and resistance on snow-covered slopes are difficult to obtain, and the author is not aware of any such data. Results of go–no-go tests on various snow-covered slopes were presented by Green and Blaisdell (in prep.) and by Osborne and Guitar (1986).

The main effect of slopes is the redistribution of the force of gravity on the vehicle body forces (Yong et al. 1984). This redistribution is seen as an additional resistance term due to gravity and a reduction of the normal load on each wheel (track). In cases of marginal mobility, vehicle momentum must also be considered. This analysis examines snow-covered slope mobility and compares predictions with available test data.

TRACTION

On level, snow-covered ground, the gross traction generated by a vehicle can be estimated by

$$T_g = 0.851\ (N/A)^{0.823} \qquad \rho \le 550\ \text{kg/m}^3 \qquad (1)$$

$$T_g = 0.321\ (N/A)^{0.97} \qquad \rho > 550\ \text{kg/m}^3$$
(Richmond et al. 1990) (2)

where T_g is the gross traction generated per driven wheel (track) in kilopascals, (N/A) is the normal load on the wheel (track) divided by the contact area in units of kilopascals and ρ is the snow density. If we assume that

there is no change in the failure mode of snow under a wheel (track) on a slope then,

$$N_S = N \cos\phi \tag{3}$$

can replace N in eq 1 and 2 where ϕ is the slope angle. (N_S is the normal force acting on the tires or tracks of a vehicle on a slope.)

RESISTANCE

A number of equations exist to determine the motion resistance due to deformation of a snow cover. In selecting an algorithm for the CRREL shallow snow mobility model, Blaisdell et al. (1990) choose a model proposed by Liston (1974).

$$R_S = pbh\rho_o\{[1/(\rho_f - \rho_o)] \ln(\rho_f/\rho_o) - (1/\rho_f)\}$$

$$\rho_o < \rho_f \ (z > 0) \tag{4}$$

$$R_S = 0 \qquad \rho_o = \rho_f \ (z = 0)$$

where p = tire inflation pressure
b = maximum tire or track width
h = *snow depth*
ρ_o = initial snow density (prior to tire or track passage)
ρ_f = maximum (final) snow density (after vehicle passage)
z = sinkage.

Richmond et al. (1990) tried to develop a general empirical relationship from a large data base of different vehicles (which included both wheeled and tracked vehicles); however, on the average it was not any better than that proposed by Liston (only within 50% on average, for resistance). Richmond et al. (1990) presented relationships for each vehicle they tested and Richmond (1990) combined some of these data and presented separate empirical relationships for wheeled and tracked vehicles. These equations are presented in Table 1.

A vehicle attempting to negotiate a snow-covered slope must overcome gravity in addition to expending energy in compacting and deforming the snow. The resistance due to gravity R_g can be described by

$$R_g = W \sin\phi \tag{5}$$

where W is the weight of the vehicle.

By use of this approach, the general mobility equation for vehicles on slopes is

$$T_{net} = T_g - R_S - R_g \tag{6}$$

where each term represents the sum of traction or resistance for the whole vehicle. The resistance due to running gear, tire deformation, etc., has already been removed in obtaining the T_g term (eq 1 or 2). T_{net}, the net traction, must be positive for vehicle mobility.

MOMENTUM

Vehicles can negotiate short, steep slopes by making use of momentum built up during the approach to the slope, i.e., a running start. Using Newton's second law ($F = ma$), the work required to move an object can be written

$$\text{Work} = \int F\,dx = \int mv dv. \tag{7}$$

Solving the right side equality for F, we can obtain an average force in terms of vehicle speed, which can be added to the traction generated on the slope in question if required (i.e., we only need to account for this if the net traction is negative).

$$F = \frac{W}{2gx}\left(v_1^2 - v_0^2\right) \tag{8}$$

Table 1. Empirical equations used to predict R_S, from Richmond (1990) and Richmond et al. (1990).

*Constant** (d)	*Exponent* (e)	*Vehicle data used*
100.8	0.59	HMMWV
146.7	0.6	LAV25
275.43	0.5	HEMTT
137.25	0.61	HMMWV, HEMTT, LAV25†
145.18	0.8	SUSV
14.71	1.6	M113A1
306.54	0.9	BFVS
157.54	0.83	M113, SUSV, BFVS**

* The equations are of the form

$$y = dx^e$$

where x = parameter ($\rho_0 \times b \times a$)
a = length of wheel (track) in contact with snow
b = tire (track) width
ρ_0 = initial snow density
y = external motion resistance due to snow on a per tire or per track basis.

The SUSV was assumed to have two tracks because of its extremely low ground pressure, and thus the second pair of tracks do not seem to behave as trailing tires.

† Used for M34 truck predictions.

** Used for M60 tank predictions

where W = vehicle weight
v_0 = initial velocity (base of slope)
v_1 = final velocity (crest of slope)
x = length of the slope
g = gravitational constant.

RESULTS

Go–no-go data for vehicles on slopes were obtained from two sources, Green and Blaisdell (in prep.) and Osborne and Guitar (1986). All of the tests reported were done on slopes at the Keweenaw Research Center (KRC), in northern Michigan. The author was also able to obtain video tapes of some of the tests reported by Green and Blaisdell. The test slopes, along with other roads and test areas at KRC, generally become underlaid with a layer of packed snow as the winter progresses. Even though the slope surfaces are soil, for snow test purposes, the underlying surface must be considered hard packed snow. This observation is confirmed by the tapes, which show, for example, an M113 with its tracks locked, sliding backwards down a slope. Table 2 contains vehicle characteristics data for the vehicles used in these comparisons. Tables 3 and 4 present the go–no-go data and calculations of T_{net}. Results of 38 tests are presented. Equations 1 and 2 were used to estimate gross traction (eq 2 was only used for the 560-kg/m^3-density snow case). R_s, used in eq 6 to determine T_{net}, was calculated using the equations from Table 1, since it was thought that these individual vehicle equations would provide more accurate resistance values than the more general relationship (eq 4) used in the CRREL shallow snow model. Total resistance from the CRREL shallow snow model is presented for reference and the overall slope prediction performance is not different from using the empirical resistance equations. Equation 5 was used for calculating the effect of the slope angle (R_g). Equation 8 was not included since most of the tests were done from a standing start at the base of the slope. The relative magnitude of this term is discussed below.

DISCUSSION

Initially, 13 mobility predictions indicated that the vehicles should be able to successfully negotiate the slopes where they did not. There were no cases where no-go conditions were predicted and the vehicles did negotiate the slopes. This means that the analysis either under-predicted resistance or over-predicted gross trac-

Table 2. Tire and track data for military vehicles.

Vehicle	*Tire nomenclature*	*Inflation pressure (kPa)*	*Radius* (m)*	*Width† (m)*	*Contact area** (m²)*	*Weight (kN)*
HMMWV	37.00 × 12.5 R 16.5	138/152	0.429	0.33	0.074	33.45
	36.00 × 12.5 LT	138		0.425		
HEMTT	16.0 R20	241/276	0.617	0.475	0.171	268.56
		139/207	0.589	0.483	0.149	
LAV25	12.50/75 R20XL	207	0.445	0.378	0.100	119.63
		103	0.414	0.343	0.141	
	11.00 R 16 × L	290	0.434	0.314	0.058	
		165	0.417	0.332	0.102	
M34 2.5T	11.00-20 NDCC	241	0.536	0.287	0.063††	75.62
SUSV	Track	—	32.5°	0.6096	1.180	61.34
BVFS	Track	—	25°	0.533	2.090	223.30
M113A1	Track	—	21°	0.381	1.020	104.09
M60	Track	—	35°	0.66	2.80	467.06

* Radius for wheeled vehicles, entrance angle for tracked vehicles.
† Maximum deformed width.
** Hard surface contact area, per tire (track)
†† Data from Harrison (1975).

Table 3. Tracked vehicle data.

Snow depth (cm)	*Snow density (kg/m³)*	*Slope tested (%/°)*	*Go–no go*	T_g *(kN)*	R_g *(kN)*	R_s* *(kN)*	R_s† *(kN)*	R_{net}** *(kN)*
SUSV (after Green and Blaisdell, in prep.)								
5	560	19/11	go	17.9	11.7	0	—	6.2
30–60	230	30/17	go	32.0	17.9	10.1	1.9	4.0
5	560	25/14	go	17.9	14.4	0	—	3.5
5	560	25/14	no go	17.9	17.9	0	—	0
10–15	80	25/14	go	32.3	14.4	2.0	4.6	15.9
10–15	80	30/17	no go	32.0	17.9	2.0	4.6	12.1
30–60	150	19/11	go	32.6	11.7	8.8	2.1	12.1
30–60	150	25/14	no go	32.6	14.4	8.8	2.1	9.4
M113A1 (after Green and Blaisdell, in prep.)								
5	560	19/11	go	29.2	19.9	0	—	9.3
5	560	16/9	go	29.3	16.3	0	—	13.0
5	560	19/11	no go	29.2	19.9	0	—	9.3
10–15	80	19/11	go	43.5	19.9	1.3	11.0	22.3
10–15	80	25/14	no go	43.1	25.2	1.3	11.0	16.6
30–60	150	16/9	go	43.7	16.3	24.6	5.0	2.8
30–60	150	19/11	no go	43.5	19.9	24.6	5.0	−1.0
30–60	230	25/14	no go	43.1	25.2	32.1	4.7	−39.0
M113 (after Osborne and Guitar 1986)								
17	300	25/14	go	43.1	25.2	4.0	1.1	13.9
14	130	19/11	go	43.5	19.9	2.1	1.2	21.5
14	130	25/14	14 m††	43.1	25.2	2.1	1.2	15.8
18	130	30/17	7.6 m††	42.6	30.4	3.1	1.5	9.1
BFVS (after Green and Blaisdell, in prep.)								
5	560	19/11	go	62.5	42.6	0	—	19.9
30–60	230	25/14	no go	91.7	54.0	36.6	6.9	1.1
M60 (after Osborne and Guitar 1986)								
23	190	19/11	go	178.9	89.1	5.5	5.4	84.3
23	190	25/14	go	178.9	113.0	5.3	5.4	60.4

* Using equations from Table 1.
† CRREL shallow snow mobility model (eq 4).
** T_{net} using equations from Table 1.
†† Distance traveled up a 20-m slope (no go).

tion. The simple resistance equations used here do not take into account two potentially large contributors to resistance: belly drag and slip–sinkage. An examination of vehicle sinkage calculations and ground clearance showed that unless significant slip–sinkage occurred, belly drag would not be a reason for underpredicting snow resistance under these snow conditions. Slip–sinkage is generally small compared to sinkage due to snow compaction; its effects become greater as a vehicle bogs down.

Since the greatest amount of data is for the M113, these data were examined first. Tables 3 and 4 indicate that in some cases a range is given for the snow depth. When this occurred I used the maximum value in the resistance calculations. Additionally, for the data of Green and Blaisdell (in prep.), the snow densities were not measured on the slopes but in an adjacent area, so they are only indicators of what the actual snow densities might be.

Figures 1–4 illustrate these uncertainties by showing a plot of net (available) traction predicted using eq 6 versus snow density for various depths of snow. The shaded areas in these figures show the snow conditions and results of the actual tests. Where the lines of equal snow depth pass below the 0 net traction line the prediction is no go.

In Figure 2 (the 19% slope) a large shaded area is indicated as no go. This agrees with the predicted

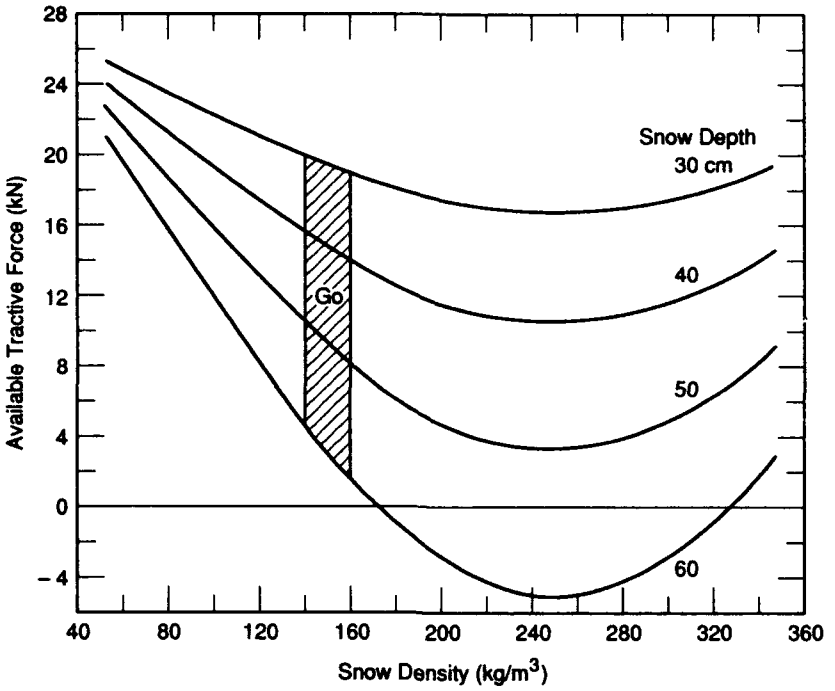

Figure 1. Mobility of the M113 on a 16% slope.

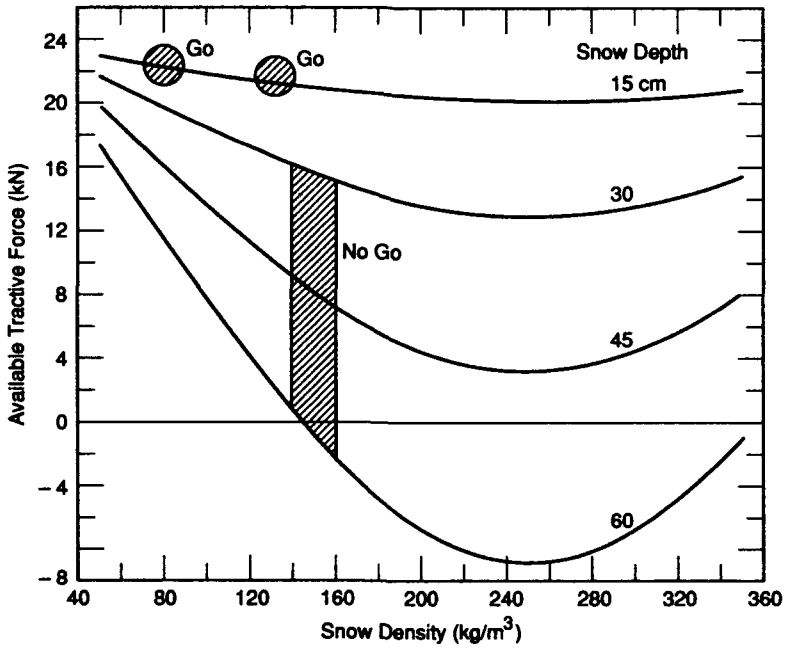

Figure 2. Mobility of the M113 on a 19% slope.

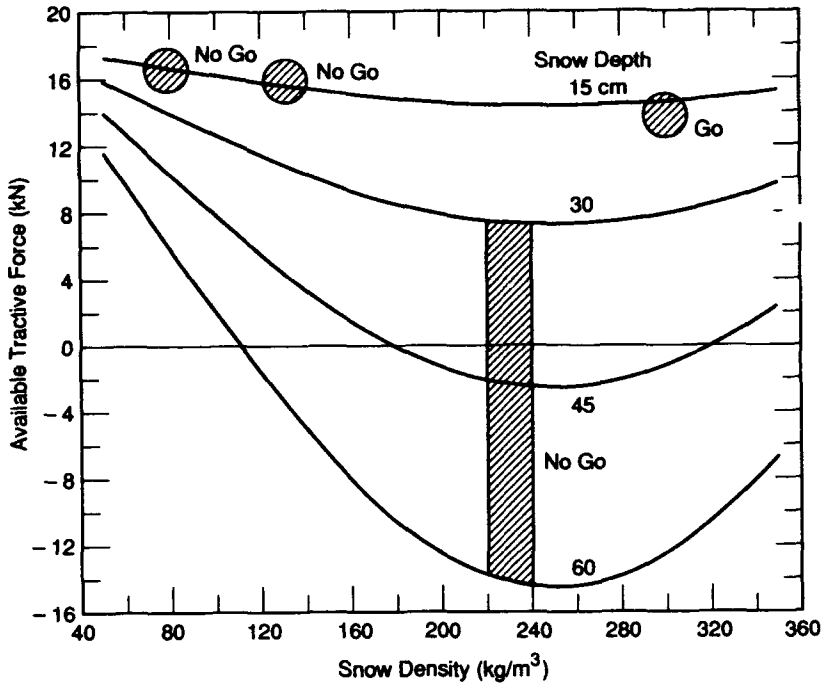

Figure 3. Mobility of the M113 on a 25% slope.

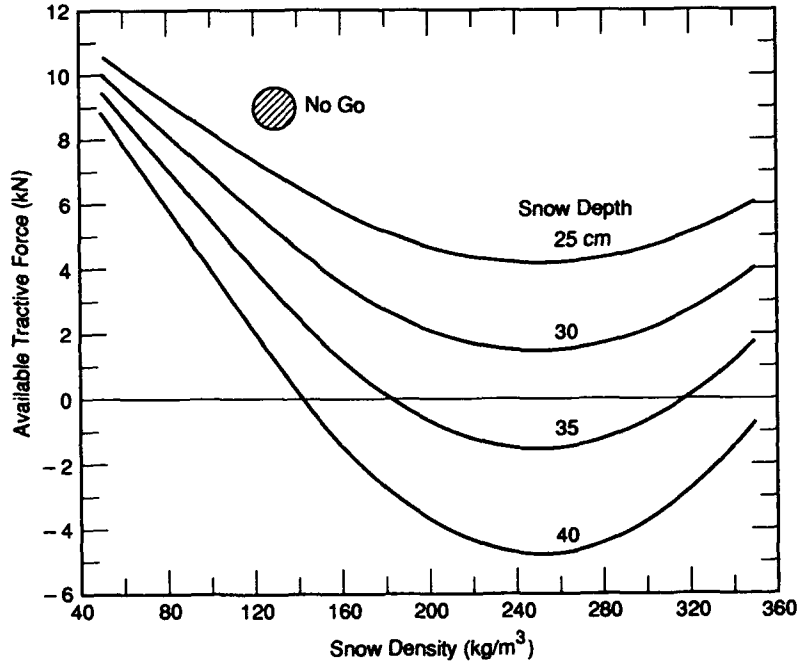

Figure 4. Mobility of the M113 on a 30% slope.

Table 4. Wheeled vehicle data.

Snow depth (cm)	*Snow density (kg/m³)*	*Slope tested (%/°)*	*Test results Go–no go*	T_g *(kN)*	R_g *(kN)*	R_s* *(kN)*	R_s† *(kN)*	T_{net}** *(kN)*
HEMTT (after Green and Blaisdell, in prep.)								
5	560	19/11	go	52.8	51.2	0.0	—	1.6
30–60	230	25/14	no go	87.6	65.0	18.2	30.1	4.4
5	560	19/11	go	52.8	51.2	0.0	—	1.6
5	560	25/14	no go	52.2	65.0	0.0	—	−12.8
30–60	150	17/7	go	89.2	32.7	15.5	32.6	41.0
30–60	150	16/9	no go	88.7	42.0	15.5	32.6	31.2
HMMWV (after Green and Blaisdell, in prep.)								
5	560	19/11	go	38.9	6.4	0.0	—	32.5
30–60	230	25/14	no go	12.0	8.1	3.8	11.2	0.1
10–15	80	25/14	go	12.0	8.1	1.6	3.0	2.3
10–15	80	30/17	no go	11.9	9.1	1.6	3.0	0.5
LAV25 (after Green and Blaisdell, in prep.)								
5	560	19/11	go	31.9	22.8	0.0	—	9.1
30–60	230	25/14	no go	37.7	28.9	10.3	17.6	−1.5
10–15	80	19/11	go	37.5	22.8	4.1	4.1	10.6
10–15	80	25/14	no go	37.7	28.9	4.1	4.1	4.7
M34 2½-ton truck (after Osborne and Guitar 1985))								
23	130	5/3	7 m††	25.2	4.0	4.3	6.7	16.9

* Using equations from Table 1.
† CRREL shallow snow mobility model (eq 4).
** T_{net} using equations from Table 1.
†† Distance traveled up 20-m slope (no go).

performance only for the greatest snow depth. It was not clear from the video tape of this test if the vehicle's belly was dragging in the snow, but calculations showed that ground clearance would be marginal at a snow depth of 60 cm. For the 25 and 30% slopes shown in Figures 3 and 4, no-go conditions were observed in shallow, low density snow. Speculation that excessive slip–sinkage may occur under these conditions led to the sinkage without slip being examined. From the shallow snow mobility model, the sinkage estimates were 12.6 cm (initial snow depth 15 cm), 10.4 cm (initial snow depth 14 cm) and 13.3 cm (initial snow depth 18 cm). It would be reasonable to assume that the small layer of compacted snow (2–5 cm) could easily be ejected from under the spinning track. The underlying layer of packed snow (mentioned earlier) would then provide the tractive surface and probably offer a smaller amount of gross traction. Equation 2 would then be more appropriate for calculating gross traction. A recalculation of the net traction using this assumption showed that the M113 would still be able to make it up the 25 and 30% slopes, but with a lot less available traction in reserve.

The data from other vehicles with this snow condition (snow depth 10–15 cm, ρ_0 = 80 kg/m³) were examined in this light. The SUSV prediction would now agree with the observed no-go performance on the 30% slope, and a go prediction is still obtained for the same snow condition on the 25% slope, which the vehicle negotiated. The LAV25 prediction also becomes no go for the 25% slope (agreeing with the observed performance) and is still a go for the 19% slope. The HMMWV was able to climb the 25% slope (and was barely predicted to). Changing the traction equation for this case causes the prediction to change to no go. On the 30% slope a go prediction was changed to no go, agreeing with the test results. Review of the video tapes showed that that the HMMWV had no difficulty climbing the 25% slope under these conditions. Table 5 summarizes the above discussion.

From the data in Table 4, it appears that the 25% slope is about the limit for wheeled vehicles. Figure 5 shows available traction for the HEMTT, HMMWV and LAV25 on a 25% slope with 60 cm of snow. Tests showed that none of the vehicles could climb this slope when the snow cover had a density of 230 kg/m³. The

Table 5. Comparison of the observed and calculated available traction on snow-covered slopes. (Snow depth: 10–15 cm; initial density: 80 kg/m³.)

Vehicle	*Slope (%/°)*	*Test results*	*Predicted traction (kN)* T_{net}*	T_{net}†	T_{net}**
M113A1	19/11	go	22.3	8.0	–1.7
M113A1	25/14	no go	16.6	2.3	–7.4
SUSV	25/14	go	15.9	1.3	–1.3
SUSV	30/17	no go	12.1	–2.4	–5.0
LAV25	19/11	go	10.6	5.0	5.0
LAV25	25/17	no go	4.7	–1.4	–1.4
HMMWV	25/14	go	2.3	–0.3	–2.0
HMMWV	30/17	no go	0.5	–2.5	–3.9

* T_g using eq 1 and R_s from Table 1.
† T_g using eq 2 and R_s from Table 1.
** T_g using eq 2 and R_s from Table 1.

predictions bear this out, except for the HEMTT, which in general had difficulty climbing slopes. It is not clear why this was.

In the above analysis, momentum was not considered. Green and Blaisdell (in prep.) did most of their tests from a standing start at the base of the slopes, although in some cases a short running start was used if a no-go condition prevailed in an initial test. In general, running starts did not improve slope negotiation. Osborne and Guitar did their tests at the fastest speed possible or prudent.

If it is assumed that the vehicle speed was 16 kmph (10 mph) at the base of the slope and that the vehicle is still moving at 1.6 kmph (1 mph) at the crest of the slope,

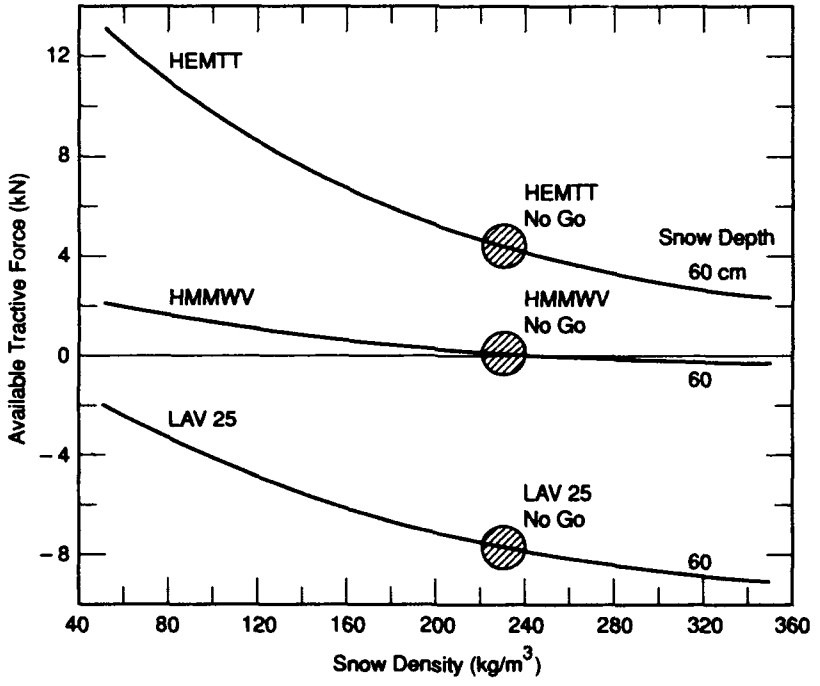

Figure 5. Mobility of three wheeled vehicles on a 25% slope.

Table 6. Effective force due to momentum.

Vehicle	F* (kN)
M113	5.2
SUSV	3.1
BFVS	11.1
LAV25	5.7
HMMWV	1.7
HEMTT	13.4

* Initial velocity: 16 kmph.
Final velocity: 1.6 kmph.
Slope length : 20 m.

then for any vehicle, eq 8, in terms of force (kN) becomes

$$F = 0.997 \frac{W}{x} \tag{9}$$

where x is the slope length in meters and W is the vehicle weight (kilonewtons). It can be clearly seen that this momentum "force" will have the greatest effect on short slopes and with heavy vehicles. The slopes at KRC are about 20 m long; using this length in eq 9 for various vehicles produced the values in Table 6. Given the same hypothetical snow conditions and the values in Table 6, these vehicles could negotiate slopes about 2.5 degrees steeper when momentum is used compared to when it is not. In marginal cases of slope negotiation, momentum could provide enough force to make the slope negotiable, particularly if the slope is short.

CONCLUSIONS

Elements of the CRREL shallow snow mobility model and empirical resistance equations were combined with a simple method of introducing the effect of slopes (i.e., adding gravitational resistance and reducing normal load on the driving elements) to obtain values of net predicted traction. These values were compared with the results of go–no-go tests. It was shown that this model works fairly well. Additionally, it seems that for thin layers of snow (<15 cm), the underlying material is more important on slopes than on level terrain. After taking this into account, the predictions of go–no go were correct 28 times out of 39. Similar results (26 out of 39) were obtained using the the more general equations of the shallow snow mobility model, but with the effects of slopes included and selecting the packed snow traction equation for conditions when the snow layer was thin. There does appear to be a problem predicting performance of the HEMTT (a heavy wheeled vehicle), but the reason did not become clear during this study.

ACKNOWLEDGEMENTS

I would like to thank Charles Green of the Waterways Experiment Station for the providing CRREL with the video tapes of his tests and for some additional unpublished notes on his tests. I also express my appreciation to S. Shoop and G. Blaisdell who provided technical reviews of this paper.

LITERATURE CITED

Blaisdell, G.L, P.W. Richmond, S.A. Shoop, C.E. Green and R.A. Alger (1990) Wheels and Tracks in Snow: Validation study of the CRREL shallow snow mobility model. USA Cold Regions Research and Engineering Laboratory, CRREL Report 90-9.

Green, C.E. and G.L. Blaisdell (In prep.) U.S. Army wheeled versus tracked vehicle snow mobility program. Waterways Experiment Station, Vicksburg, Mississippi, WES Technical Report.

Harrison, W.L. (1975) Vehicle performance over snow. USA Cold Regions Research and Engineering Laboratory, Technical Report 268.

Liston, R.A. (1974) Operation of the M151 1/4-ton truck in shallow snow. USA Cold Regions Research and Engineering Laboratory, Technical Note (unpublished).

Osborne, M.D. and S. Guitar (1986) Determining the effectiveness of snow-covered slopes as vehicle obstacles. Keweenaw Research Center, Michigan Technological University, Houghton, Michigan.

Richmond, P.W., G.L. Blaisdell, G.L. and C.E. Green (1990) Wheels versus tracks in snow: Second validation study of the CRREL shallow snow mobility model. USA Cold Regions Research and Engineering Laboratory, CRREL Report 90-13.

Richmond, P.W. (1990) Vehicle motion resistance due to snow. 1990 Army Science Conference.

Yong, R.N, E.A. Fattahand and N. Skiadas (1984) *Vehicle Traction Mechanics*. New York: Elsevier.

An Experimental Method for Vehicle Mobility Research on Freezing/Thawing Soil

S. SHOOP, E. BERLINER AND S. DECATO
U.S. Army Cold Regions Research and Engineering Laboratory
Hanover, New Hampshire 03755-1290

ABSTRACT

The Cold Regions Research and Engineering Laboratory has constructed a test basin where full scale vehicle mobility testing can be performed under simulated winter conditions. Although mobility testing is primarily performed on freezing and thawing soil, other surfaces can also be used. The test basin is 36.6 meters long, 12.3 meters wide and 3.6 meters deep. The deeper part of the basin is filled with a gravelly sand in which a water table can be allowed to fluctuate. In the top 106 centimeters of the basin is the test soil, which is changed periodically. Refrigeration panels are used to freeze the soil from the top down. Soil moisture and temperature are monitored during the freeze/thaw and can be varied as desired. The soil is generally first tested in an undisturbed condition, and then again after trafficking. Soil parameters such as moisture, density, cone penetration, and strength are measured prior to vehicle testing.

An instrumented Jeep Cherokee is used for traction and motion resistance testing. The vehicle has load cells and velocity sensors on the front wheels and both a sonic speed sensor and a fifth wheel to measure vehicle speed. The sensors are read and recorded using a computer-controlled data acquisition system. A typical test sequence consists of three traction and motion resistance tests, as well as a baseline hard surface resistance test, for each tire pressure or type.

INTRODUCTION

Freezing and thawing ground can cause difficult conditions for vehicle mobility. Vehicle traffic on unpaved and secondary roads is often restricted or even prohibited during thawing periods. Even when passage is possible, it can result in severe environmental damage (i.e. rut formation and consequent erosion). Although thawing ground conditions are common, field vehicle mobility testing on thawing ground can be difficult because of the short and erratic nature of the thawing events. Therefore, researchers at the Cold Regions Research and Engineering Laboratory (CRREL) have constructed a test basin where full scale vehicle mobility testing can be performed under controlled conditions (Shoop, 1989).

The test basin is located within the Frost Effects Research Facility (FERF) along with other freeze/thaw experiments. Our experimental program is designed to study the effects of different soil parameters (primarily soil type, moisture and density) and conditions (rate and depth of freeze/thaw and depth of water table) on vehicle mobility. Tests are performed in a large basin where freezing and thawing are controlled by varying air temperature and using refrigeration panels placed on the soil surface. Moisture content in the soil is varied by changing the water table depth, by adding surface water to simulate rain or snow melt, and by controlling the rate

of frost penetration. The soil temperature and moisture are recorded throughout freezing and thawing. The amounts of frost heave and ice formation are measured by surface elevation surveys and inspection of soil cores, respectively.

To date, a large number of mobility tests have been completed on various conditions of a thawing silty sand. Results indicate that the thaw depth strongly affects both traction and motion resistance, the degree of influence depending primarily on the moisture content of the soil. However, since the frozen layer restricts soil drainage, and water accumulates in the thawing layer, thawing soils become even wetter than under unfrozen conditions. These results have been discussed (Shoop, 1989, 1990) and will not be addressed here.

MOBILITY TEST BASIN

Frost Effects Research Facility

The unique capabilities of the FERF allow full scale vehicle testing to be conducted under carefully controlled experimental conditions. Freezing conditions can be created throughout the year. Refrigeration panels can supply temperatures from –40°C to +50°C, and the air temperature can be dropped to –10°C or raised as high as +30°C, depending on ambient outside temperatures. Thus freeze and thaw rate, as well as soil moisture, can be controlled.

The mobility test basin occupies the entire north half of the FERF. It is 36.6 meters long and 12.3 meters across, as shown in Figure 1. The mobility testing area is divided in half longitudinally. Testing occurs on one half of the test basin during thawing while the other half of the test basin is being frozen. This large area allows a complete suite of full scale mobility tests, including repetitions, on undisturbed soil. With a skilled driver, several test suites can be completed within the area.

Soils

The test section currently consists of a bottom layer of fill and a top layer of test soil separated by a geotextile (Figure 2). The purpose of the fill material is to simulate a natural environment (i.e. to eliminate having a rigid impermeable layer directly below the layer of test soil) and to allow for a water table to be added and varied relatively quickly. The fill soil is a bank run sand from Pompy Pit, located in Thetford, Vermont. The top 106 centimeters of soil is the material to be tested. The first soil tested (1988–1990) was a silty sand, and the present soil type is a clayey silt, both from Lebanon, New Hampshire. The test soils are marginal road material and are typical subgrade or off-road material in New England. The grain size distribution curves of the three

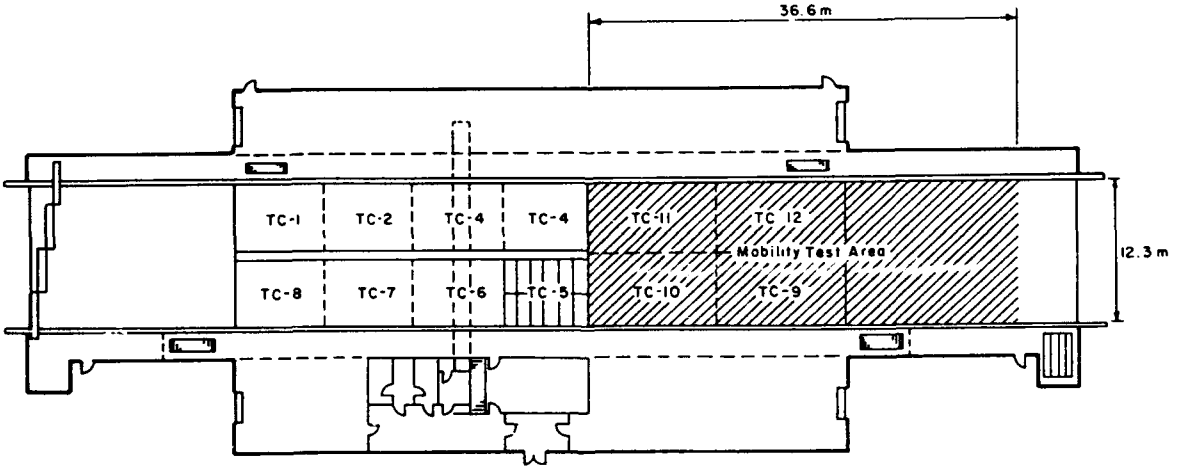

Figure 1. Plan view of the soil test basin in the Frost Effects Research Facility (hatched area). TC refers to Test Cell.

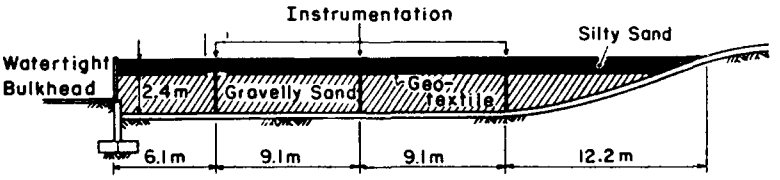

Figure 2. Cross section of the mobility test basin showing configuration of test soil, base fill and geotextile as well as location of instrumentation.

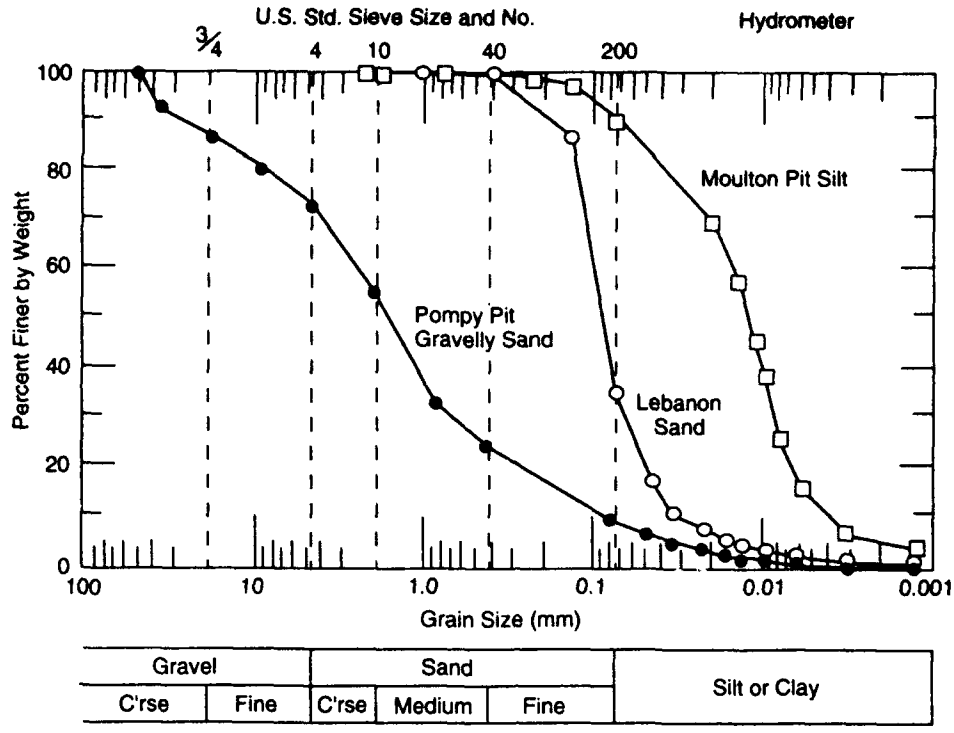

Figure 3. Grain size distribution curves of the test soils (Lebanon sand and Moulton Pit silt) and the base fill (Pompy Pit gravelly sand).

soil types mentioned are shown in Figure 3. Based on results from the standard CRREL frost heave test (Chamberlain, 1987) and the Army Corps of Engineers soil classification scheme (Berg and Johnson, 1983), frost susceptibility of the base fill material is low, while both test soils are highly frost susceptible.

Geotextile

A needle-punched polyester geotextile separates the test soil and the base fill at a depth of 107 cm. It was chosen as a separator for the two soils based on Corps of Engineers Civil Works Guide Specification CW-02215, March 1986, using Filter Design Criteria. It is placed over the entire test basin with the exception of two circular holes of 1.2 meters (4 ft) diameter cut in the fabric, each containing a vertical string of tensiometers and thermistors in the center. These sections without fabric are used as reference sections to monitor the effect of the fabric on moisture migration during the freeze/thaw cycles (Shoop and Henry, 1991). The fabric is present at all other instrumentation locations.

Test cell instrumentation

Temperature and soil moisture tension are monitored using thermistors and tensiometers throughout each freeze/thaw cycle. The instrumentation is concentrated in the upper 30 cm because this is the area of most concern to vehicle mobility on thawing ground. Near the surface, the thermistors are placed at 2.5-cm intervals and the tensiometers at 5-cm intervals. The vertical distance between the instruments increases with depth. The basin is instrumented at six locations, three on each side, approximately 9 meters apart. Figure 4 shows the vertical configuration of the instrumentation and the location of each instrumented section in the test basin.

The thermistors were installed on a polyethylene rod and then placed in a hole drilled in the soil. The tensiometers are each placed individually within the soil by careful augering and backfilling at each location. The top 30 cm of instrumentation is removed after vehicle testing so that the soil can be rototilled and recompacted to specifications before freezing for the next test series.

The soil temperature is recorded every 2 hours throughout the freeze and thaw cycle using a computer-controlled data acquisition system. These data are reduced and compiled automatically every 24 hours to calculate frost depth and thaw depth. Tensiometers are read manually, as these instruments need more human attention (i.e. they need to be checked for air in the tube linings and periodically refilled with glycol). The tensiometer data are then entered into a spreadsheet and used to track the moisture migration in the soil as a result of the advancement of the freezing front or other conditions. Figure 5 illustrates the workings of a tensiometer.

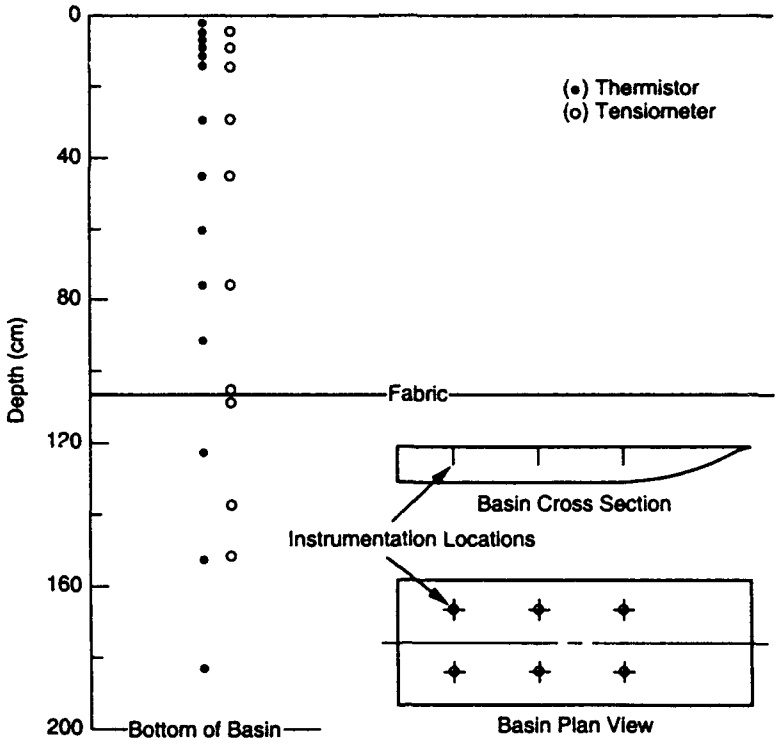

Figure 4. Instrumentation configuration in the test basin.

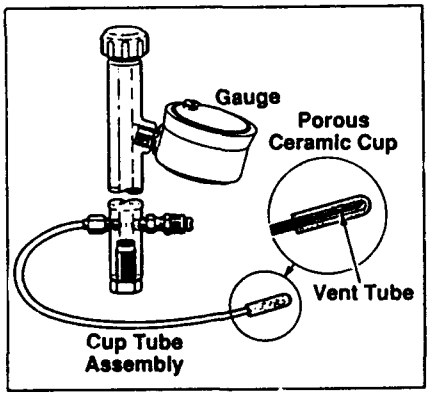

Figure 5. Construction and major components of a soil moisture probe tensiometer. These are filled with glycol for use in freezing environments.

Their use in monitoring soil moisture is discussed more in Shoop and Henry (1991).

Water table

One of the features of the large test basin is the capability of maintaining and controlling a water table. Water can be added to the basin through four standpipes (wells) near the corners of the basin. The vertical standpipes were connected to horizontal pipes located 1 foot from the bottom of the test cell in the base fill. These pipes are perforated to allow the water to seep into the soil and are covered with a fabric to keep the soil out. The water level is measured in each of the standpipes and is also inferred from the tensiometer data. Water can be released through four drains in the floor of the test basin.

Figure 6. The CRREL Instrumented Vehicle in the FERF mobility test basin.

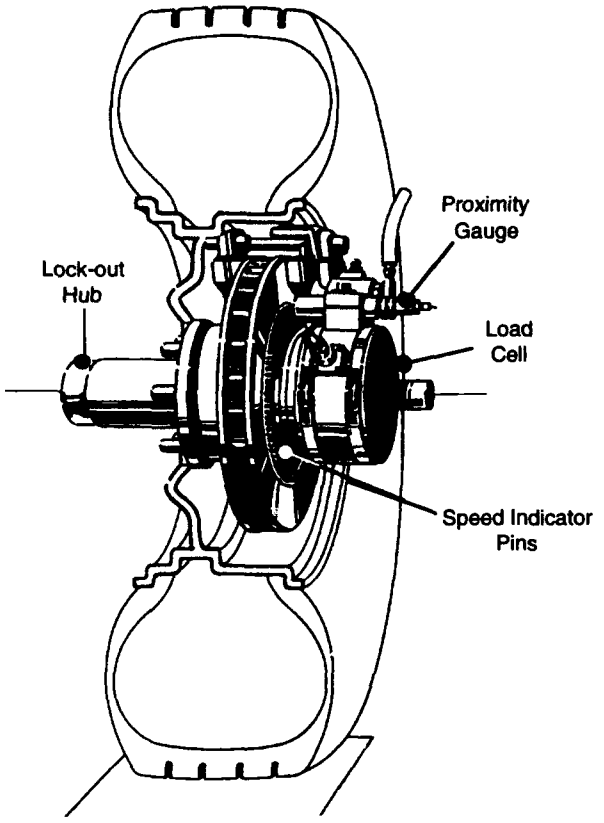

Figure 7. An annular load cell mounted on the vehicle axle.

THE CRREL INSTRUMENTED VEHICLE (CIV)

Mobility testing is accomplished using an instrumented 1977 Jeep Cherokee (Figure 6) with significant modifications. These changes include the addition of specialized equipment and the removal and modification of some stock equipment.

Each of the wheels is instrumented to measure the forces at the tire/ground interface and the wheel speed. Load cells mounted on the axles (Figure 7) measure forces up to 6000 lb in three mutually perpendicular directions: longitudinal (direction of travel), vertical, and transverse (across direction of travel, usually generated in turning maneuvers) as illustrated in Figure 8. To accommodate the annular load cells at each wheel, we replaced the stock axles with longer ones.

Aside from the triaxial load cells, a uniaxial load cell mounted on a coupling can be used to measure drawbar forces. In addition, we are considering using more sensitive torque meters, which are easily added and removed from the vehicle as needed. These would be attached to the outside of the wheel, and would be in place only during experiments needing accurate measurement of very small loads.

Individual wheel speed is measured using a proximity gauge and counter. The gauge detects the passage of the equally spaced nodes on the disk brakes, allowing for the calculation of revolutions per minute. Total vehicle speed measurements are made using a fifth wheel and an ultrasonic speed sensor (Figures 9 and 10). The fifth wheel uses a tachometer generator and an optical encoder (50-pulse-per-foot output) and can also measure distance traveled.

Wheel speed can be controlled either by the standard accelerator foot pedal or by a computer-controlled stepper motor, which governs the engine throttle. The motor controller was specially designed to provide stepping motor control from 0.1 revolution per second

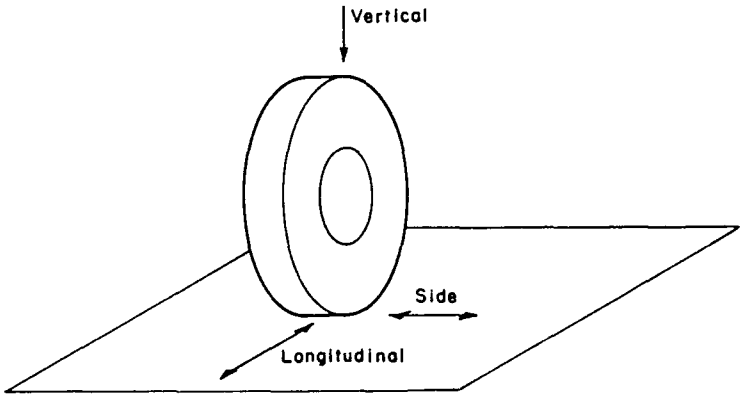

Figure 8. The load cells measure force in three mutually perpendicular directions.

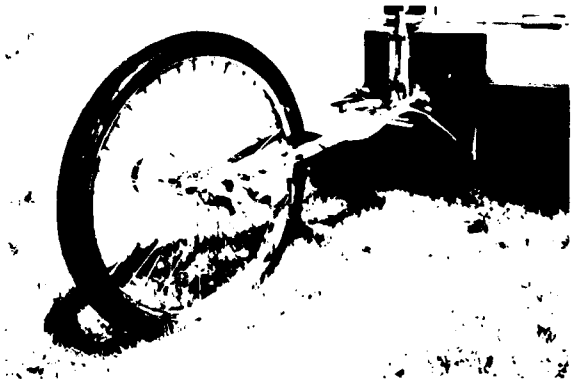

Figure 9. Fifth wheel used for measuring vehicle speed and distance traveled.

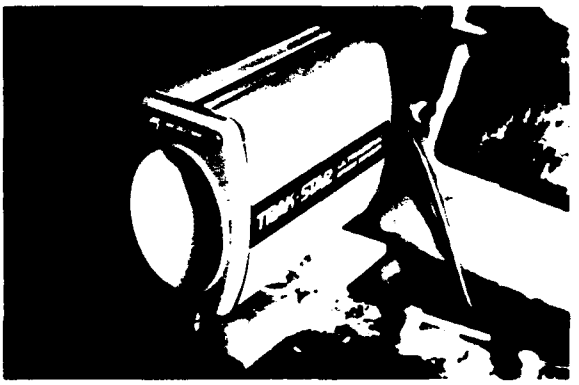

Figure 10. Ultrasonic speed sensor used as an alternative method of measuring vehicle speed.

Figure 11. Heath/Zenith industrial computer and monitor which controls data acquisition and testing.

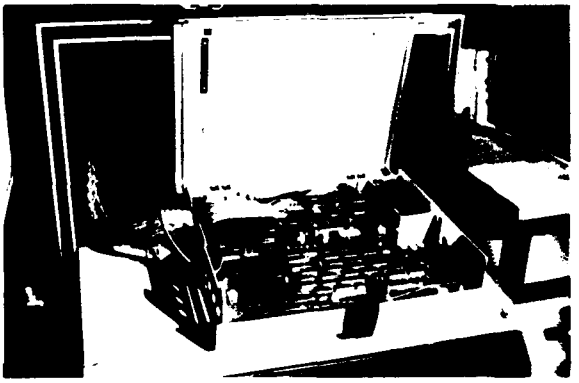

Figure 12. Keithley Model 575 Measurement and Control System.

to 9.9 revolutions per second in 0.1-revolution-per-second increments and from 10 revolutions per second to 99 revolutions per second in 1.0-revolution-per-second increments (Blaisdell, 1983).

Warn locking hubs were installed on all axles. These hubs, combined with the Jeep's emergency four-wheel-drive system, provide for any combination drive system: four-wheel-drive, front-wheel-drive, or rear-wheel-drive. The emergency drive system ensures that engine torque is transferred equally to the four wheels through the stock series of differentials, overcoming the Jeep's standard Quadra-Trac.

Three further modifications have been made to the vehicle. Additional braking capability is provided by dual calipers at each wheel. As with the drive system, braking is applied to either the disk brakes on all four wheels, or only through the front or rear brakes. The engine contains an additional heavy-duty alternator, which is used for recharging a pair of 12-volt deep-cycle marine batteries located in the rear of the vehicle. They power the data acquisition system through a sine-wave static inverter, which converts from 12 volts dc to 115 volts ac power. Also, to allow more variation of wheel and tire size, we installed a 4-inch lift kit at each axle.

Data acquisition system

In November of 1990, a high-performance, PC-based data acquisition system replaced the outdated configuration. The new computer is a 386, 16 MHz, rack-mountable industrial grade computer with a VGA monitor (Figure 11). Data acquisition is accomplished through a fully software programmable commercial measurement and control system (Figure 12) with additional in-house-designed signal conditioning. The software is a combination of product-specific software and CRREL-developed programs written in compiled BASIC and C.

Signal conditioning is handled separately for the load cell and proximity gauge inputs. The load cell inputs first pass through a shunt/short circuit. The function of this circuit is determined by either a set of DIP (Dual Inline Package) switches on the circuit

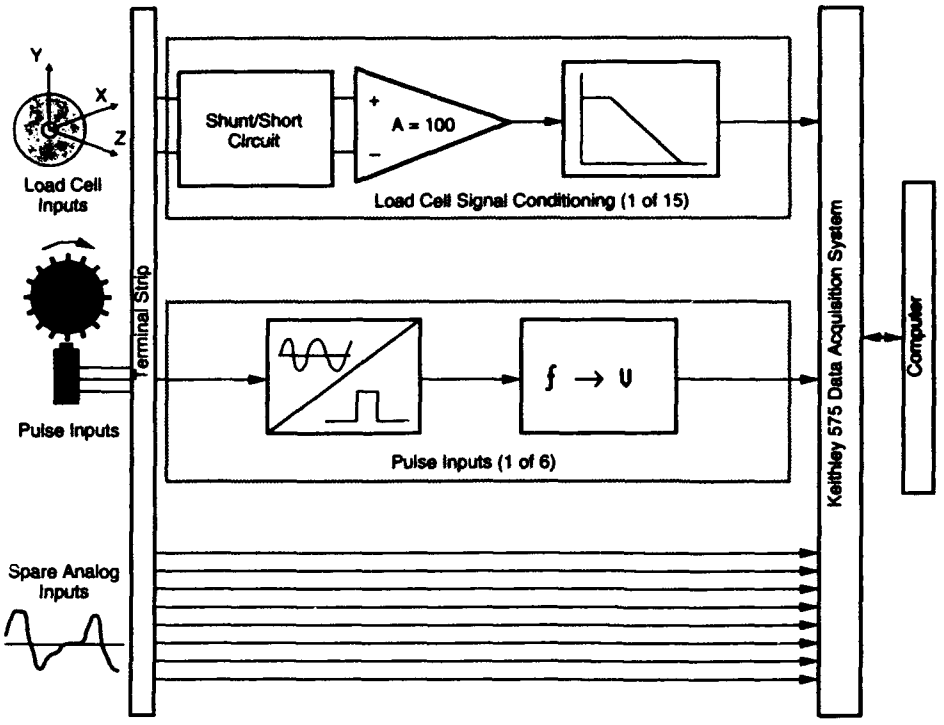

Figure 13. Block diagram of the signal conditioning circuit.

board, or by a remote, user-accessible switch. If the switch is in the neutral position, there is no change in the signal. When the switch is held in the shunt position, a precision resistor is placed in parallel with the signal. This simulates a known load, and is used for calibration purposes. With the switch in the short position, the load cell signal is ignored, and system diagnostics can be performed. Because the load cell signals are on the order of millivolts, it is important to amplify the signal before processing. Thus the next step in the signal conditioning is to amplify the signal by 100. Also, at this time the signal is changed from double-ended to single-ended. Finally, the signal goes through a low-pass filter and on to the data acquisition system. Input from 15 load cells can be processed with this system.

Conditioning of the six velocity (or pulse) signals is more straightforward. The signal is first conditioned into a square wave and then passes to a frequency-to-voltage converter. From there, it feeds directly into the data acquisition system. A schematic of the signal conditioning is shown in Figure 13.

Software

Data acquisition is controlled by one of two software programs written at CRREL. One is a compiled BASIC program which scans all of the assigned channels, writing all data to the screen only. This program is used primarily for system diagnostics. The other is a menu-driven program written in C, which prompts the user through vehicle calibration and a set of resistance and traction tests. This program acquires and stores to disk up to 1800 data points per test, although increased memory on the computer will allow more data points to be taken.

Once the data have been written to a C array, they are converted from voltages to the appropriate engineering units, kilometers (or pounds) per hour and Newtons (or pounds) for the velocities and loads, respectively. The data are then saved to an ASCII file on a floppy disk for further manipulation after testing is complete.

After testing, the data are imported into a spreadsheet-based analysis program where they are graphed, and calculations are performed to yield traction and resistance data. The spreadsheet contains a series of macros which arrange and manipulate the data. Averages and standard deviations are calculated and plots of all the data are created. If the file is from a resistance test, the process ends there. For traction tests, the macro then begins a series of calculations: differential interface velocity (DIV = wheel velocity–vehicle velocity), slip (slip = DIV/wheel velocity), tractive coefficient (μ = longitudinal force/vertical force), and the average peak tractive force (average of top 20% of the longitudinal forces).

A more complete description of the CRREL Instrumented Vehicle and its components can be found in Berliner et al. (in prep) and Berliner and Shoop (in prep).

MOBILITY TESTING PROCEDURES

Soil preparation

To prepare a frozen or thawed soil for vehicle testing, freezing panels are placed on the soil surface and the soil is frozen from the surface downward. The freeze rate is controlled by adjusting the temperature of the coolant in the refrigeration panels. When the desired frost depth is obtained, generally a depth of 40 cm or more, the panels are removed. The soil surface is surveyed to determine the amount of frost heaving, and soil cores are taken to determine ice lens growth and for soil strength measurements in the laboratory. The soil is then allowed to thaw by maintaining "spring-like" conditions within the building (7° to 13°C). Vehicle mobility is tested primarily while the soil is thawing. After vehicle testing on the undisturbed soil, the surface is often trafficked by running 50 passes with a truck (to simulate the passing of a military company) and then tested again. When the soil is thoroughly thawed, the top 30 cm of instrumentation is removed and the surface is tilled and recompacted for the next freeze/thaw cycle.

Vehicle calibration

The vehicle instrumentation is calibrated at the beginning of each test series and intermittently if it is turned off, if the conditions change significantly, or if the tests take a very long time to complete. Although there are several methods of calibrating the vehicle, they contain mostly similar elements. A standard calibration before testing in the FERF is as follows.

The first step is always to temperature-soak the vehicle in the FERF. This involves activating all mechanical and electronic systems and allowing the vehicle to sit in the FERF for not less than 20 minutes. When the vehicle temperatures have stabilized, the front end of the vehicle is jacked clear of the ground so the wheels are free from load, and the two wheels are manually spun and allowed to come to rest. In this position, the vertical channels of the load cells are read and equated to zero load and the velocity channels are read and equated to zero velocity.

The vehicle is then lowered and a dynamic calibration is performed. This entails driving the vehicle with the rear wheels on a smooth level surface at 1.6 kilometers per hour while reading the longitudinal and horizontal channels. These readings are then taken to be zero value or datum for the horizontal loads. The load cells are very sensitive to the load distribution (and, therefore, tilt) of the vehicle; even very small slopes affect load transfer on the wheels. Therefore, the vehicle must be calibrated on as level and smooth a surface as possible.

Finally, the vehicle is driven on a smooth, flat surface at 8 kilometers per hour, and the velocity readings are equated to that speed to calibrate the velocity channels.

Vehicle mobility testing

A mobility test sequence consists of both traction and motion resistance tests. To measure traction, the vehicle is driven at a constant speed (generally 5 or 8 kilometers per hour) in front-wheel-drive. The speed of the front wheels is then gradually increased (either manually or automatically using the stepper motor) while the brakes are applied to the rear wheels to hold the vehicle speed constant. The resulting slip of the front wheels is reported as the wheel-to-ground differential interface velocity (DIV), which is equal to the speed of the wheel minus the speed of the vehicle. Traction is reported as a tractive coefficient (longitudinal force divided by vertical force) and is plotted as a function of the DIV.

Motion resistance is determined by measuring the longitudinal force on the front wheels with the vehicle in rear-wheel drive. Again, the vehicle is operated at a constant speed. Motion resistance is reported as the average longitudinal force or as a motion resistance coefficient (longitudinal force divided by vertical force). The motion resistance on deformable terrain is sometimes reported as terrain resistance (also called external resistance), which is that part of the motion resistance caused only by the terrain deformation (i.e. it does not include the effects of tire deformation or flexing of the running gear). Terrain resistance is calculated by subtracting the motion resistance measured on a hard surface from the total motion resistance measured on the deformable terrain. The hard surface motion resistance is measured on a level paved road just outside the FERF.

General guidelines and recommended procedures for testing with the CRREL Instrumented Vehicle are outlined in Shoop (1991). As applied to the FERF, they are as follows.

1) Before testing, calibrate the vehicle as described above. Temperatures should be periodically monitored using thermocouples at various places inside and outside the vehicle and recorded. If the temperature or other conditions change significantly during the course of the tests, it should be noted and the vehicle recalibrated.

2) Execute a hard surface motion resistance measurement for each set of test conditions. This should be performed immediately prior to or after mobility testing

on the deformable terrain, and for each tire inflation pressure used. The hard surface information will serve as a baseline for the mobility measurements taken throughout the day.

3) Perform either one long rolling resistance test (the full length of the test section) or three shorter tests, followed by three traction tests.

4) Record the time of the calibration and of the subsequent tests. Additional information that should be recorded for each test series includes calibration method, speed of tests, etc.

A full complement of tests will usually include three tire pressures: 240 kilopascals, 180 kilopascals, and 103 kilopascals. At each tire pressure a hard surface rolling resistance is performed for approximately 20 seconds, followed by one to three rolling resistance tests on the test material (approximately 20 seconds of data or 200 individual data points) and at least three traction tests.

SUMMARY AND CONCLUSIONS

Part of the CRREL mobility research program is the study of vehicle mobility on thawing ground. When frozen ground thaws, from the surface downward, the underlying frozen soil acts as an impermeable layer and traps any moisture from rain or snow melt in the thawing layer on the surface, forming a very wet, weak soil layer over strong frozen ground. This creates problems for vehicle mobility. Roads are often closed or weight restrictions applied and off-road mobility may be impossible.

These conditions are difficult to test in the field because of the erratic nature of thawing soil. However, in the FERF, thawing conditions can be created throughout the year and soil conditions can be carefully controlled.

From this type of study we can determine the mechanisms involved in vehicle mobility in thawing soils and the soil parameters critical to vehicle mobility in thawing ground. This information will be used to develop a scheme for predicting vehicle mobility under thawing conditions.

Acknowledgments

The authors thank Paul Richmond, Dr. Richard Berg, and Stephen Bowen for their thoughtful reviews of the paper.

LITERATURE CITED

Berg, R. and T. Johnson (1983) Revised Procedure for Pavement Design under Seasonal Frost Conditions. CRREL Special Report 83-27.

Berliner, E., S.A. Shoop, G.M. Trachier and G.L. Blaisdell (1992) Upgrades and Modification to the CRREL Instrumented Vehicle. CRREL Special Report.

Berliner, E. and S.A. Shoop (1992) An Instrumented Vehicle for Traction and Motion Resistance Measurements. In Proceedings of the Symposium on Pavement Response Monitoring Systems for Roads and Airfields, Lebanon, NH, September 1991.

Blaisdell, G.L. (1983) The CRREL Instrumented Vehicle, Hardware and Software. CRREL Special Report 83-3.

Chamberlain, E.J. (1987) A Freeze–Thaw Test to Determine the Frost Susceptibility of Soils. CRREL Special Report 87-1.

Shoop, S.A. (1991) Precision Analysis and Recommended Procedure for Vehicle Mobility Measurements Made Using an Instrumented Vehicle. CRREL Special Report (in prep).

Shoop, S.A. (1990) Mechanisms Controlling Vehicle Mobility on a Thawing Soil. In Proceedings of the 10th International Conference of the International Society of Terrain Vehicle Systems, Kobe, Japan, August 1990, Vol. I, p. 301–312.

Shoop, S.A. (1989) Vehicle Mobility on Thawing Soils: Interim Report on CRREL's Test Program. CRREL Special Report 89-31.

Shoop, S.A. and K.S. Henry (1991) The Effect of a Geotextile on Water Migration and Frost Heave in a Large Scale Test Basin. Transportation Research Board 70th Annual Meeting, Preprint 91-0532 (accepted for publication in TRB Record).

Ice Cleat Design And Testing For Tracked Military Vehicles

MARK D. OSBORNE
Senior Research Engineer
Keweenaw Research Center
Michigan Technological University
Houghton, Michigan 49931

ABSTRACT

The mobility of military tracked vehicles is poor on snow and ice due to the rubber pads that are typically used on tracks. Various types of ice traction aids or ice cleats have been designed and tested for all types of the military tracked vehicles ranging from the M113 APC up to the M1A1. The Keweenaw Research Center (KRC), a research agency of Michigan Technological University (MTU), has been involved in ice cleat testing for over eight years. Through the years KRC has developed a set of tests and test procedures for evaluating the performance of the ice cleats. Although they are not officially specified as a Test Operating Procedure (TOP), they have been accepted by the U.S. Army Tank-Automotive Command (TACOM). TACOM has funded the majority of the testing.

Most of the ice cleat designs have been done by TACOM. This past year KRC proposed and performed a laboratory study to determine the optimum design in a cold room and reduce testing costs. A design was developed and tested during the winter of 1991. Some redesigning was required to obtain significant improvement in tracked vehicle mobility on ice and snow. During the laboratory and field testing process a theory was developed for optimum ice cleat design.

The opinions expressed in this paper do not necessarily coincide with those of the U.S. Army or the Government of the United States and the information provided here shall not be construed as an official endorsement or approval of this product or company by the U.S. Government.

INTRODUCTION

Mobility of military tracked vehicles in northern climates is usually limited because rubber track pads are standard equipment on these vehicles. Although these vehicles are generally more capable of maneuvering through deep snow and on hard-packed snow surfaces than wheeled vehicles, handling is difficult and on ice, traction is just as poor as wheeled vehicles. These tracked vehicles weigh anywhere from 13 to 70 tons and when coupled with almost no traction on ice, present a dangerous situation for military personnel in and around the vehicle. Poor mobility has resulted in the development of traction aids to improve traction on ice and hard-packed snow.

The Keweenaw Research Center (KRC), a research agency of Michigan Technological University (MTU), has been involved in ice cleat testing and evaluation for over eight years. Most of the testing has been sponsored by the U.S. Army Tank-Automotive Command (TACOM) and has been performed at KRC. In the late winter season of 1984 the Marine Corps sponsored an ice cleat evaluation during NATO war exercises in northern Norway.

KRC has tested several tracked vehicles including the M113 APC, M109 self-propelled howitzer, the M110, the Bradley IFV, the Marine Corps Amphibious Assault Vehicle, M60 tank and the M1 and M1A1 Main Battle Tank (MBT).

Over the years, KRC has developed a test course

specifically designed for testing and evaluating military tracked vehicles. The test course includes an ice rink which is 200 feet wide by 700 feet long, a hard-packed snow test loop consisting of winding curves, gentle hills and straight sections, deep snow areas and iced slopes. There are two types of iced slope areas, a vertical variable slope ranging in grade from 0 to 30 percent and a variable side slope ranging in grade from 0 to 25 percent. Shown in Figure 1 is a diagram of the hard-packed snow test area. Figures 2 and 3 show the layout of the variable vertical and side slopes, respectively. The ice surfaces are constructed by first packing snow and allowing the ground to freeze. Next, the packed snow surface is flooded lightly in several layers to build up a strong, smooth ice surface. The surfaces are maintained by grading the snow off of the ice surface, plowing with pick-up trucks, sweeping the surface with a rotary broom and finally flooding with a water truck. Through trial and error KRC has found that this is the best method for maintaining a consistent, smooth surface which is necessary for comparable evaluation of ice cleat performance.

KRC is located on the Keweenaw Peninsula, which is nearly surrounded by Lake Superior. The climate is ideally suited for testing as winter temperatures average 10 to 20°F and rarely rise above freezing or drop below −10°F. The winter season generally runs from mid-November through the end of March. The annual snowfall of over 200 inches provides plenty of fresh snow for creating deep snow areas and resurfacing the hardpacked snow areas.

DESCRIPTION OF TESTS AND PROCEDURES

KRC has developed a specific set of tests and test procedures for evaluating ice cleats on tracked vehicles. The tests include braking on ice, slalom on ice, slope climbing and side slope traversing on ice, speed and handling on hard-packed snow, drawbar pull and motion resistance on snow and ice and deep snow mobility.

Braking tests demonstrate a vehicle's stopping ability on ice. The best ice cleat design will provide the

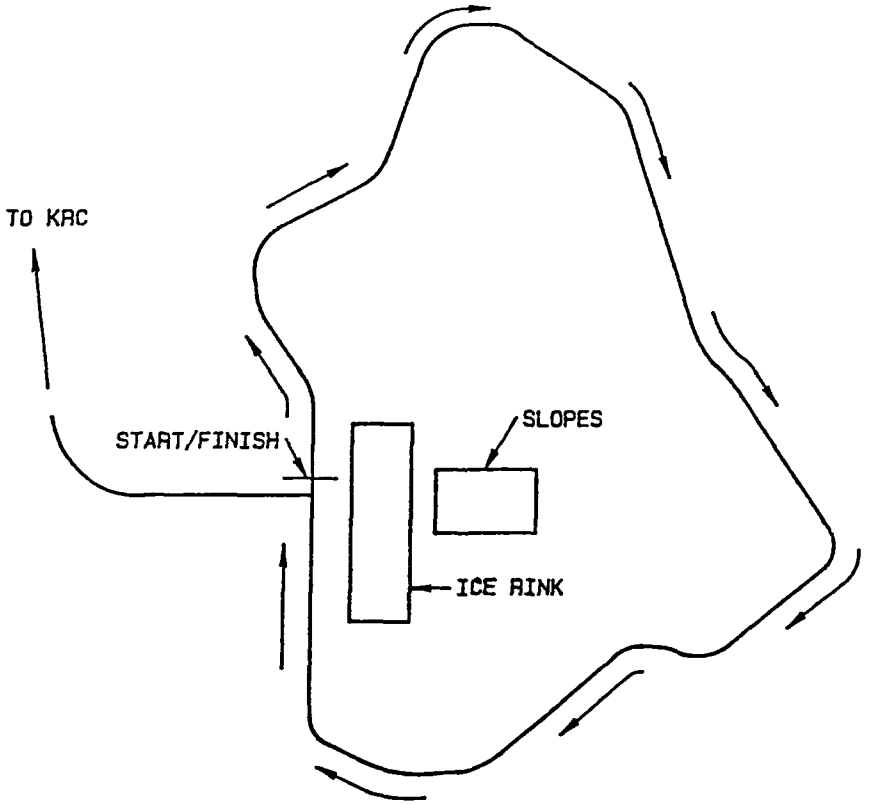

Figure 1. Diagram of hard-packed snow test area.

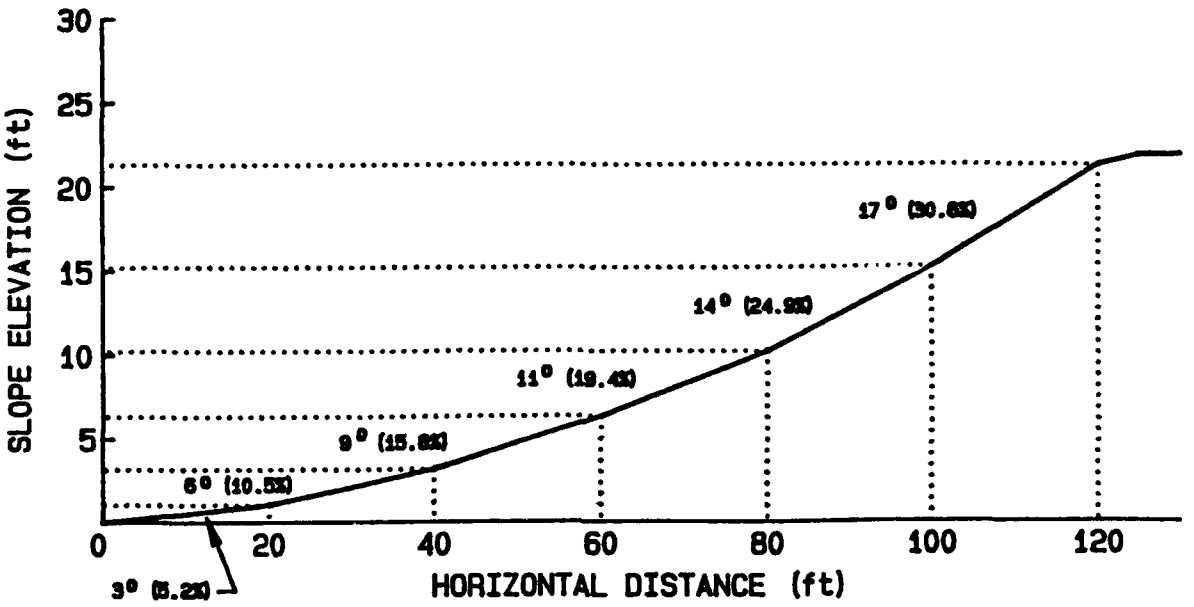

Figure 2. Diagram of the variable vertical slope.

shortest stopping distance of all designs tested on the same vehicle, under the same conditions and at the same speeds. Tests are conducted at vehicle speeds of 5, 10, 15 and 20 miles per hour. The vehicle is accelerated to and held at the desired speed prior to entering the ice rink area. The driver is signaled to apply and hold the brakes. With the brakes locked, the vehicle slides to a complete stop and the distance of the skid is measured. Stopping distance is measured to the front of the vehicle such that if the vehicle turns slightly the added distance is accounted for. Vehicle speed is measured using a radar gun as the vehicle speedometer is typically inaccurate. Vehicle speed is radioed to the driver so he can control his final speed just before applying the brakes. Braking decelerations are recorded using a commercially available electronic accelometer. The accelometer is interfaced with a laptop portable computer and braking deceleration data is transferred to floppy disks. This data

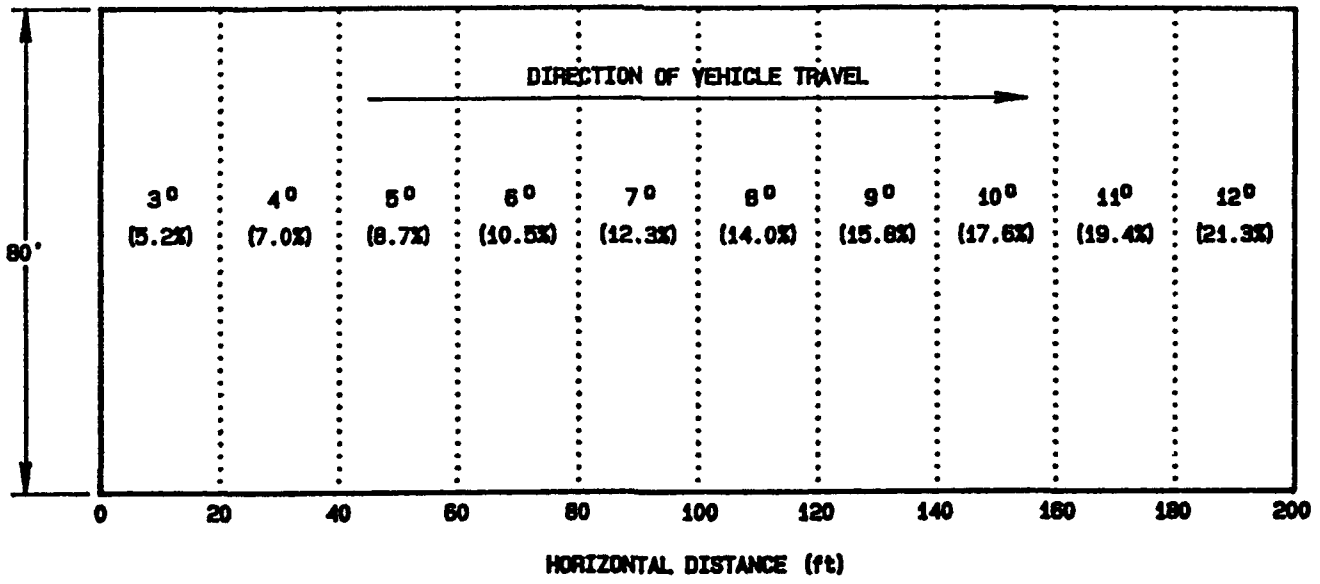

Figure 3. Diagram of the variable side slope.

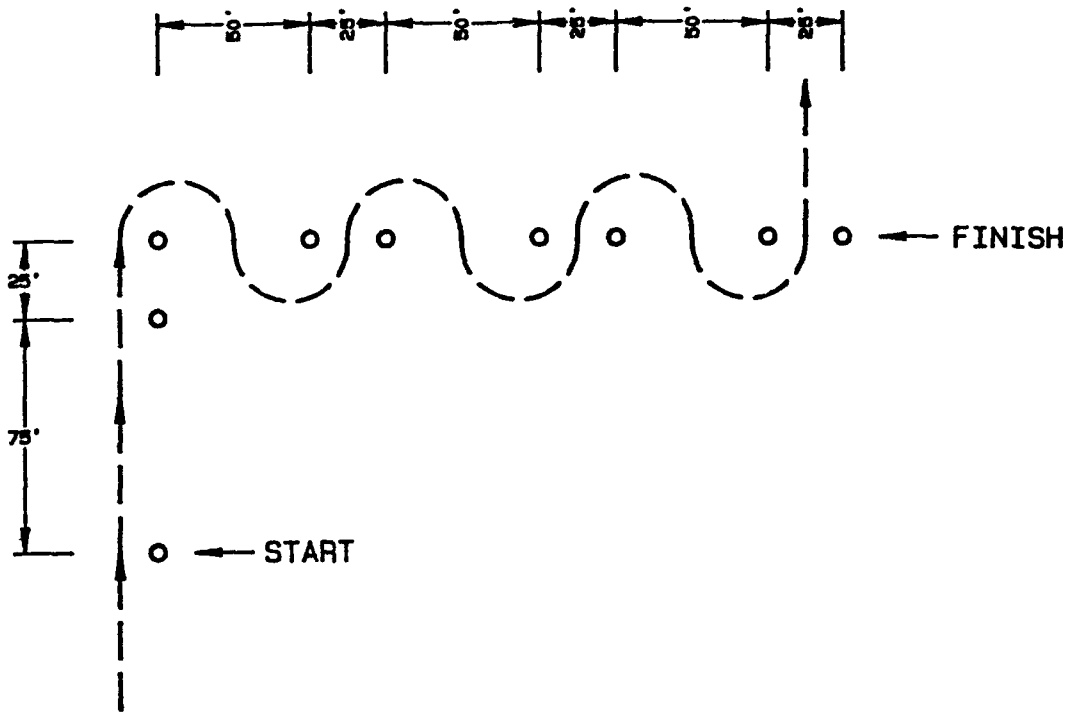

Figure 4. Diagram of slalom on ice.

is used to generate representative plots showing fore and aft accelerations and decelerations, and right and left accelerations which occur during each braking test. A minimum of six tests are run at each speed in an attempt to obtain a statistical data base.

The speed test on hard-packed snow is a timed test of vehicle maneuverability. The test is conducted on a closed-loop course adjacent to KRC and which is shown in Figure 1. The course is 1.3 miles long, consisting of a mixture of straight-aways, gradual curves and tight curves. The objective of this test is to maneuver the test vehicle over the course in the fastest time possible. To minimize driver bias, six runs are conducted, three in a clockwise direction and three in a counter-clockwise direction for each arrangement tested. Data is then statistically analyzed to determine the average speed for each ice cleat type or track arrangement.

The slalom test is designed to assess a vehicles' maneuverability on ice. A diagram of the slalom course is shown in Figure 4. The objective of this test is to negotiate the course in the fastest time possible. Typically, six runs are made to obtain a statistical average of the vehicles handling capabilities by measuring the time required to maneuver through the course without hitting the pylons. The driver has to be careful not to accelerate too fast or he may lose control of the vehicle.

The track holding test is conducted on the ice covered variable vertical slope which varies from 0 to 30 percent in grade. To conduct this test the vehicle is positioned at the base of the slope. When given a signal, the vehicle is driven up the slope approximately 20 feet. The driver is then signaled to stop. When signaled again, he drives another 20 feet up the slope. This procedure is continued until the vehicle either climbs the hill, can not advance up the hill any further or slides down the hill. The point of the vehicle's furthest ascent up the hill is marked for distance and inclination. Three runs are usually conducted during this test because of the damage that occurs to the ice on the slope by the time this test is completed.

The vertical hill climb test is similar to the track holding test in that it involves the negotiation of an ice covered variable grade slope. The difference between the two tests is that instead of advancing up the slope in short stop-and-go steps as is done in the track holding test, the hill climb involves driving the M1A1 up the slope in one continuous attempt from a dead stop at the base. To run this test, the vehicle is positioned at a starting point at the base of the slope. When given a signal, the driver drives the vehicle up the slope until it either climbs the slope or loses traction and slides down the slope. The point of furthest advancement up the slope is marked and measured for distance and inclination. Three tests are usually conducted.

The side slope tests a vehicle's ability to traverse across an icy slope. The slope used for this test varies from 0 to 25 percent. To run this test, the vehicle is positioned at the starting point, which is at the 0 percent end of the slope. When given a signal, the driver drives the vehicle across the slope at approximately 5 mph. He continues until the vehicle traverses the entire slope or the vehicle loses traction and slides sideways down the slope. The point where the vehicle begins sliding is measured for inclination. This test is conducted three times for each track configuration.

The deep snow mobility test is subjective and is conducted to determine if the vehicle performs better in snow two to four feet deep with a particular track arrangement. For this test, the driver negotiates the vehicle through a large snow covered field. The snow generally consists of several layers of snow ranging from a strong, dense layer near the bottom to a light, fluffy layer near the top. Normally the driver does not have any problem in negotiating this terrain, even with pads, but ice cleats do tend to help control the vehicle. Deep snow mobility would be improved more if the track had a larger surface area to provide better flotation.

Drawbar pull and motion resistance tests are conducted with the vehicle to determine maximum pulling power or tractive effort on hard-packed snow and ice. A load cell of appropriate size is normally used to measure pulling force and resistance to motion as a function of time. All data is recorded using a portable computer and is saved on floppy disks for later analysis. Actual track speed is measured by D-C tachometers mounted on each sprocket of the vehicle. Actual vehicle speed is measured using a D-C drum tachometer instead of a fifth wheel which may slip or may produce noisy results on the rough terrain. This past year an ultrasonic speed sensor was also used to measure actual vehicle speed and appeared to produce fairly good results. The main emphasis in these tests is to measure maximum pull force and resistance to motion. The procedure for conducting the drawbar pull tests requires connecting a pull cable, block and tackle and the load cell between the test vehicle and a load vehicle. In situations where more than one load vehicle is required to stop the test vehicle, another cable is fastened between the first and second load vehicles. All drivers and the engineer operating the computer data acquisition system communicated using two way radios. The test vehicle is brought to a speed of approximately 5 mph and held as constant as possible at that speed. When this speed is attained a load is applied by braking the load vehicle(s) until the test vehicle is stopped completely. The procedure for conducting the motion resistance tests is similar to the drawbar pull tests except the load vehicle pulls the test vehicle along at approximately 5 mph and the test vehicle is usually kept in neutral. The steady state force required to pull the test vehicle in neutral at a steady speed is then measured and recorded for both ice and hard-packed snow conditions with the same load cell and data acquisition system used for the drawbar pull tests. At least three drawbar pull and motion resistance tests are conducted for each track configuration for comparison.

For all of these tests it is important to ensure that the test surfaces are as consistent as possible to obtain comparable results. KRC generally measures the static coefficient of friction of the ice surface for comparison purposes. Unfortunately, for tests with ice cleats, friction measurements are not critical. What needs to be measured is strength of the ice. This should be a dynamic compression and shear strength test. To date there is no known method that is widely accepted for measuring ice strength. KRC has several ideas but has not had the funding to develop and refine this idea. Strength of ice may change by the hour, depending on temperature, solar radiance, etc. This has been one of the problem areas in the past.

ICE CLEAT DESIGN

Over the years, several ice cleats have been designed for many vehicles. Because each vehicle has its own type of track, each vehicle has its own ice cleat design. Most have been the "X" shaped grouser type that fit in the shoe on a replaceable pad track. Some have been designed for installation on non-replaceable pad tracks such as the crows foot T156 ice cleat that bolts onto the center guide. FMC has designed a slightly different ice cleat for a replaceable pad track, the T157 cleat. These designs are shown in Figure 5. Ice cleat design theory will be discussed later in this paper.

KRC has run a number of tests on different vehicles to determine the optimum configuration and spacing. On tracks with two pads side by side ice cleats were installed side by side and staggered, i.e., on one side at the first installment and on the other side on the next installment and so forth along the entire length of track. The side by side installation always provided the best traction. Also, when cleats were installed on every fifth track shoe performance appeared to be optimized. Cleats on every third shoe did have better traction but the improvement over every fifth shoe was insignificant and for the extra work involved to install the additional cleats, it was not worth the extra effort.

Typically, cleats are designed at TACOM and then

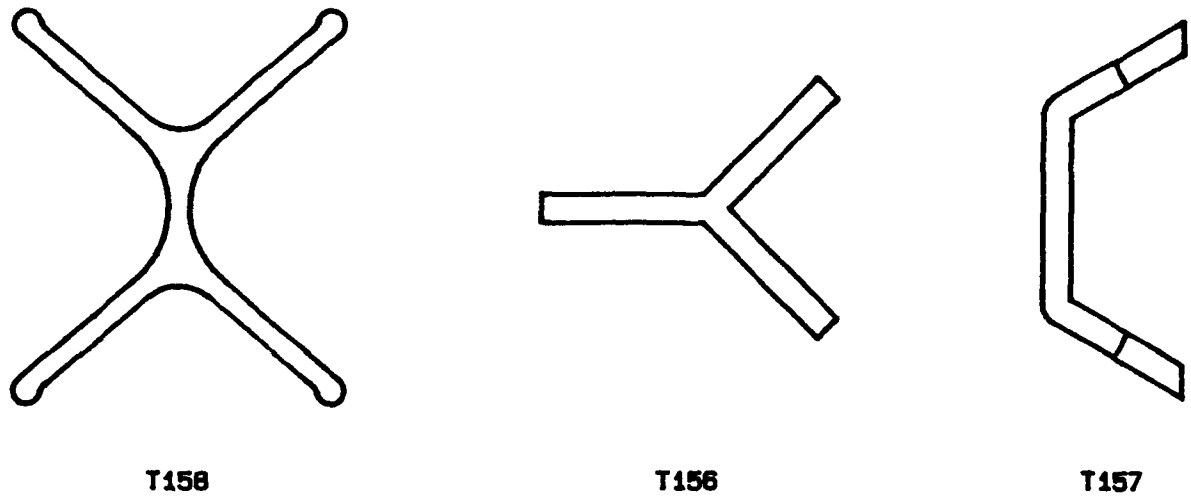

Figure 5. Typical ice cleat designs for military tracked vehicles.

field tested at KRC during the winter season. If the results are not good they are redesigned and then tested the following winter. As an example, the ice cleat for the M1A1 T158 track was originally designed and tested in 1986. KRC recommended that performance may be improved by increasing ice cleat ground pressure. TACOM redesigned the T158 ice cleat in 1989, increasing ground pressure by milling out the center area of the cleat. Tests conducted in 1989-90 showed an insignificant improvement. The 86 original and 89 modified designs are shown in Figure 6. Building a test course and conducting tests is expensive. Being able to test one or two designs per winter season is an expensive way of arriving at a final product. In 1990 KRC proposed running a series of tests in a cold room to determine an optimum design. By testing on a fixture in a cold room

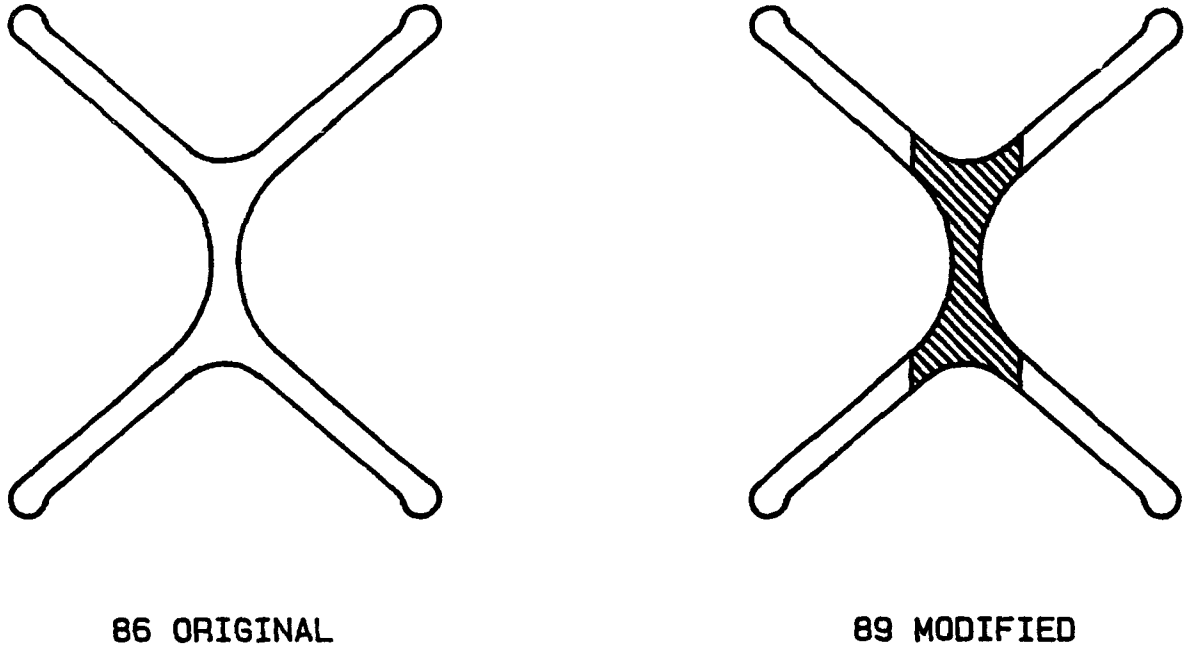

Figure 6. Drawing of the 86 original and 89 modified T158 ice cleat designs (actually bottom view).

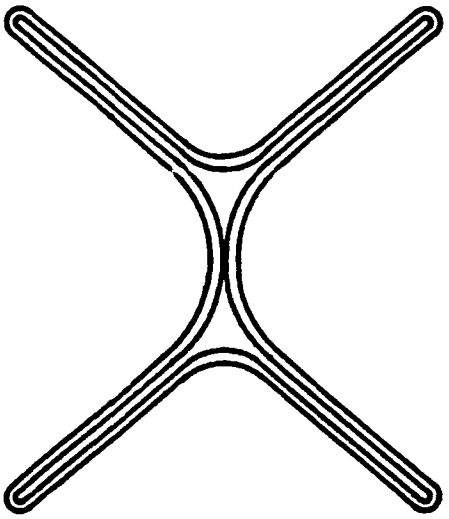

Figure 7. Drawing of the 90 radius cleat design for the M1A1 T158 track.

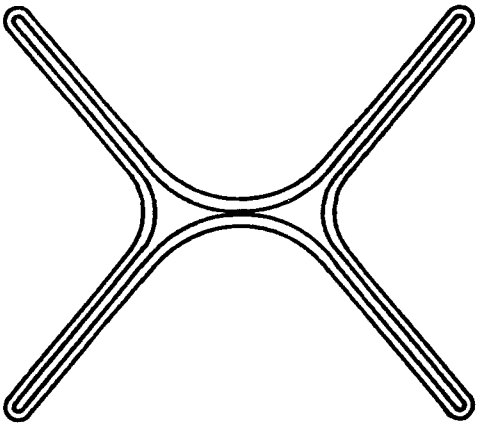

Figure 8. Drawing of 91 taper ice cleat design for the M1A1 T158 track.

a number of designs could be tested inexpensively, thereby screening out the poor ones and leaving the best designs for the winter field test.

A test fixture was constructed out of steel to test the ice cleats for the resistance to motion. This would directly simulate two of the most critical areas, braking and slope climbing on ice. It did not account for dynamic effects because the cleats were pulled at slow, steady rates rather than at the high speeds that are typically seen on the test course. A hydraulic cylinder was used to apply the normal load to the track block simulating the roadwheel load. Load cells were used to monitor normal load and the force necessary to pull the track block across the ice surface. An ice surface was formed in a steel box for each test and room temperatures were kept as constant as possible to evaluate ice cleat performance on an equal basis. Data was collected and recorded using a computerized data acquisition system.

A large number of tests were conducted for several designs at various normal loads. It was decided that the 5,500 pound normal load (for one half track block) was the appropriate normal load as it is the approximate average maximum load applied to an ice cleat on the M1A1 tank. The final design was developed through several iterations or modifications of the original 86 cleat. The final design was a cleat with 1/4 inch thick webs and a radius on the edge of the web. A simple structural analysis showed that the web would be strong enough to withstand loading on concrete. The rounded bottom edge appeared significantly better in the laboratory tests as compared to the flat edge with the same thickness or the original 86 and 89 designs. Figure 7 shows a drawing of the 90 radius cleat.

Winter tests showed improvement with the 90 radius cleat in all areas except braking. For example, this was the first time ever that the M1A1 was able to climb the entire slope (30%) using ice cleats. The problem with the braking results was thought to be due to the radius edge. The edge was milled flat and the cleats were raised supposedly to the same height as the 90 radius cleat. It was felt that the dynamic action was not accounted for during the laboratory tests and that the radius allowed the tank to ride up on top of the ice at high speeds after initial penetration. This 91 taper design, shown in Figure 8, was tested with about the same results as the 90 radius design. It was then found that the 90 radius cleat was 0.125 inches lower in height than the 86 and 89 designs and that the 91 taper design was 0.205 inches lower than both. (TACOM was concerned that too high a cleat would damage the tank sponson units but the height difference was really either an oversight or the 86 and 89 designs were out of tolerance in terms of height). Since the 91 taper design performed as well or better than the 90 radius design even though it was lower in height, it was decided that the final design would be the 91 taper design raised to the same height as the 86 and

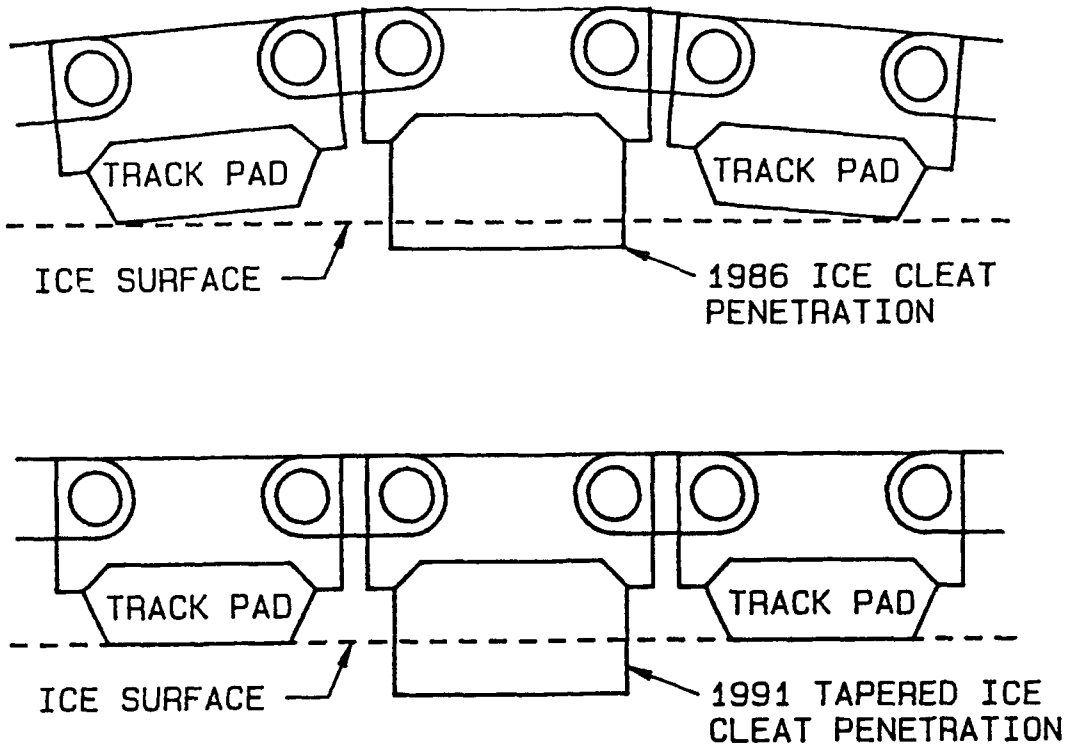

Figure 9. Illustration showing how ice cleat penetration is limited by either ground pressure or track pad thickness.

89 designs. The cleats were raised to this height but not tested due to the early spring weather. This study also resulted in a theory for ice cleat designs.

For optimum traction, ice cleats need maximum penetration and maximum interfacial area. The 91 taper design with its thinner web area has high ground pressure yet still has plenty of strength. Our theory is that penetration is limited by the height of the cleat and the surrounding track pads. Figure 9 illustrates this point. As shown in the upper portion, it is felt that the 86 design was not penetrating to the pad surface. The higher ground pressure of the 91 taper design allows this penetration.

The 86 original cleat design had an estimated ground pressure of 797 psi while the 89 modified design was 1,060 psi. The 90 radius had a ground pressure of 1,410 psi while the 91 tapered design has a ground pressure of 982 psi.

The 91 taper design ground pressure was nearly the same as the 89 design but the 91 design has a larger interfacial area. As illustrated in Figure 10, the larger the interfacial area the better the stopping ability because the force is distributed over a larger area. For equal penetration depth, the cleat with the largest area will perform the best. Also, the squared off edges will perform better than a radiused edge.

SUMMARY

A standard method for testing traction aids on military tracked vehicles has been developed at KRC. Specific test courses allow these tests to be conducted under relatively the same conditions. Through field experience and laboratory testing, a theory for ice cleat design has been developed at KRC. Effective ice cleat design requires the following and depends on the vehicle's track shoe design:

1.) As thin a web as possible for highest ground pressure possible.

2.) Web thickness has to be thick enough not to break while driven on concrete.

3.) As large of an interfacial area as possible.

These criteria allow for the greatest penetration and tractive forces, whether they are stopping, accelerating, slope climbing or handling.

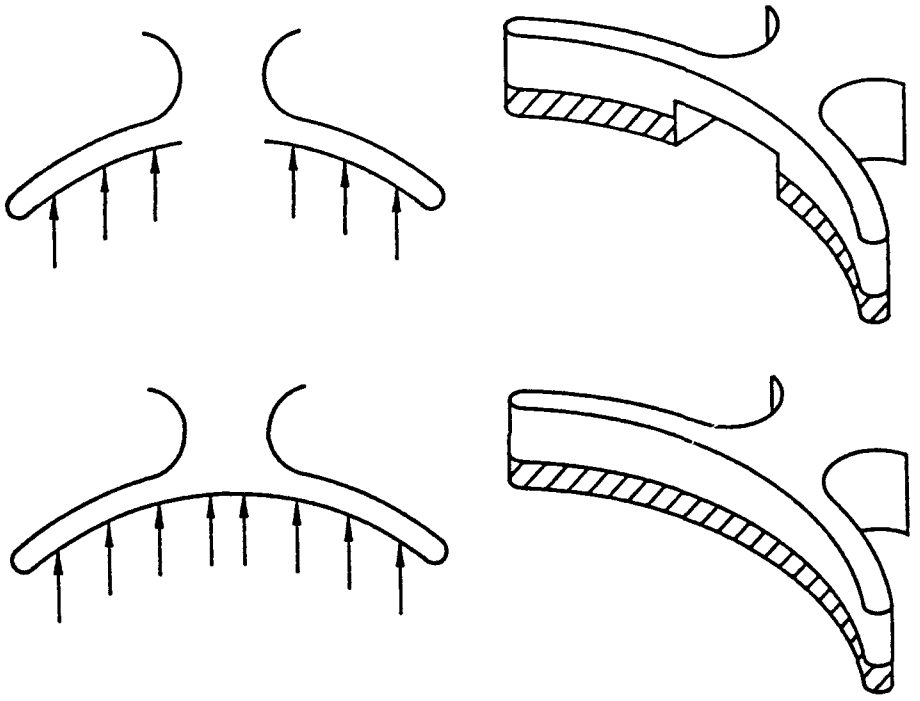

Figure 10. Drawing illustrating the interfacial area concept.

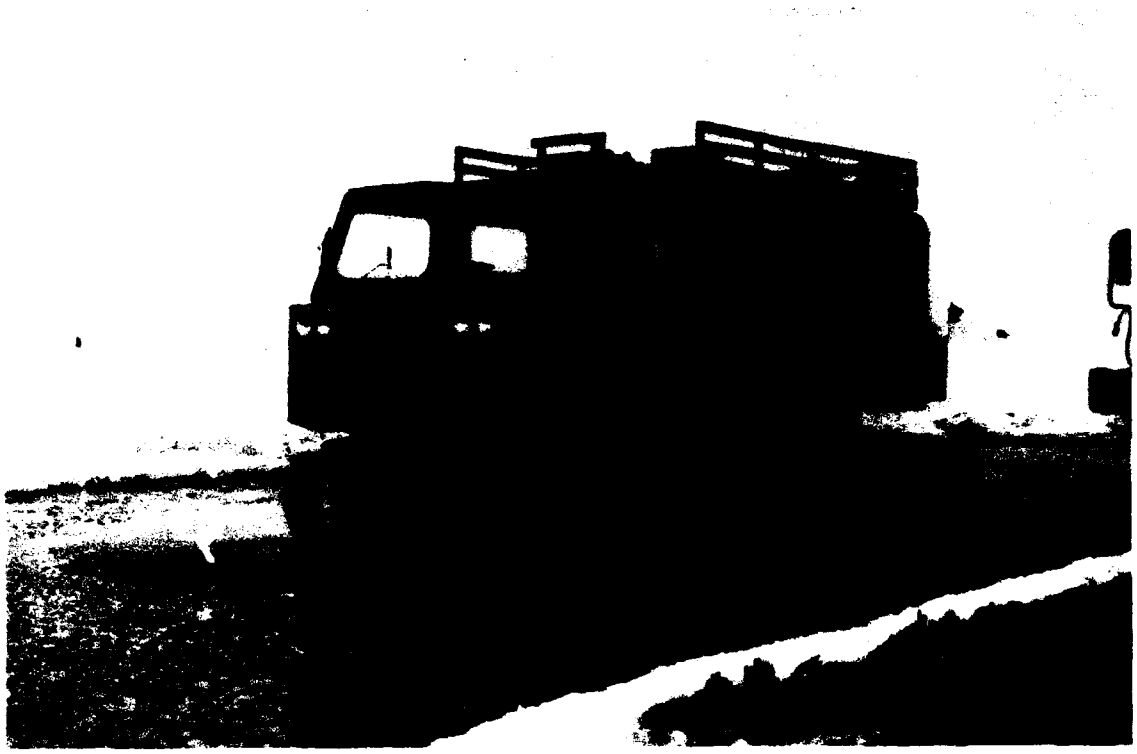

3. VEHICLE MOBILITY

BV 206
A Proven Concept In Winter Mobility

JAN LJUNGGREN, MME
Design Manager, BV 206
Hägglands Vehicle AB
Örnisköldsvik, Sweden

ABSTRACT

In the early seventies the Swedish Army Materiel Administration started to plan for a successor to the Bv 202, which was one of the most capable All Terrain Vehicles in the world. The technical specification for the new vehicle was naturally set higher in all important areas, for instance higher payload, 2,000 kg vs 800, higher top speed 55 km/h vs 35 and no increase in overall dimensions. There was also a very high requirement on reliability, availability and maintainability. On top of this, there was a requirement that the maintenance cost for the vehicle was to be stated in the tender and to be tested on production vehicles and have a considerable influence on the price of the vehicle.

In 1974 Hägglunds was chosen, in competition with other Swedish manufacturers, to develop and produce the Bv 206.

The Bv 206 is an articulated steered vehicle with all four tracks driven. It is to be used to support army units carrying 2,000 kg payload or 17 combat equipped soldiers on or off roads, summer and winter. It will also be used towing trailers up to 2.5 tons.

The low ground pressure in combination with the articulated steering gives the vehicle a very high degree of mobility over soft grounds such as swamps and snow. It is also amphibious without preparation, propelled in water by the tracks and steered by the articulation.

INTRODUCTION

The story of Bv 206 starts in the early seventies, when the Swedish Army started to look for a successor to the old Bv 202, which had been in service since 1965 (Fig. 2). When it was introduced, it meant an extremely high increase in the off road mobility of the army units, primarily in wintertime. Earlier they had to use horse transports, skies and sledges.

The introduction of an articulated carrier in the Swedish army units meant a very high increase in the fighting power, not primarily because of the quicker transport, but because they arrived together with their equipment and in a condition good enough to use it.

The basic design of the 202 was done in 1955–60, so it was of course a bit out of date. The characters they primarily wanted to improve were load capacity and maintenance cost. The mobility capacity of the 202 was considered adequate, but one weak point was the risk for shedding a track. This risk had to be minimized. Some other drawbacks with the 202 were also the ergonometric conditions for the driver, with high noise level, poor visibility and heavy steering.

DEVELOPMENT

The invitation for tenders for the new vehicle was sent out in 1971 with the technical requirements, which had a strong concentration on total lifetime cost. The companies giving a quotation had to state a maintenance cost, which was to be tested in a carefully specified test.

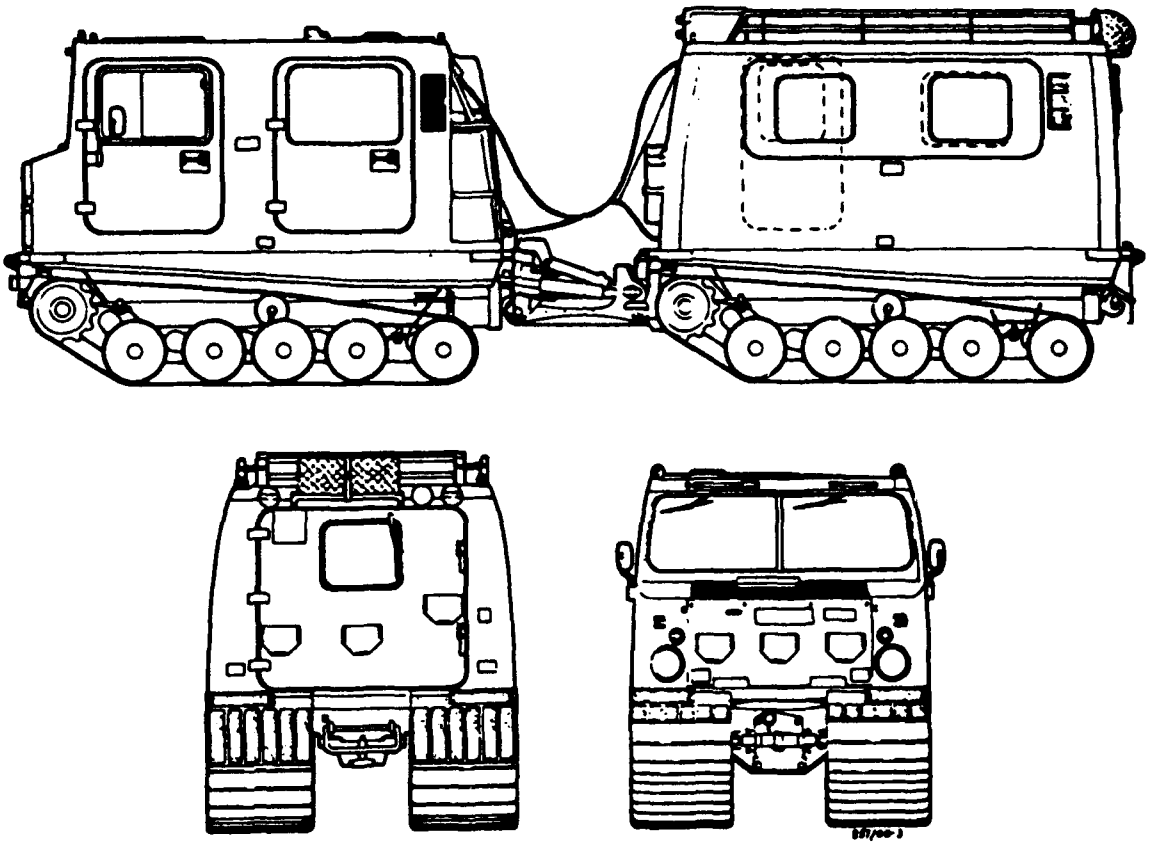

Figure 1. BV 206.

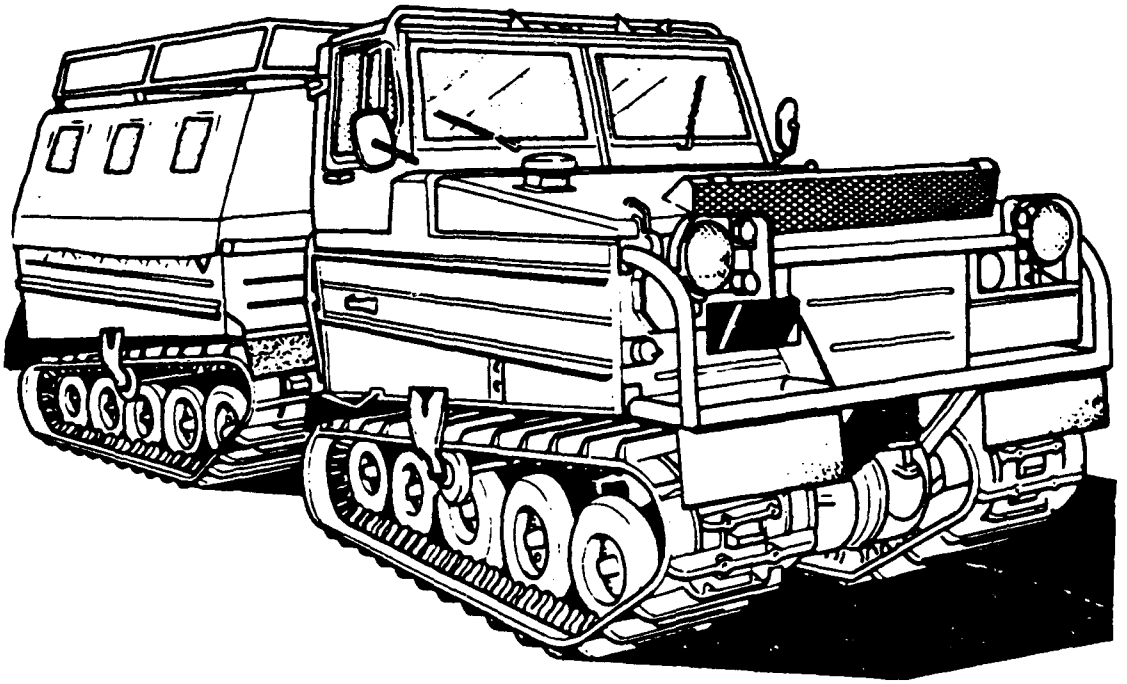

Figure 2. BV 202.

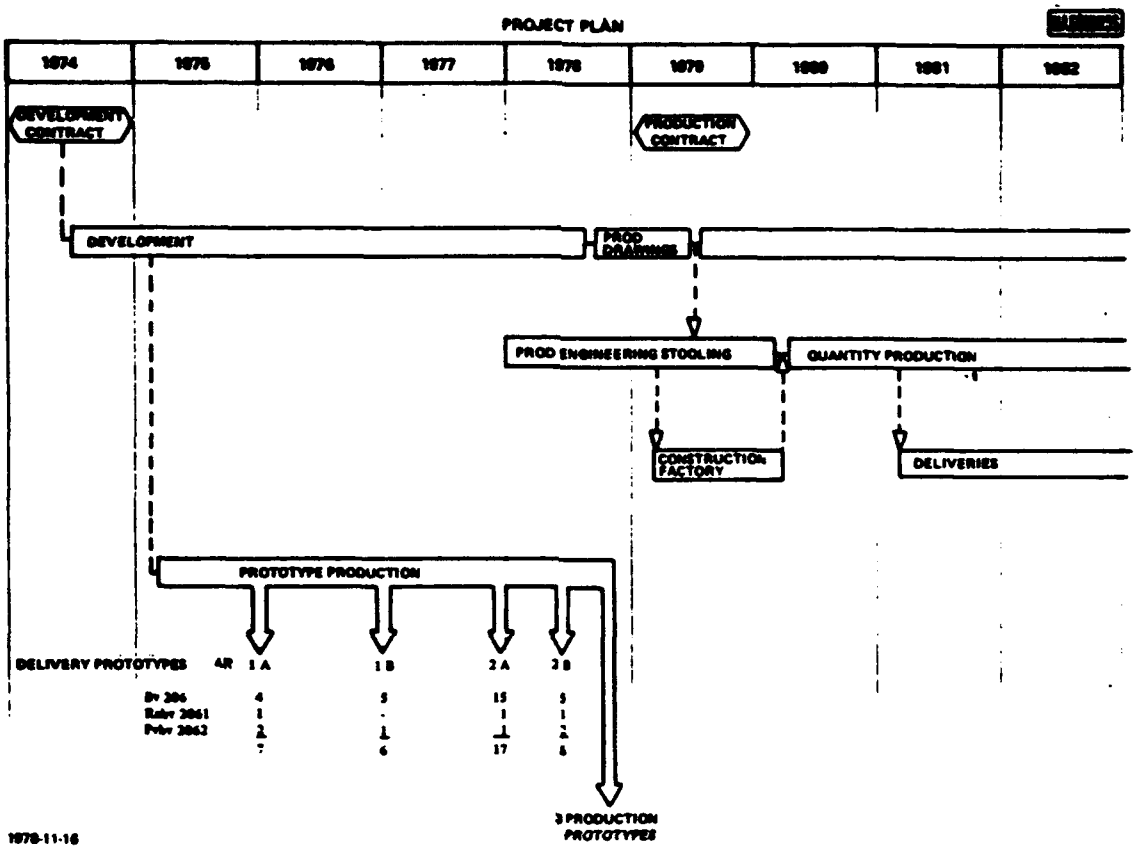

Figure 3. Project time plan.

The proved maintenance cost would then have an important influence on the final price of the vehicles, so that a low maintenance cost gives a higher price to the producer. The most important requirements for the new vehicle were:

1. Load capacity 2,000 kg
2. Articulated steering, amphibious
3. Lifetime 15 years or 30,000 km
4. Spec. ground pressure 12 kPa
5. MDBF 2,500 km (prohibitive failures)
6. MTTR 1.8 h

In June 1974 Hägglunds was awarded the contract to design and manufacture a number of test vehicles in three different batches. If the technical tests came out successfully, we were guaranteed to get the production contract (Fig. 3). During the development, it was indicated that we had to make two more batches of test vehicles to verify the performance.

When starting the design phase of this vehicle, very few components were specified. I can only remember a small map light and the tow hook. The performance was on the other hand very carefully specified.

One important basic requirement that governs the whole design is the articulated steering principle, which needs a special explanation:

The high requirement for off road mobility rules out all other steering systems. A tracked vehicle is normally steered by varying the track speeds with some steering device. This means that you introduce brake forces between track and ground. These brake forces, which increase with smaller turning radius, mean that the force available for pulling the vehicle is reduced when it is most required. The split on two vehicle parts means that you get a more advantageous relation between track length and width for the steering forces (Fig. 4).

Another very important requirement on the vehicle was the payload capacity of 2,000 kg, which is two and a half times the capacity of the old vehicle, without

WHY ARTICULATED STEERING?

LESS STEERING FORCES → HIGHER NET PULL

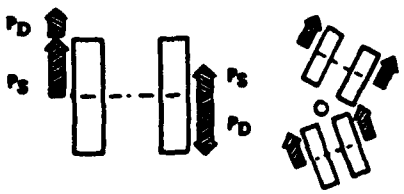

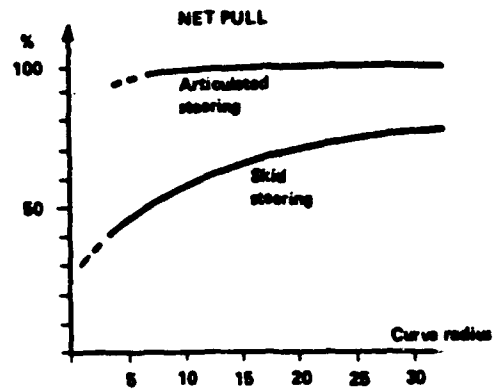

LESS SLIP → LESS DAMAGE TO GROUND SURFACE

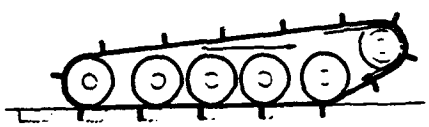

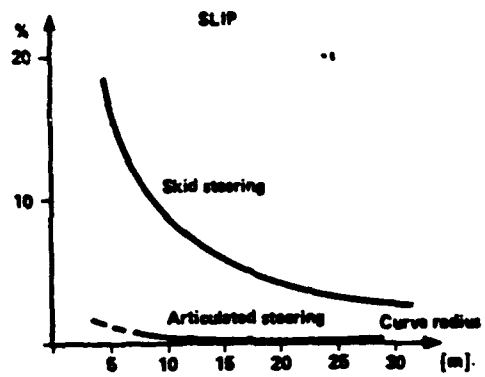

LONGER TRACK LENGTH → ENHANCED AGILITY

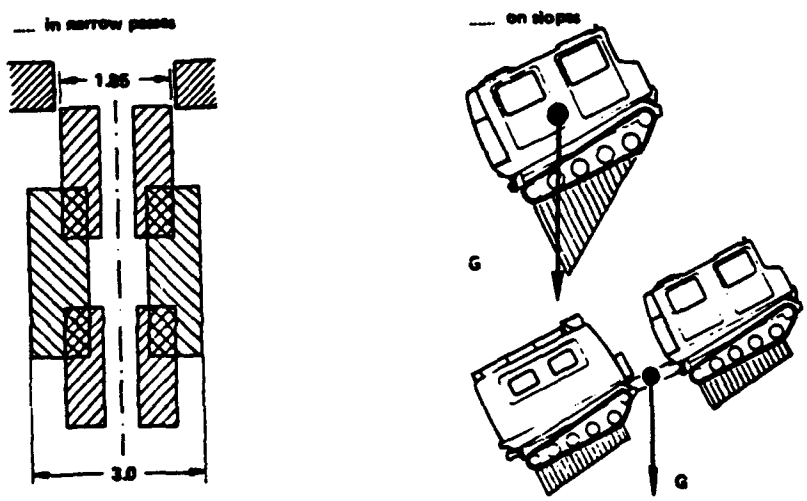

Figure 4. Reason for articulated steering.

increase in overall dimensions and ground pressure. To reach this difficult requirement, we had to use very light design solutions and use a lot of light construction material. The body is built in glassfiber reinforced plastic, which is unusual for this type of vehicle.

Another extreme solution was to make the tracks from Hytrel, a plastic material. We also did increase the width of the track from 500 mm to 620 mm. The high demand on reliability has forced us to carefully study possible trouble areas and choose design solutions according to this.

Since one of the trouble areas on the old vehicle is the clutch and the manual transmission, this is one reason for using an automatic on the new vehicle.

When designing the track assembly we had two important requirements to consider, firstly the risk for shedding a track should be minimum and secondly the need for maintenance should be as small as possible. By designing the assembly with two rows of roadwheels and double sprockets and idler, we have got a wide and solid contact base between the track itself and the track assembly. This is very important, because the track is very flexible.

Very important for a vehicle like this is that it shall be very easy to repair and maintain in field service, since the repair possibilities in field conditions are always restricted. To make this easier, we have designed Bv 206 so that it is very easy to exchange broken parts, if they cannot be repaired on the spot. The whole track assembly can be removed after loosening four bolts. The track can be exchanged by three men in less than 20 minutes when ambient temperature is –15°C. A complete power unit can be replaced in less than one hour.

When selecting components for this vehicle, we have tried to use components manufactured in large quantities and available also in the future.

When entering the production phase, we had produced 46 test vehicles in five different batches with redesigning and modifications. The test vehicles have a total mileage of 400,000 km. Looking back at the development phase, there are a lot of things to remember.

The development of a new track has been long and very troublesome. The first test vehicles were equipped with tracks made from Hytrel, a new plastic material produced by DuPont. The track was injection molded in sections, which could be joined together to a complete track. This new material meant that track weight was reduced by 50% compared to a rubber track. Unfortunately, this new material did not correspond to our expectations. We ran into problems with cracking, low friction on icy roads and high wear rate. The cracking occurred in temperatures around –10°C, although the basic material does not become brittle until –45°C or lower. The low friction on icy roads meant that the vehicle was very difficult and dangerous to drive on roads. The high wear rate meant that the life requirement of at least 6,000 km could not be met. We reached only 2,000 km, so we had to go to a conventionally designed rubber track of the same type as on Bv 202. This meant a weight increase of 350 kg. These tracks were naturally not completely trouble-free either, but after some development of the integral steel parts we have reached a life of at least 10,000 km, which is adequate. The track has been developed in cooperation with the manufacturer, Skega AB.

The development of the track assembly has, like for the track itself, been difficult. The first test vehicles had six pair of roadwheels (Fig. 5) mounted on three sub frames individually sprung from the track beam (Fig. 6).

This system was much too optimistic on dynamic forces, and we quickly had to introduce a stronger design. Therefore, we made the roadwheels bigger (Fig. 7), and we reduced the number of roadwheels to four pairs, mounted on two sub frames with four wheels in each track assembly (Fig. 8).

This design was much better in mechanical strength, but the spring rate was too high, so we got a very bumpy ride and too high vibration level. The final solution turned out to be very fortunate. It is designed with a cylindrical rubber torsion spring carrying two railing arms for a pair of roadwheels.

The steering device is another very complex unit, which is evident from Figure 9 showing the required relative movements between the two vehicle parts. To complete the picture, one should remember the shaft transmitting power to the rear car.

The first steering device was a welded construction with a conventional design and very heavy (Fig. 8). To improve the situation we redesigned it, and it is built with an open box torsion bar instead of a bearing for roll movement.

We have tested three different petrol engines and one diesel engine during the development period. The requirement said that we should have a petrol engine of approximately 100 kW. The first engine we tested was Volvo B30, a 3 L, 6-cyl. in-line engine, but it was rather difficult to install and was to go out of production 1978, so we left it after the first test batch. The second engine was the English built 3 L, 60° V-6 engine 2614E. It was very easy to install due to its compactness, but production plans for it did not suit us, and we also had some problems with overheated pistons. The third engine,

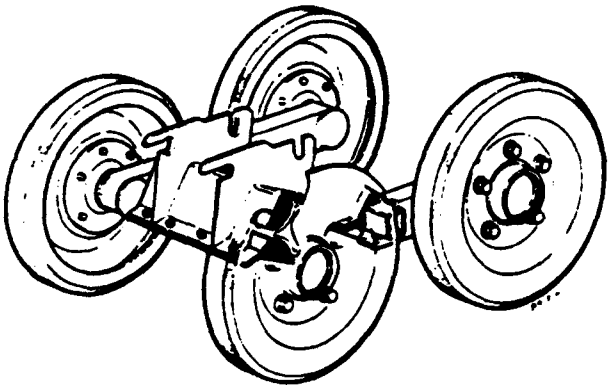

Figure 5. Wheel unit, first design.

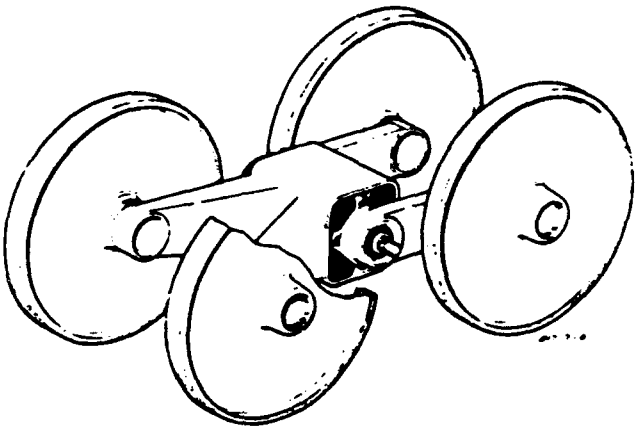

Figure 7. Wheel unit, second design.

which we finally selected, was the German built Ford 2,8 L, 60°, V6, 2658E. This engine was equally easy to install and has proved to be very tough, though the mean power output is much higher in Bv 206 than in a normal passenger car.

We have also tested Mercedes turbocharged diesel engine, an in-line 5-cyl. and 6-cyl. prechamber diesel. These are very qualified engines for this vehicle, but it was on the market too late for being evaluated by the Swedish Army. We expect other buyers of Bv 206 to select this engine.

The automatic transmission was with the Volvo engine a Borg Warner BW 35 unit, but this was not mechanically strong enough, and we soon switched over to Mercedes W4 A-018 and we now use W4 A-040, which are a development of their transmissions for passengers cars.

In our model, the transmission has a special shift pattern to suit the Ford engine. The fitting of the engine to the gearbox and the connecting development worn has all been done by Hägglunds .

Although the development line has not always been so straight, the basic concept for this has remained unchanged, and in June 1979 we received the production order from the Swedish Army of some 3,500 vehicles.

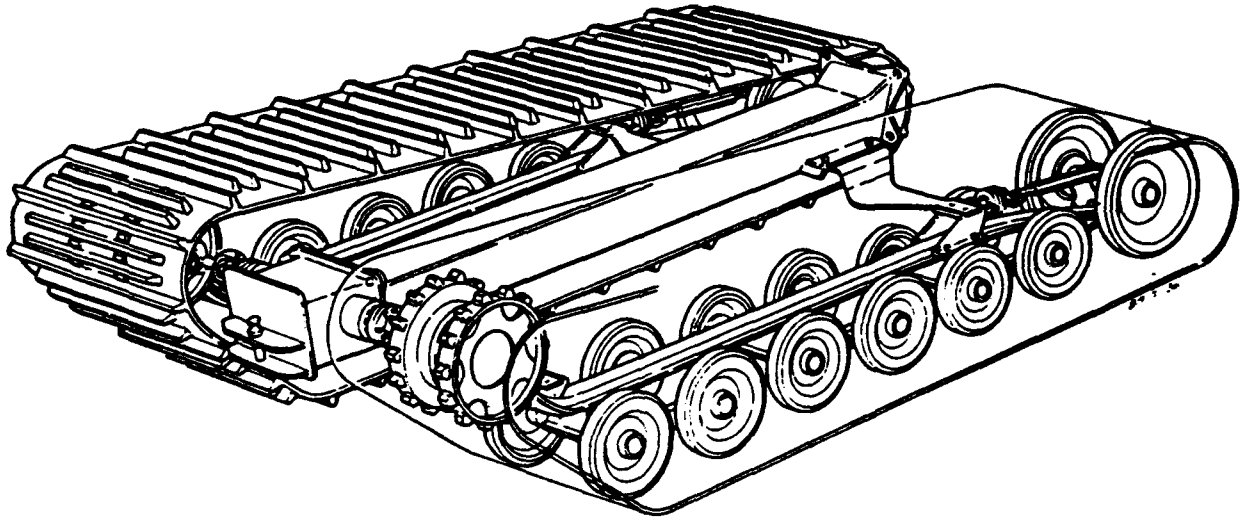

Figure 6. Chassis, first design.

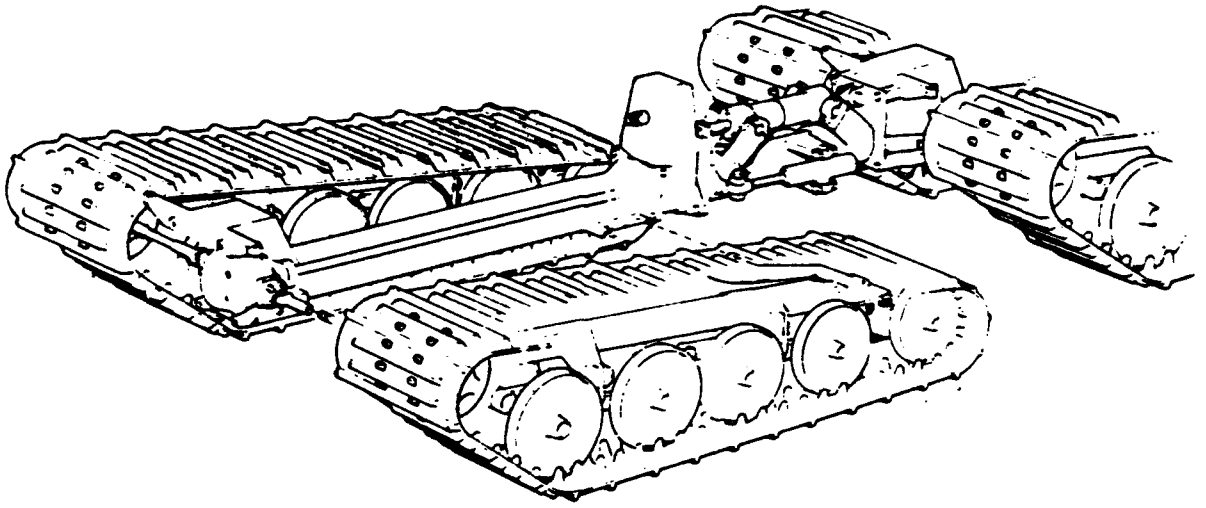

Figure 8. Chassis, second design.

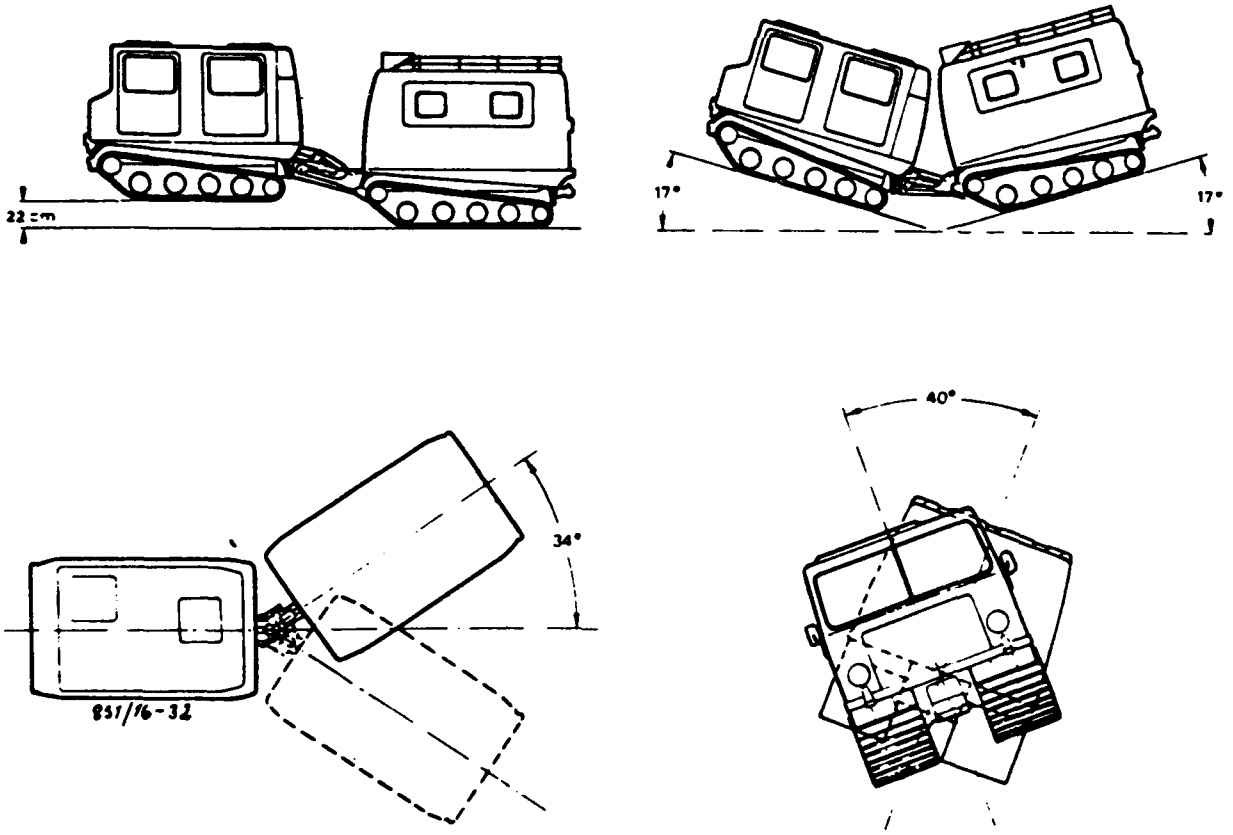

Figure 9. Required relative movements between the two vehicle parts.

DESIGN

The engine was originally the gasoline engine Ford 2658E. We used this engine for the Swedish Army and initial export orders from Finland and U.K. This compact V-6 engine has been very successful, although the mean power output is 2–3 times higher than in the passenger car.

Today, we use Mercedes 6 cyl. turbocharged diesel engine. This design is very unique, using aluminum cylinder head and light designs, resulting in same weight and higher power output than the Ford gasoline engine. For very dusty environment, the engine can be equipped with a heavy duty air filter of self cleaning cyclon type.

Driveline

The automatic transmission is a Daimler Benz W4 A-040 four speed unit. The transmission is controlled the normal way by a hand lever, with which you select a suitable range, Reverse, Neutral or Drive. Since we have modified the shift pattern to suit this type of vehicle and engine, it is very easy to operate the gearbox by the accelerator. The transmission has a secondary pump, which makes tow starts possible.

Transfer gearbox is a manually operated two step gearbox, which distributes the power to the front and rear differentials. High, neutral or low range can be selected by the driver with a hand lever, but the lever must not be operated when the vehicle is in motion. The transfer gearbox is bolted between the central beam of the front chassis and the steering unit. The housing of the gearbox is an integrated part of the chassis structure.

The differential is a hypoid unit conventionally designed. Front and rear units are identical. Like the transfer gearbox, the differential housings are parts in the chassis structure.

Chassis

Each chassis consists of a central beam, two transverse leaf springs and two track assemblies (Fig. 11). In the front chassis, the central beam also houses the propeller shaft from transfer gearbox to front differential. Each track assembly consists of track, track beam, sprocket assembly, four pair of roadwheels mounted on trailing arms to four cylindrical torsion rubber springs, and idlers sprung identical to roadwheels. The track tension is adjusted with a bolt between the idlers accessible through tooth gap.

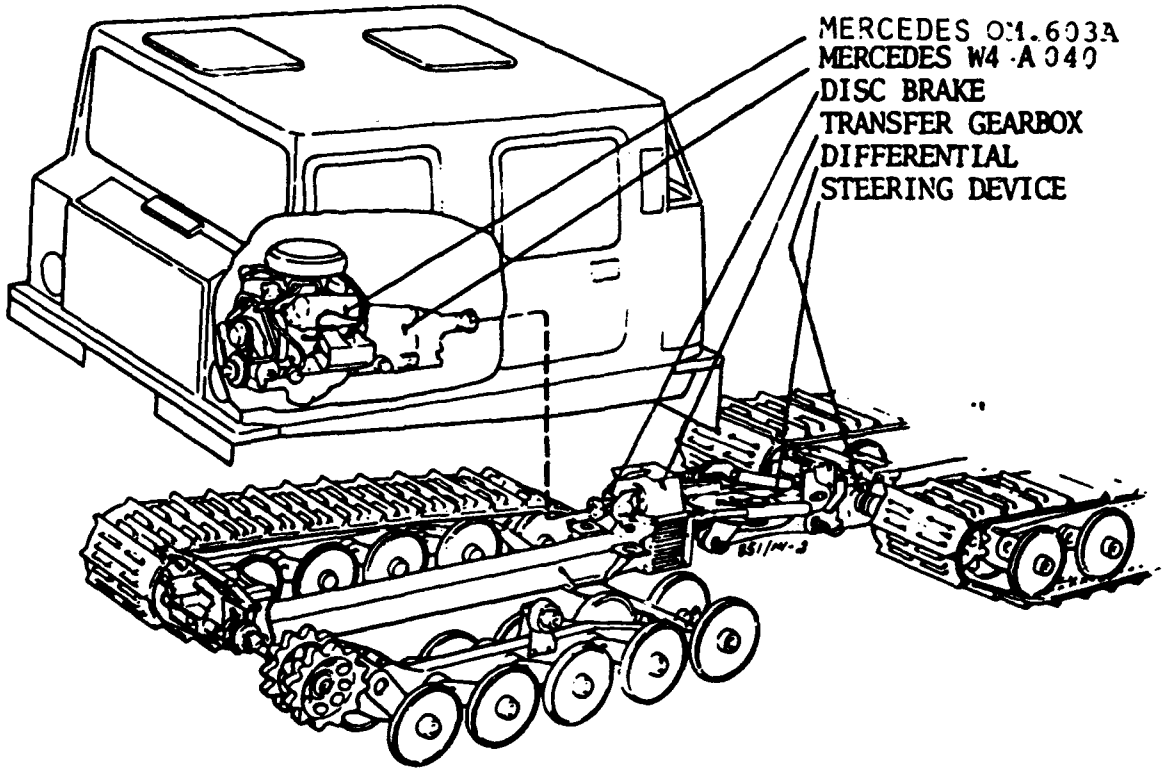

Figure 10. Driveline.

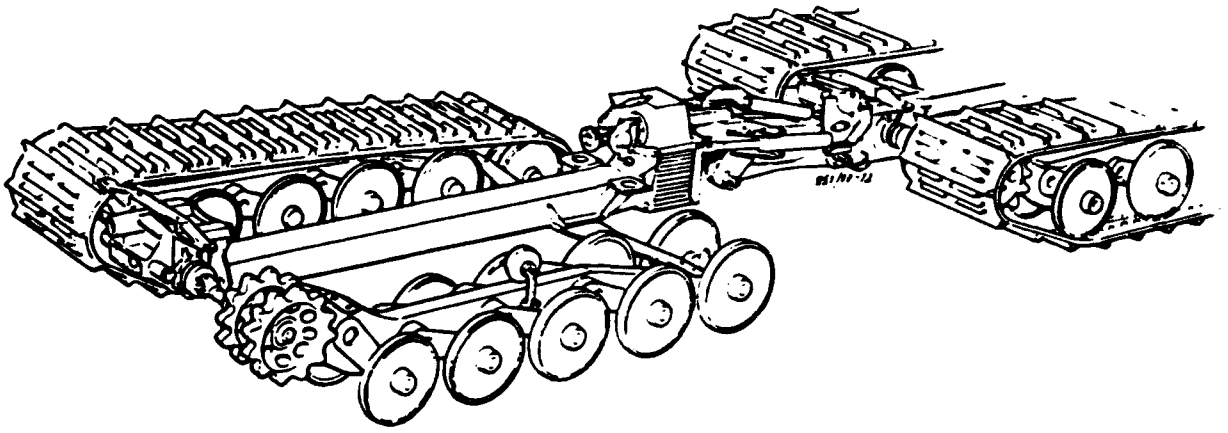

Figure 11. Chassis, final design.

The track is an endless unit made in rubber, reinforced crossways with steel beams and lengthwise with glassfiber. The guide horns are bolted through the steel beam.

Steering System

The steering system of Bv 206 is a hydrostatic articulated steering system operated by a steering wheel and activated by hydraulic cylinders on each side of the steering unit (Fig. 12). The hydraulic components are some of the few components that have been unchanged throughout the development phase.

Brake System

The brake system consists of a hydraulic service brake and a mechanically operated parking and emergency brake. Both systems operate on one single disc, mounted on a separate hollow shaft on the transfer gearbox, always in connection with the output shaft, independent of the position of gear lever.

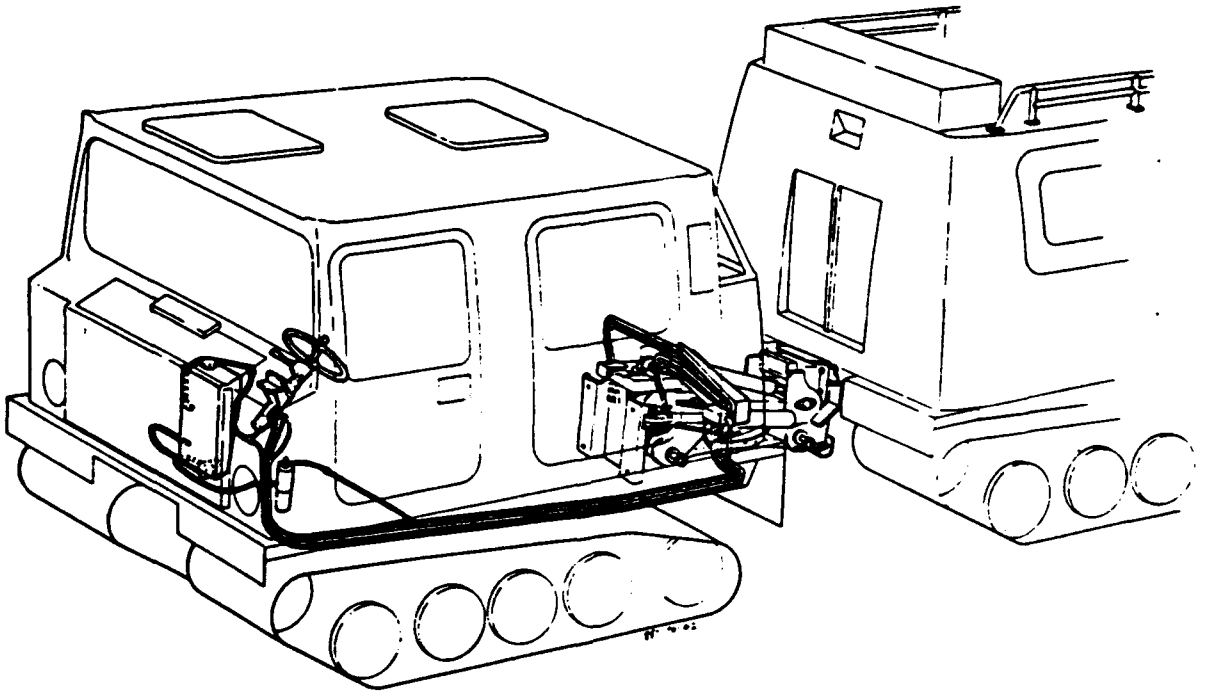

Figure 12. Steering design.

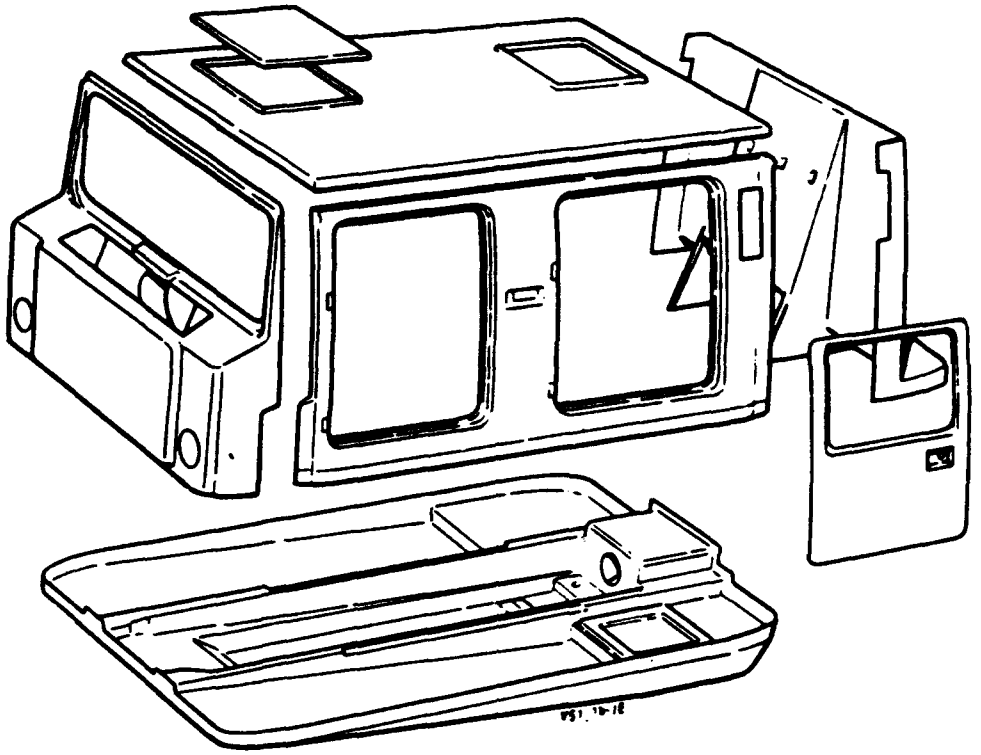

Figure 13. Body panels, front car.

Body

The body is made in glassfiber reinforced plastic, and most of it is a sandwich construction with PVC foam as distance material. Steel reinforcements and strong points are embedded in the structure. The bodies are built from a number of panels, which are bonded together (Fig. 13). The panels are manufactured in the reinjection method. They have been developed in cooperation with the maker, AB Bofors Plast.

For the Swedish Army we have developed three different versions of the vehicle, firstly standard version or the carrier, secondly an anti-tank version (Fig. 14) armed with a 90 mm recoilless gun or a Tow missile and thirdly a command post vehicle fully radio suppressed.

PERFORMANCE

Bv 206 has off road mobility far above most other vehicles. It is as standard designed for operation in temperatures ranging from –45°C to +35°C and with minor modifications, it can operate up to 49°C (120°F). It is fully amphibious without any extra kits, propelled in water by its own tracks. Its oversnow capacity is very good compared to a skid-steered vehicle, especially when you have to make sharp turns.

Payload is 2250 kg or 17 combat equipped soldiers, and it can tow trailers up to 2500 kg.

Top speed on paved roads is 55 km/h and in water approximately 3 km/h.

Grade ability is limited only by the friction between track and ground. 40° has been recorded. Sideways it can take 42° before tilting over.

The vehicle is extremely simple to operate and handle, so driver's training is very short. It has been driven by a 10 year-old girl.

PRODUCTION AND SALES

From Bv 206 production plant, the first vehicles rolled out March 1981. The first years, the production rate was some 50–200 vehicles and the capacity is now 800 vehicles per year.

The original contract from the Swedish Army was on 2000 vehicles, but was later increased to 4500 vehicles. The export sales have been very successful, and the vehicle is now in service in more than 20 countries. Most of the vehicles are in operation in the armed forces,

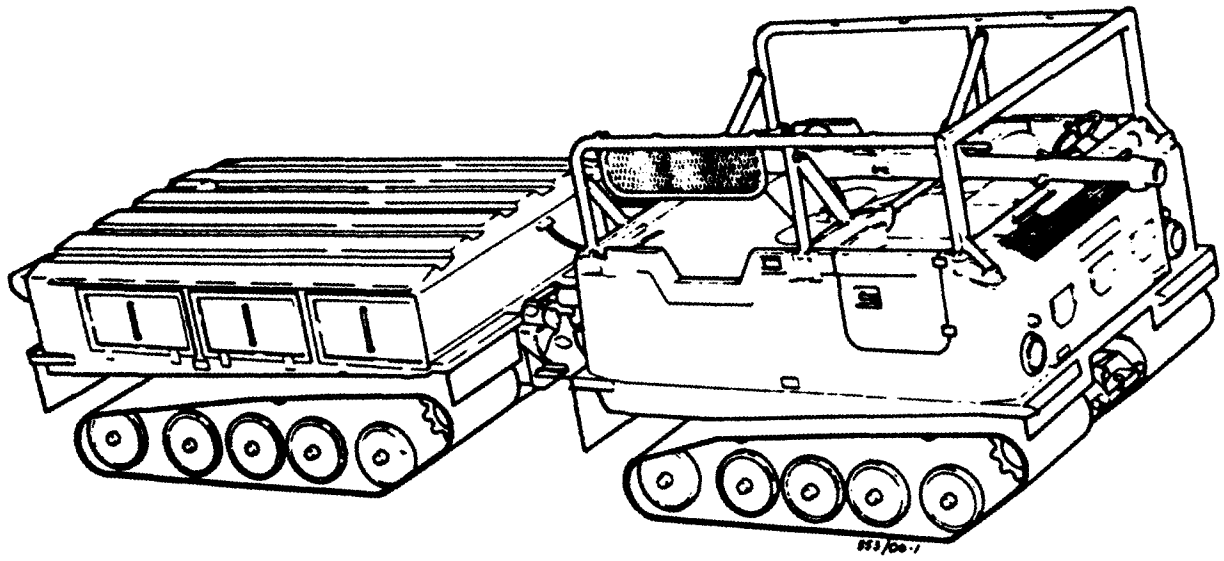

Figure 14. Anti-tank version.

but some are also used in important civilian roles, such as rescue vehicles in airports and general transport vehicles in Antarctica. Yellowstone Park operates some vehicles for passenger transport in wintertime. We have today sold more than 9000 vehicles.

Our biggest customer is, of course, the Swedish Army. Outside Sweden, it is in the armed forces of most NATO-countries and also in Finland who is operating a large fleet of Bv 206 in Northern Finland. One very interesting customer is Pakistan who operates the vehicle in high mountains. It is in regular service at altitudes above 4000 m. For these and other extreme conditions, we have developed a special snow track, which mounts outside the standard rubber tracks. This snow track gives you a very high mobility in soft deep snow and high inclinations. With this track, we have climbed more than 28° in deep snow. The snow depth was up to 9 feet.

In Antarctica, the Bv 206 is in use by Australia, U.S.A., New Zealand, Finland and Sweden. It is used as a general transporter, and to tow sleds with weights up to 10 tons. The Bv 206 can be used anywhere a job needs to be done in a roadless country, independent of weather conditions.

Operability: The First Step To Mobility

DEBORAH DIEMAND
U.S. Army Cold Regions Research and Engineering Laboratory
Hanover, N.H. 03755-1290

ABSTRACT

Virtually all major operations on earth involve the use of automotive and construction equipment. Although most of these operations are located in relatively undemanding surroundings, some take place in extremely inhospitable environments. Special provision is necessary to assure reliable operation of the equipment under these adverse conditions. One of the most difficult environments for effective operation of this sort of equipment is extreme cold.

All engineering equipment has some problems, even in ideal conditions. As winter approaches and temperatures fall, problems gradually become more frequent, more numerous, and more serious. At about 0°C their number rapidly increases as the performance of the soft and fluid elements of the engine and associated systems begins to deteriorate. Lubricants thicken, seals stiffen, batteries lose power and freeze, and ice forms in fuel lines, carburetors, and anywhere else water can possibly enter. Difficulty in engine starting is encountered. These problems slowly proliferate down to about –40°C at which temperature another rapid increase in problems occurs. This is because problems with hard parts are added to the gallery of already existing difficulties. Differential expansion and contraction of different metals cause jamming. Metals, rubbers, and other elastomers become brittle; structural members crack; push rods and cylinders break. Below this temperature, equipment operation becomes extremely difficult and in some cases impossible. Since very few vehicles are designed specifically for performance in cold regions, the remedies for these problems have largely resulted from local ingenuity fueled by the need of the moment. This paper describes some general solutions for many operational problems encountered at –40°C and below.

INTRODUCTION

Many of the problems associated with equipment operation at low temperatures are familiar to most of us. Below the freezing point of water, antifreeze must be used in water-cooled engines. Engines become hard to start because of decreased battery power and increased oil viscosity. This can usually be overcome by tuning the engine and changing to a lighter oil. Tires lose some of their pressure in the cold. These sorts of concerns are common in the continental United States and have little more than nuisance value. However, in extremely cold areas such as Alaska, Canada, and Antarctica, where temperatures may hover around –40°C or below for long periods, these problems evolve from a nuisance into a very serious operational problem.

The primary area of concern is starting the equipment. Diesel engines are especially difficult in this regard because of the nature of the fuel and the ignition process, and many modifications are usually needed to assure that a machine designed for use in temperate areas will function in extremely cold climates. In general, this involves the installation of heaters for various components, devices to improve heat retention in the engine compartment, and measures to improve ignition.

Once the engine is operating normally, its excess heat can be used to warm other parts of the machine, such as the cab, fuel tank, and hydraulic reservoir.

While there are many auxiliary heaters on the market for these purposes, a properly winterized engine should produce enough excess heat to satisfy all of the equipment's heating needs. Therefore, the proper operation of the engine itself is the most important concern, and it is the primary focus of this paper.

WINTERIZATION MEASURES

The winterization of equipment broadly includes any measure that will help to mitigate the adverse effect of cold on normal operation. This includes the use of arctic-grade lubricants and seals, the implementation of heat retention devices, and the installation of heaters.

Lubricants

There are a number of lubricants currently on the market that give satisfactory service at very low temperatures. 0W20 or 0W30 motor oils remain fluid down to –50°C or slightly below. These oils are often used in hydraulic systems, certain transmissions and other applications where the standard fluid becomes too viscous to use in the extreme cold. There are drawbacks in the use of these oils, however.

First, if the oil is not changed often enough, the viscosity index improver additive may deteriorate, resulting in loss of the oil's high-temperature properties. This additive is a very large branched molecule that contracts at low temperatures and exerts little influence on the base oil's viscosity. At high temperatures, it expands, effectively thickening the oil and increasing its viscosity. However, in the high shear conditions in the cylinders the branches of these large molecules can shear off, and in extreme cases what remains is the very light base stock, which cannot adequately lubricate the engine at operating temperatures.

Second, some machinery cannot tolerate arctic-grade oils at all and must use standard 30 weight oils or heavier. Most light machinery can use 0Wxx oils, but the heavier the equipment, the more likely it will be that they will be adversely affected by these oils. The problems and use of lubricants are discussed further in reference 1.

Batteries

The best way to ensure reliable battery power at low temperatures is to keep the battery warm at all times. Since this is not always feasible, batteries for arctic use usually use heavier electrolytes than those in warm areas, often with a specific gravity of 1.300, which improves low-temperature performance and lowers the freezing point. Nevertheless, some heating will still be necessary to achieve sufficient power output for starting and subsequent recharging. Batteries should be housed in an insulated box equipped with either an electric heater (usually about 100 W) or a thermostatically controlled coolant heater. Excessive heat can damage the battery because of the higher acid concentration.

Since more electric power is needed in cold regions because of increased engine resistance on start-up and greater use of lights, pumps, and so forth, a higher capacity battery should be used than that normally called for, or more than one should be installed. Further information on the use of batteries at low temperatures is given in reference 2.

Elastomers

Fluid leakage reaches epidemic proportions at low temperatures, especially in hydraulic systems where the fluid pressures are higher than in other systems. However, oil commonly leaks out of transmissions, power steering, and other systems as well. Some of this leakage may be due to metal contraction affecting clearances between mating parts and the tightness of fasteners. However, the greater part of the problem is because the materials used in seals, gaskets, and hoses shrink, crack, and lose their flexibility. Arctic-grade seals and hoses should be used on all parts of the machine that will be exposed to temperatures of –40°C and below. Silicone rubbers have proven very useful in these applications, and a great number of seals and hoses are commercially available using this material. At temperatures above –40°C, standard parts may be satisfactory in many passive applications and need not be replaced unless leakage problems develop. These problems are discussed in reference 3.

Another factor that should be considered in selecting suitable materials is their ozone resistance. In snow-covered regions ozone concentrations are higher than normal and many products will degrade in its presence.

Heat Retention Devices

A cold-soaked, uninsulated engine at –40°C will be almost impossible to start and, once started, will never achieve normal operating temperatures. The result will be frequent breakdowns and high maintenance and repair costs. In an average machine operating under normal conditions about a third of the energy available in the fuel is used for useful work; another third is lost through exhaust heat, while the remaining third is transferred to the cooling system. In a well-insulated engine, much of this waste heat can be retained, and the engine will achieve normal operating temperatures while the excess can be used to warm other areas of the machine such as the cab, batteries, hydraulic reservoir, and so forth by installation of suitable heat exchangers in the cooling system.

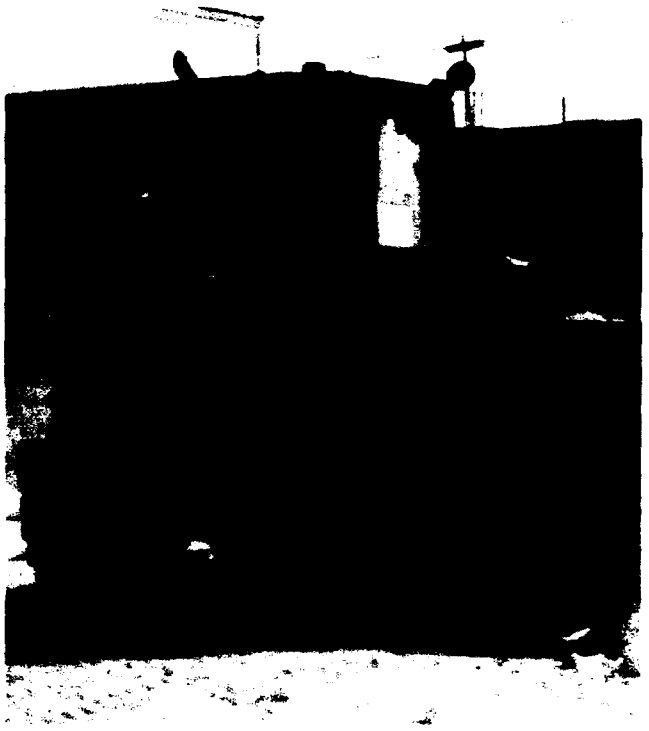

Figure 1. This loader is equipped with both winterfront and side blankets to minimize heat loss from the engine compartment. The winterfront can be partially opened using the horizontal and vertical zippers that meet at its center point.

Closed cell vinyl insulation 6 mm thick or greater is a popular choice for insulation in cabs and can be used in the engine compartment as well if treated with a flame retardant. A protective steel liner is also a good idea. Many vehicles are equipped with sound-insulating foam in the engine compartment, which also serves as thermal insulation to a degree.

Other commonly used heat retention devices are winterfronts and side blankets such as those shown in Figure 1. Virtually all machinery in use on Alaska's North Slope in the winter is equipped with winterfronts, which are usually designed so that they can be partly or fully opened in case the temperature rises. These prevent ambient air from entering the engine compartment during operation and restrict heat loss during shutdown. Side blankets serve the same purpose in machinery with open side panels. Under-engine protection is also used either in the form of a plastic or metal shield or a more or less closely fitting insulated covering for the oil pan.

Thermostatically controlled cooling fans reduce or eliminate fan operation, again reducing heat loss from air infiltration. High-temperature thermostats are also routinely used to increase the maximum temperature the engine can achieve before heat is removed by the cooling system.

The implementation of winterization measures will improve the engine performance at low temperatures and in some cases may enable starting and operation at temperatures as low as –30°C, but below this, the addition of heat is desirable in all cases and inescapable in most. Further discussion of winterization measures is given in reference 4. The following sections give a brief discussion of the types of heaters commonly used in automotive applications and criteria for their selection. More information on heaters and heating is given in reference 5.

TYPES OF HEATERS

Engine preheating is either continuous during shutdown (standby heating) or on demand for a short time prior to starting a cold-soaked engine (quick-start). The main difference between standby and quick-start heaters is the heat output. Standby heaters are either run continuously or controlled thermostatically while en-

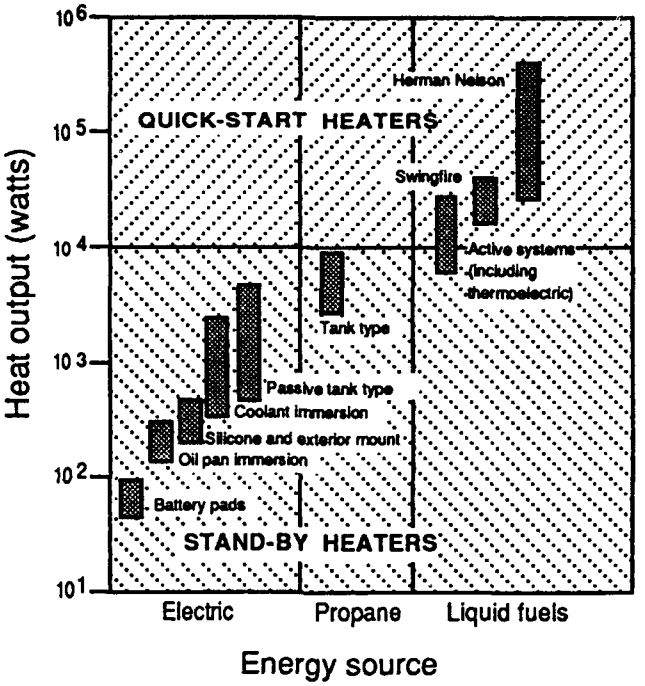

Figure 2. Heat output ranges for various types of automotive heaters.

gines are not operating and are often manually or automatically turned on as soon as the engine is stopped. They maintain the engine temperature, therefore, only at a sufficient level to ensure startability. Quick-start heaters must have a much greater heat output than standby heaters because they must heat a cold-soaked engine to normal operating temperature within a relatively short time.

Most heaters either supply heat directly to the component being heated or indirectly through the coolant, a notable exception being the Herman Nelson, which uses forced hot air. The heat output of the many units used in automotive applications ranges from about 50 to 1,000,000 watts. In general, stand-by heaters produce up to about 100 kW, while quick-start systems fall into the higher output ranges. Within this wide range the specific heater types occupy a narrower niche, as shown in Figure 2.

For the most part, electric heaters are the easiest to install, most convenient to use, and easiest to control. They are available in a great number of types, sizes, and power densities. There is really no engine component that cannot be heated electrically. Figure 3 shows three of the most common types of electric heaters used for automotive heating.

Immersion heaters are used in the cooling system and in the oil sumps of both the engine and gear boxes. The wattage of those used in the cooling system is usually much higher than for those used for warming oil because of the danger of charring or degrading the oil. Immersion heaters for these two applications should not be interchanged. These units are either mounted into existing ports in the engine, such as the oil drain plug or frost plugs in the water jacket (which they replace), or are preassembled as a unit designed to replace a small section of the lower radiator hose so that the warmed fluid will rise by convection, flowing into the block to be replaced by cold fluid from the radiator.

Externally mounted pads or coils are commonly used where an immersion heater cannot be used. The so-called silicone heater is widely used in Alaska, where it is commonly used to warm the oil pan as well as components such as the hydraulic reservoir, fuel tank, or other parts with a flat surface. The wire heating element is sandwiched between two thin layers of silicone rubber resulting in a flexible unit about 2 mm thick that is applied to the metal surface with high-temperature silicone cement. Silicone pads are commonly available in sizes ranging from about 10 × 15 cm to 15 × 30 cm with wattages from 150 W to 450 W. Other sizes can be custom made, and special-purpose pads are manufactured for drums, cylinders, and the like.

Batteries are normally heated with very low-power plates (underneath the battery) or blankets (surrounding the battery). Batteries should only be heated enough to assure sufficient power output and should never be

exposed to elevated temperatures for extended periods.

The last common type of electric heater is the tank-type, which is plumbed into the cooling system in such a way that water is drawn in from a point near the bottom of the system and returned to it at the top. The power output is usually greater than that of the other types of electric heaters, but this advantage is partially diminished by the increased heat loss to the engine compartment. These heaters are usually passive systems and rely upon convection to circulate the heated coolant. They are therefore limited as to the areas to which heat can be distributed.

Fuel-fired heaters have a similar design in which the water jacket surrounds the combustion chamber, as shown for a propane-fired heater in Figure 4. Heaters of this type have the highest heat output of the on-board units and are often supplied with pumps so that the heated coolant can be distributed to many different areas in the equipment rather than just the block. Heat exchangers can be installed in the cab (usually standard), oil pan, battery box, fuel line, hydraulic reservoir, rearview mirror, air intake, and other areas where space permits the installation of the necessary tubing. Active systems of this sort are often used for stand-by heating, and the larger units can be used as quick-start heaters to preheat a cold-soaked engine, although this could take as long as several hours. Their major disadvantages are that they need electricity to run the pump and they are subject to the same fuel problems as the engines themselves, i.e., waxing and low volatility. The problems of fuels at low temperatures are discussed in reference 6.

Thermoelectric generators are very reliable, if costly, devices that convert heat directly to DC electricity through a solid-state energy converter. They produce electrical power at about 7–9% efficiency and produce a large amount of waste heat. Small units that use diesel fuel, kerosene or gasoline have been designed for use on automotive equipment. Heat from combustion of the fuel is applied to one side of the energy converter. The other side is cooled by circulating engine coolant. The resulting temperature differential causes DC power to be produced. The electricity produced runs the pump, and any excess power can be used to charge the battery, if desired. The net power output is about 60 to 400 W. The excess heat is absorbed by the coolant and amounts to about 6 to 12 kW. Power required for startup is about 420 W maximum (15 amps at 28 V), but the unit is self-sustaining during normal operation. These heaters would appear to have great potential value in cold regions where electric power is limited.

In many cases the use of an auxiliary quick-start system is the most effective choice in terms of both fuel economy and heating time before start-up. The gasoline-fired Swingfire heater used by the military is a

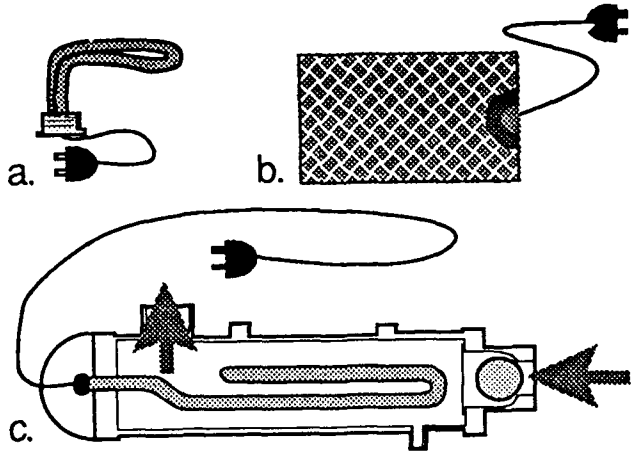

Figure 3. Common types of electric heaters. a) Immersion heaters designed for installation in existing ports in the engine; b) silicone pads attach to any flat metal surface on the engine or elsewhere in the machine; c) passive tank-type heater in which the coolant flows by convection through the heater. The ball at the intake prevents backflow of the coolant when the engine is shut down.

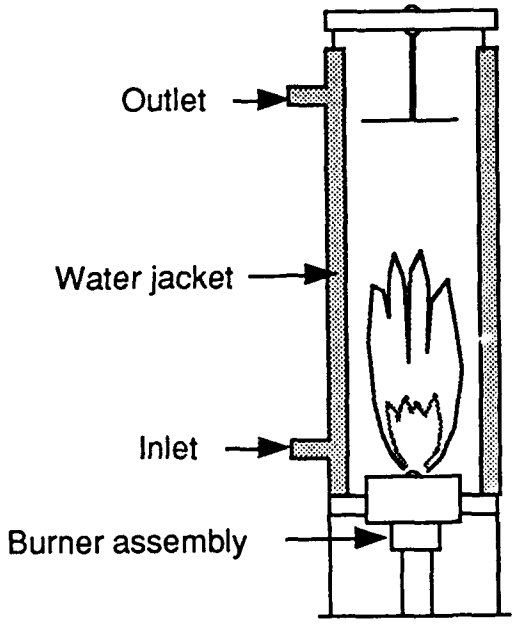

Figure 4. Fuel-fired heater in which the coolant flows through a water jacket surrounding the combustion chamber. It may be either passive, in which the coolant flows by convection, or active, with an associated pump.

multipurpose device that can be used for coolant heating, space heating, forced hot air heating, and so forth. A heat exchanger designed to accept the Swingfire is installed on the machinery to be heated, and the unit is moved from one machine to the next. Their heating capacity ranges from about 10 to 20 kW, and they require only a small amount of electricity on start-up and none thereafter.

Other types of coolant preheaters use fast-disconnect couplings to connect the heating unit to the cooling system and pump the hot coolant through whichever heat exchangers are enabled. The power for the pump can be taken either from the battery of the unit being heated or from the vehicle used to transport the heater. These heaters are designed to use various kinds of fuel and can be almost any size.

The Herman Nelson heater is a fuel-fired forced hot air heater that blows hot air through conduits to the parts to be heated. It is normally used in conjunction with a shelter of some sort, whether an insulated compartment integral to the machine or a temporary shelter enclosing all or part of the equipment. The heat output may be as high as 1,000 kW.

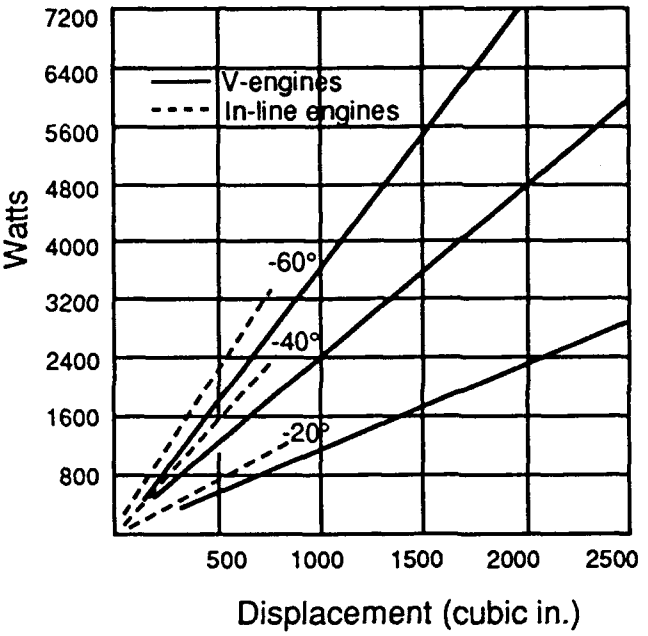

Figure 5. The amount of heat required to warm the block of engines of various sizes to –1 °C from the indicated ambient temperatures using immersion heaters. Additional heat would be required if a tank type heater were used or if other areas were heated.

MAGNITUDE OF HEAT INPUT REQUIRED

At temperatures below –30°C most equipment that is not stored in a heated garage will require at least some heat input for starting. The amount of heat applied and to which parts of the machine depends on many factors:

Engine size

The size of the engine has a strong influence both on the rate at which heat is lost from an engine and the amount of heat that must be applied for a successful start from a cold-soaked condition. Figure 5 shows the size of the heater required to warm the block to 1°C for engines of various displacements. The data from which this graph was drawn were derived from measurements made on engines in still air equipped with immersion heaters that were able to bring the block temperature up to –1° in 12 hours, with 80% of the temperature rise taking place in the first 5 hours. If a shorter heating period is required, a larger heater must be used. If tank type heaters are used, the wattage values should be 50% higher than those shown. Any other necessary heat input such as for the oil pan, battery, or cabin would be in addition to this. Note also that in-line engines need more heat input than V-engines with the same displacement.

Type and configuration of the equipment

Diesel equipment requires more attention than gasoline-powered equipment because the fuel is more viscous and harder to vaporize and because ignition depends on the heat of compression alone, which is often insufficient at ambient temperatures below about –10°C. There are a number of devices in use to heat the intake air either electrically or through the use of coolant heat exchangers or partial combustion of the fuel before it reaches the combustion chamber. One of these should be used on diesel equipment even in moderately cold conditions, and at extremely low temperatures the intake air should be heated even during normal operations. This is often accomplished by locating the intake near the supercharger or some other hot place in the engine compartment.

In terms of engine configuration, the more compact V-type engines require less heat than in-line types.

In terms of the overall machine configuration, the more compact the design, the easier it will be to warm the necessary components. If the fuel tank and hydraulic reservoir can be enclosed in a common insulated envelope, both can be heated more effectively. On the other hand, some machinery such as cranes by their very nature cannot be made in a compact configuration. These are difficult to winterize and are usually not used at very low temperatures if it can be avoided.

Operational schedule

The length of time a machine will be shut down in the

course of normal operations has a considerable influence on the amount of heating it will need before it is restarted. A machine that is used continuously may not need any integral engine heaters. For example, in a mining operation where the equipment is used on a 24-hour basis and is never turned off except when it is in the heated maintenance facility, the engine will never cool sufficiently to need heat input for starting. On those rare occasions when such equipment has been allowed to cold soak, it can be warmed in a temporary shelter using a quick-start heater.

A well winterized engine may retain enough heat to start after 4 to 8 hours without additional heating depending on ambient conditions. However, an engine that has been allowed to cool for as much as 16 hours must be considered cold-soaked and treated accordingly. If the equipment is routinely shut down for a period that might be long enough to cold-soak the engine it should be equipped with a stand-by heating system that will maintain a sufficiently high temperature in the engine for reliable starting throughout the shutdown period.

Length of time available for heating

For several reasons the most efficient engine preheating technique is the quick-start method where a relatively large amount of heat is applied in a relatively short period. The shortest possible time is desirable, but because of the size of heater required and the damaging effect of raising the temperature of engine parts too rapidly, heating time should not be less than 15 minutes to 1 hour at –55°C (–65°F), depending on engine mass. In general, the shorter the time allotted for preheating, the greater the size of the heater required and the greater the complexity of the preheating system. Quick-start systems are virtually essential when cold-soaking of a vehicle is unavoidable. Usually quick-start heaters are stand-alone units exterior to the machine such as Herman Nelson heaters or a hot coolant transfusion unit, and usually there is not a large number of them available at a particular site. Therefore, if many machines must be started up at the same time, a single heating unit would have to be shared by a number of machines, so that it could take several hours to start up all the engines. In this situation it would make sense to install high-capacity preheating units on each machine capable of warming the engine to starting temperature in a few hours. The preheating system can be controlled by a timer that would automatically start up the heaters at a preselected time so that all machines should be ready to start when they are needed.

Type of shelter available

Very little equipment used in cold regions can be kept in heated garages except certain emergency vehicles. However, whenever possible equipment should be kept in a shelter of some kind to retard heat loss from wind chill and to prevent infiltration of blowing snow. In windy conditions the amount of energy required to preheat an engine is greatly increased and the period of time the engine will retain enough heat to start unassisted is much reduced.

Temporary shelters are commonly used when using a hot air quick-start heater to preheat cold-soaked machinery. Parachutes are often used, as shown in Figure 6, or a tent or tarpaulin—anything, in short, that will cut the wind and reduce heat loss. Coolant heaters are less dependent on wind conditions since they pump heated coolant directly to the heart of the engine.

Degree of winterization

The use of heat retention devices is a good idea because they will improve engine life and performance by ensuring that the engine will be able to reach and maintain its design temperature and will increase the amount of engine heat that can be made available for other uses. A closed and insulated engine compartment also indirectly assists cold-starting by reducing the amount of heat that must be applied for a successful start.

Availability of electric power

If virtually unlimited electric power is available, electric heaters can be used to warm all necessary parts of the engine. They are reliable, inexpensive, compact, easily controlled, and available in an enormous number of sizes, types, and power outputs. However, a large piece of equipment may need an intolerably large amount of electricity to preheat it in a reasonable amount of time. Similarly, the electric power supply may simply be inadequate to meet the heating demands of the number of machines needing preheating. In this case fuel-fired heaters should be used. Many of these need a small amount of electricity to start up or to operate pumps, but the heat itself is produced through the combustion of fuel.

CONCLUSIONS

There is no way to achieve flawless operation of automotive equipment at very low temperatures. However, by proper winterization of the equipment, use of arctic-grade lubricants and fuels, and choice of a suitable heating system, the life and performance of the equipment can be much improved. Unless it is run continuously, all machinery will need some degree of heat input below –30°C. The choice of an appropriate heating package depends upon:

Figure 6. A bucket loader is heated prior to operation by enclosing it in a parachute and blowing hot air into the enclosed space through elephant-trunk conduit from the space heater on the left. The ambient temperature is about –35°C.

- The size of the engine
- The type and configuration of the equipment:
- The operating schedule: If the engine is normally shut down for a relatively short period, a standby system would probably be the best choice; if the equipment is often shut down for long periods, a quick-start system would be the most efficient.
- The amount of time available for heating: The shorter the heating time available, the larger and more complex the heating system.
- Available shelter
- The degree of winterization
- The type and number of auxiliary heating units that are available
- The availability of electric power.

LITERATURE CITED

1. **Diemand, D.** (1990) Lubricants at Low Temperatures. U.S.A. Cold Regions Research and Engineering Laboratory, Cold Regions Technical Digest No. 90-1, December 1990.

2. **Diemand, D.** (1991) Automotive Batteries at Low Temperatures. U.S.A. Cold Regions Research and Engineering Laboratory, Cold Regions Technical Digest No. 91-4, May 1991.

3. **Diemand, D.** (1991) Automotive and Construction Equipment for Arctic Use: Materials Problems. U.S.A. Cold Regions Research and Engineering Laboratory, Cold Regions Technical Digest No. 91-5, November 1991.

4. **Diemand, D.** (1992) Winterization and Operation of Automotive and Construction Equipment in Arctic Use. U.S.A. Cold Regions Research and Engineering Laboratory, Cold Regions Technical Digest No. 92-1, September 1992.

5. **Diemand, D.** (1991) Automotive and Construction Equipment for Arctic Use: Heating and Cold Starting. U.S.A. Cold Regions Research and Engineering Laboratory, Cold Regions Technical Digest No. 91-3, April 1991.

6. **Diemand, D.** (1991) Automotive Fuels at Low Temperatures. U.S.A. Cold Regions Research and Engineering Laboratory, Cold Regions Technical Digest No. 91-2, March 1991.

Wheeled Vehicle Mobility Evaluation In Deep Snowpack

D.M. XU, A.M.O. MOHAMED, R.N. YONG
Geotechnical Research Centre
McGill University
817 Sherbrooke St. West
Montreal, Quebec, Canada H3A 2K6

G.J. IRWIN
Defence Research Establishment Suffield
Vehicle Mobility Section
P.O. Box 4000
Medicine Hat, Alberta, Canada T1A 8K6

ABSTRACT

This paper proposes a computational model to evaluate the wheeled vehicle mobility in deep snow pack. The snow plate footing and the snow direct shear test data are used to offer the basic parameters required in the model. The contact length under the vertical load on the tyre is determined at first so that the average normal and shear stresses on the contacting surface can be evaluated. The energy conservation principle is subsequently employed to evaluate the tractive efficiency, etc. A computational example is given for demonstration which offers a great deal of information for vehicle design.

1.0 INTRODUCTION

Present procedures utilized for predicting vehicle-snow performance are by and large *ad hoc* in nature, or based on adaptations of methods used in the field of vehicle mobility on soil terrain. In the case of vehicle-soil interaction, the methods used for predicting vehicle-soil performance rely on procurement of soil material property on information through field testing tools. These tools, e.g. cone, vane-cone, bevameter, etc. together with their associated methods of data interpretation and application presume a certain degree of material property invariance. This assumption is not valid in the strictest since, but finds some measure of application in the field of mobility on soil material because the widespread difference in vehicular loading schemes and surficial topography are by and large significantly greater than the general differences in local soil properties.

Variations in soil conditions encountered when measuring vehicle performance in soil influence the response of different loading system. In view of such circumstances the need to account for soil property variation for correlation between changes in soil properties and vehicle performance is obvious. Thus, measurements of penetration resistance or shear resistance in soil material appear to be acceptable for application with the associated methods of analysis for both description of and assessment of soil-vehicle performance.

Snow however presents a different picture. The problems existing in ordinary vehicle-soil interaction become significantly more complex in a vehicle-snow interaction phenomenon because the material (snow) properties are significantly more complex. An insight into some of the reasons why snow is much more complex responsive material compared to soil in the area of vehicle performance predictions follows.

Density

Snow pack density is a very popular measurement in snow classification schemes but tells little about the snowpack without knowledge of grain size, *in situ* temperature and thermodynamic history. By and large, snowpack density varies with age and normally has a

profile of values increasing from the surface downward. A knowledge of this is important not only from the density-variation point of view but also from the viewpoint of detailing with respect to stratigraphy. Since initial vehicle flotation relies on snowpack stability *vis-a-vis* bearing support, structural configurations in the snowpack are important conditioners. Thus, one can note that various methods of packing can produce identical density. In turn, these various packing or structural configurations can produce varying strengths due not only to packing states, but also bonding mechanisms. Density measurements do not reflect these aspects of the phenomenon. Note also that the snowpack is subject to large changes in density during vehicle-snow interaction.

Grain size distribution

This is an important factor relates to shear strength and potential or actual bonding. It also is a factor in the density of the pressure bulb which forms beneath the vehicle traction element. The grain size distribution characteristics of a snowpack is affected by age, temperature variations, climatic conditions during and after deposition, and possibly other cases.

Temperature

Local temperature has a pronounced effect on the strength properties of snow. It is not uncommon for the near surface layer in a snowpack to vary 20°C in a 24-hr. period. It is also significant to note that in conjunction with elapsed time, the variations in temperature will contribute to the thermodynamic history of the snowpack. Thus, the corresponding or related changes in snow resistance properties can be identified.

Depth

Whilst a knowledge of the depth of the snowpack gives only documentary information, by itself it becomes extremely important when coupled with vehicle dimensions. The method of performance analysis for operations in a snowpack which completely contains the effects of vehicle sinkage is different than for operations where the snowpack behaves as a layer compacted between the vehicle and the ground. These vehicle performance conditions are labeled as *over snow* and *through snow*, respectively

Snow-soil analogy

If analogies were attempted between soil and snow, the closest and most realistic analogy would be between dry sand and granular (dry) snow. Both materials can be considered as two phase materials where porosity and grain size distribution are reasonable descriptors of the materials. Beyond this particular context, however, the analogy fades because:

(a) the mechanical properties of sand are by and large insensitive to seasonal temperature variations—as opposed to snow. Note that in most locations and instances, snow completely disappears in the summer period and that the properties of the material throughout its seasonal life are reflective of the life cycle.

(b) The effects of stress history in sand strain-rate loadings are vanishing small. These effects are significant and influential factors in production of snowpack response.

(c) Volume changes under loading in sand are small in comparison to snow.

Devices for measuring snow properties for mobility prediction purposes

In the examination of devices presently used for measuring snow properties for mobility prediction purposes, it is significant to note that technology transfer (from mobility on soil to mobility on snow) has been made on a one-to-one basis. Relegating snow as another kind of soil material, and using not only the same testing tool but also the same kind of data reduction, analytical techniques and equations, can lead to severe errors in assessment of vehicle-snow interaction. This kind of technology transfer ignores the true and real differences in material response—which are indeed large in the case of snow and assumes that the interactions themselves are identically duplicated *vis-a-vis* vehicle-soil and vehicle-snow interaction.

Thus for example, if one presumes that soil can be modelled according to elastic-plastic and elastic-work hardening relationships, the implication from technology transfer thinking is that snow will conform to the same requirements befitting that of elastic-plastic or elastic-work hardening materials. Note that the extremely high volume change effect is not satisfactorily accounted for in the above models. Hence, one compounds the difficulties indirect transfer through not only the large difference in volume change and linearity performances but also the attendant problems of temperature and strain-rate.

In addition to the requirement of likeness in constitutive performance between soil and snow as a natural consequence of the application of technology transfer, the adoption of the soil-snow analogy carries on the imposition of the two-parameter Mohr-Coulomb theory as a "valid" failure criterion for snow. The consequences of the application of the theory of a failure to snow can be dramatic since the outcome of the theory is the identification of two material strength parameters C (cohesion) and ϕ (angle of internal friction). Since the theory of failure requires that the total energy needed to

fail a test sample is expended along a rupture plane, and not in volume change or any part thereof, it is clear that the application of such a theory to materials which suffer undue volume change under loading cannot be directly accomplished without accountability for volume change energy expenditure. Thus the concepts or values of C and ϕ obtained in medium to high volume change materials need to be properly scrutinized and placed in perspective in order that their application to problem analyses may be correctly situated. Note that in the case of soils, the volume changes encountered under loading are generally sufficiently small—thus allowing for a viable application of the two-parameter Mohr-Coulomb theory of failure.

The preceding highlights that in order to predict vehicle snow performance, it is essential that the mechanism of compaction and shear between the traction elements and the snow is understood. If the prediction is based upon sampling the reactions of the snow to external forces and imposed deformations, logic dictates that if a proper rational prediction of performance is to be made, a similarity in the development of snow response between the reaction element and test and direct shear tests are used to obtain the required parameters which characterize the snowpack. In this study a plate loading and direct shear tests are used to obtain the required parameters which characterize the snowpack. Furthermore, a wheeled vehicle mobility model is derived based on the energy conservation principle. In brief, the method works with an analysis of the displacement around the contact boundary between the loaded tyre and the supporting snowpack. The contact length is first determined so that the subsequent calculated stresses on the contact boundary can be specified. The slip rate and the traction efficiency are given as a natural outcome based on shear test data and the energy conservation principle.

2.0 THEORETICAL FORMULATION

In applying the principle of energy conservation to the evaluation of tyre performance on deep snowpack, the different energy components participating in the interaction between the loaded tyre and snowpack need to be calculated. The energy concept for evaluation of traction was formally introduced by Yong and Webb (1969) for motion performance of rigid wheels on soft soil. Subsequently, the energy model was extended by Yong and Fattah (1976), Yong et al. (1978, 1980), and Xu et al. (1990) and (1991) to predict pneumatic tyre performance on soft soils.

The basic principle used in the energy model evaluates the moving performance of the tractive element (tyre) on snowpack in terms of the well known energy balance equation.

$$\text{Input energy} = \text{output energy} + \text{energy losses} \quad (1)$$

With the quasi-static assumption, the vehicle is assumed to move on the snowpack at a relatively low speed so that dynamic effects (including vertical vibration of vehicle system and snow damping) can be neglected. The energy balance equation in terms of power can be written as:

$$P_{use} = P_{input} - (P_{slip} + P_{snow} + P_{tyre}) \quad (2)$$

where: P_{use} = the useful power; P_{input} = the total power input to wheel; P_{slip} = the power dissipated due to tyre slip; P_{snow} = the power dissipated in snow deformation, and P_{tyre} = the power dissipated in tyre deformation.

This method of mobility evaluation (Xu et al. 1990 and 1991) is especially suitable for the initial stage when the vehicle begins to move on a specified terrain surface from the "at-rest" condition. It not only answers whether the vehicle can or cannot move i.e., "go or no go" question, but also gives a reasonable estimation of vehicle mobility for the assumed conditions: (1) slow speed, and (2) no vibration effect.

Input energy

The input energy, through the applied torque T_o on the tyre during time t_o is given by:

$$E_{input} = T_o \omega t_o \quad (3)$$

or

$$P_{input} = T_o \omega \quad (4)$$

where: E_{input} = total input energy (kN.m.rad); P_{input} = total input power (kN.m); ω = tyre angular velocity (rad/sec); T_o = applied torque (kN.m), and t_o = time (sec).

Slip energy

The slip (dissipated) energy due to the applied torque T_o on the tyre during time t_o is given by:

$$E_{slip} = T_o \omega t_o S \quad (5)$$

or

$$P_{slip} = T_o \omega S \quad (6)$$

where: E_{slip} = the dissipated (lost) energy due to tyre slip (kN.m.rad); P_{slip} = the dissipated power due to slip (kN.m), and S = the slip rate, which is given by:

$$S = \frac{\omega r - v}{\omega r} \tag{7}$$

where: S measures the efficiency of the transfer of the tyre rotational motion into the horizontal vehicle motion; r = rolling radius (m), and v = translational velocity (m/sec).

Snow dissipated energy

When the vehicle moves on the snowpack, it continuously "loads" the undisturbed snow and hence snow will be deformed and energy will be dissipated due to snow deformation. This energy is directly related to the normal stress distribution on the contact area between tyre and snow surface. For the snow surface, the loading situation can be considered in terms of a distributed stress along the contact length moving at vehicular speed.

The moving boundary loading condition can be specified as follows, any concentrated point load F(kN) acting at a distance x_o from the origin of the coordinates may be described by

$$F(t) = F\delta(x - x_o) \text{ or } F < x - x_o >^{-1} \tag{8}$$

where $\delta(x - x_o)$ is the Dirac-delta function defined by:

$$\delta(x - x_o) = \lim_{\varepsilon \to 0} \begin{cases} 0 \text{ when } x < \left(x_o - \frac{\varepsilon}{2}\right) \\ \frac{1}{\varepsilon} \text{ when } \left(x_o - \frac{\varepsilon}{2}\right) < x < \left(x_o + \frac{\varepsilon}{2}\right) \\ 0 \text{ when } x > \left(x_o + \frac{\varepsilon}{2}\right) \end{cases} \tag{9}$$

For the problem under consideration, the point load F and the distance x_o take the following relations:

$$F_v = b \int_{-\ell}^{\ell} \sigma(u)du, \text{ and} \tag{10}$$

$$x_o = vt \tag{11}$$

where: $\sigma(u)$ = normal stress distribution along the contact length (kN/m^2), ℓ = half contact length (m); b = tyre width (m), and u = distance ranges between $-\ell$ to ℓ (m). It can be noted that Eq. (10) implies that along tyre width b the stress distribution is uniform. Substituting Eqs. (10) and (11) into Eq. (8), the vertical load $F_v(t)$ is given as:

$$F_v(t) = F_v < x - vt >^{-1} = b \int_{-\ell}^{\ell} \sigma(u)du. < x - vt >^{-1} \tag{12}$$

where: x = the transverse coordinate measured from the tyre centre to a stationary reference (m), and F_v is the axial load on the wheel from the vehicle weight.

The simplification of a quasi-static assumption is to guarantee that the normal force F_v is constant, which in turn is not violated by the dynamical effects. Therefore, one can evaluate the snow dissipated energy using a simplified set of calculations. To calculate the snow dissipated energy, the normal stresses on the contact area must be calculated first. The normal stress distribution on the contact area is usually assumed as a parabolic shape according to Hertz contact theory as:

$$\sigma(u) = \frac{3F_v}{4\ell b}\left(1 - \frac{u^2}{\ell^2}\right) \text{ for } 0 \le u \le \ell \tag{13a}$$

$$\sigma(-u) = \sigma(u) \tag{13b}$$

where: F_v = the axial load on the wheel (kN). To simplify the calculation an average normal stress σ_{av} is suggested as follows

$$\sigma_{av} = \frac{F_v}{2\ell b} \tag{14}$$

When the vehicle moves a distance Δx, the energy dissipated in deforming a new undisturbed snow element takes the following form:

$$\Delta E_{snow} = \sigma_{av} b \delta_s \Delta x \tag{15}$$

where δ_s is the snow sinkage (m). Substituting Eq. (14) into (15) gives

$$\Delta E_{snow} = \frac{F_v \delta_s}{2\ell} \Delta x \tag{16}$$

Furthermore, if the vehicle moves from $x_o = 0$ to $x = x_1$, the total dissipated energy is given by

$$E_{snow} = \frac{F_v \delta_s}{2\ell} \int_0^{x_1} dx = \frac{F_v \delta_s}{2\ell} x_1 \tag{17}$$

Since $x_1 = vt_1 = (1 - S)\omega r t$, one obtains

$$E_{snow} = \frac{F_v \delta_s}{2\ell}(1 - S)\omega r t_1 \tag{18}$$

The corresponding dissipated power is given by:

$$P_{snow} = \frac{F_v \delta_s}{2\ell}(1 - S)\omega r \tag{19}$$

Tyre dissipated energy

The tyre dissipated energy can be calculated in a similar way to snow dissipated energy. The resultant equations obtained are:

$$E_{tyre} = \frac{F_v \delta_t}{2\ell}(1 - S)\omega r t_1 \tag{20}$$

$$P_{tyre} = \frac{F_v \delta_t}{2\ell}(1-S)\omega r \qquad (21)$$

where: δ_t = the tyre sinkage (m).

Useful energy

According to Eqs. (2), (3), (6), (19) and (21), the useful energy or power can be calculated as follows:

$$P_{use} = T_o\omega - \left[ST_o\omega + \frac{F_v\delta_s}{2\ell}(1-S)\omega r + \frac{F_v\delta_t}{2\ell}(1-S)\right]$$
$$= \omega(1-S)\left[T_o - \frac{F_v r}{2\ell}(\delta_t + \delta_s)\right] \qquad (22)$$

Traction efficiency

The traction efficiency h takes the following form:

$$\eta = \frac{P_{use}}{P_{in}} = (1-S)\left[1 - \frac{F_v r}{2\ell T_o}(\delta_t + \delta_s)\right] \qquad (23)$$

Draw-bar pull

It has been known that the useful power is given by the following

$$P_{use} = F_{DP} \times v \qquad (24)$$

where: F_{DP} = Drawbar pull (kN). Substituting Eq. (24) into Eq. (22), the draw-bar pull takes the following expression

$$F_{DP} = \frac{\omega(1-S)}{v}\left[T_o - \frac{F_v r}{2\ell}(\delta_t + \delta_s)\right]$$
$$= \frac{T_o}{r} - \frac{F_v}{2\ell}(\delta_t + \delta_s) \qquad (25)$$

The draw-bar pull presented by Eq. (25) is the force required to mobilize the traction forces minus the motion resistance of the wheel. It can be seen that as the input torque increased the draw-bar pull increased and the draw-bar pull is not a function of the slip rate. At a given constant tyre rotational velocity ω, the horizontal translation velocity v is affected by slip rate S. At $S = 0$, $v = \omega r$, while at $S = 100\%$, $v = 0$. Furthermore as the input torque on the wheel increases, the slip increases. At certain limit of torque values, the slip reaches 100% and the vehicle is not able to move because the soil loses its shear resistance. At the same time, the attached drawbar pull F_{DP} reaches maximum value at S = 100%. However, this force is "handicapped," with no ability to do any useful work (as the vehicle does not move). Based on such observation, it is wise to take the constant velocity ωr as observational base and express the useful power P_{use} as:

$$P_{use} = T_{TF} \times \omega r \qquad (26)$$

where T_{TF} = tractive force (kN), which is the force capable of doing useful work. Substituting Eq. (26) into Eq. (22), the following expression for the tractive force can be obtained

$$F_{TF} = (1-S)\left[\frac{T_o}{r} - \frac{F_v}{2\ell}(\delta_t + \delta_s)\right] \qquad (27)$$

It can be seen from Eq. (27) that when the slip rate equals zero, the tractive force reduces to the same expression presented by Eq. (25). Furthermore, when the slip rate equals 100%, the tractive force is reduced to zero.

3.0 PARAMETER CALCULATION

The following parameters: (1) half contact length (ℓ); (2) snow sinkage (δ_s); (3) tyre sinkage (δ_t), and (4) the slip rate (S) need to be calculated.

(1) Contact length

Since both the tyre and the soil are assumed to be deformable, curve AB, as shown in Fig. 1, is the resultant contact profile which represents a compatible displacement curve in the final state after the load F_v is applied. The curve AB depends on both tyre and soil compression characteristics. Two extreme cases as shown in Fig. 2 can be discussed: (1) the soil can be considered as a rigid surface, hence the resultant curve AB is a line as shown in Fig. 2a, and (2) if one considers the tyre as a rigid disk, the resultant curve AB is a part of the tyre circumference as shown in Fig. 2b. The real situation is somewhere in-between the two extreme cases.

Let us compare the contact length $2\ell_1$ (Fig. 2a) and $2\ell_2$ (Fig. 2b), in the case that the tyre size and the inflation pressure are the same but one is rigid terrain while the other is a deformed terrain. The conclusion can be reached that $2\ell_1$ is larger than $2\ell_2$. Since the terrain is deformable, it allows the tyre to sink more. The spring constant of two springs connected in series is always less than that of either spring taken individually. That is why one cannot just take the tyre compression test data to obtain the contact length without considering the terrain characteristics.

Hertz theory has been widely used to calculate the contact length by many authors. The subsequently obtained contact length, which based on presumed displacement field, yields the following approximate relation

$$\ell = \left[\frac{4F_v r}{\pi}\left(\frac{1-\nu_s^2}{E_s} + \frac{1-\nu_t^2}{E_t}\right)\right]^{\frac{1}{2}} \qquad (28)$$

where: E_s and E_t modulus of elasticity for soil and tyre

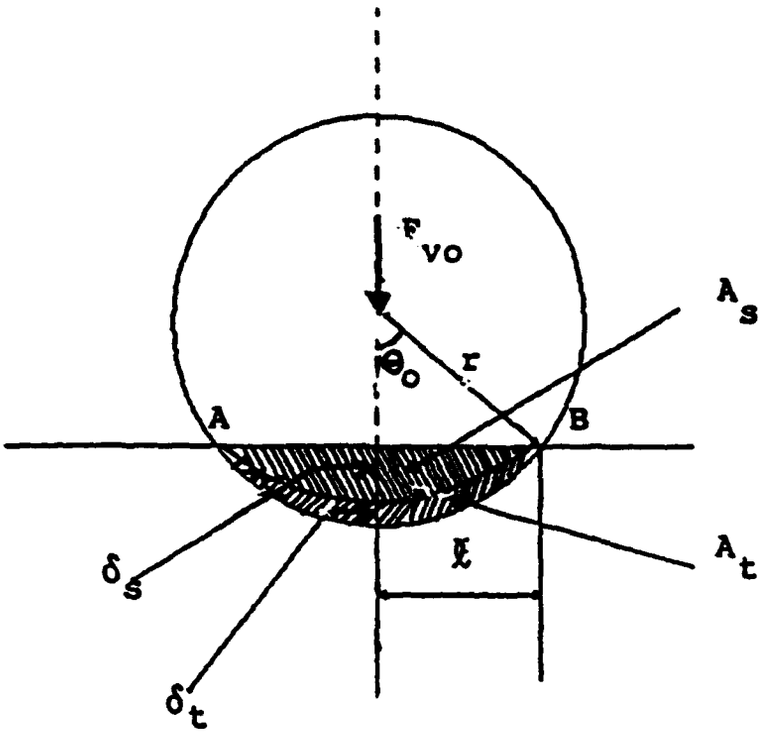

Figure 1. Geometric representation of soil and tyre compression areas.

tyre respectively. Since, neither soil nor tyre are elastic, one has to search for a new method to calculate the contact length based on both tyre and snow characteristics. The following highlights the technique used in this study to calculate the contact length.

From a rigid circular plate load test data on snow, one obtains a relationship between the vertical applied load, F_v, and the snow deformation, Δ_s. The theoretical relationships between snow deformation, Δ_s and the vertical applied load, F_v, can be represented by the following equation after Yong et al. (1990):

$$\Delta_s = \frac{1}{3}\left(\frac{\rho_c - \rho_o}{\rho_o}\right)\left(\frac{\sigma_p D}{c + \sigma_p \tan\phi}\right)\left(\frac{\sigma_p}{\sigma_c}\right)^{\frac{1}{k}} \qquad (29)$$

where: ρ_o = initial snow density; ρ_c = critical snow density; σ_p = stress distribution on the plate = $\frac{4F_v}{\pi D^2}$; D = plate diameter; σ_c = stresses at critical snow density; c, ϕ, and k = snow material parameters which can be

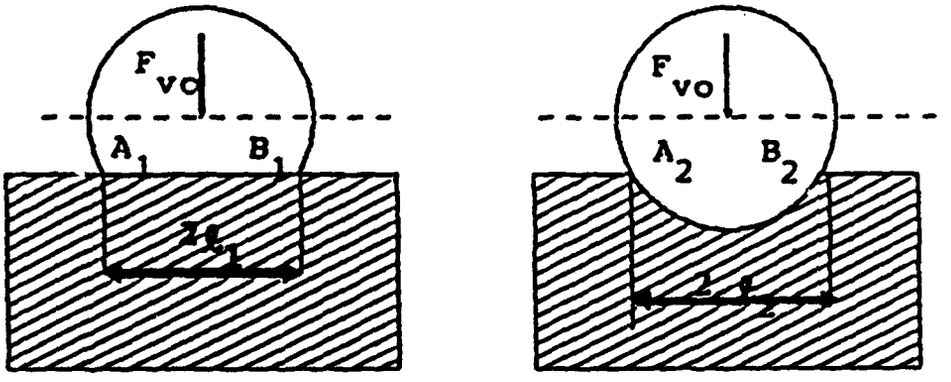

a. Contact length A_1B_1 for soft tyre and rigid terrain.

b. Contact length A_2 and B_2 for rigid tyre and soft terrain.

Figure 2. Schematic diagram showing contact length.

determined from Eq. 31 and the experimental relation between σ_p and Δ_s.

Since plate disk loading is different from rigid wheel type loading on a snow, transformation of plate type sinkage into wheel type sinkage has to be performed. After transformation, the final Δ_{so} takes the following form:

$$\Delta_{so} = \frac{2}{3}\left(\frac{\ell b}{\pi}\right)^{0.5}\left(\frac{\rho_c - \rho_o}{\rho_o}\right)\left(\frac{\sigma_t}{c + \sigma_t \tan\phi}\right)\left(\frac{\sigma_t}{\sigma_c}\right)^k \quad (30)$$

where: ℓ = half the contact length; b = tyre width; σ_t = average stress distribution on the contact length = applied load on the tyre/contact area; contact area = $2\ell b$. From experimental data on different types of snow, the following material parameters are assigned: $c = 3$ kPa; $\phi = 5.7°$, $\sigma_c = 423$ kPa; $k = 0.25$, and $\rho_c = 0.597$ Mg/m^3. It should be noted that these parameters are similar to those determined by Blaisdell et al. (1988). However, from the geometrical relation, Δ_{so} can be determined from the following relation.

$$\Delta_{so} = r - (r^2 - \ell^2)^{0.5} \quad (31)$$

To solve for the appropriate Δ_{so} numerically, an iteration technique is used. Given a firs. tried value $\ell = r$, from Eqs. 32 and 33, one determines two values for Δ_{so}, named $\Delta_{so}(1)$ and $\Delta_{so}(2)$. *Since ℓ is tried value,* $\Delta_{so}(1)$ is not equal to $\Delta_{so}(2)$. If $ABS[(\Delta_{so}(1) - \Delta_{so}(2))/\Delta_{so}(1)]$ is not less than 1%, then $\ell = \ell - d\ell$, where ℓ is a small value = $r/1000$. Such an iteration procedure will continue until the above comparative condition is satisfied. The corresponding ℓ and Δ_{so} are the solution.

(2) Tyre and soil deformations

As a vertical load F_V applied on the axis of a tyre, which is exerted through the vertical total weight, both tyre and snow will be deformed after contact. The total sinkage of the tyre, δ, can be determined. The detailed algorithm to calculate δ involves the following steps:

(a) from a tyre compression test data for a given tyre inflation pressure on a rigid surface, one obtains a relationship between the applied load, F_v, and the corresponding deformation of the tyre, Δ_t. By using a numerical interpolation method, the tyre deformation, Δ_{to}, which corresponds to the vertical load, F_{vo}, on the tyre to be modelled can be determined from the following relationship:

$$\Delta_{to} = \Delta_{ti} + \left(\frac{F_{vo} - F_{vi}}{F_{vi+1} - F_{vi}}\right)(\Delta_{ti+1} - \Delta_{ti}) \quad (32)$$

where: Fv_o = the vertical load between the two points i and $i + 1$. The tyre deformed area A_t, in a vertical cross section can be determined from the following relation as shown in Fig. 2a:

$$A_t = r^2(\theta_1 - \sin\theta_1 \cos\theta_1) \quad (33)$$

where: r = tyre radius; θ_1 = an angle which characterizes half contact length, which can be determined from the following relation

$$\theta_1 = \arccos\left(\frac{r - \Delta_{to}}{r}\right) \quad (34)$$

(b) from a rigid circular plate test data and Eqs. (30) and (31), Δ_{so} can be calculated. The snow deformed area, A_s, in a vertical cross section can be determined from the following relations as shown in Fig. 2b.

$$A_s = r^2(\theta_2 - \sin\theta_2 \cos\theta_2) \quad (35)$$

where: θ_2 = an angle which characterizes half contact length, which can be determined from the following relation

$$\theta_2 = \arccos\left(\frac{r - \Delta_{so}}{r}\right) \quad (36)$$

(c) in considering the real case whereby both the tyre and the snow are deformable, the total sinkage δ can be determined by considering Δ_{to} and Δ_{so} as representing the displacement of two springs connected in series. Once δ is obtained, the tyre sinkage, δ_t, and the snow sinkage, δ_t, can be determined according to the ratio of δ_t to δ_s. It should be noted that δ_t and δ_s are not Δ_{to} and Δ_{so} The relationship between A_s and A_t is given by

$$A = A_s + A_t = r^2(\theta_o - \sin\theta_o \cos\theta_o) \quad (37)$$

where: θ_o = an angle which characterizes half contact length as shown in Fig. 1. Based on the geometrical representation in Fig. 1, the following relationships can be obtained:

$$\ell = r\sin\theta_o \quad (38)$$

and

$$\delta = \delta_s + \delta_t = r - r\cos\theta_o = r - (r^2 - \ell^2)^{0.5} \quad (39)$$

Eq. (37) can be written as follows:

$$A = A_s + A_t = r^2\left(\theta_o - \frac{\sin 2\theta_o}{2}\right) \quad (40)$$

when θ_O is small

$$\sin 2\theta_o = 2\theta_2 - \frac{(2\theta_o)^2}{2} + \cdots, \text{and} \quad (41)$$

$$\cos\theta_o = 1 - \frac{\theta_o^2}{2} + \cdots \quad (42)$$

Substituting Eq. (41) into Eq. (40), the following relations can be obtained

$$A \approx r^2\left(\theta_o - \frac{1}{2}\left(2\theta_o - \frac{4\theta_o^2}{2} + \cdots\right)\right) \approx \theta_o^2 r^2 \qquad (43)$$

Substituting Eq. (42) into Eq. (39), the following relation can be obtained

$$\delta \approx r\left(1 - \left(1 - \frac{\theta_o^2}{2}\right)\right) \approx \frac{1}{2} r\theta_o^2 \qquad (44)$$

From Eqs. (43) and (44), the relationship between A and δ can be expressed as follows

$$A = 2r\delta \qquad (45)$$

Since A is proportional to δ, A_s and A_t can be assumed to be proportional to δ_s and δ_t respectively. The relationship can be written as follows:

$$\frac{A_s}{A_t} = \frac{\delta_s}{\delta_t} \qquad (46)$$

With the aid of Eqs. (37), (39), and (46) the snow and tyre deformed areas can be obtained as follows:

$$\delta_s = \frac{A_s}{A}\delta \qquad (47)$$

$$\delta_t = \frac{A_t}{A}\delta \qquad (48)$$

and

$$\delta = r - \left(r^2 - \ell^2\right)^{0.5} \qquad (49)$$

where: δ = total deformation due to tyre deformation, δ_t, and snow deformation, δ_s.

(3) Slip rate, S

In the original sense, slip rate S is defined as represented by Eq. (7). If the rotation of the tyre is completely transferred to a horizontal motion, $v = \omega r$ and $S = 0$. This situation requires that snow is very stiff. However, in case of fresh snow, a backward movement of the snow takes place due to the induced shear stresses. In order to calculate the slip rate direct shear tests on the specified snow are required. The reduction of data from direct shear test into slip rate of a tyre can be proceed as follows:

(a) For a circular sample in a direct shear test, the sheared area i.e. the contact area can be expressed as:

$$A_{sh} = \frac{\pi}{4} d_{sh}^2 \qquad (50)$$

where: A_{sh} and d_{sh} = cross sectional area and diameter for the tested sample in the direct shear test.

(b) The equivalent contact length, L, for a tyre with width (b) is:

$$L = \frac{\pi d_{sh}^2}{4b} \qquad (51)$$

(c) Assuming that a wheeled vehicle moves a circumferential distance L during the forward movement of the vehicle, a horizontal backward movement U of the snow due to shear stresses is induced. The slip rate S can then be obtained as follows:

$$S = \frac{U}{L} = \frac{4Ub}{\pi d_{sh}^2} \qquad (52)$$

(d) Eq. (52) is valid only for smooth tyres. To include the effect of treads, one has to calculate the effect of snow-snow and rubber-snow contact and their ratios. Since, the tyre has a unique shear displacement, U, the following condition has to be satisfied

$$\xi_s \tau_s + \xi_r \tau_r = \tau_{av} \qquad (53)$$

where: τ_{av} = average shear stress on the contact area which is given by

$$\tau_{av} = \frac{T_o}{2b\ell r}; \qquad (54)$$

ξ_r and ξ_s = fractions of treaded and nontreaded areas respectively, and τ_r and τ_s = the developed shear stresses at the contact areas for rubber-snow and snow-snow respectively.

(e) From direct shear experimental data, the relationships between τ_s vs U_s and τ_r vs U_r can be obtained and represented by the following relationships:

(1) Snow-snow condition

$$\frac{\tau_s}{\tau_{smax}} = \begin{cases} \left(\dfrac{U_s}{U_{smax}}\right)^a & \text{for } U_s < U_{smax} \\ 1 & \text{for } U_s \geq U_{smax} \end{cases} \qquad (55)$$

where a = a positive number, and τ_{smax} = maximum shear strength. If τ_s is beyond τ_{smax} the snow is considered to be in a state of shear failure. From experimental data, the following empirical formulas are obtained:

(a) parameter, a

$$a = 0.7 - 2.0\left(\frac{\rho_o - 0.025}{\rho_c}\right) \qquad (56)$$

(b) maximum horizontal backward movement, U_{smax}

$$U_{smax} = 20.0 - 76.0\,(\rho_o - 0.25) \qquad (57)$$

where: U_{smax} in mm and ρ_o in Mg/m^3

(c) maximum shear strength τ_{smax}

$$\tau_{smax} = 40.0 - 2.5\,(\rho_o - 0.25) + 3.5\sigma_n \qquad (58)$$

where: σ_n = the normal stress in kPa.

(2) Snow-rubber condition

Rubber material at the tyre contact with snow appears to have different characteristics compared with the snow-snow contact case. The most obvious differences is that the shift shearing displacement, U_r, is small at the initial stage of loading. As shear load increases, shear failure occurs at relatively lower shear stress, τ_r. These data show that the $\tau_r - U_r$ curves are very sharp. Since the tread effect must be considered in the mobility evaluation, this type of contact is as important as snow-snow contact. The test data were analyzed to yield the general empirical formula as follows:

$$\frac{\tau_r}{\tau_{rmax}} = \begin{cases} 127.29\dfrac{U_r}{\sigma_n} & \text{for } \tau_r < \tau_{rmax} \\ 1 & \text{for } \tau_r \geq \tau_{rmax} \end{cases} \qquad (59)$$

where: $\tau_{rmax} = 0.5265\sigma_n$; σ_n = normal stress in kPa.

(f) for tyre movement on snow the total backward movement U is equal to both U_s and U_r, i.e.

$$U = U_s = U_r \qquad (60)$$

The shift displacement, U, is calculated by using iteration method as a numerical technique. This can be explained as follows: Given an initial value of U, which should be a small value, let us say $U = 0.001$ mm, τ_s, τ_r and τ_{av} can then be calculated from Eqs. (55), (59), and (54) respectively. The iteration procedures will be continued with new values of $U = U + dU$, where dU = a small increment, until the following criteria satisfied.

$$\left| \frac{\xi_s\tau_s + \xi_r\tau_r - \tau_{av}}{\xi_s\tau_s + \xi_r\tau_r} \right| < 1\% \qquad (61)$$

The slip rate, S, can then be calculated from Eq. (52).

4.0 COMPUTER SIMULATION

A computer program named "TR89SNOW" has been developed for the wheeled vehicle mobility evaluation over a deep snow. An example is given here to show the simulation results.

Table 1 shows the input parameters and tyre specification. The tyre used in this study is Michelin 7.0 (treaded). The initial snow density is 0.34 Mg/m^3. Figure 3 pictorially shows the tyre size and loading conditions.

Table 2 and Fig. 4 show the tyre compression test data on a rigid surface for a specified inflation pressure. This was done at the Geotechnical Research Centre of McGill University. Furthermore, Fig. 5 and Fig. 6 show the snow footing curves and the snow shearing curves respectively. These curves were obtained from the analyzed formula demonstrated in material parameters determinations. The physical results are presented in Table 3. These results are produced for a specified

****
* Input data *
****

a) Constant Parameters:
Tyre name=Michelin 7.0(treaded)
Tyre inflation pressure= 34.50(Kpa)
Snow initial density=0.34(Kg/m3)

Table 1: Parameters

Param.	R	d	R1	R2	P0	T0	OMEGA
Value	0.39(M)	0.20(M)	0.400	0.600	1.60(KN)	0.14(KN-M)	0.78(rad/s)

Note:R1,R2-area ratios of tread & nontread parts of tyre, respectively

Figure 3. Tyre size and loading conditions.

b) Tyre compresion test data:
(Tests are done in GRC.)

Table 2:P-L & P-delta data

NO.	P(KN)	L(M)	delta(M)
1	0.00	0.000	0.0000
2	0.43	0.069	0.0062
3	0.70	0.093	0.0113
4	1.00	0.112	0.0165
5	1.30	0.126	0.0210
6	1.60	0.142	0.0270
7	1.90	0.150	0.0300

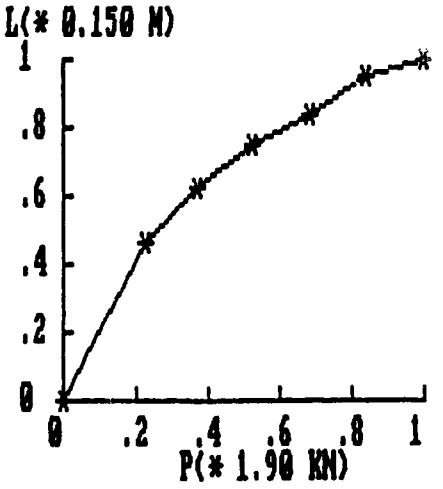

Figure 4. P–L *curve of tyre.*

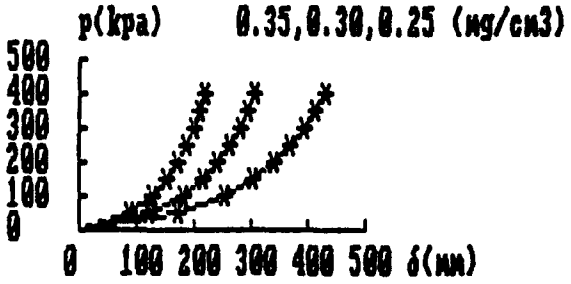

Figure 5. Snow footing curve.

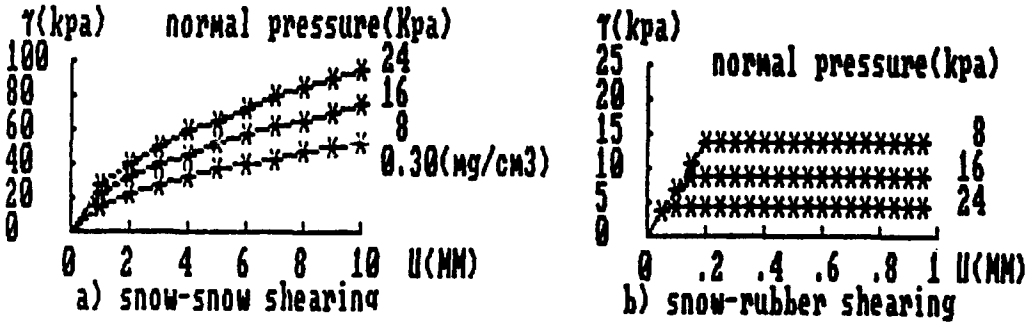

Figure 6. Snow shearing curves.

Table :3 Physical results

Slip rate	slip	3.820 (%)
Input power	P1	0.109 (KN-M/s)
Slip dissipated energy	P2	0.004 (kN-M/s)
Snow dissipated energy	P3	0.05683 (KN-M/s)
Tyre dissipated energy	P4	0.022 (KN-M/s)
Useful power	P5	0.026 (KN-M/s)
Tractive efficiency	ETA	24.077 (%)
Draw-bar pull	DP	0.007 (KN)

For same tyre & loading conditions on the same soil, for other data points request, procedure continues by specifying new torque.

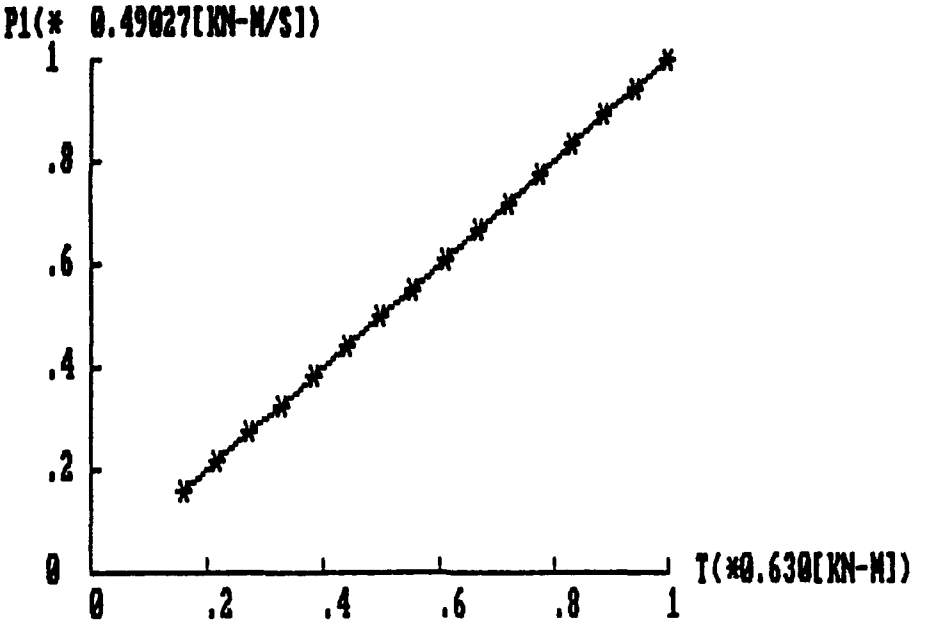

Figure 7. Input power P_1 *versus torque* T.

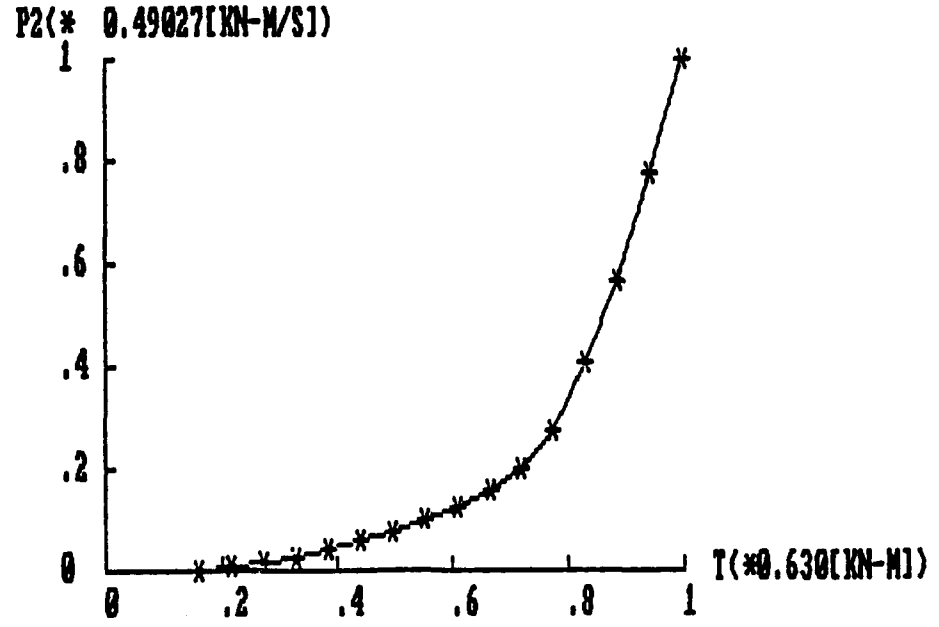

Figure 8. Slip dissipated power P_2 *versus torque* T.

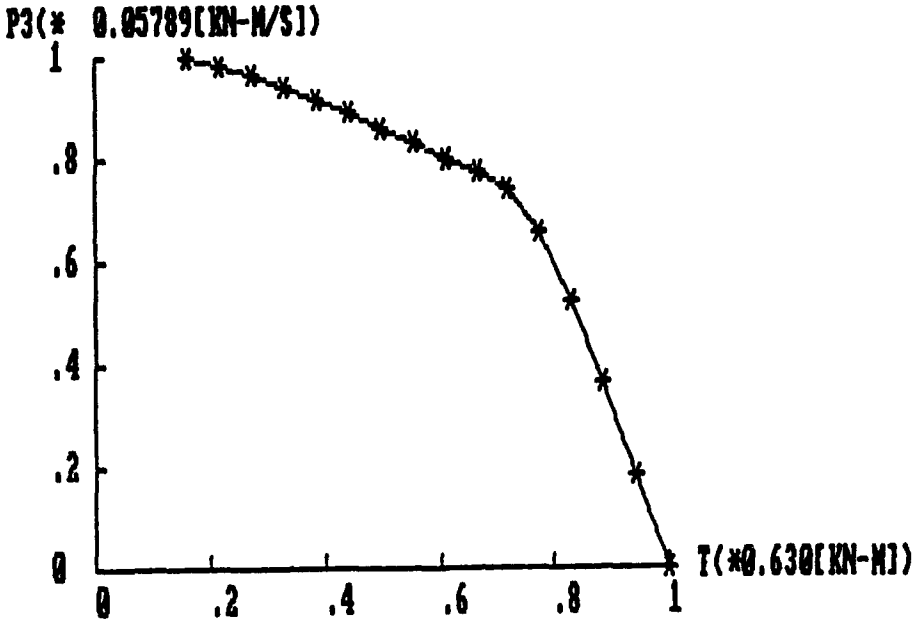

Figure 9. Soil dissipated power P_3 *versus torque* T.

torque value. If the applied torque T varies, one will be able to obtain more computational results. In program "TR89SNOW" this is judiciously programmed so that torque T varies properly. The calculated change of power P_1 P_2, P_3, P_4 and P_5 with the increased torque T are presented in Figs. 7–11. The change of tractive efficiency η, slip rate S and draw-bar pull DP with torque T are presented in Figs. 12 to 14. From Fig. 12, one concludes that the highest tractive efficiency η is about 57%, which is at torque $T = 0.36$ KN.m. From Fig. 13, one observes that slip rate S sharply increases with increased torque T. The maximum DP is about .65 kN at $T = .42$ KN.m as shown in Fig. 14.

The relation between η and S is presented in Fig. 15. It is noted that the best tractive efficiency occurs at slip rate, S, around 20%. When the slip rate increases, the tractive efficiency decreases quickly.

The relation between motion resistance MR and the driving force TR is presented Fig. 16. With an increase in driving force, the motion resistance MR increases. It is clearly evident that a high driving force is not good for the vehicle driving since the resistance increases in an exponential manner.

The relations betweer P_1, P_2, P_3 and slip, S are presented in Fig. 17. One notices the following: 1) the slip rate dissipated power is more harmful, and 2) high tractive efficiency occurs at slip rate (S) around 20%.

5.0 CONCLUSION AND REMARKS

The present model is a sound tool to investigate the vehicle mobility over a snow covered road, offering a great deal of information to vehicle engineers. The model not only answers the basic question that the vehicle can or cannot go over a snow covered road, but also gives detailed information as to how it can achieve the best benefit according to the payload requirement. This model is easy to use in a personal computer. Any parameters can vary to visualize the adequate change which brings the vehicle designer the best benefit.

The following points are under investigation at the

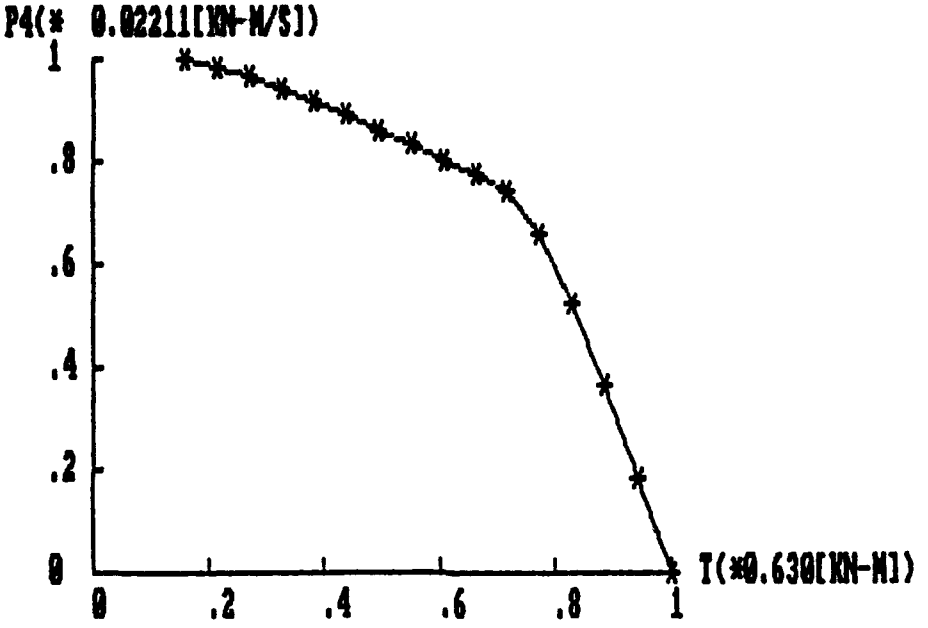

Figure 10. Tyre dissipated power P_4 *versus torque* T.

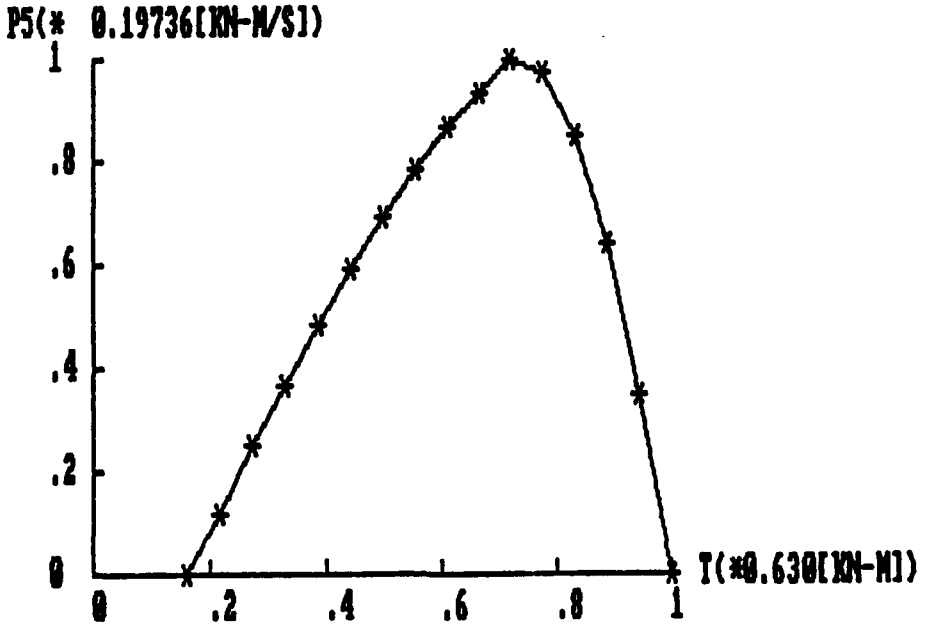

Figure 11. Remain useful power P_5 *versus torque* T.

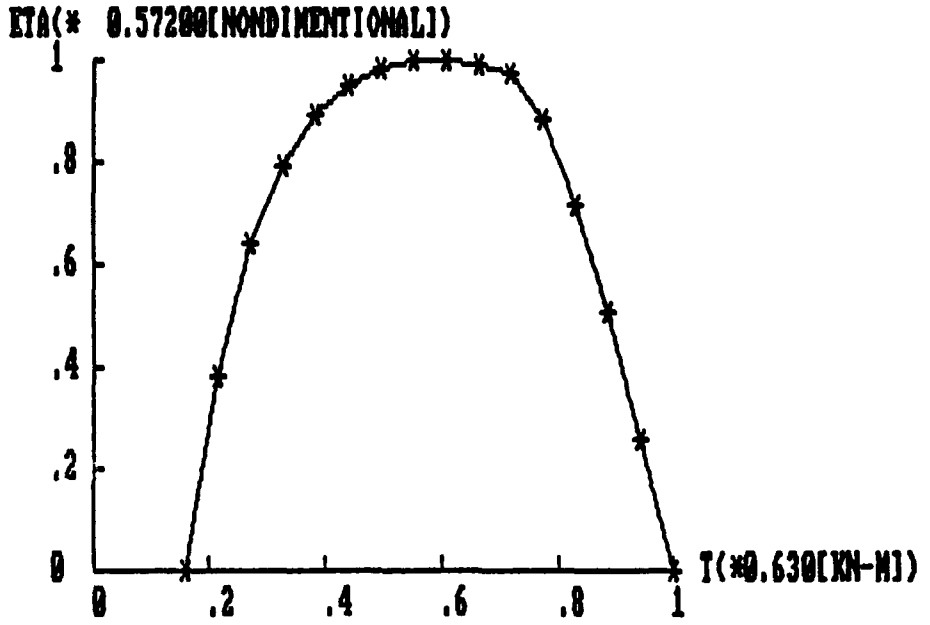

Figure 12. Tractive efficiency ETA *versus torque* T.

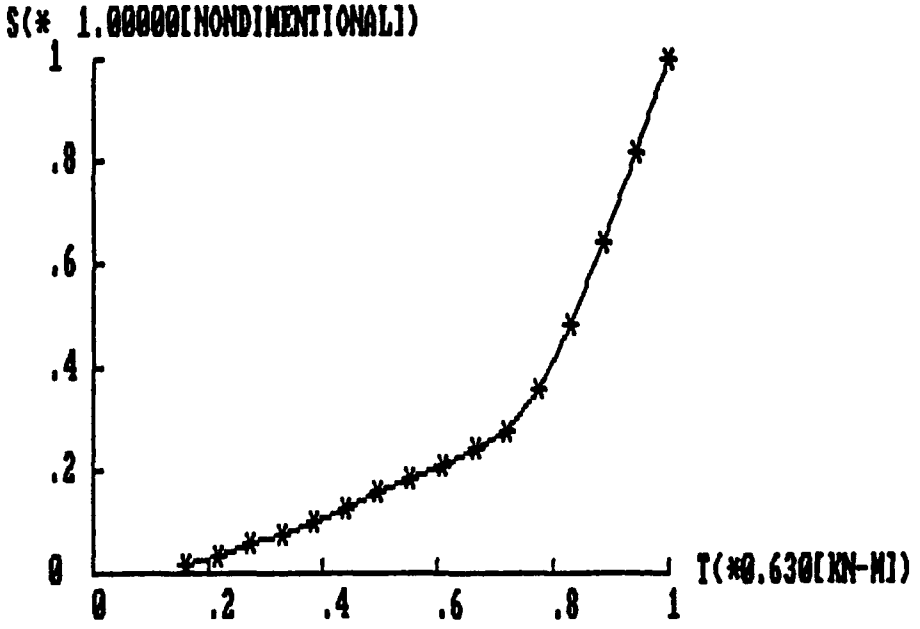

Figure 13. Slip rate S *versus torque* T.

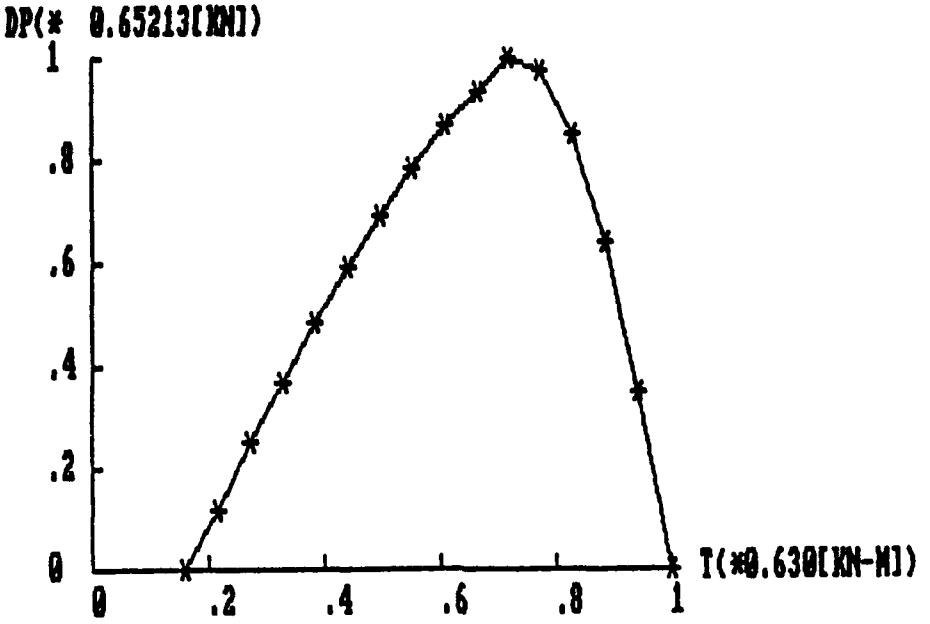

Figure 14. Draw-bar pull DP *versus torque* T.

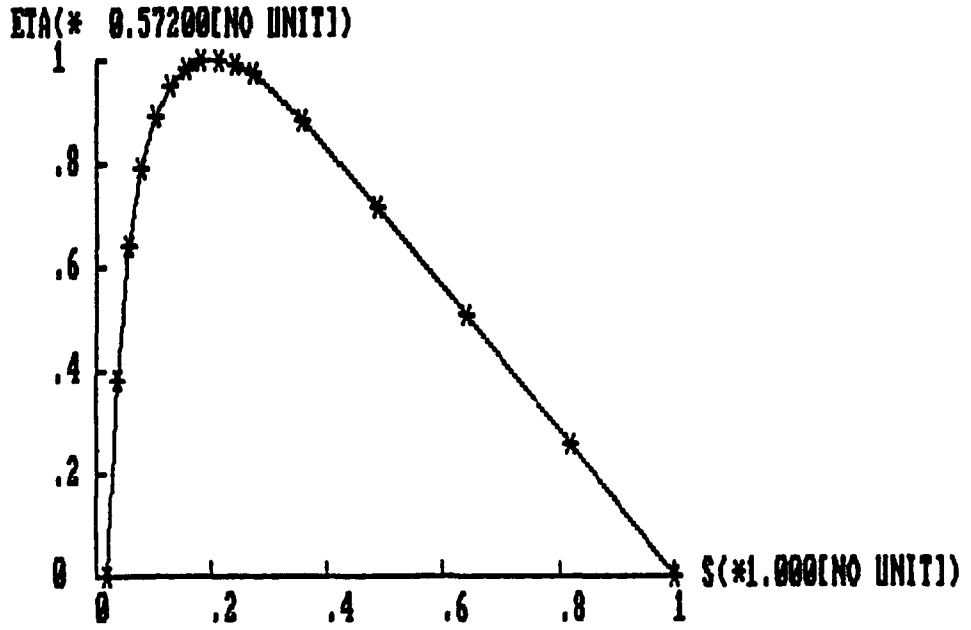

Figure 15. Tractive efficiency ETA *versus slip rate* S.

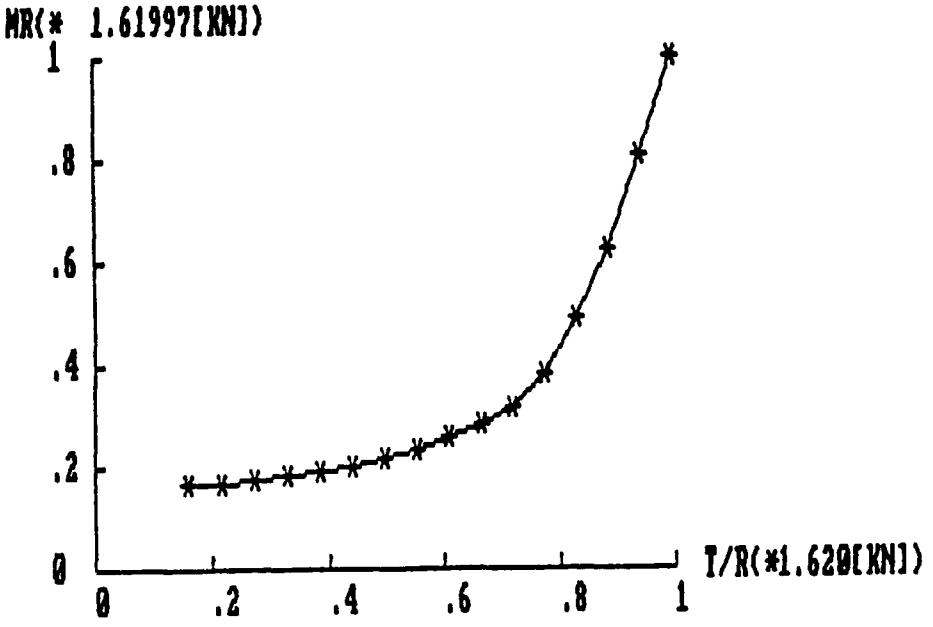

Figure 16. Motion resistance MR *versus driving force* T/R.

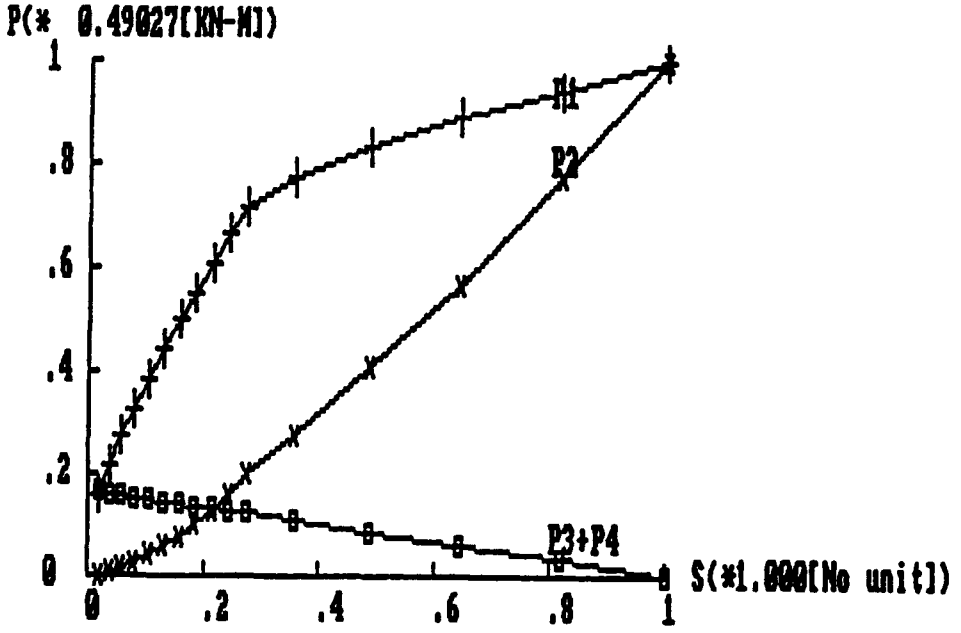

Figure 17. Power versus slip rate S.

Geotechnical Research Center to enhance the model capability:

(a) a field snow compression test under loading of the rigid tyre-shaped disk.

(b) dynamical effect and the road roughness effects will be considered in the further development of the model.

(c) upgrading TR89SNOW to predict the performance of the whole wheeled vehicle. This can be achieved by taking into consideration vehicle axle/wheel configuration and the difference between driving and towed wheels.

(d) calibration of the developed wheeled-vehicle model with the actual field data of an instrumented wheeled vehicle in measured snow conditions.

ACKNOWLEDGMENTS

The work performed in this study was in partial fulfillment of the study requirements for Defence Research Establishment Suffield (DRES) under contract arrangement with Department of Supply and Services (DSS), Canada.

LITERATURE CITED

Blaisdell, G.L., Richmond, P.W., Green, C.E., and Alger, R.G. (1988) "Wheels and Tracks in Snow (Validation Study of the Shallow Snow Mobility Model)" Report, CRREL and WES, Hanover, New Hampshire.

Xu, D.M., Yong, R.N., Mohamed, A.M.O., and Irwin, G.J. (1990) "Tyre Performance Prediction Using a Quasi-Static Moving Boundary Displacement Method" Proceedings of the IASTED International Symposium Modelling, Simulation and Optimization, Montreal, Canada, May 22-24, ed. Jacyno, 2. pp. 107-110.

Xu, D.M., Yong, R.N., and Mohamed, A.M.O. (1991) "Modeling of Tyre-Clay Soil Interaction Via Quasi-Static Moving Boundary Displacement Method" J. of Forest Engineering, Vol. 2, No. 2., pp. 7-19.

Yong, R.N., and Webb, G.L. (1969) "Energy Dissipation and Drawbar Pull Prediction in Soil-Wheel Interaction" Proc. 3rd Int. Conf. ISTVS, Essen, Vol. 1,

Yong, R.N., and Fattah, E.A. (1976) "Prediction of Wheel-Soil Interaction and Performance Using The Finite Element Method" J. Terramechanics, Vol 13, No. 4, pp. 227-240.

Yong, R.N., Fattah, E.A., and Boonsinsuk, P. (1978) "Analysis and Prediction of Tyre-soil Interaction and Performance Using Finite Elements" J. Terramechanics, Vol. 15, No. 1, pp. 43-63.

Yong, R.N., Boonsinsuk, P., and Fattah, E.A. (1980) "Tyre Load Capacity and Energy Loss with Respect to Varying Soil Support Stiffness" J. Terramechanics, Vol. 17, No. 2, pp. 131-147.

Yong, R.N., Mohamed, A.M.O., and Xu, D.M. (1990) "Correlation of Snow Trafficability with the Physical Properties and Conditions of Deposited Snow" Defence Research Establishment Suffield, DSS file No. 0-3SG.27702-6-02884. P. 84.

The Army MANPRINT Program and Its Relationship To Industry

DAVID A. SLOSS AND MICHAEL A. KRIZ
Emerging Systems, Concepts and Planning Directorate
U.S. Army Tank-Automotive Command
Warren, Michigan 48397-5000

MANPRINT DEFINITION

MANPRINT is an Army term which refers to the comprehensive technical effort to assure total system effectiveness by integrating into the materiel development and acquisition process all information concerning:

a. Manpower—The human resource requirements and authorizations needed to operate, maintain, and support an item of hardware.
b. Personnel—The aptitudes, experience, and other human physical and mental characteristics required to operate, maintain, and support equipment.
c. Training—The instruction, time, and other resources necessary to impart the requisite knowledge, skills, and abilities to qualify personnel for operation, maintenance, and support of fielded equipment.
d. Human Factors Engineering—Designing materiel to ensure that its use is compatible with the capabilities of the individual soldier in an operational environment.
e. System Safety—The attainment of the optimum degree of safety consistent with mission requirements.
f. Health Hazards—Applying medical knowledge to identify, evaluate, and control risks to the health and effectiveness of the personnel who use the equipment.

The objective is to ensure that Army systems can be operated and maintained by the fully equipped soldier within stated mental and physical limits; i.e., the "target audience description." It is up to the Army and industry to take the actions necessary to ensure that this question is answered: Can the soldier, with this training, perform these tasks, to these standards, under these conditions?

RELATIONSHIP TO INDUSTRY

MANPRINT success depends on the combined efforts of specialists in the Army and industry. Although they each have their own responsibilities, their interests mesh in the communication on MANPRINT requirements and the development of design solutions. The Army must articulate its MANPRINT goals and constraints throughout the acquisition process, and industry must strive to deliver products that will compensate for the finite capabilities of soldiers and training bases. Chart 1 depicts the MANPRINT crosswalk/relationship between the Army and industry for developmental systems. The Training and Doctrine Command (TRADOC) represents the soldier or "market." The Army Materiel Command (AMC) is the system developer or manager. The builder or producer of the system is industry. TRADOC develops a statement of needs, AMC interprets the needs into technical terms for industry which proposes a design, schedule, and cost. Note: There is extensive interaction between the Army and industry throughout the acquisition process.

MANPRINT is also an important element in the acquisition of nondevelopmental (NDI) systems, in which the government does not pay research and developmental costs. During the search for a NDI solution, the market investigation, the Army identifies potential MANPRINT problems and addresses them in detail in the requirements documents, solicitations, and in the user criteria portion of the market investigation. The Army then uses the MANPRINT data obtained from the market investigation to influence the selection of items or components to be assembled, the design of any modifications, and the integration of the components. This is true even for "off-the-shelf" items.

MANPRINT is a critical element in the Source Selection Evaluation Process. Offerer's proposals are evaluated on:

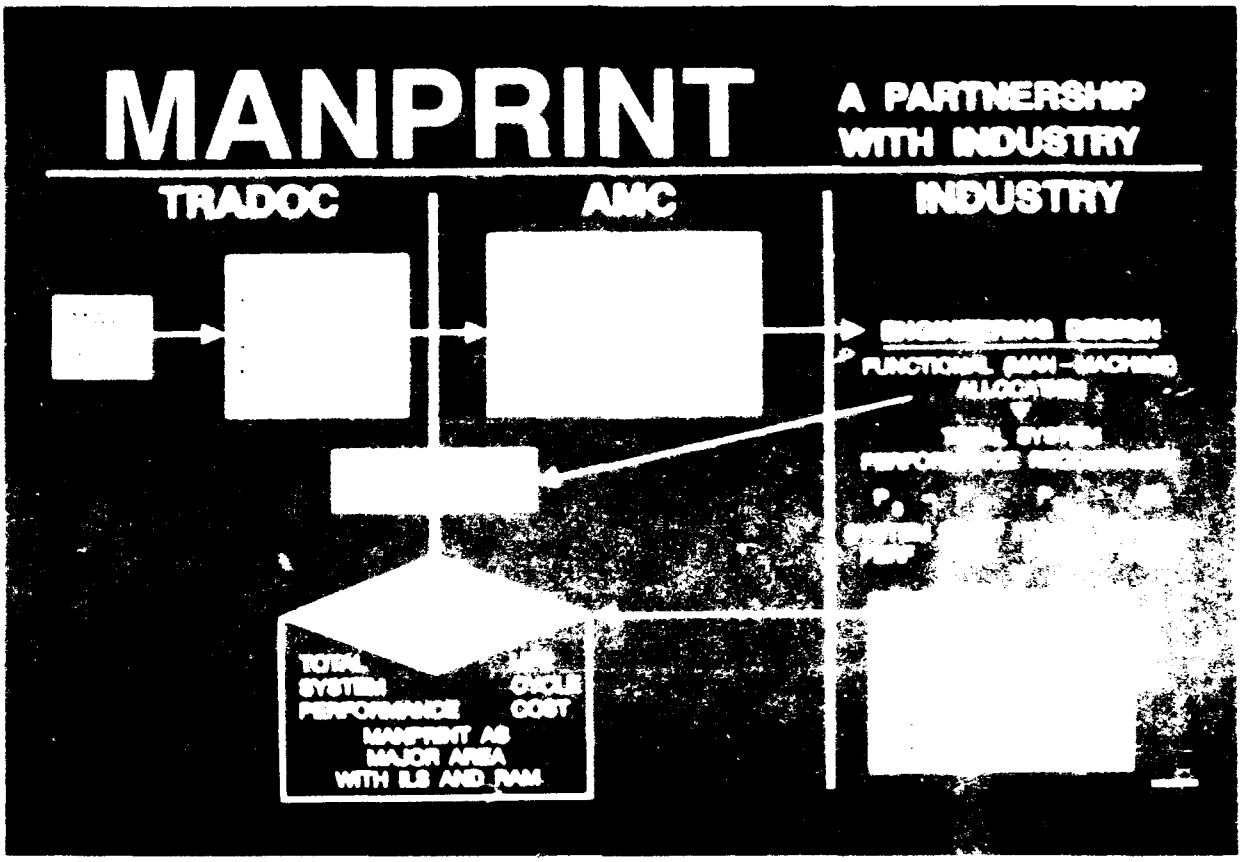

CHART 1

a. The ability of a contractor to integrate MANPRINT related alternatives, constraints, and analysis results.

b. The proposed methods by the contractor to document and report MANPRINT related alternatives, trade off analyses and design implications.

Industries that have no intention or desire to do business with the Army can still benefit from MANPRINT methodology. Essentially, the process examines how well a product can be used and supported. The problems that the general public has had with programming VCRs are a good example of industry's failure to understand the capabilities of its "target audience." It has been stated that less than 30% of VCR owners are capable of programming their equipment to record a television program.

METHODOLOGY TO SUPPORT MANPRINT

The Army developed a computerized MANPRINT analysis called "HARDMAN." HARDMAN is an analytical tool which predicts the quantitative manpower, personnel, and training demands required to support a developmental system. All of these elements are significant cost drivers. This type of analysis is normally performed in the concept phase of a program and is usually combined with an "Early Comparability Analysis" (ECA). ECA feeds HARDMAN by examining the "higher driver" or resource intensive manpower, personnel, and training tasks that were associated with the predecessor system(s). The product of these two processes is quantified data that provides decision makers with information on competing proposals that allows them to assess the impact of manpower, personnel, and training requirements on system effectiveness, supportability, and life-cycle costs. The Army's HARDMAN methodology (hardware versus manpower) is illustrated in Chart 2.

MANPRINT AND OPERATIONS AND SUPPORT (O&S) COSTS

There is a major effort in the Army to reduce O&S costs by "up-front" analysis and planning. The reason for this emphasis is shown in Chart 3. By the time we have completed the Concept Formulation Process (CFP) program documentation, we have built in about 70 percent of the system's life cycle costs.

HARDMAN METHODOLOGY

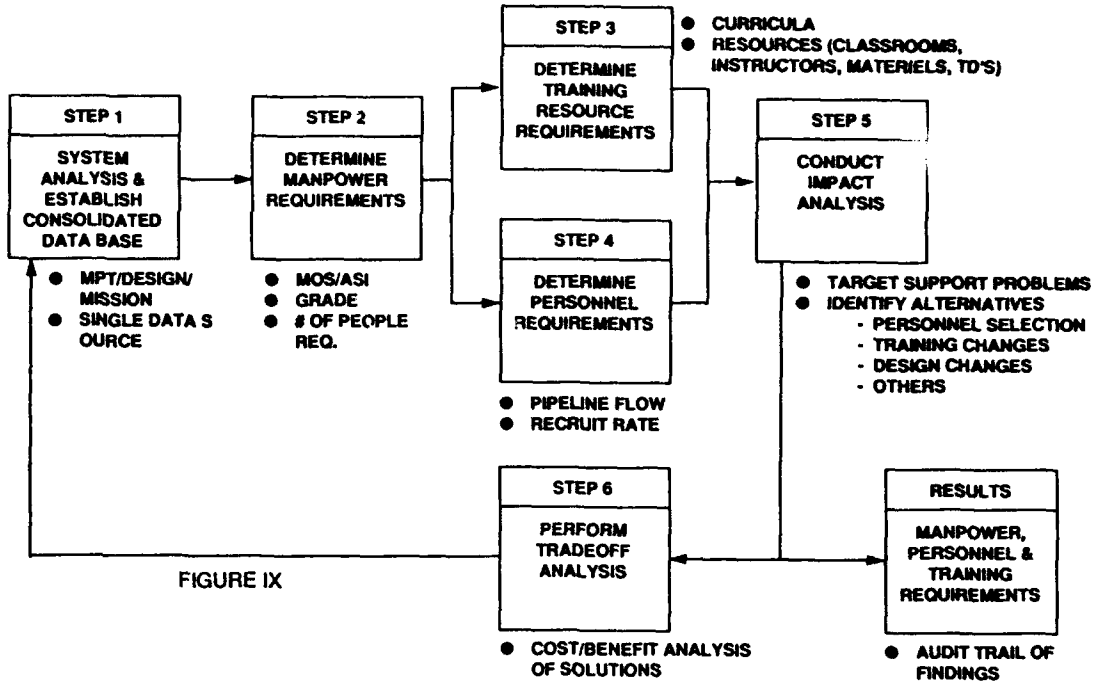

FIGURE IX

CHART 2

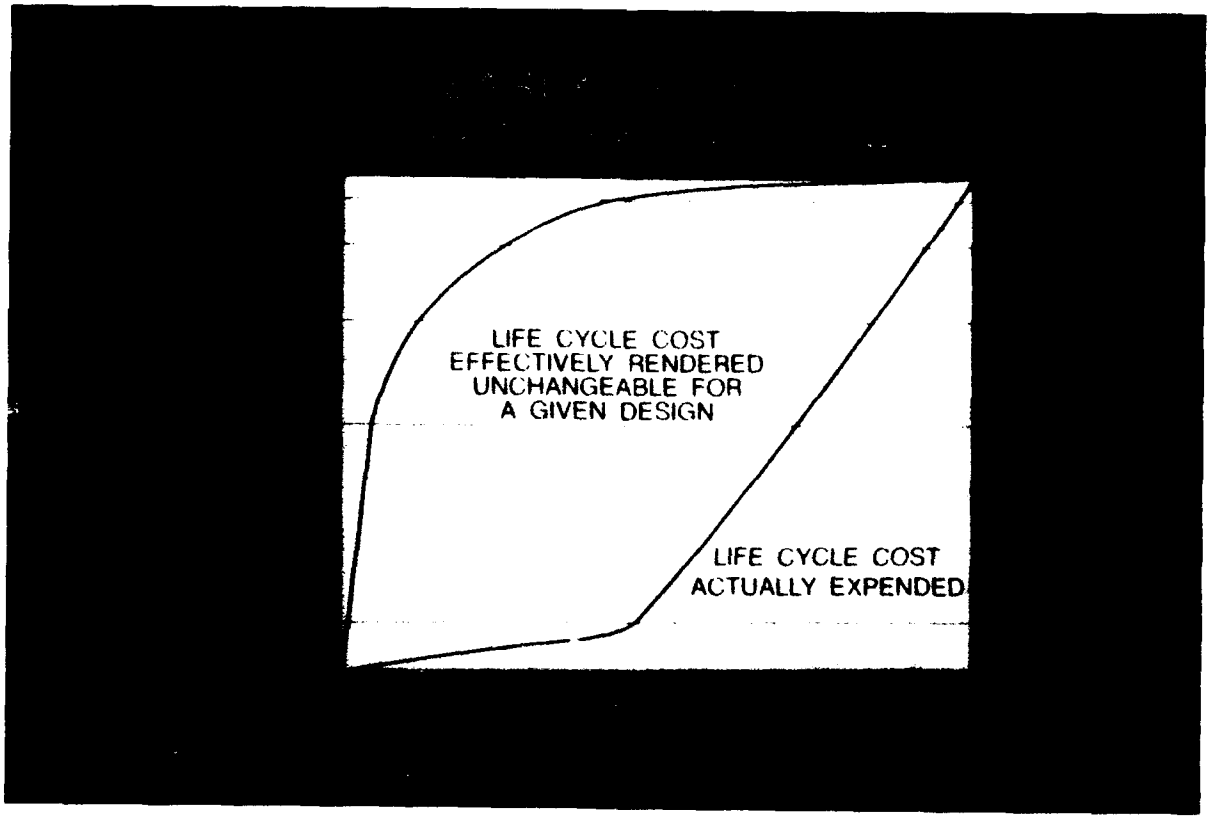

CHART 3

There are several studies which show that a problem that can be corrected for a dollar in the concept stage will cost between $1,000 and $10,000 to correct in the production stage. From this perspective, an unparalleled opportunity exists in the initial phases of a program to save an enormous amount of money. This can also translate into higher potential profits for industry.

MANPRINT is the Army's effort to control one of the major O&S cost drivers—personnel. The up-front planning document for MANPRINT is the System MANPRINT Management Plan (SMMP). The SMMP identifies the important MANPRINT issues anticipated in the system acquisition and functions as an audit trail to record decisions affecting these issues. The SMMP will be discussed in detail later. In general, the SMMP is used to plan for the acquisition of soldiers needed to operate and maintain a system; to plan for resources needed for required training; and to predict the amount of time needed to complete maintenance and mission support activities. All of these aforementioned resources affect the life-cycle costs (LCC) of the item. For industry, this translates into lower warranty costs and added value for the customer.

MANPRINT PLANNING

The Army SMMP provides the strategy to be employed in implementing the MANPRINT concept for a specific system. The SMMP considers the materiel deficiency being addressed, mission, operational environments, design versions or alternatives, and essential total system (Man in the Loop) performance characteristics.

The SMMP is updated at each system review point and serves as an audit trail of all of the decisions made which will have a direct impact on the system design and/or MANPRINT issues. The plan also identifies all assumptions being made which are not documented elsewhere. For example, the average soldier operating the present system is mental category IIIB*; therefore, the average soldier operating the new system will also be mental category IIIB.

A critical element of MANPRINT planning is a determination of what data will be available to support the associated analysis activities and a corresponding risk assessment. The risk assessment includes the impact of the level of MANPRINT effort and when the various analyses are to be conducted based on the availability of data and resources.

Planning activities include a comprehensive MANPRINT schedule showing what is to be done by whom from research exploratory development through first-unit-equipped. The "what is to be done" is documented with Task Descriptions.

Task Descriptions list the following information:

a. Task Description (narrative)
b. Rationale (why is it necessary)
c. Resources (personnel and dollars)
d. Time to Complete (optimistic, normal, pessimistic)
e. Responsible Agency (lead agency)
f. Dependencies (prior tasks which must be completed first)
g. Feeds (tasks requiring completion of this task first)

There are other aspects to the SMMP; however, this overview demonstrates the complexity of the effort; the commitment by the Army; and the potential payoff to the Army and potentially to industry.

MANPRINT AS PART OF THE ARMY MATERIEL ACQUISITION PROCESS

MANPRINT is only one of a number of activities that occurs before a commitment is made to allocate development or procurement dollars. Chart 4 shows the acquisition documentation required to initiate a program. Each of the 73 documents shown forms the basis for contractual requirements. Specific documents relating to MANPRINT are:

a. System MANPRINT Management Plan (SMMP)
b. Manpower, Personnel & Training (MPT) Assessment
c. System Safety Assessment Report (SSAR)
d. Human Factors Engineering Assessment (HFEA)
e. Health Hazard Assessment Report (HHAR)
f. MANPRINT Assessment (MA)

The total acquisition process which is a process where the soldier's need is defined and a solution developed. The process is depicted in Chart 5. At program initiation, the "environment" in which the system is initiated is considered, as is the total program life cycle that ends at system upgrade or disposal. The purpose is to insure that a process is set in motion to develop all necessary information for a future "business" decision consistent with today's technology, policies, and legal prerequisites. It is essential that this "up-front" work be done as thoroughly as possible, or a penalty will be paid throughout the life cycle of the system.

Each phase of the life cycle—definition of what is needed; development of a solution; production and support of the system; and improvement or replacement—has distinctive documentation. The Operational and Organizational (O&O) Plan developed by the soldiers provides the authority for program initiation. The plan describes how a system operates, its role in the

AD-A271 946 FIRST INTERNATIONAL CONFERENCE ON WINTER VEHICLE MOBILITY SANTA BARBARA CALIFORNIA JUNE 1991(U) COLD REGIONS RESEARCH AND ENGINEERING LAB HANOVER NH

UNCLASSIFIED G L BLAISDELL JUL 93 93-17 XA-CRREL NL

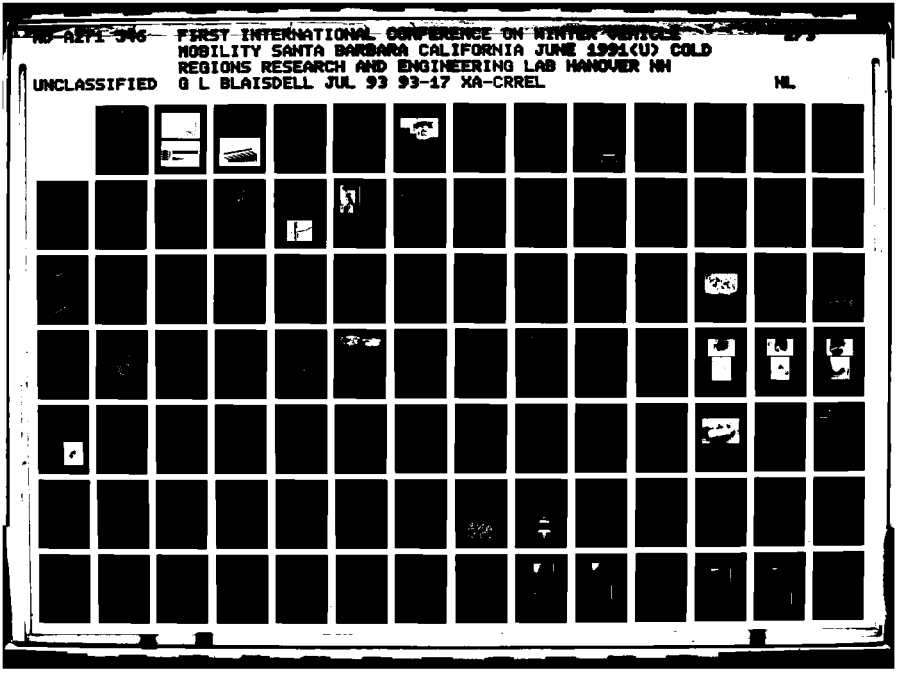

Association for Information and Image Management

1100 Wayne Avenue, Suite 1100
Silver Spring, Maryland 20910

301/587-8202

Centimeter

1 2 3 4 5 6 7 8 9 10 11 12 13 14 15 mm

1 2 3 4 5

Inches

MANUFACTURED TO AIIM STANDARDS
BY APPLIED IMAGE, INC.

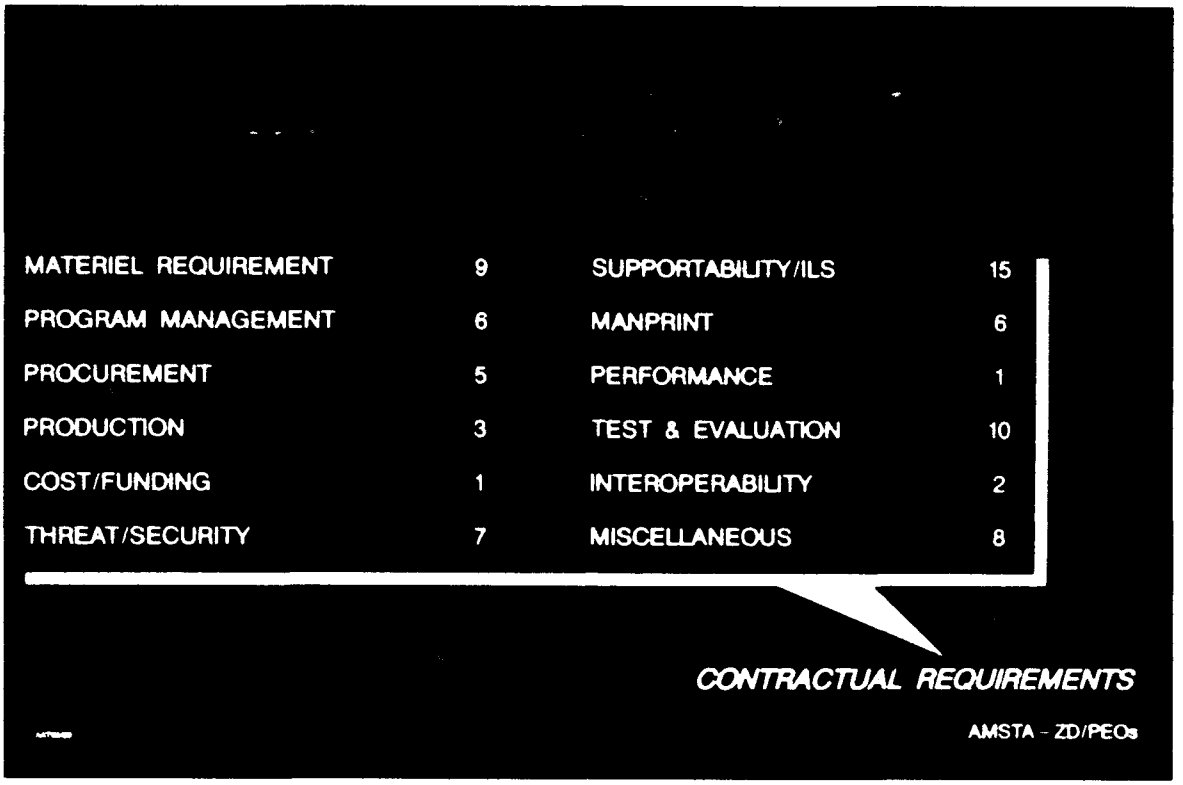

CHART 4

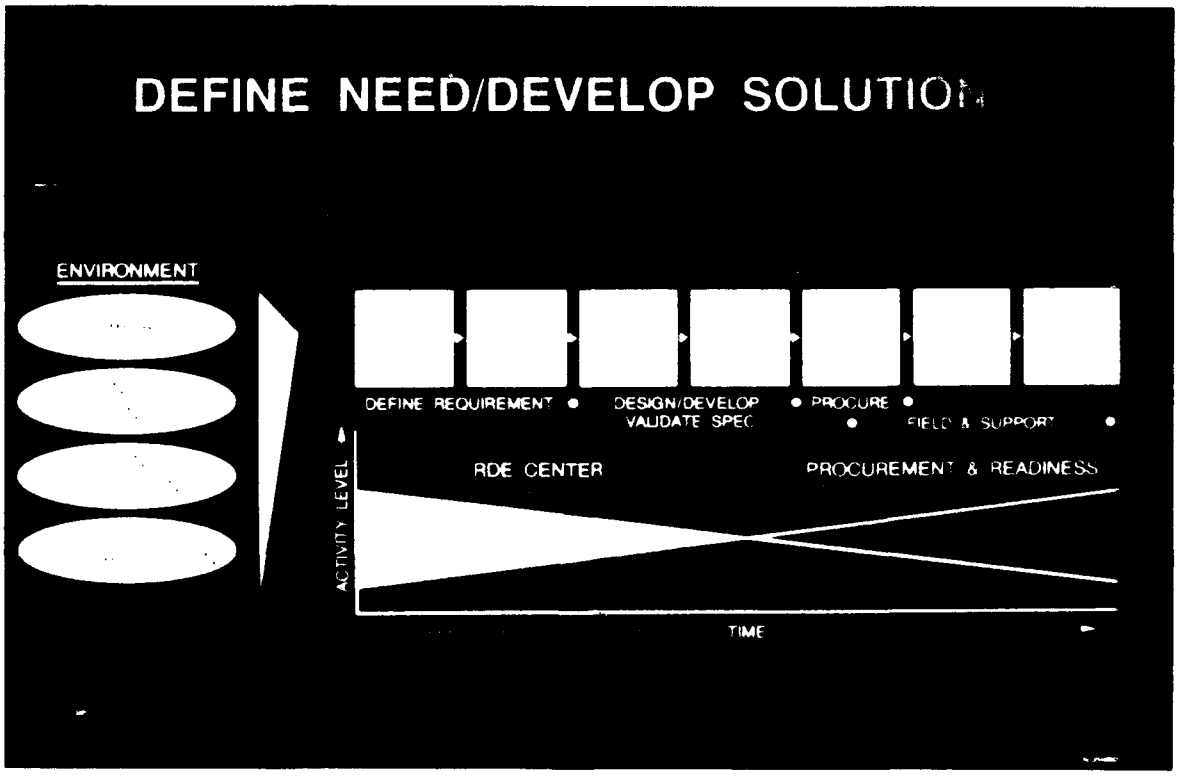

CHART 5

Army's organizational structure, how it will be used, and what it will do toward solving the apparent deficiency. The plan also addresses two significant system considerations: logistics and MANPRINT.

Although the majority of the process discussed is Army-specific, there is a movement toward a Department of Defense Acquisition System which uses many of the Army processes. If industry has any real interest, or if there is an intention to compete for development or production of an Army system, then it is to industry's advantage to know the process. In addition, many aspects of the Army acquisition process can provide a potential benefit to the industry by providing a systematic way to produce an optimized system.

THE ACQUISITION SPECTRUM (AND MARKET INVESTIGATION)

The Army looks at a variety of "materiel solutions" to meet a specific or general requirement. Chart 6 illustrates the "Acquisition Spectrum." The ideal solution is something we already have in the DOD system or a modification of an existing system. The next best choice is an "off the shelf" item. An example of the latter is commercial construction equipment. The soldier usually assumes that a developmental program is the most desirable. The premise is that the desired system will be custom designed and built for a specific application. When cost, schedule, and technical risk are considered, the attractiveness of a development system fades.

The initial documentation for any system requires a market investigation. Available information on commercial, developmental, foreign and existing systems are examined for candidates. An advertisement is placed in the Commerce Business Daily to solicit information on systems that are not generally known or advertised. The results of the market investigation are used to determine if a commercial item can be used (or modified), or if a development program is required.

NONDEVELOPMENT ITEM (NDI) EXAMPLE

The Special Operations Forces (SOF) came to the Army with a request for a snowmobile, which in Army

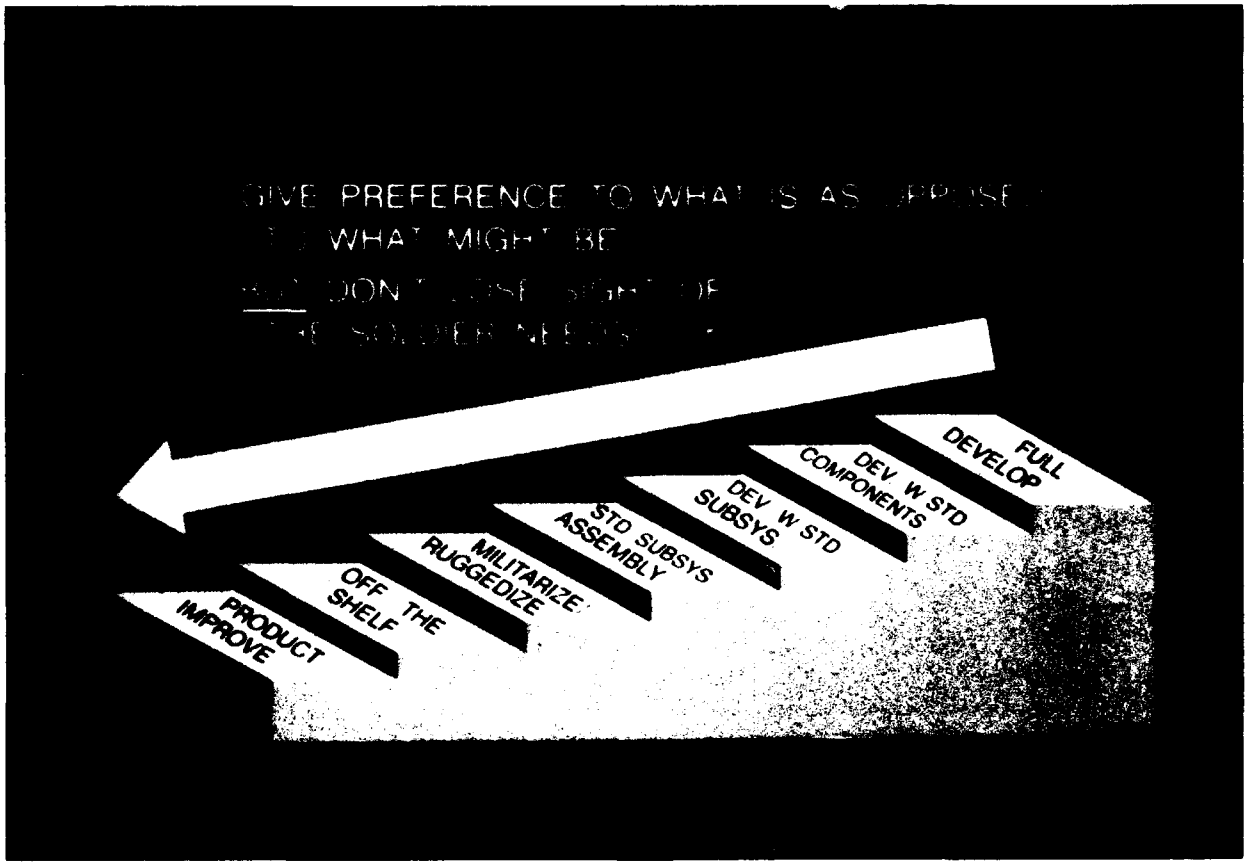

CHART 6

terms became the Mobile Over-Snow Transport or MOST. Our initial perception was that this was a straightforward procurement. The SOF used snowmobiles and sleds in Colorado and encountered no problems.

The Army has a program for testing NDI candidates to develop realistic performance specifications. NOTE: The purpose is not to select a specific candidate but to become knowledgeable in the use and performance of the system in general. NDI tests also provide the soldier an opportunity to refine operational doctrine. MANPRINT issues are developed during this period.

Tests were conducted in Alaska where the environmental and operational conditions were similar to those that could be expected in SOF operations. These conditions were distinctly different from those encountered in Colorado. The test results showed that:

a. The snowmobiles became immobilized in deep new snow.
b. Required loads could not be carried on the snowmobile.
c. Required loads could not be carried on towed sleds.
d. Sled durability was low.
e. Sled stability was poor.
f. The snowmobiles could not be started below –40°F.

The last point provided some insight into the differences between "sport" use of snowmobiles and the needs of the SOF.

The Alaskans normally keep their snowmobiles in a garage or sheltered area. They start the machines up before leaving home and carry them with the engine running, usually in a pickup truck, to wherever it is they want to use the snowmobile. The SOF want to leave the machines for up to two weeks in –65°F temperatures and have trouble-free starts after that period.

The impact of the tests was that a "sport" type snowmobile did not meet the requirements by a wide margin. It also was apparent that the use of this type of machine could lead to mission failure.

The test series was very successful in identifying the MANPRINT issues shown in Chart 7. Fortunately, we found through continued market investigation that several manufacturers were developing "workhorse" snowmobiles. This type of snowmobile solves most of the technical problems related to load carrying and stability. We are continuing to try different sleds and modifications to resolve those problems.

We were able to establish that:

*NOTE: Mental category IIIB is the second lowest of five categories in the Armed Forces Qualification Test (AFQT). It represents the 31–49 percentile of the general population.

SYSTEM MANPRINT MANAGEMENT PLAN QUESTIONS TO BE RESOLVED

- MANPOWER INCREASE WHEN SYSTEM FIELDED?
- CAN SFOD-A TEAM MEMBERS BE TRAINED TO DO LIMITED IDS MAINTENANCE IN THE FIELD?
- OPERATION/MAINTENANCE IN ARTIC/NBC GEAR?
- WILL EXHAUST BE A PROBLEM?
- MISSION PROFICIENCY AFTER 6 HOURS ON SNOWMOBILE OR SLED?
- WHAT SAFETY HAZARDS CAN BE EXPECTED FROM COMMERCIAL SNOWMOBILES?

TAC/2379-6-81/A2

CHART 7

a. A new "MOS" or Military Operational Specialty was not required for "Snowmobile Driver" or "Snowmobile Mechanic."
b. A small increase in mechanics will be required because mechanized equipment is replacing skis and snow shoes.
c. The operator can be trained to perform limited direct support maintenance. This may be very difficult at times, due to environmental conditions and arctic clothing, but it is doable.
d. Exhaust discharge can be directed to avoid CO poisoning.
e. Further testing is required to determine if soldiers can perform their mission after operating a snowmobile for six hours.
f. Noise levels require ear protection.
g. No hazards from edges, rotating/reciprocating parts were found.

A follow-on study is being conducted to determine if a cold start kit can be developed. The objective is to acquire a kit that could be applied to any snowmobile selected. There is no commercial interest in such a kit.

We believe that the MOST program demonstrates that the MANPRINT process is both workable and necessary for nondevelopment equipment purchased by the Army.

SUMMARY

MANPRINT is an integral part of the way the Army does business and part of "up front" planning required for new Army systems. We demonstrated that MANPRINT issues can be integrated into the acquisition process and can have an impact on improving human performance, while reducing life-cycle costs. It calls for an expanded focus which encompasses the man-machine interface and addresses the total system, increasing customer satisfaction and product value. The objective of the MANPRINT program is to optimize system performance and to provide our soldiers with the best and safest equipment possible.

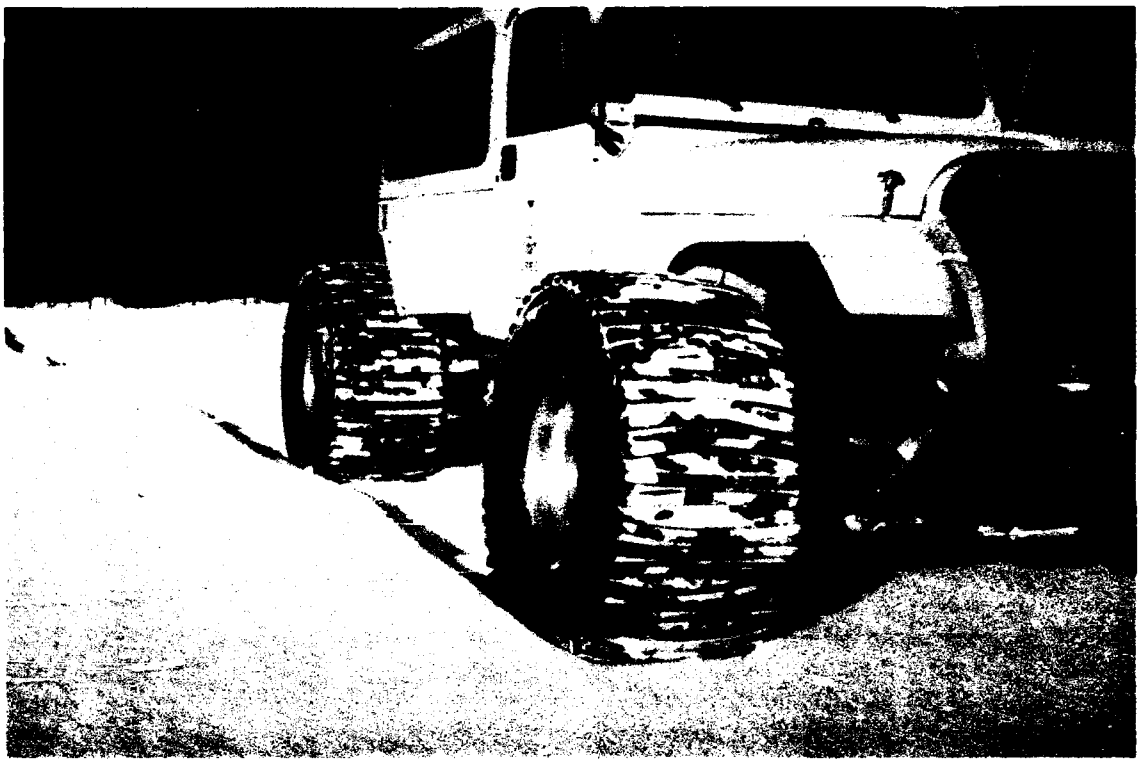

4. MOBILITY ENHANCEMENT

Cross-Country Mobility of Tracked Vehicles

BJORN ANDERSSON

Since the beginning of the sixties terrain vehicles have been developed with very high intensity. The reason for this has partly been an increasing need for military and civilian transports as well as the technical development has made it possible to make terrain-adjusted tyres and tracks with good durability and acceptable prices.

Good cross-country mobility often results in high purchase and operational costs in relation to the transport capacity and must therefore not become an end in itself. Needs and costs must be weighed.

On hard ground, marsh and in snow the tracked vehicles with low ground pressure are superior to wheeled vehicles, no doubt.

One should, however, state that in forestry almost exclusively wheeled vehicles are used. Forest terrain is often troublesome but a combination of good cross-country mobility of the vehicle and the options to reinforce the ground result in a transport capacity worth its price. For military vehicles cross-country mobility in all sorts of terrain is often required without preparation in order to make it possible for the vehicle to fulfill its mission. In this case tracks are a must.

The criterion of cross-country mobility is that available tractive force and friction coefficient at all stages shall exceed the external rolling resistance. The rolling resistance is caused by sinking down on soft ground, grade-ups, local obstacles etc., while the tractive force very often is dependent on available friction coefficient. The cross-country mobility of a vehicle is governed by a number of parameters.

The essential ones are:

—specific ground pressure

—capability to negotiate obstacles

—steering system

Various types of vehicles, tracked or wheeled vehicles, slip steered or articulatedly steered offer different types of space for these parameters.

SPECIFIC GROUND PRESSURE

On hard ground, roads, dry meadows and so on the specific ground pressure is of very little importance. In snow, on marshland and wet meadows it could be a matter of go-no go.

Definition

The specific ground pressure of tracked vehicles is defined as G/A

where G = gross vehicle weight

A = ground contact area of tracks = $(L_1 (+L_2)) \times 2b$

With $G = 20$ tons, $L_1 = 3.5$ m and $b = 0.5$ m the ground pressure is p

$$\frac{20{,}000}{350 \times 100} = 0.57 \text{ kp/cm}^2 \text{ or}$$

$$\frac{204{,}000}{3.5 \times 1} = 58.2 \text{ kPa}$$

A low ground pressure gives in principle a low sink-down, low rolling resistance and low shear force to the ground.

On soft ground, the rolling resistance increases in principle quadrangularly by the weight, decreases quadrangularly by the track length in contact with the ground and decreases proportionally by the track width.

A high rolling resistance results in a high shear force per unit area on the part of the ground under the tracks. If this shear force is limited and not directly proportional to surface pressure and friction coefficient there is a risk that the ground will break which generally means additionally reduced tractive force and thereby bogging down.

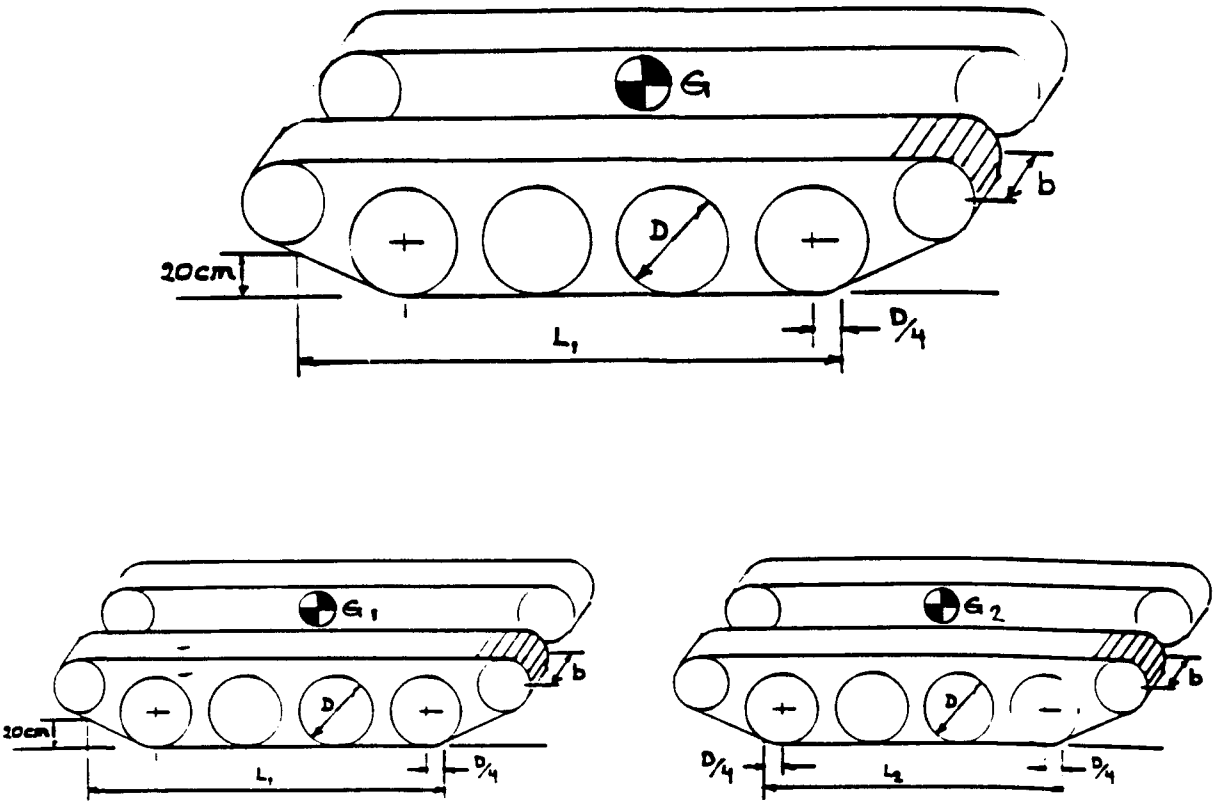

Figure 1. Track steered vehicle; articulatedly steered vehicle.

The design of the track assembly is of great importance.

Rowland and Wong have developed methods for the estimation of effect on sink-down, rolling resistance etc in view of the geometry of the track assembly.

Track steered and articulatedly steered vehicles have different possibilities to meet the requirement of a low ground pressure.

On a track steered vehicle the track relation, i.e. the contact surface area of the track divided by the track gauge, should not exceed 1.6–1.8. The vehicle will thus be relatively quadrangular.

On an articulatedly steered vehicle the track relation is of no importance. Compared to a track steered vehicle of the same size, the articulatedly steered vehicle is slimmer and longer.

On Bv 206 the tracks are wide and they are positioned under the bodies. This results in a large area of the tracks and a low ground pressure. At the same time the vehicle is slim and can be driven through narrow passages.

A long track on a track steered vehicle results, on the other hand, in lower rolling resistance compared to two short tracks after one another provided the specific ground pressure is the same. As the ground pressure of the articulatedly steered vehicle is considerably lower, its sink-down and consequently its rolling resistance will be lower in comparison with corresponding track steered vehicle.

CAPABILITY TO NEGOTIATE OBSTACLES

The suspension of a tracked vehicle is to offer increased comfort for the crew and thereby permit higher speed on road and in terrain.

The capability of the suspension to level out the vehicle pressure against the ground is, however, of great importance to the mobility as well. It is essential to avoid comprehensive raising of the centre of gravity which might result in a high friction coefficient between ground and tracks.

In very rough terrain the suspension cannot level out all the uneven parts of the terrain. One must therefore see to that the vehicle is completed with some kind of turning joint, bogie function or similar in order to avoid a dramatic raising of the centre of gravity, which will require a high friction coefficient.

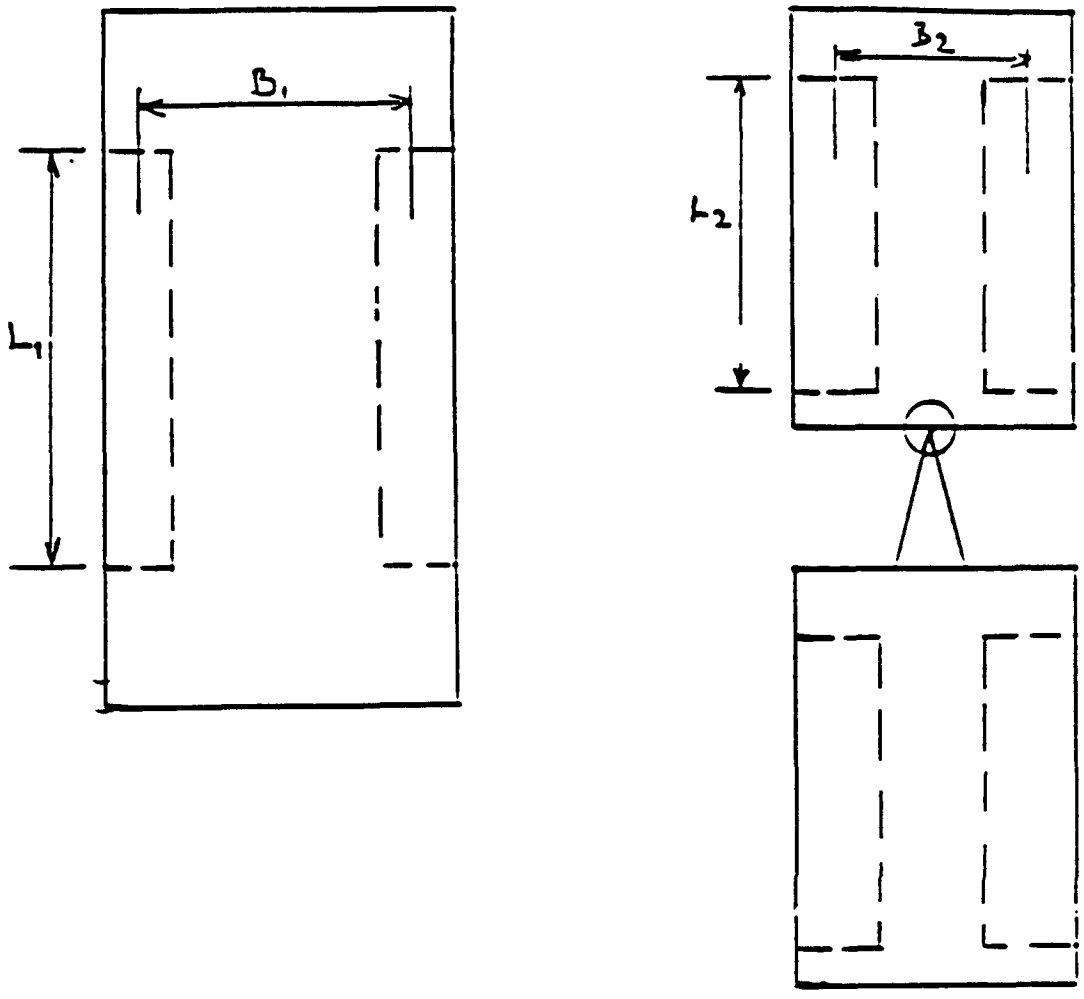

Figure 2. Example of track and articulatedly steered vehicles of the same size.

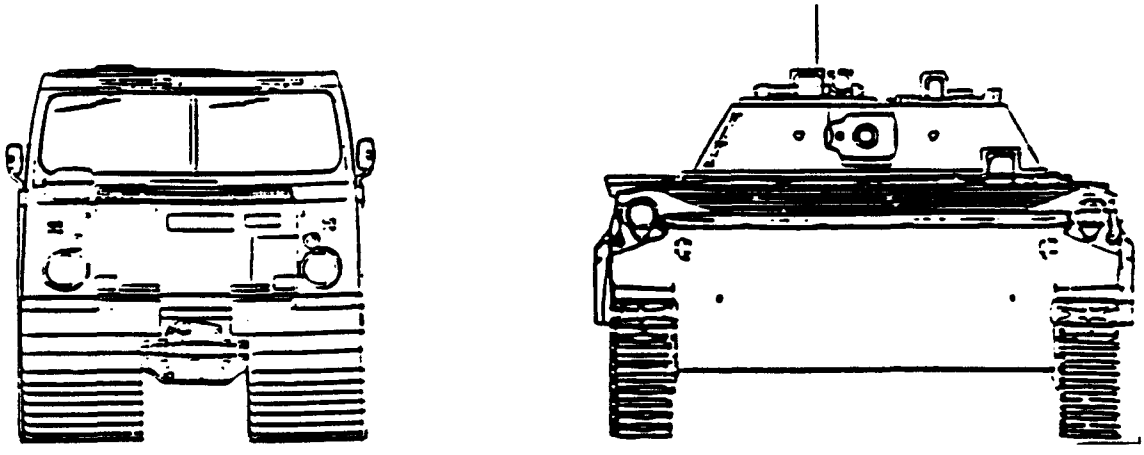

Figure 3. Track width–total width of articulatedly steered vehicle Bv 206 and armoured tracked vehicle BMP R (Spähpanzer).

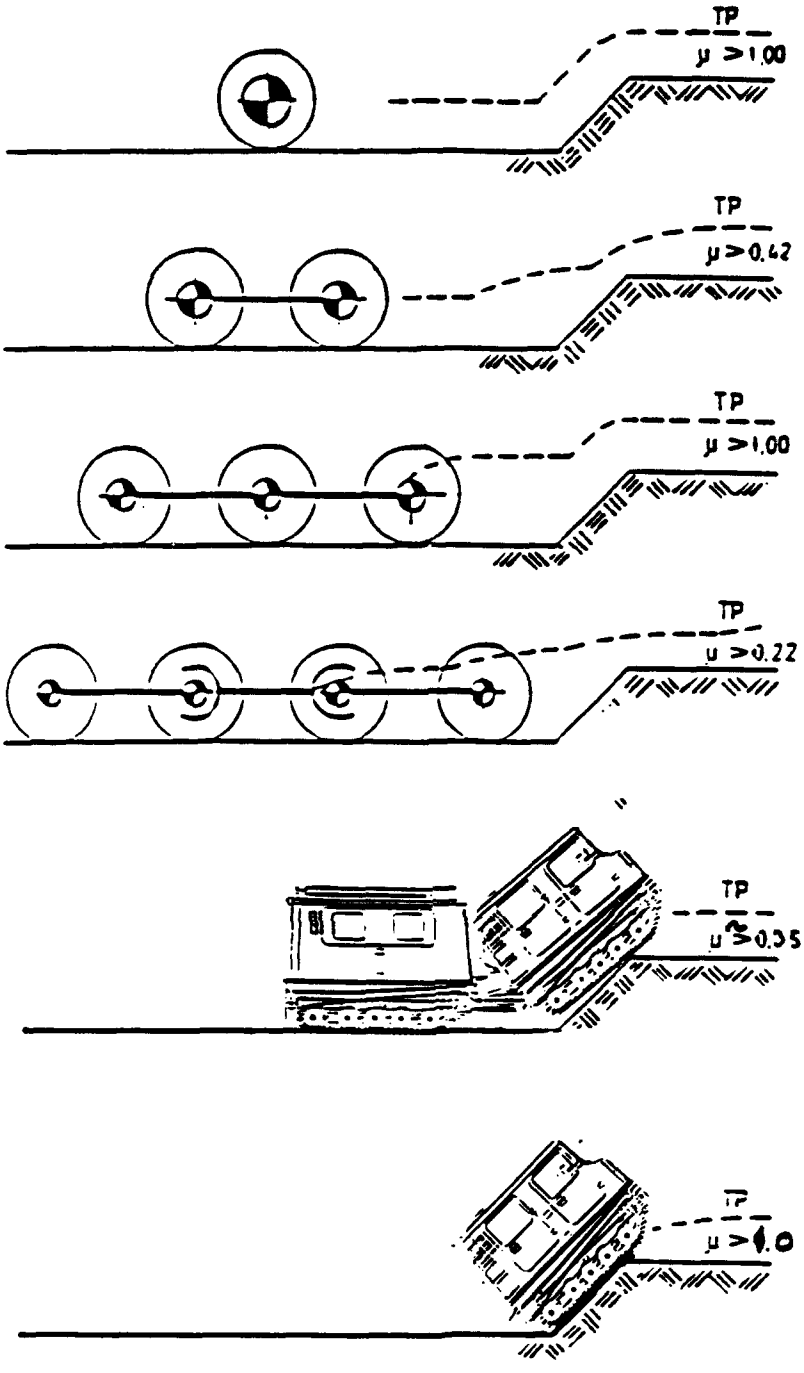

Figure 4. The raising of centre of gravity for stiff respectively articulated vehicles.

Off-road trucks generally have a weak frame which enables it to turn, e.g. forwarders and dumpers have a kind of turning joint and often bogie-suspended wheels. This gives an even pressure against the ground and a minimum raising of the centre of gravity.

In Fig 4 is indicated the raising of the centre of gravity and required friction coefficient for various track and wheel assemblies.

One can see here that a single vehicle (A) which has to negotiate the obstacle on its own requires a high friction coefficient while two vehicles linked together (B) manage the obstacle even though the friction coefficient is considerably lower.

Note that the raising of the centre of gravity can be relatively flat during the major part of the negotiating of an obstacle but steep during a short period of time. It is,

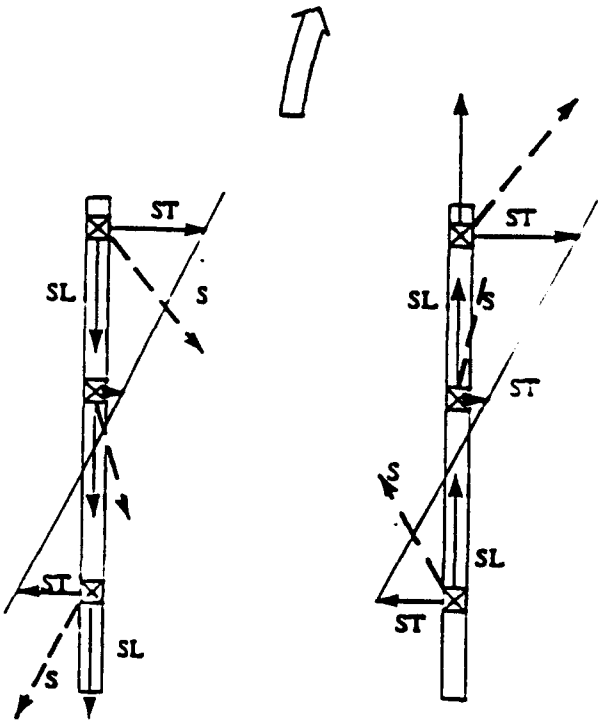

Figure 5.

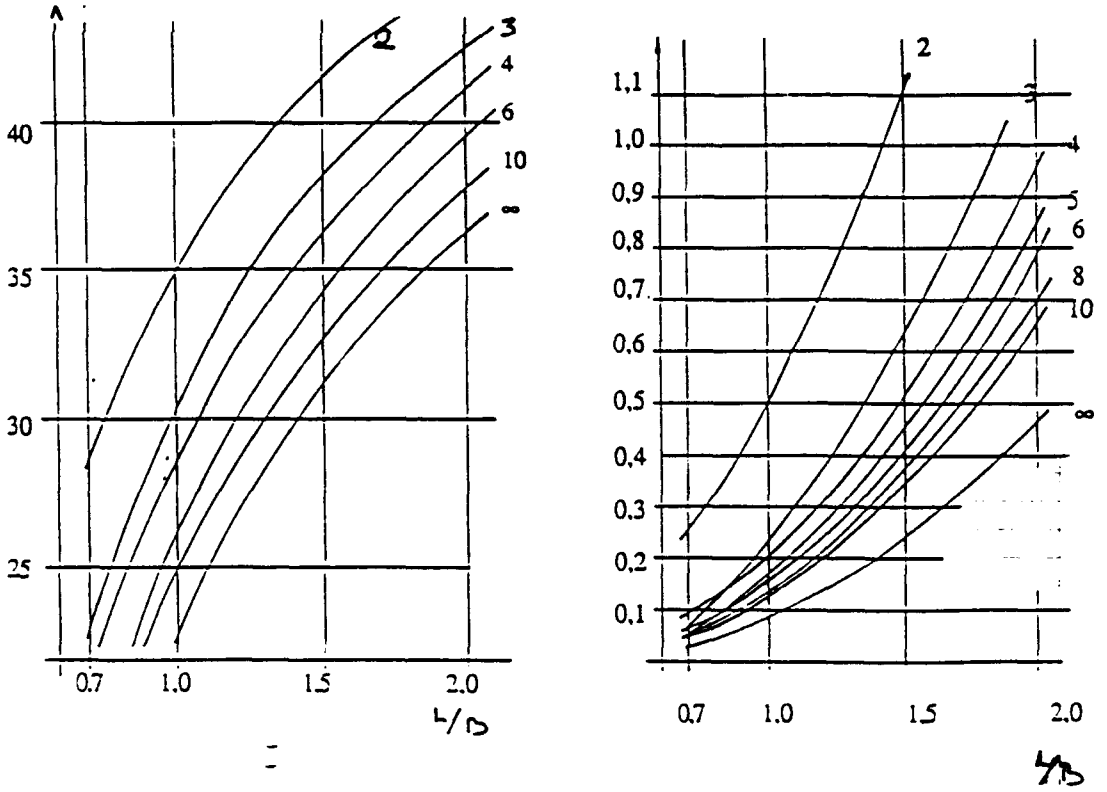

Figure 6. Track force in % of GVWX coefficient of friction. Different Nos. of road wheels. Track slip in M/rad and different Nos. of road wheels. Value must be multiplied with distance between track centre.

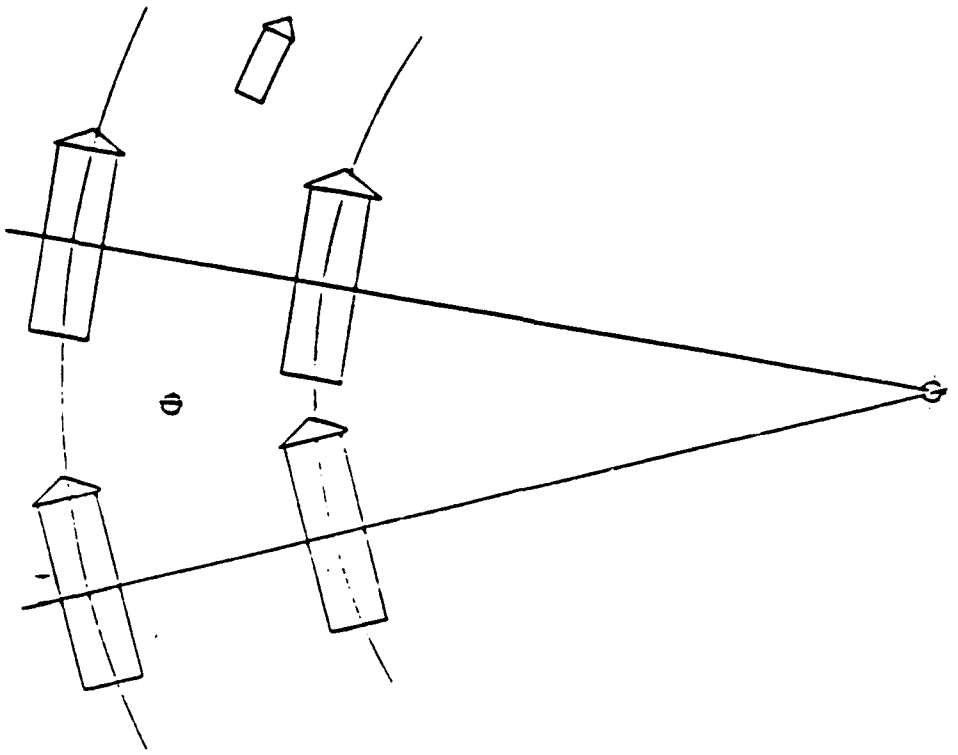

Figure 7.

however, the steepest part that is crucial to GO-NO GO. When negotiating an obstacle the raising of the centre of gravity should be as even as possible.

STEERING OF TRACKED VEHICLES

The steering of a tracked steered vehicle is accomplished by giving outer and inner tracks various speeds. Thus the tracks slip longitudinally and laterally against the ground.

When steering an articulated vehicle the front and rear cars are turned round a common steering joint. Even in this case the tracks will slip but considerably less.

In both cases the track forces and track slip can be calculated as a function of the geometry of the track assemblies. It should be observed that the forces and slip which are a fact when driving through a curve with track steered vehicles are completely independent of the design of the steering system. In order not to complicate the calculations certain idealizations have been made regarding the incorporated parameters:

1. The substructure is completely flat and plane
2. The friction coefficient is the same in all directions
3. The track width = Nought
4. Vehicle speed is low and invariable

The general case, track steered vehicle

A track steered vehicle is steered by giving the outer track a higher speed than the inner track. Thus the outer track will slip backwards while the inner track slips forwards.

The longitudinal slip is invariable along the whole track while the lateral slip is proportional to the distance from the centre of the track *Y*.

The slip of a partial element longitudinally (*SL*) and laterally (*ST*) results in a slip (*S*) which varies in size and direction according to Figure 5.

On top of this slip which results in a turning of the vehicle the rolling of the vehicle is stored and the combination results in a steering radius.

Based upon this the track forces and slip can be calculated resulting in Figure 6.

Articulatedly steered, tracked vehicles

When steering a tracked steered, tracked vehicle the inner track must be braked or given less tractive force than the outer track. This is detrimental to the mobility. An articulated vehicle is steered by angling the front and

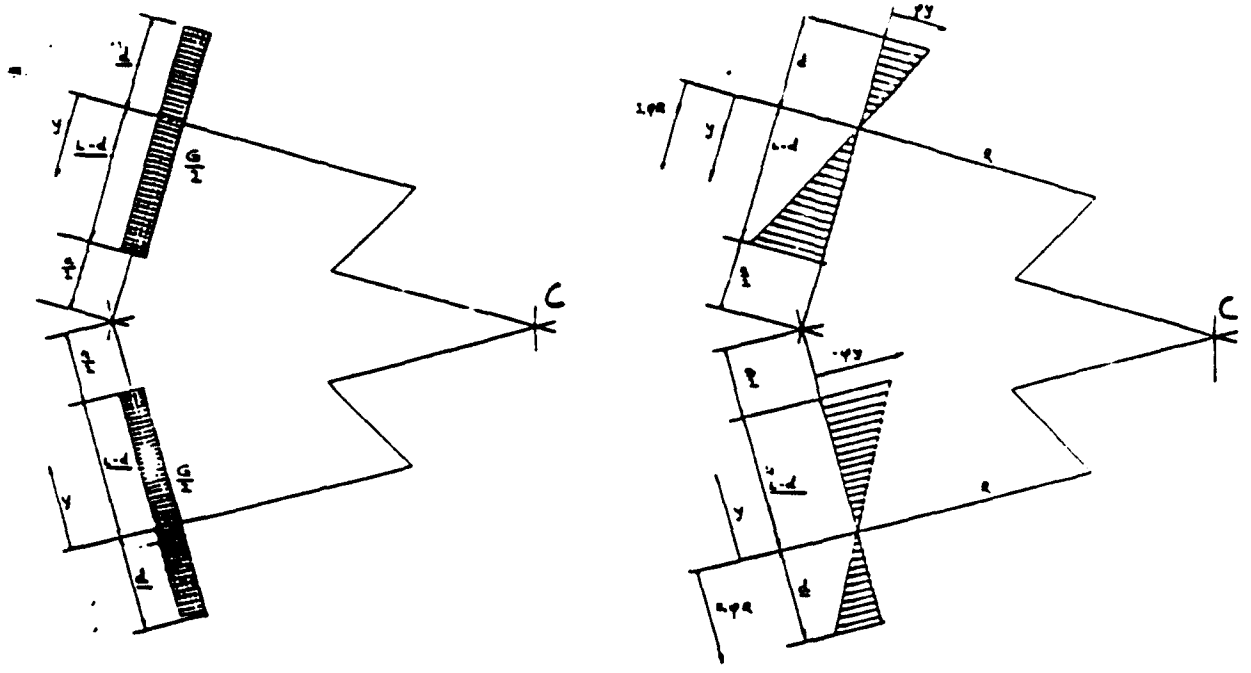

Figure 8.

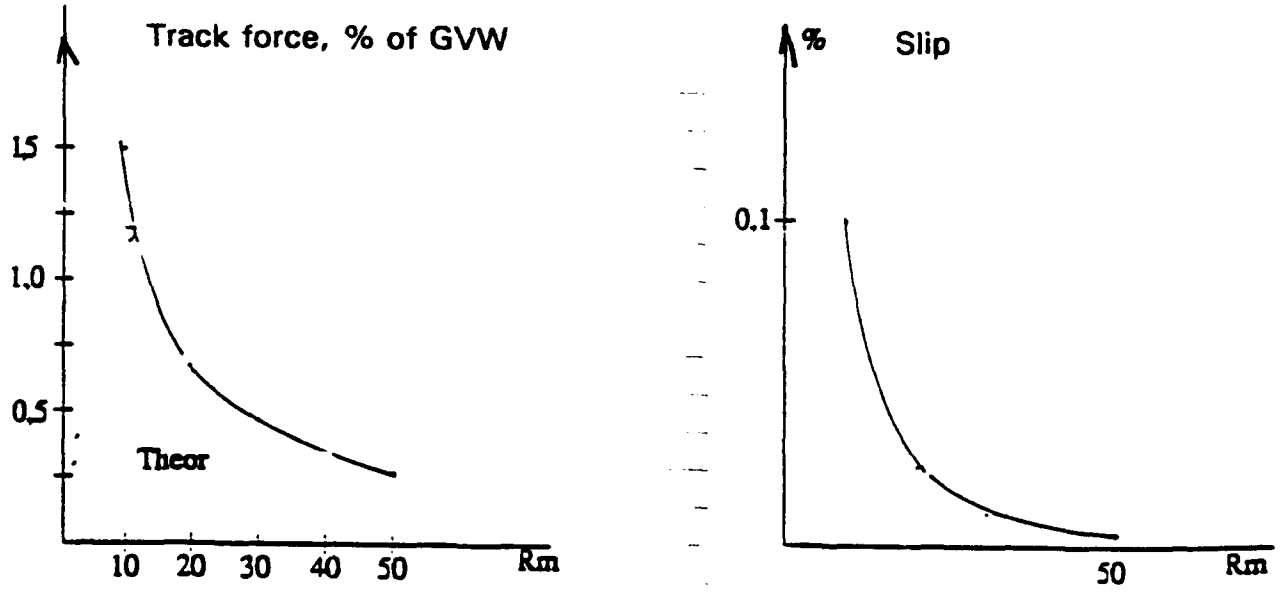

Figure 9.

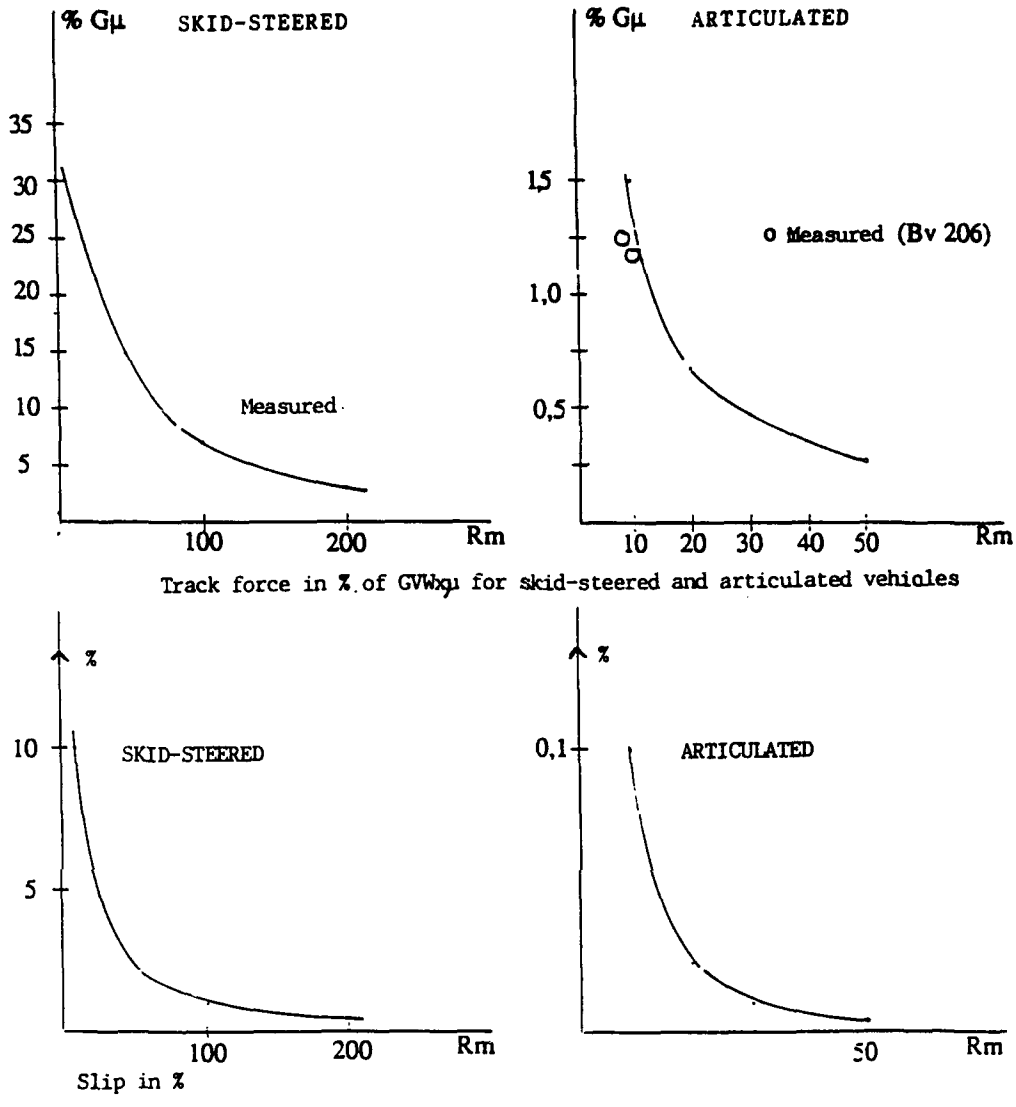

Figure 10.

rear car to each other. Thus full tractive force can be maintained on all tracks. A certain slip, however, is a fact. This is due to the tracks which through their length primarily skid laterally when driving through a curve, and this creates a moment around the fulcrum which must be compensated by tractive force in the tracks.

When calculating, the simplification is permissible, that the vehicle is considered single-tracked:

One cannot suppose that the tracks are turned around their centres, i.e. $d = L/2$.

The driving moment around the fulcrum C is then:

$$M_1 = \frac{G\mu}{L} R \int_{-d}^{L-d} \frac{SR}{\sqrt{S^2R^2 + Y^2}} dy$$

The braking moment M is:

$$M_2 = \frac{G\mu}{L} R \int_{-d}^{L-d} \frac{Y^2}{\sqrt{S^2R^2 + Y^2}} dy$$

To achieve moment equilibrium of the vehicle the following applies:

The integrated turning moment around any optional point of the vehicle is to be equal to nought.

For the sake of simplicity the centre of the steering unit is chosen and the moment is calculated for one car.

$$M_3 = \frac{G\mu}{2L} R \int_{-d}^{L-d} \frac{y}{\sqrt{S^2R^2 + y^2}}$$

$$\left(\frac{a}{2} + L - d - y\right) dy = 0$$

Conditions: $M_1 = M_2\ M_3 = 0$

This gives:

$$1.\ \frac{G\mu}{L} R \int_{-d}^{L-d} \frac{S R\, dy}{\sqrt{S^2R^2 + y^2}} = \frac{G\mu}{L} \int_{-d}^{L-d} \frac{y^2\, dy}{\sqrt{S^2R^2 + y^2}}$$

$$2.\ \frac{G\mu}{L} R \int_{-d}^{L-d} \frac{S R\, dy}{\sqrt{S^2R^2 + y^2}} \left(\frac{a}{2} + L - d - y\right) = 0$$

After calculation the following curves are obtained: with

$L = 2.0\ a = 1.0$ m
$G = 8000$ kg $\mu = 1.0$

The following curves for track force and slip are obtained:

A vehicle with good cross country mobility must be design with:

—low ground pressure
—low weight
—many road wheels
—high track tension
—good suspension
—articulated steering

A carefully designed track steered vehicle can have a very good cross-country mobility. The Swedish IFV 90 has seven road wheels and a GVW of 22 metric tons. It uses M2 tracks. It has an excellent mobility in snow.

Articulated steering anyhow increases the mobility dramatically and must be recommended for highly mobile vehicles.

Investigation of Forces Incurred During Snow Plowing

WADE STEIGER, ANDREW HANSEN AND KYNRIC PELL
Center for Information Technology
Department of Mechanical Engineering
University of Wyoming
Laramie, Wyoming 82071

INTRODUCTION

In 1988, the University of Wyoming was awarded the Strategic Highways Research Program contract H-206, "Improved Displacement Snowplow and Blowing Snow Control." The goal set out for this project was to decrease the energy consumption of a snowplow by 20%. Under this contract, the University of Wyoming designed, fabricated and tested a snowplow that incorporated several new design features. A variable geometry ultra high molecular weight polyethylene moldboard and a double blade cutting edge were two of these design features. During testing at West Yellowstone, Montana, the double cutting edge was found to be successful both in reduction of the power required to push the snowplow and in improving the handling of the truck. This work is continuing with further analysis of the data and the fabrication of a second experimental plow and two prototypes to be tested in the winter of '91–'92.

DESIGN OF THE EXPERIMENTAL SNOW PLOW

The snowplow used in the testing was designed and built by the Department of Mechanical Engineering at the University of Wyoming. The plow is a 12' reversible geometry, incorporating a husting hitch, designed to mount to a Ford F9000 truck supplied by the Wyoming Highway Department. This snowplow incorporated a new moldboard and cutting edge design. The design of this plow was done using the software package I-DEAS from Structural Dynamics Research Corporation.

The design of the moldboard is an extension of the Frink America Reverse-a-Cast plow. This design uses an ultra high molecular weight polyethylene (UHMWPE) moldboard 48" × 144" × 7/16" supported only on the top and bottom edges. The moldboard was mounted in this way to allow the geometry to be varied. The UHMWPE material was chosen because, in addition to allowing variable geometry, it has exceptional abrasion and impact resistance as well as low friction.

The arms shown in Figure 1 can be adjusted, by means of turnbuckles, thus changing the shape of the moldboard. This plow used five 1 1/2" turnbuckles and one 3/4" turnbuckle to control the shape of the moldboard.

The design of the cutting edge was prompted by analytical work concerning energy dissipation caused by a plastic wave leading the snowplow, as well as the comments made by numerous plow operators and maintenance personnel. During displacement plowing a nonlinear compression wave leads the snowplow in the snow in front of the cutting edge. This compression wave absorbs a significant amount of energy. Recent work has shown that the energy adsorbed by this compression wave could be reduced by using an inclined cutting edge (Hansen (1991). The snowplow operators indicated that a snowplow will cut ice much better if the cutting edge is nearly normal to the road. This design is an attempt to address both concerns.

The cutting edge used on this plow consisted of one blade at a near normal angle to the road and one blade laid back at approximately 45 degrees. The front blade is made out of one inch thick UHMWPE. The rear blade was a standard American Association State Highway and Transportation Officials blade. The idea behind the two blades was that the front blade would remove the loose snow on the road while the rear blade removed the

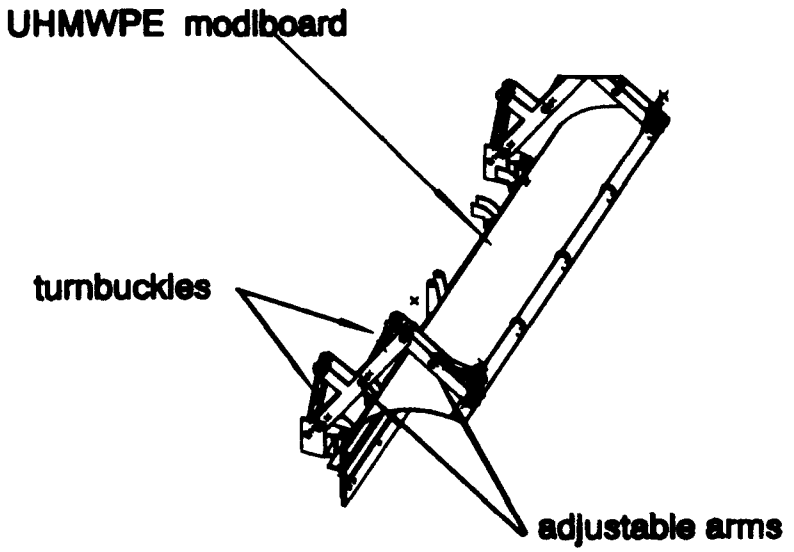

Figure 1. Variable geometry, reversible plow.

hard packed snow and ice from the road. The gap between the two blades allows the material cut by the rear blade to flow up to the moldboard. The UHMWPE blade will be referred to as the snow scoop in this report. There are three four foot wide segments of the cutting edge. Each of these segments is able to trip independently. The trip action is controlled by a four inch diameter air cylinder attached to the back of each trip edge segment. The UHMWPE snow scoop will deflect sufficiently, or break off during a tripping event.

A diagram of the cutting edge is shown in Figure 2.

DATA ACQUISITION

A personal computer based data acquisition system was installed on the snowplow. A portable IBM 80386 computer with a Metrabyte 16 channel analog to digital

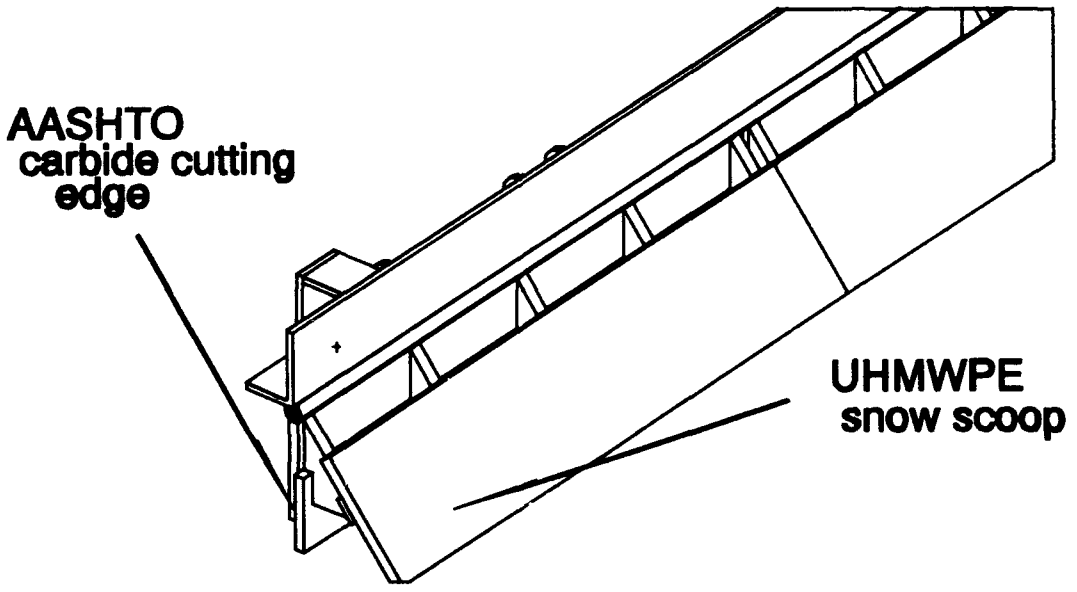

Figure 2. Dual cutting edge design.

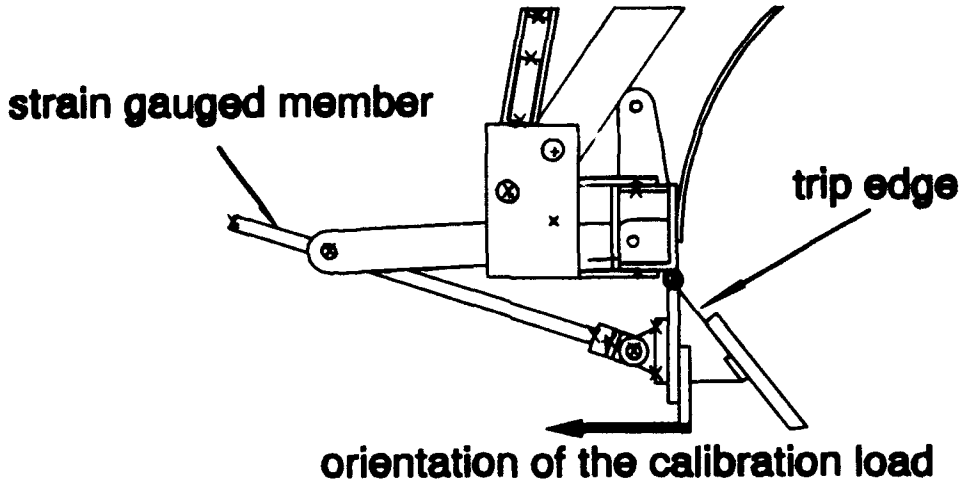

Figure 3. Tripping edge instrumentation.

converter was used to record the data. With this system, sampling rates of 10 to 1000 Hz per channel were used. There are eight strain gauge based load cells mounted at the plow-truck interface. For testing, three more strain gauge based load cells are mounted in place of the air cylinders on each trip edge. There are also two stain gauge based load measuring devices in the moldboard positioning arms at each end of the moldboard. Each of these load cells is connected to the data acquisition computer board through a line conditioning amplifier.

The load cells on the trip edge are calibrated to measure the horizontal force at the cutting edge/road surface interface on each of the three individual trip edges. These load cells were calibrated using a reference load cell. The configuration of the loading was such that the load cells on the snowplow measured the horizontal force at the bottom to the trip edge directly. The resulting linear calibration curves were put into the

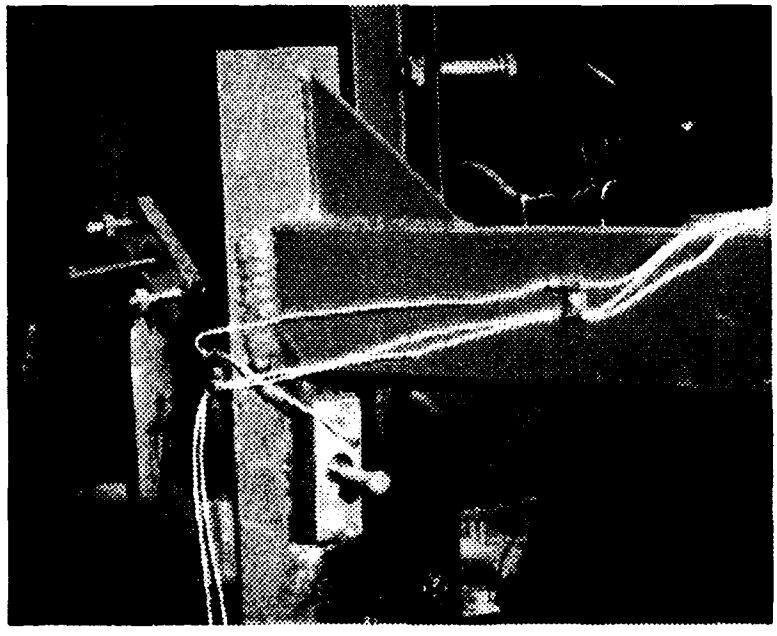

Figure 4. Hitch mounted load cells.

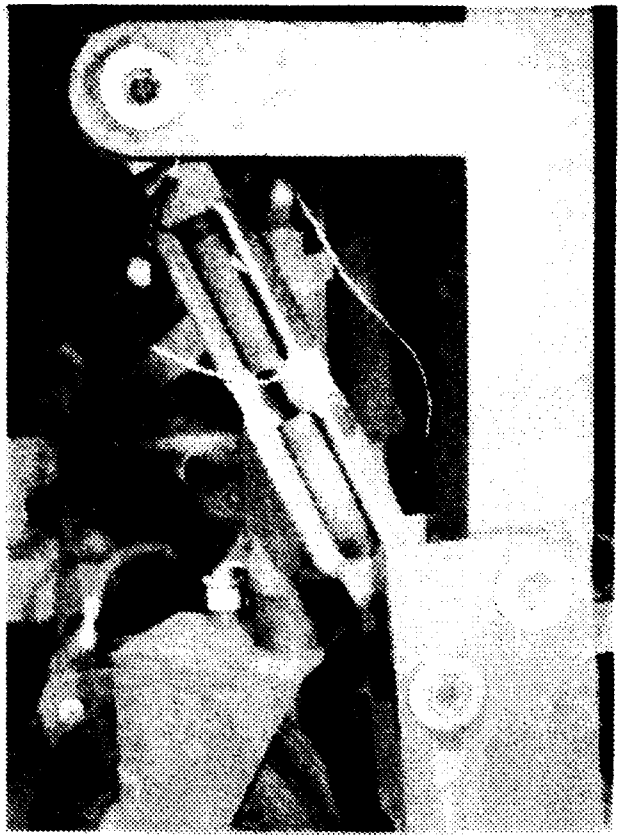

Figure 5. Strain gauged turn buckle.

data acquisition software such that loads are output directly in pounds force. A diagram of the calibration loading is shown in figure 3.

Micro-Measurements CEA-06-125UW-120 strain gauges were used in a full bridge circuit. The load cells were made of annealed 17-4 stainless steel, which was subsequently heat treated.

The eight load cells mounted on the plow hitch were calibrated in an Instron axial test machine in compression only. An offset was introduced into the calibration due to mounting the load cells on a surface that was not as flat as the surface on which they were calibrated. The calibration curves were also put into the data acquisition program, as was done with the load cells on the trip edge. These load cells used Micro-Measurements CEA-06-125TW-120 strain gauges in a full bridge circuit. These load cells were also made of 17-4 stainless steel in the same manner as the ones on the trip edge. The mounting of these load cells is shown in figure 4.

The load measuring devices in the control arms were created by strain gauging the turnbuckles that control the shape of the moldboard. To do this, the turnbuckles had to be machined down enough that the strains were high enough to measure accurately. Because the moldboard changes shape, a Fortran program was written to convert the force measured at the turnbuckle to the force applied to the top of the moldboard. These turnbuckles were calibrated in the Instron machine, as well as on the snowplow. These load measuring devices are shown in Figure 5.

A Hall Effect proximity switch was put in the brake backing plate in the front right wheel, and five magnets were mounted in the brake drum of the same wheel. This pulse generator was connected to the counter on the A to D board in the computer. This creates a digital speedometer. By knowing the distance traveled between each pulse and using the internal clock in the computer to time-stamp the data, a speed can be calculated. The five magnets used increased the resolution of the speedometer. No signal conditioning was needed on the speedometer other than that done by the A to D board. A time and speed were recorded for each data set.

The test program was conducted on the entrance road to the West Yellowstone airport in Montana. This airport is closed for the winter months so the access roads made a good closed test course.

The goals set out for the trip to West Yellowstone, Montana were to document the performance of the snow scoops and various geometries of the moldboard in terms of energy consumption, cast distance, and moldboard flow. Energy consumption estimates were based on the recorded load cell data. The cast distance tests were based on mass displacement measured on a discrete grid. The moldboard flow tests were done by video-taping the flow of painted snow over the moldboard.

In West Yellowstone on March 2, 1991, a power consumption test was conducted. This test was run to determine the effectiveness of the UHMWPE snow scoops. Before each test, a data set was taken with all the load cells in an unloaded state. This allows the offsets induced in mounting the load cells to be taken out numerically. Conditions for this test were as follows: temperature, 24°F; snow depth, 2.75"; snow density, 8.73 lb/ft^3. The moldboard shape is the unsymmetric shape, which was consistent thought this test. This moldboard shape closely resembles a conical one way snowplow. To do this test, the snow scoops were on for the first runs and were then taken off for the following runs. Plots of the resulting data are shown in Figures 7–9.

The tests conducted involving different moldboard shapes had the same goal as that for the trip edge geometry, that is to measure the energy consumption. In addition, measurement of cast characteristics was also attempted. Due to limitations imposed by time and the size of the test course these tests were not done in

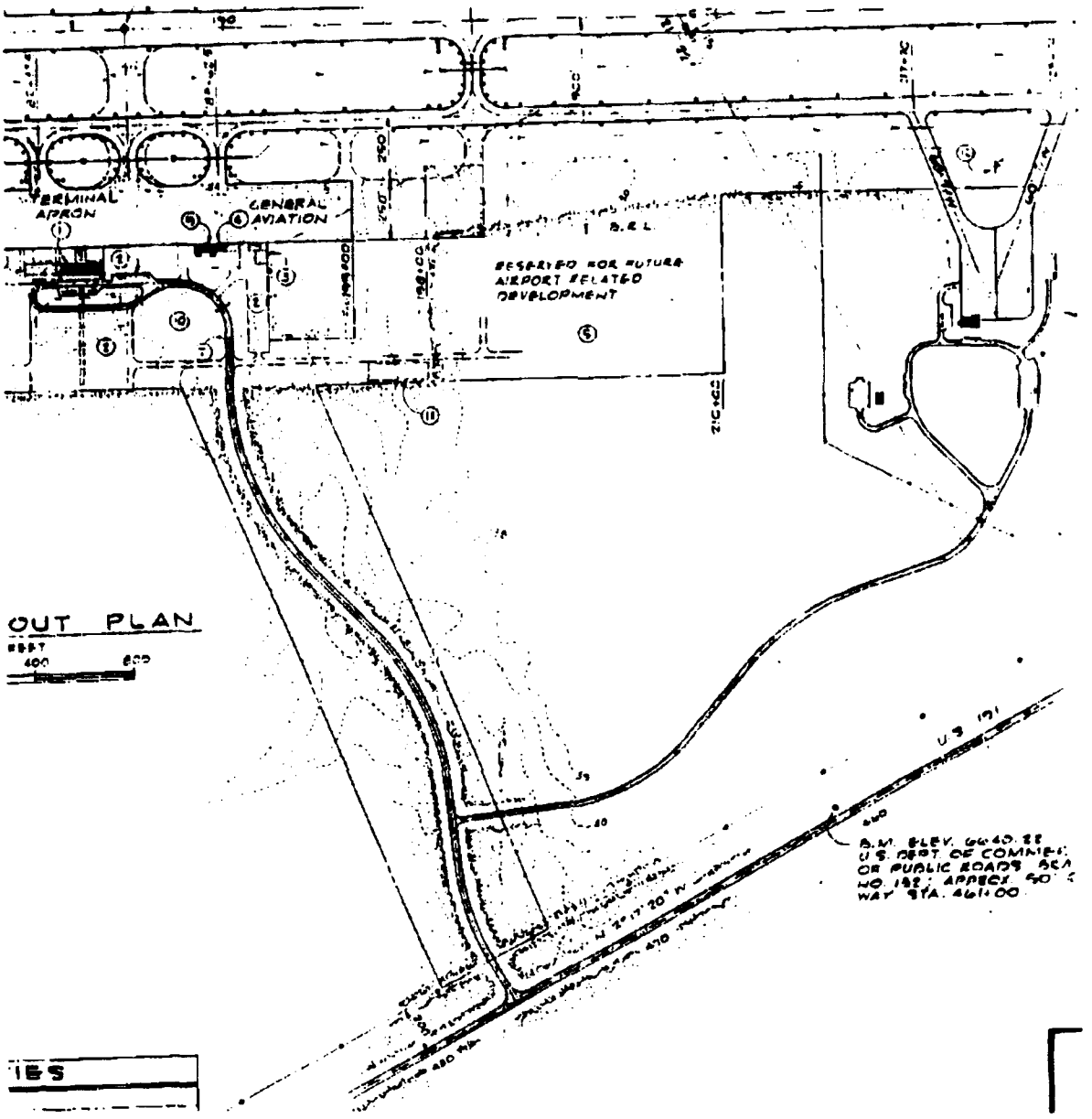

Figure 6. Map of the roads used on the West Yellowstone Airport.

identical snow conditions. Due to the various conditions the comparison of the forces involved were done in a nondimensional way. The nondimensional force parameter used was

$$\frac{F \times g_c}{\rho \times V^2 \times D \times W}$$

where,

F = force,
ρ = density of the snow,
V = velocity of the truck,
D = depth of the snow,
W = width of the plow cut, and
g_c = gravitational constant

The data shown in the next three plots were taken with the snow scoops on. Figures 10 and 12 show that

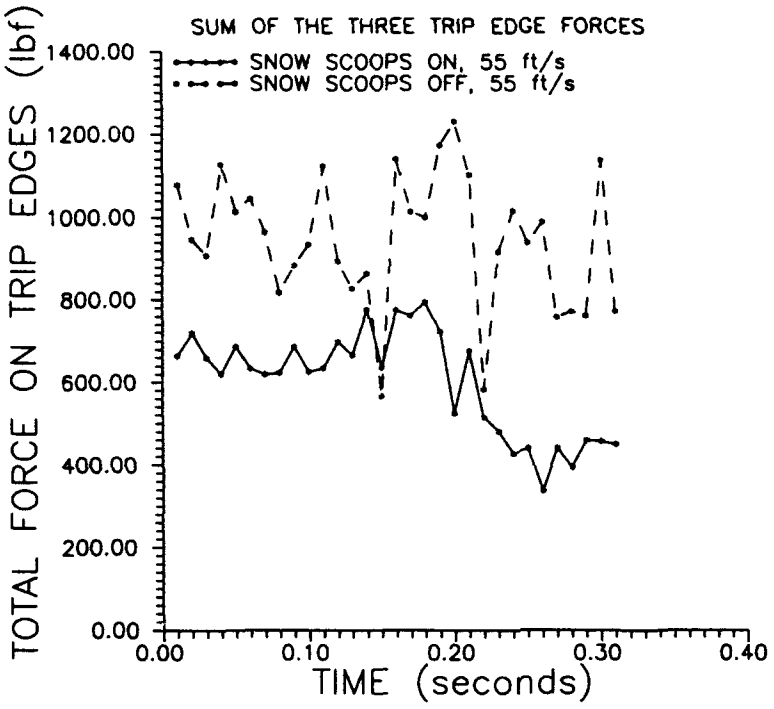

Figure 7. Plot of the sum of the force measured by the three trip edge load cells.

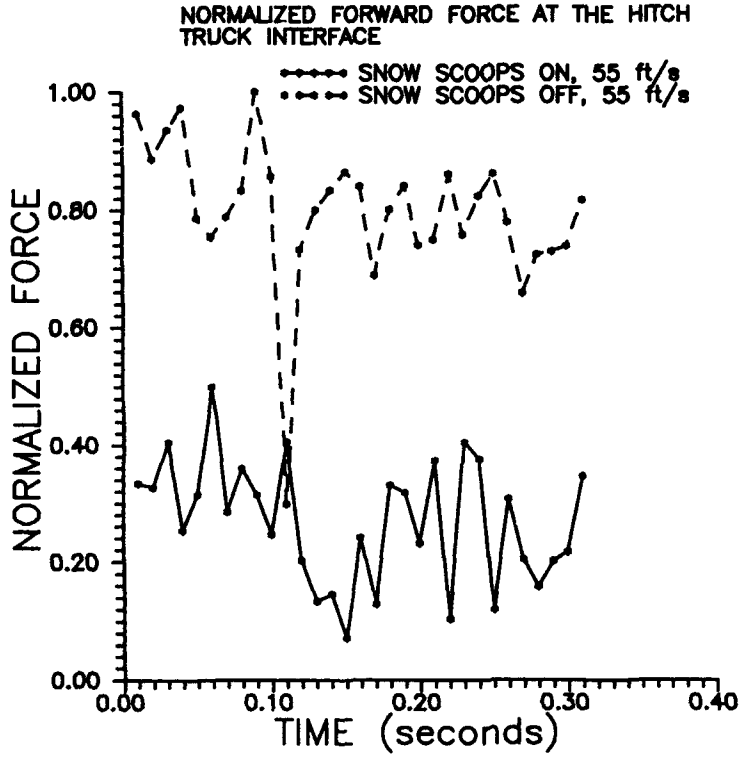

Figure 8. Forward force on the hitch, sum of four load cells.

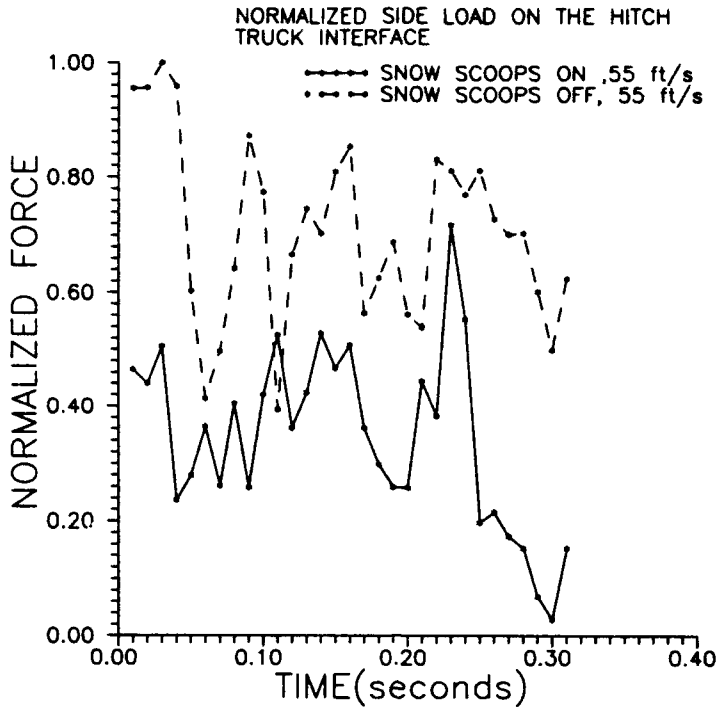

Figure 9. Sum of the two load cells on the right side of the hitch.

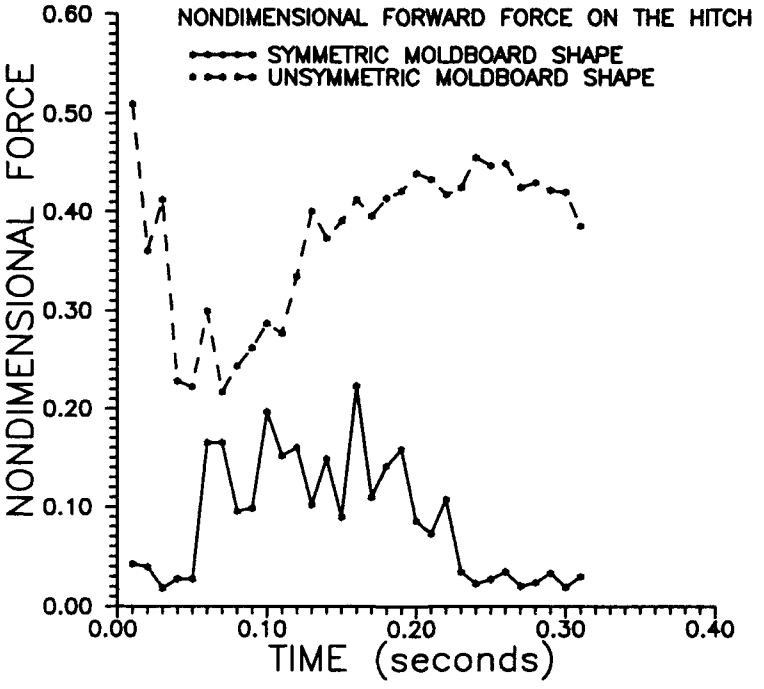

Figure 10. Nondimensional forward force on the hitch.

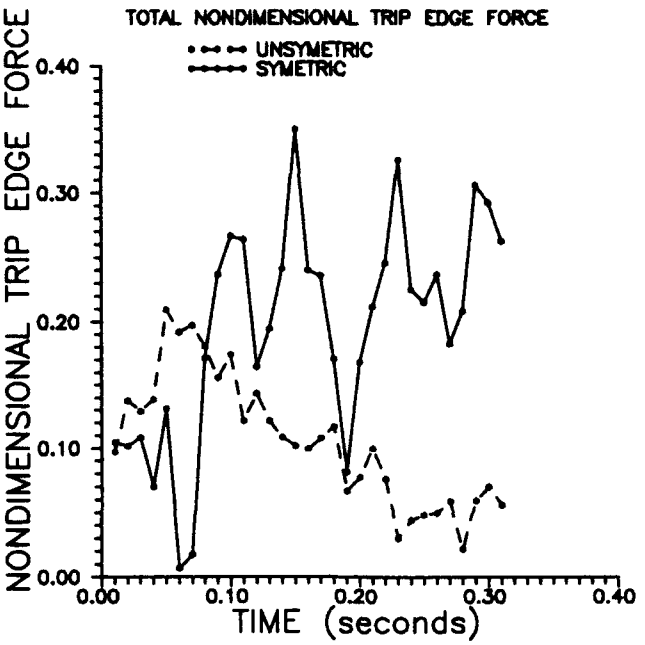

Figure 11. Nondimensional force on the trip edge.

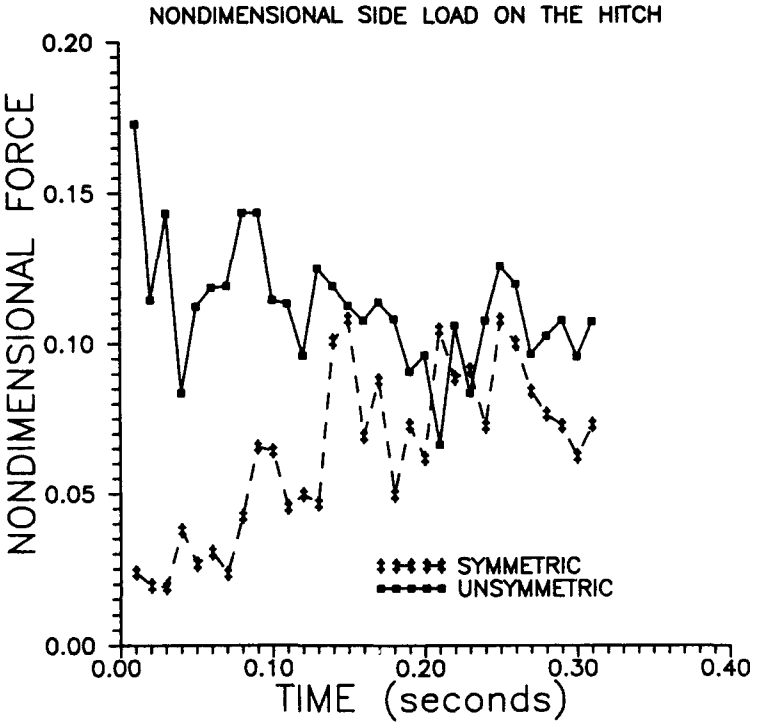

Figure 12. Nondimensional side load on the hitch.

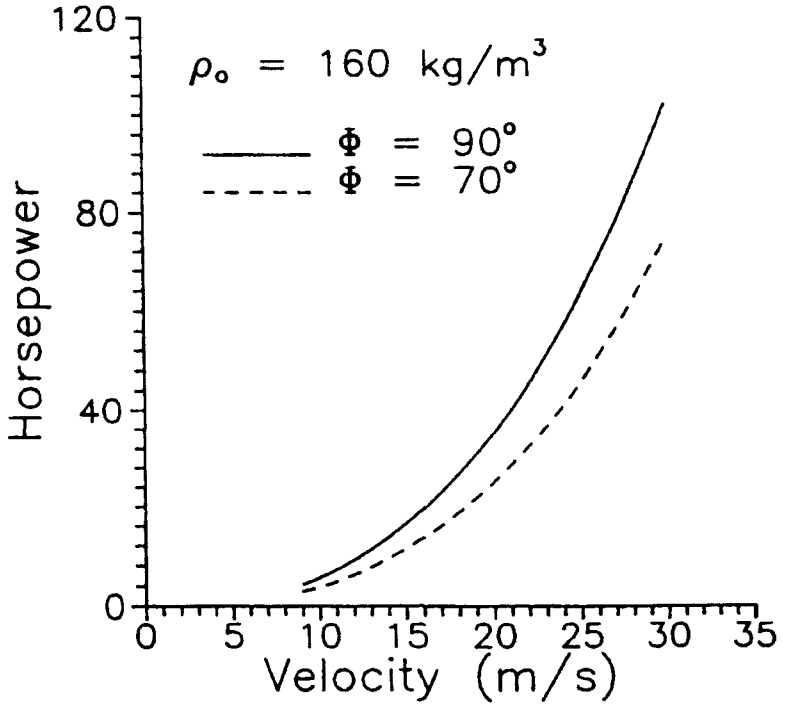

Figure 13.

the forces for the unsymmetric moldboard shape are higher than those for the symmetric moldboard shape. This can be attributed to increased rehandling of the snow done by the unsymmetric shape shown in the video data.

Figure 13 taken from Hansen (1991) may explain part of the reduction in force seen with the snow scoops on. The angle represents the angle of the cutting edge with $\Phi = 90°$ representing vertical orientation. The reduction in force shown in this plot is due to a reduction in the compression wave that leads the snowplow. The reduction in force is predicted to be even greater at 45° than at 70° but still not enough to explain the entire decrease in force that is seen in the test results.

PROJECT CONTINUATION

The reduction of the data obtained in West Yellowstone is still underway. Current analytical work is focusing on a finite difference code to predict the compression wave leading the snowplow. This work and more testing may yield a better understanding of the energy absorption mechanisms involved in plowing

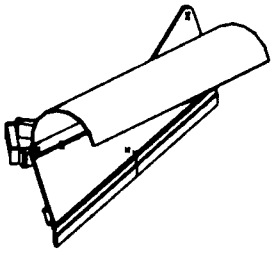

Figure 14. Cast right configuration.

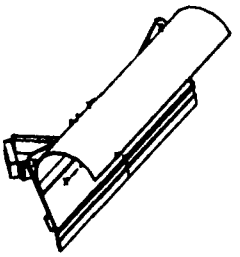

Figure 15. Center configuration.

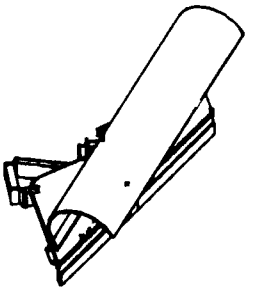

Figure 16. Cast left configuration.

snow. There is also work being done in reducing the cast characterization data.

The other aspect of continuation of this project is the design and fabrication of a second experimental snowplow. This second snowplow will be designed with the same cutting edge geometry, but with a different moldboard. The reason behind the new moldboard is the complex control system that was required by the current moldboard design. The new design will have a two piece moldboard with only one control element to control the shape of the moldboard. Diagrams of this moldboard are shown in figures 14-16.

In the design of this second snowplow, emphasis is being placed on reduction of weight and cost, as well as improving the mechanical systems involved. The test program for this snowplow will be quite similar to the one done for the first experimental snowplow so the results from the West Yellowstone testing can be verified.

CONCLUSION

The work done to date shows that significant reductions in the energy required for snowplowing can be made with the use of better cutting edge geometries. Further analysis of the data from the West Yellowstone testing should yield a better understanding of how these improvements are made. A second experimental snowplow and two prototypes currently being designed and fabricated will be field tested next winter.

LITERATURE CITED

Hansen, A.C. (1991) "An Analysis of Energy Dissipation Caused by Snow Compaction During Displacement Plowing," Transportation Research Board (In Press).

ACKNOWLEDGMENT

The research described herein was supported by the Strategic Highway Research Program (SHRP). SHRP is a unit of the National Research Council that was authorized by section 128 of the Surface Transportation and Uniform Relocation Assistance Act of 1987.

DISCLAIMER

This paper represents the views of the authors only, not necessarily reflective of the views of the National Research Council, the views of SHRP, or SHRP's sponsors. The results reported here are not necessarily in agreement with the results of other SHRP research activities. They are reported to stimulate review and discussion within the research community.

Theoretical and Experimental Results of Using Binders for Snow Roads and Runways in Antarctica

MICHAEL BARBER AND ROBERT L. BROWN
Civil/Ag Engineering
Montana State University
Bozeman, Montana 59717

ABSTRACT

The consequences of adding wood as a binder material to snow is discussed in this paper. A modified mixture theory, based upon volume fraction, is proposed. Field and laboratory experiments, conducted in the laboratory using a 50k MTS press with a cold chamber, are presented. The laboratory samples were allowed to sinter and then compressed at two different strain rates. This laboratory data suggests the suitability of binders to strengthen the snow matrix. Mixtures of wood/snow pavement test sections were constructed in the Antarctic at two sites, McMurdo and Amundson-Scott South Pole Stations. Test sections were monitored for three months during the austral summer and tested again a year later. Rammsonde penetrometer, density and temperature profiles were used to evaluate material behavior. Field results indicate snow pavement strength depends upon temperature history, initial material properties, and construction processing techniques. Satisfactory strengths, for supporting wheeled aircraft, were obtained at depths below 20 cm at both stations. Field evidence shows that with an improved surface processing technique, such as heat processing, adequate strength may be obtained to support wheeled aircraft landing in the antarctic.

INTRODUCTION

During World War II wood was used with ice to create "ice-crete ships" for use in the North Sea, as described by Moser (1963). During the Olympics at Squaw Valley, wood was used to strengthen and increase the durability of the parking lot. When mixed with wood, the characteristics of snow undergo a change in mechanical behavior. When the need to improve the roads and runways in Antarctica became evident, the compaction and use of binder materials was investigated. This study investigates the change in material properties when sawdust is added as a binder to a snow matrix.

McMurdo has runways and taxiways that exist on approximately eight feet of snow atop of the Ross Ice Shelf. During the austral summer the temperatures rise above freezing for several weeks, causing the surface layer of snow to become isothermal, resulting in some melting. Trucks and vans equipped with special tires transport materials from the aircraft into McMurdo, via a five mile long snow road. When temperatures rise, these vehicles have difficulty on the snow road. In particular, the reduced strength due to the snow becoming wet resulted in rutting, formation of potholes and washboarding. A process whereby the road is made passable for all vehicles during the entire season would increase the efficiency of the support services. This technique would also facilitate landing the aircraft on snow runway with wheels instead of skis.

South Pole station has consistent low temperatures and exists at an altitude of 2805 m. Due to the altitude and cold temperatures, aircraft are taxed in their ability to carry heavy payloads out of this site. The increased ski friction below –20°C and decreased performance of the aircraft at that altitude could be enhanced by aircraft on wheels. If the runway and taxiway were constructed such that wheeled aircraft were able to land, it may be possible to utilize aircraft with a larger payload, allowing fewer flights to provide the necessary resupply each

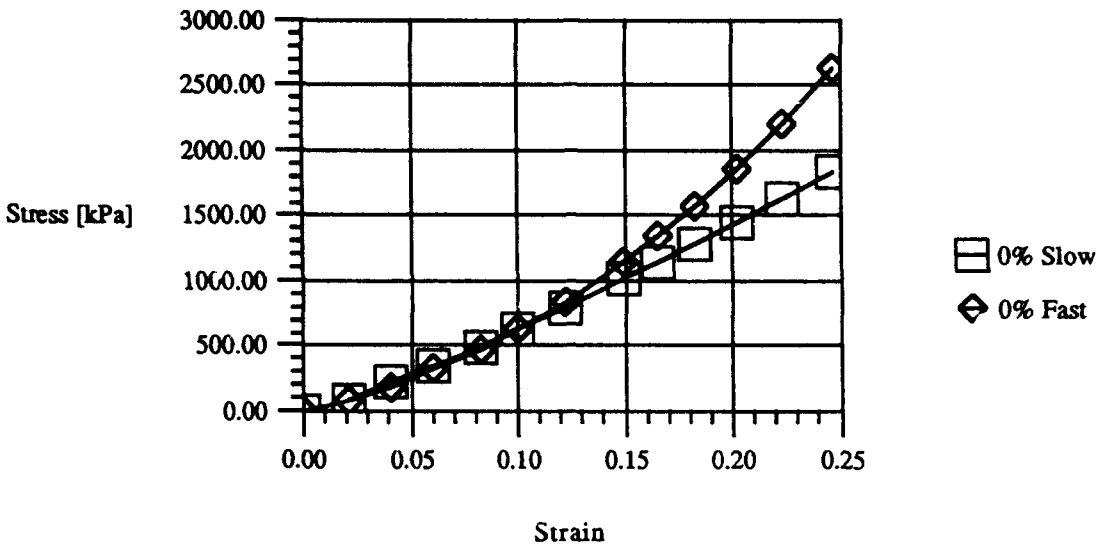

Figure 1. Stress-strain curves (100% snow at 2.5 mm/s and 25.0 mm/s).

season. In addition, use of C-141 aircraft on wheels would allow nonstop flights from Christchurch, New Zealand, an obvious improvement in the logistics problem for the South Pole.

Over the past 20 years, much research has been conducted on ways to develop and improve snow compaction techniques. For example, a well known fact is that snow sinters and hardens at a faster rate than the normal metamorphic process when it is agitated and compacted, Abele and Frankenstein (1967). Past research utilizing sawdust and woodchips as binders in a snow matrix is reported by CRREL, Abele (1963).

The mechanics of the process whereby snow and wood bonds together is not totally understood, but a method of constructing a useful mathematical model is proposed as well as the field and laboratory test results.

LABORATORY TEST RESULTS

Snow from Grayling Pass in Montana was stored in the cold room at Montana State University for a period of 2 months. This snow was then agitated and mixed with the appropriate amount of sawdust to achieve the correct mixture contents. The samples were placed in sonotubes and compressed at the rate of 2.5 mm/s until a stress of 0.2 MPa was reached. The entire batch was then stored in the cold room for 27 days until testing.

Mixture contents of 0%, 2.5%, and 10% wood were tested. Those samples without wood were mixed and compacted in the same manner as those containing wood. Two strain rates, 25.0 mm/s and 2.5 mm/s (in this paper referenced as fast and slow), were used to compare the rate effect on the stress-strain relation. The average density of the snow samples were 0.532 g/cm^3 plus or minus 0.007 g/cm^3. Samples with a larger wood content had a lower density, while those without wood were more dense.

Figure 1 shows the general difference between strain rates for snow without any wood content. This is as expected, for the higher the strain rate the stiffer the matrix should be. Figures 2 and 3 indicate how the percent of wood effects the stress-strain behavior of the snow matrix for the two different strain rates. Notice, for the faster strain rate, the pure snow matrix is stiffer for small strains than that achieved with wood added. As the strain increases, the effect of the added wood becomes more influential and the strength exceeds that of pure snow. This becomes more pronounced with the slower strain rate. From figure 3 we can conclude that with wood the stress-strain relationship does increase for strains exceeding approximately 8% strain.

As previously mentioned, the density for pure snow was higher than for wood/snow mixtures. It is further proposed by Barber, Brown, and Lee (1989) that the sintering process is different for the ice grains than with ice and wood particles. As deformation takes place, bonds fracture, allowing the pure snow samples to decrease in relative strength. The ice grains in the snow matrix containing wood will also fracture, but the wood/ice bonding may not fracture giving larger particles within the collapsing matrix from which to gain strength.

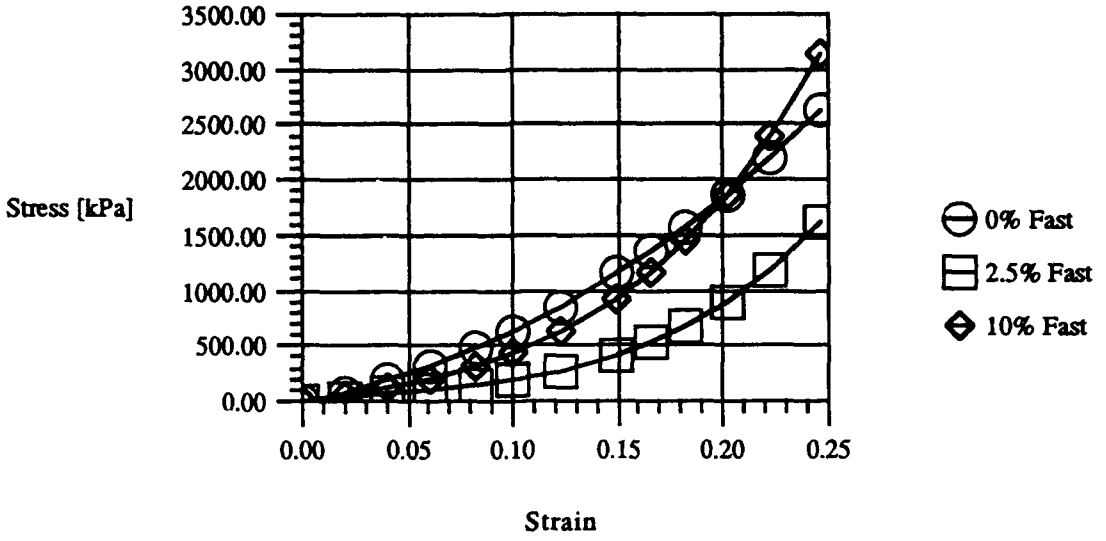

Figure 2. Stress-strain curves (% wood at 25.0 mm/s).

ANTARCTICA TESTING

A testing program was established at McMurdo Station, Antarctica and at South Pole Station, Antarctica to evaluate the properties of wood/snow mixtures in the field. The data taken for evaluation were temperature profiles, density profiles, California Bearing Ratio test (CBR), Clegg impact tests and the Rammsonde penetrometer test (resulting in a Ram value). This paper does not address the CBR and Clegg test results.

During the austral summer at McMurdo the temperatures ranged from −17°C to +5°C. The in-situ snow grains are approximately 0.2 mm with rounded edges and some minor faceting. Initial densities were on the order of 0.35 g/cm^3 to 0.45 g/cm^3. Early in the summer the snow had a low free water content while later in the season it rose dramatically. The snow road and runway are on the lee side of a ridge that descends from Mt. Erebus, which causes significant deposition of snow adjacent to the ridge than near the runway. The snow, about 2.5 m deep at the runway and 5 m deep near the beginning of the snow road, lies on top of the Ross Ice Shelf which is approximately 8 m above sea level at this point. Most of the melt runoff from the ridge runs onto

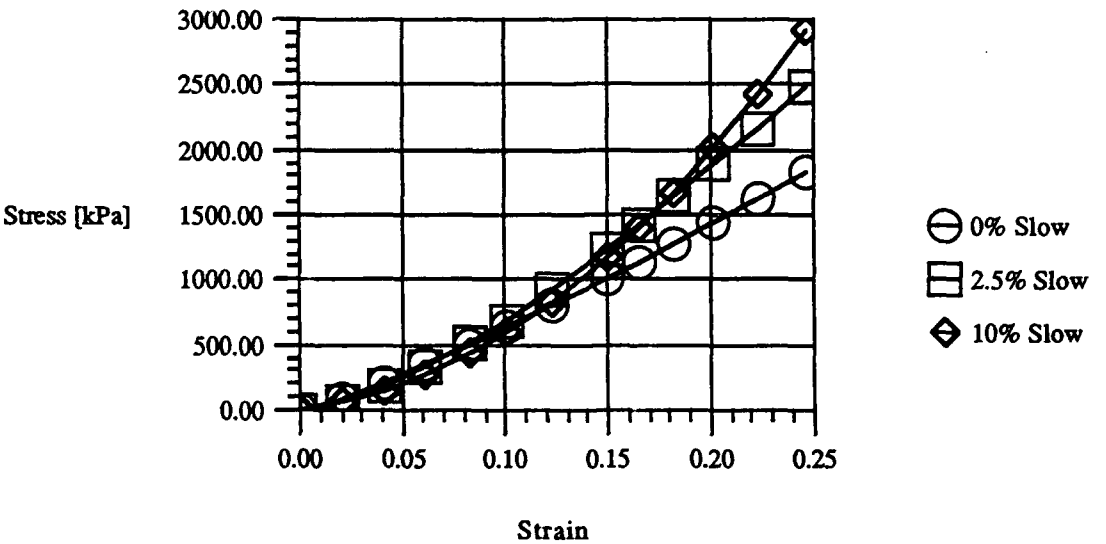

Figure 3. Stress-strain curves (% wood at 2.5 mm/s).

the ice shelf near the transition zone of the dirt road with the snow road.

South Pole Station temperatures ranged from –45°C to –17°C during the initial testing while during the winter months temperatures can be lower than –80°C. The snow grains are about 0.1 mm, rounded and very dry. These grains precipitate from the atmosphere and then blow about the surface for many years. Due to the blowing ice particles and the 10 cm per annum accumulation, the initial densities are higher than at McMurdo. There is a moderate transition from the ice granular surface to the ice approximately 30 m below. However the firn at the South Pole does show a definite stratigraphy Gow (1965) which has an annual periodicity showing alternating layers of a wind crust formed during the winter and a temperature gradient layer formed during the summer and fall. The maximum solar intensity available is at an angle of incidence, 23.3°.

Four testing plots were established, two at each base. At both McMurdo and South Pole stations, a test plot was situated on a taxiway. In addition, McMurdo had a plot on the shuttle road used by vans, and the South Pole had a plot on the cargo berm area utilized by tracked vehicles for cargo and personnel transport. Each sample section was 6 m wide by 12 m long by approximately 1 m deep, except for the McMurdo taxiway section, which was 9 m by 8 m to allow aircraft use. Each plot was constructed by a bulldozer (D-6), equipped with low ground pressure width tracks. After scraping out to a depth of one meter, four lifts of 15 cm each were placed on top of a 30 cm layer of compacted snow. Sawdust was then placed over each lift and mixed with a Honda snow blower. In the control sections (100% snow, no sawdust) pulverization was achieved by using the snow blower. Each lift was then compacted by a low ground pressure bulldozer traversing the test sections twenty times. Optimal mixing was not achieved at either site, since the snow blower did not have sufficient power to adequately pulverize the dense snow, characteristic of Antarctic snow.

Temperatures during construction of the snow road at McMurdo Station ranged from –5°C to –15°C, and the snow had ambient temperatures of –5°C to –10°C. During the construction of the taxiway site the ambient temperatures ranged from –1°C to +1°C with snow temperatures of 0°C to –8°C. When building the snow road test site, the weather was clear and sunny. With afternoon temperatures near the freezing mark, the sun warmed the wood so quickly that the snow became very wet and difficult for the snowblower to process. When the taxiway site was constructed the weather was overcast and heating of the sawdust was not such a problem.

At the South Pole Station similar techniques were used except for the area between the depths of 20–40 cm. Due to the altitude and the hardness of the existing snow, the snow blower ceased functioning properly. A Sprite, similar to a van with 2 cleated tracks, was used to try to mix the wood into the snow until the snowblower was repaired. As will be noted later, the properties of this 20 cm layer were quite different from the other layers above and below it. The snow temperature was –30°C to 49°C while the ambient temperature during construction was –40°C and a windchill of –80°C. It was not possible to break the existing snow matrix into a fine powder, due to the density.

At both the South Pole and McMurdo, test sites had plots of 10% sawdust/90% snow and 5% sawdust/95% snow to volume ratios plus a 100% snow plot used as a control. In all plots, pulverization and compaction were identical except for the 20 cm layer in the South Pole taxiway. After initial construction of the plots the Rammsonde penetrometer test (with a 30° cone), temperature profiles and density profiles were performed to monitor the change in properties as it varied with time. In addition, at the end of the season core samples were taken to determine density and temperature profiles within the sample plots.

Ram values presented demonstrate the change in material properties due to processing, temperature fluctuations, material composition and aging. The surface temperature represents the current ambient air temperature. Ram values are not given for the first 15 cm below the surface, since this distance is needed before the cone is fully inserted into the snow. The densities for the region from the surface to a depth of 50 cm are given.

McMurdo Station results

The results of the field studies at McMurdo (Williams Field road and taxiway) are illustrated in Figures 4–7. The temperature profiles were obtained at the time of density determination, Figure 4 gives a typical profile. Temperatures are recorded starting with the surface, then to a depth of 70 cm. There had been approximately one week during which temperatures exceeded +4°C each day; then a cold front with wind and snow arrived to lower the air temperature. Daily highs were about 0°C on the day the snow road sections were tested for the last time, while the high temperature was –2°C when the taxiway sections were finally tested. For the snow road the 10% wood mixture cores ranged from –2.2°C to +0.4°C, the 5% wood mixture ranged from –2.2°C to 0.0°C, an average of –1.0°C to –2.5°C for the 100% processed snow and for the 100% unprocessed snow the temperature ranged from –0.8°C to –0.2°C. At the taxiway site the 10% wood mixture cores had temperatures of +0.5°C to –2.0°C, the 5% wood mixture ranged from –0.5°C to –3.0°C and the 100% processed snow ranged from –1.0°C to –5.0°C. It should

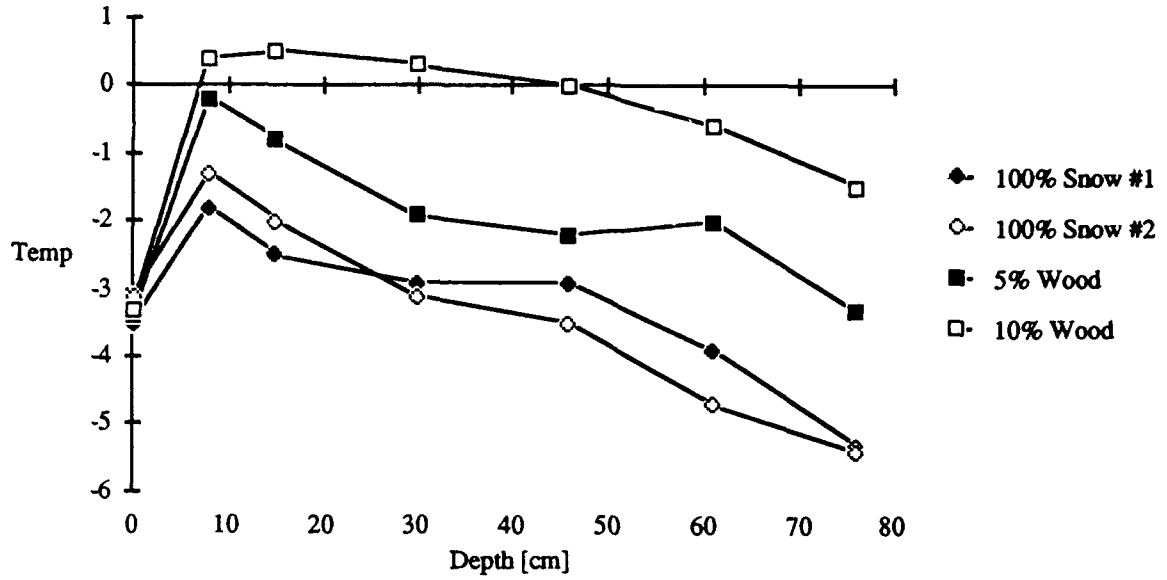

Figure 4. McMurdo Station temperature profile final day of testing.

be noted that these test sites are only one kilometer apart, across the flat Ross Ice Shelf, with tests done on succeeding days.

Rammsonde value measurements were taken throughout the austral summer. The average Rammsonde values taken at 15 days and the average of tests between 15 days and 47 days yielded the following results in Table 2. Table 1 shows how density varied with wood content and location. Additionally, the density changes during the year are recorded. Notice how the maximum densities increased with those sections containing wood.

The densities for the 10% wood mixture were higher than the 5% wood mixture and the 100% snow sections. With high temperature gradients, there was not a large change in the densities. It must be remembered that extreme melting took place in the wood sections due to the solar insolation. This meltwater percolated downward and refroze, thereby increasing densities further

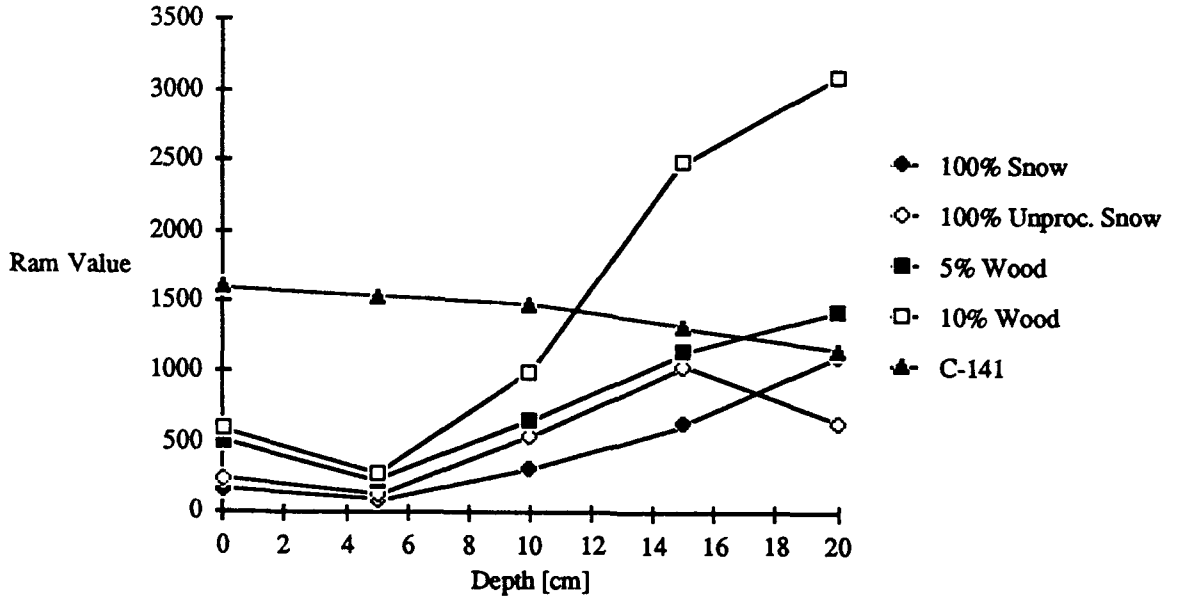

Figure 5. McMurdo Station Rammsonde values (15 days).

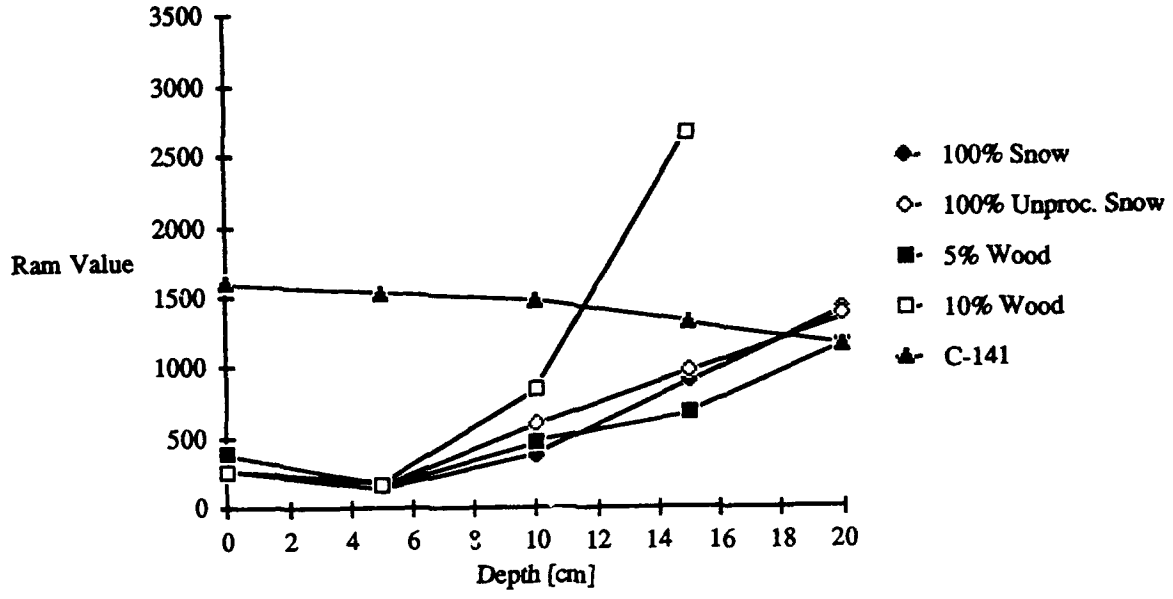

Figure 6. McMurdo Station Rammsonde values (23 days).

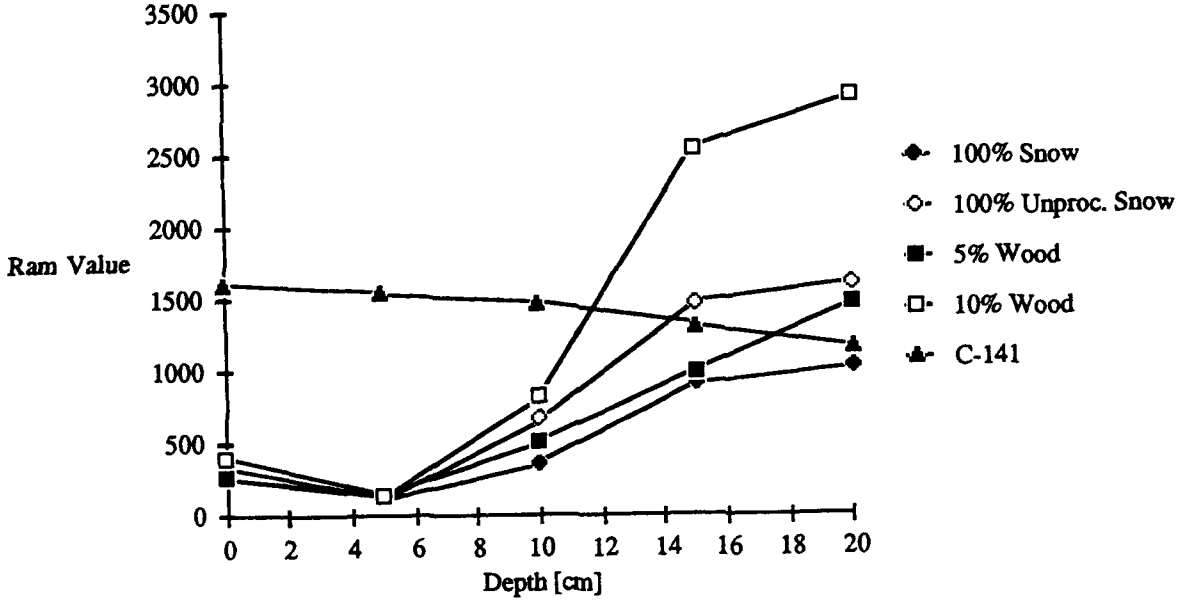

Figure 7. McMurdo Station Rammsonde values (37 days).

Table 1. McMurdo Station density ranges.

% Wood	*Minimum density*	*Maximum density*
0% (Taxiway)	0.62 g/cm³	0.62 g/cm³
5% (Taxiway)	0.65 g/cm³	0.74 g/cm³
10% (Taxiway)	0.70 g/cm³	0.80 g/cm³
Unprocessed (Snow Road)	0.60 g/cm³	0.60 g/cm³
0% (Snow Road)	0.65 g/cm³	0.70 g/cm³
5% (Snow Road)	0.70 g/cm³	0.75 g/cm³
10% (Snow Road)	0.65 g/cm³	0.85 g/cm³
Unproc. (Snow Road 1 yr.)	0.41 g/cm³	0.60 g/cm³
0% (Snow Road 1 yr.)	0.66 g/cm³	0.79 g/cm³
5% (Snow Road 1 yr.)	0.73 g/cm³	0.86 g/cm³
10% (Snow Road 1 yr.)	0.70 g/cm³	0.87 g/cm³

Table 2. McMurdo Station Rammsonde values.

% Wood	*Average value*	*Range of values*	*Maximum value*
0% (Taxiway)	450	375–870	1050
5% (Taxiway)	750	525–1125	1950
10% (Taxiway)	1050	750–1500	1950
0% (Snow Road)	450	300–750	2250
5% (Snow Road)	750	600–1050	2700
10% (Snow Road)	1050	900–1200	3000

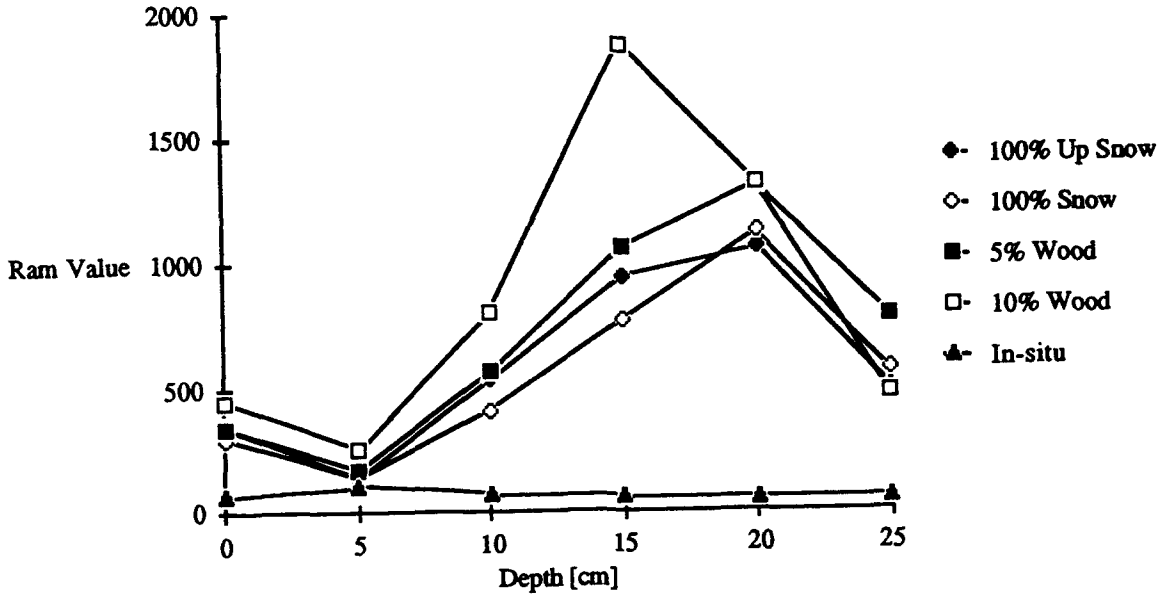

Figure 8. McMurdo Station Rammsonde values (season average).

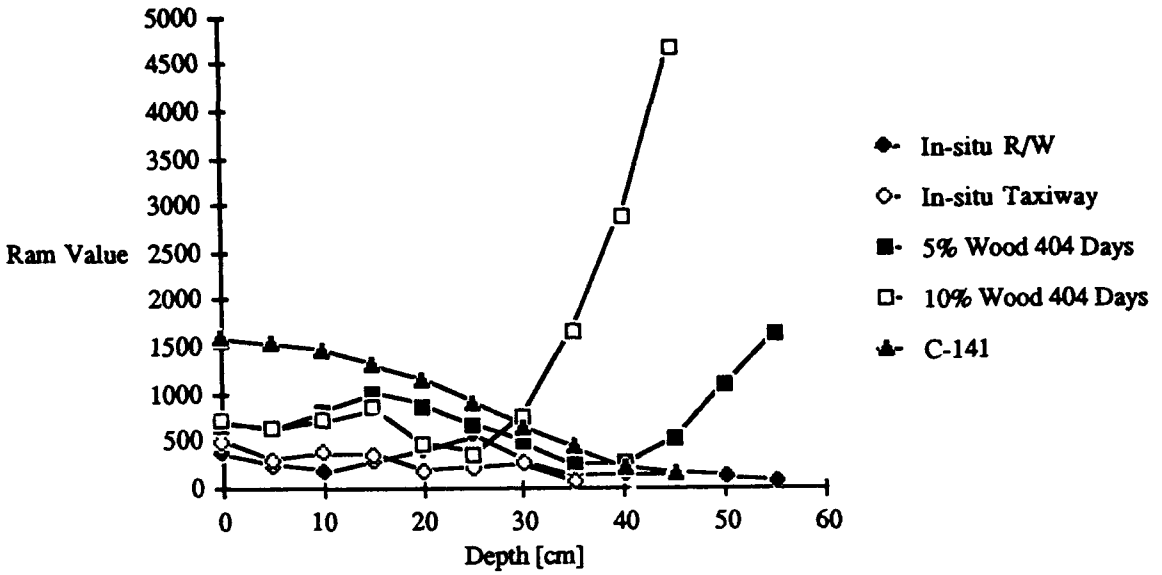

Figure 9. South Pole Station Rammsonde values (1 year).

down in the snow cover.

From Table 2 and Figures 5–8, it may be observed that as the percent of wood increases so does the average Ram value. This must be contrasted with the observation that densities did not differ greatly between different wood contents. Notice, the maximum Ram values occur in those sections with the highest percent of wood. Additionally, the highest lower bounds for the Ram value also occur in the sections with the highest percent of wood. The average Ram values for McMurdo Station taken as one sample are given in Table 2.

South Pole Station results

The effect of the processing may be observed by examining Figure 9 and comparing the profiles of the test plots, existing taxiway and the runway, thereby indicating how the processing increases the Rammsonde values.

The decrease in density from the surface to 40 cm is due to the change in compaction and mixing technique as noted in the processing procedure. The expectation of a large difference with the in-situ density versus the compacted density was not evident; this may be attributed to the high initial density as it exists at the South Pole in the cargo berm and taxiway, both areas of heavy traffic. Further, the density in the sections containing sawdust were slightly higher than the 100% snow samples although there is a moderate drop in the samples taken during the initial season compared with later samples.

The Rammsonde profiles reflect the layering process in the taxiway test section. The values decrease in the region 20–40 cm below the surface where there was inadequate compaction and mixing due to the snow blower becoming inoperable, requiring hand mixing and compaction by the Sprite. This demonstrates the

Table 3. South Pole Station densities.

% Wood	*Minimum density*	*Maximum density*
0% (Cargo Berm)	0.64 g/cm^3	0.69 g/cm^3
5% (Cargo Berm)	0.62 g/cm^3	0.66 g/cm^3
0% (Taxiway)	0.55 g/cm^3	0.58 g/cm^3
5% (Taxiway)	0.50 g/cm^3	0.61 g/cm^3
10% (Taxiway)	0.58 g/cm^3	0.59 g/cm^3

Table 4. South Pole Station Rammsonde values.

% Wood	Average Rammsonde value	Range of Rammsonde values
0% (Cargo Berm)	993	750–1633
5% (Cargo Berm)	1977	982–3261
0% (Taxiway)	567	99–1401
5% (Taxiway)	562	145–1308
10% (Taxiway)	1092	192–2610
0% (Taxiway 1 yr.)	792	439–1639
5% (Taxiway 1 yr.)	837	472–1561
10% (Taxiway 1 yr.)	1599	370–3108

necessity of thorough pulverization and compaction for obtaining high strengths.

Temperature gradients from the South Pole show that there was not an appreciable effect of the wood mixture on the temperature profiles. Average temperatures ranged from –22°C at the surface to –23°C at a depth of 60 cm at the time of final coring.

For the 10% wood mixture the Ram values had higher average numbers then either the 5% wood mixture or the 100% snow. Ram values increased with respect to time faster for the 10% wood mixture than for 100% snow and the 5% wood mixture. At depths below 40 cm, the average Ram value for the 10% wood mixture was much greater than the other samples, particularly after 404 days. As noted above, the density for the 10% wood mixture was slightly higher than the other mixtures.

MATHEMATICAL MODEL

Snow is an elastic-viscoplastic material. Many physical and mathematical models have been proposed in the past. Here, we propose to model snow mixtures using a modified mixture theory proposed by Hansen (1989). Classical mixture theory, as proposed by Truesdell and Toupin (1960) considers each constituent within the mixture separately. Balance equations are proposed for each constituent which depend upon the independent variables of that constituent. A rigorous development of classical mixture theory may be found in the work of Bowen (1976).

Truesdell and Toupin (1960) introduced the notion of baricentric velocity given by

$$\tilde{\mathbf{x}} = \frac{\sum_{\alpha=1}^{n} \omega_\alpha \dot{\mathbf{x}}_\alpha}{\sum_{\alpha=1}^{n} \omega_\alpha} \tag{1}$$

where $\omega_\alpha \in R$ is a weighting factor and

$$\sum_{\alpha=1}^{n} \omega_\alpha \neq 0 .$$

The restriction in this paper will be for the weighting factor $\omega_\alpha > 0$, for all α. The velocity of the mixture α is denoted by

$$\dot{\mathbf{x}}_\alpha = \frac{\partial \mathbf{x}_\alpha (\mathbf{X}_\alpha, t)}{\partial t} . \tag{2}$$

The choice of weighting factor ω_α will determine the mixture theory derived. Consider first the factor $\omega_\alpha = c_\alpha$, where c_α is the concentration of the αth constituent. Then,

$$\dot{\mathbf{x}} = \frac{\sum_{\alpha=1}^{n} c_\alpha \dot{\mathbf{x}}_\alpha}{\sum_{\alpha=1}^{n} c_\alpha} = \frac{\sum_{\alpha=1}^{n} \frac{\rho_\alpha}{\rho} \dot{\mathbf{x}}_\alpha}{\sum_{\alpha=1}^{n} \frac{\rho_\alpha}{\rho}} = \frac{\sum_{\alpha=1}^{n} \rho_\alpha \dot{\mathbf{x}}_\alpha}{\sum_{\alpha=1}^{n} \rho_\alpha} \tag{3}$$

which gives the classical mixture theory definition of mean mixture velocity, Truesdell and Toupin (1960) and Bowen (1976).

A different choice made by Hansen (1989) is for the weighting factor to be $\omega_\alpha = \nu_\alpha$, where ν_α is the volume fraction. This is the amount of the body that is constituted by constituent α. This results in the following definition for mixture velocity,

$$\dot{\mathbf{x}} = \frac{\sum_{\alpha=1}^{n} \nu_\alpha \dot{\mathbf{x}}_\alpha}{\sum_{\alpha=1}^{n} \nu_\alpha} = \sum_{\alpha=1}^{n} \nu_\alpha \dot{\mathbf{x}}_\alpha \tag{4}$$

since we impose the restriction that

$$\sum_{\alpha=1}^{n} \nu_\alpha = 1 \tag{5}$$

Equations (3) and (4) give very different results for the mixture velocity in both magnitude and direction. Equation (4) is associated with the mixture theory proposed by Hansen (1989), which will be called in this paper the modified mixture theory. The theory based upon eq (3) is called the classical mixture theory. There are different assumptions which are fundamental to each theory.

Truesdell (1984) lists the Three Metaphysical Principles to be followed when considering mixtures.

1. All properties of the mixture must be mathematical consequences of properties of the constituents.
2. So as to describe the motion of a constituent, we may in imagination isolate it from the rest of the mixture, provided we allow properly for the actions of the other constituents upon it.
3. The motion of the mixture is governed by the same equations as is a single body.

These fundamental principles relate the properties and field equations of each constituent to the properties and field equations of the body as a whole.

Classical mixture theory is based upon the choice of weighting factor $\omega_\alpha = c_\alpha$ and metaphysical principle number 3. These are founded upon the two assumptions.

1. The mass weighted mean velocity of the mixture is given by

$$\dot{\mathbf{x}} = \frac{1}{\rho} \sum_{\alpha=1}^{n} \rho_\alpha \dot{\mathbf{x}}_\alpha \ . \tag{6}$$

2. The sum of the constituent equations must result in the equations of the mixture.

These give the complete classical mixture theory.

Hansen (1989) has pointed out that the mean velocity of the mixture contains the notion of linear momentum. Since velocity is a purely kinematic term it does not seem reasonable to define kinematics in terms of linear momentum. Furthermore, Segev and Taragan (1989) discuss the restrictions of adding forces that are members of different vector spaces. In general, stress fields must have the same domain and the forces must be of the same vector space to add the constituents to get the results for the entire mixture.

Hansen (1989) proposed what will be called modified mixture theory. In this theory the choice of weighting function is $\omega_\alpha = v_\alpha$. Additionally, the third metaphysical principle is altered. These assumptions are as follows.

1. The mean mixture velocity is given by

$$\dot{\mathbf{x}} = \sum_{\alpha=1}^{n} v_\alpha \dot{\mathbf{x}}_\alpha \ . \tag{7}$$

2. The behavior of the mixture is governed by the summed constituent balance equations which reduces to the balance equations of a single mixture as a special case.

Notice, the kinematic definition for velocity now contains only terms that are kinematic in nature and the mixture behaves in accordance with the summed field equations. While this answers the objections of Hansen (1989), it does not answer all those of Segev and Taragan (1989). It appears that in using Eulerian coordinates the constituent spaces will have the same domain with forces from the same field. Thus this paper will limit itself to using Eulerian coordinates.

Based upon the above analysis, the modified mixture theory will be utilized to model mixtures of cohesive elastic-viscoplastic materials. For our case, these materials are mixtures of snow and wood.

The mean velocity of the modified theory does not have a good physical meaning which is very different from that mean velocity defined in classical mixture theory. This loss of physical meaning results in a gain in understanding of the physical boundary conditions.

Balance equations

With the assumptions made by Hansen (1989), the balance equations become the following,

$$\dot{\rho}_\alpha + \rho_\alpha \operatorname{div}(\dot{\mathbf{x}}_\alpha) = \overset{+}{c}_\alpha \tag{8}$$

$$\rho_\alpha \ddot{\mathbf{x}}_\alpha - \operatorname{div}(\mathbf{t}_\alpha) - \rho_\alpha \mathbf{b}_\alpha = \overset{+}{\mathbf{p}}_\alpha \tag{9}$$

$$\mathbf{t}_\alpha - \mathbf{t}_\alpha^T = \overset{+}{\mathbf{M}}_\alpha \tag{10}$$

$$\rho_\alpha \dot{e}_\alpha - \operatorname{tr}(\mathbf{t}_\alpha^T \mathbf{L}_\alpha) + \operatorname{div}(\mathbf{q}_\alpha) - \rho_\alpha r_\alpha = \overset{+}{e}_\alpha \tag{11}$$

along with the restrictions imposed by the second law which has the form,

$$\rho\dot{\eta} + \sum_\alpha \left\{ \operatorname{div}\left(\frac{\mathbf{q}_\alpha + \rho_\alpha \theta_\alpha \eta_\alpha \mathbf{u}_\alpha}{\theta_\alpha} \right) - \frac{\rho_\alpha r_\alpha}{\theta_\alpha} \right\} \geq 0 \ . \tag{12}$$

The terms on the right hand side of equations (8) to (11) are the supply terms. These account for the interaction forces between constituents. Truesdell and Toupin (1960) show that the summation of these supply terms must obey certain rules. Hansen (1990) demonstrates that to be consistent with kinetic theory the following rules must apply.

Summing rules

The rules for summing eq (8) through (11) must result in the following relations for the supply terms,

$$\sum_\alpha \overset{+}{c}_\alpha = 0 \tag{13}$$

$$\sum_{\alpha} \hat{\mathbf{p}}_{\alpha} = 0 \tag{14}$$

$$\sum_{\alpha} \hat{\mathbf{M}}_{\alpha} = 0 \tag{15}$$

$$\sum_{\alpha} \hat{\varepsilon}_{\alpha} = 0 . \tag{16}$$

As shown by Hansen (1990), this is different from the classical mixture theory which contains diffusion velocity terms, making the solution much more complicated.

Assumptions regarding the behavior of the mixture as a whole are also made. The compilation of all constituents should behave as a single constituent. This restriction is placed on the balance equations by summing the densities, stresses, heat fluxes, body forces, energies, heat sources, and entropy. The form of these summations is shown to be,

$$\rho = \sum_{\alpha} \rho_{\alpha} \tag{17}$$

$$\mathbf{t} = \sum_{\alpha} \mathbf{t}_{\alpha} \tag{18}$$

$$\mathbf{q} = \sum_{\alpha} \mathbf{q}_{\alpha} \tag{19}$$

$$\mathbf{b} = \sum_{\alpha} c_{\alpha}\mathbf{b}_{\alpha} \tag{20}$$

$$e = \sum_{\alpha} c_{\alpha}e_{\alpha} \tag{21}$$

$$r = \sum_{\alpha} c_{\alpha}r_{\alpha} \tag{22}$$

$$\eta = \sum_{\alpha} c_{\alpha}\eta_{\alpha} \tag{23}$$

Summing the constituent balance equations with the above rules then leads to a system of nonlinear partial differential equations.

Table 5. Internal state variables for a wood/snow mixture.

r	mean bond radius
l	mean bond length
L	mean grain length
R	mean grain length
n_3	mean number of bonds per grain
N_{av}	mean number of grains per unit volume
V_g	mean volume of a single grain
V_b	mean volume of a single bond
S_g	mean surface area of grains per unit volume
S_b	mean surface area of bonds per unit volume
S_{bg}	mean surface area of bond to grain contact per unit volume
σ_g	surface energy of the grain
σ_b	surface energy of the bond
σ_w	surface energy of the wood

Constitutive equations

To complete the number of differential equations with the number of variables we relate the variables through the constitutive equations. Following Coleman and Gurtin (1967) as well as Lubliner (1990), we propose modeling the elastic-viscoplastic behavior with the use of internal state variables. These variables describe the relations at the microscopic level. For our particular application, this method allows the incorporation of interactions between constituents in the form of surface energies.

Each constituent depends upon its own independent variables. In the use of mixture theory we require an accounting of how the constituents interact with each other. This is accomplished with the supply terms. Additionally, we propose a constitutive relation for each supply term. We assume that the constitutive relation for the supply terms may depend upon the independent variables of all constituents. Thus, we have two sets of constitutive equations to formulate: one for each constituent as if it behaved as a single constituent and the other, for the supply terms for each constituent.

The use of internal state variables gives us the ability to analyze the physics of the problem and to use this analysis as the basis of our constitutive equations. Hansen (1985) considered the description of snow by internal state variables. We assume some of his list but include additional terms to describe the surface energy effects between wood and snow. Internal state variables listed below are by no means independent of each other. Current research is being conducted in deriving and identifying the relations between these variables.

These variables describe the microstructure of a wood/snow mixture. The cohesive aspects of the mixture are accounted for by the surface energies, while the geometric and kinematic microstructural behavior comes from the first six variables as described by Hansen (1985) and Edens (1989).

This mathematical model allows us to describe the microstructure of the snow matrix as well as the interaction between the snow and wood constituents. Hansen (1991) has successfully used this model, without the internal state variables, to describe the behavior of composite materials. While this is not the only model available, it has an increasing usefulness to applied engineering problems. Our development will further the transition from theory to application of the valuable mathematical model.

CONCLUSIONS

Laboratory and field tests indicate that use of wood as binder material in a snow matrix increases strength.

It appears that with large strain, this increase in strength is more evident. Temperature plays a vital role in the sintering process of the mixture of snow and wood. For this reason, solar insolation may enhance or destroy the strength integrity. For laboratory tests, solar insolation was not a factor. South Pole Station was not affected by the amount of solar insolation while McMurdo Station was greatly affected.

The tests indicate that the microstructure of the snow/wood matrix is a measure of strength. Ram values that were extremely high were in regions of high wood concentrations. Note, this is true for both McMurdo and South Pole Stations. This indicates that the strength gained is from the wood interactions as well as from ice formation due to melting, for melting did not occur at the South Pole.

In order to quantify the strength of snow/binder mixtures, we chose to model the behavior with the modified mixture theory. This has often been termed too complicated, but we are rewarded with a comprehensive theory describing the microstructural behavior allowing access to the physics of stresses and deformation. The extra work seems to be worthwhile for mixtures of materials.

This model is applicable to other engineering problems. Mixtures of materials containing several constituents may be modeled by developing and relating new internal state variables. Future research will apply these theories more comprehensively to the wood/snow problem. Additionally, we can describe materials containing numerous additional constituents, limited only by our numerical methods and computing power.

ACKNOWLEDGMENTS

The authors would like thank Dr. Sung Lee, Albert Wuori, Dr. Wilbur Haas, and Mark Bott for their support in laboratory and field testing. Appreciation is also extended to the National Science Foundation for their support in funding this project under (DPP-8517148 and DPP-8612951).

LITERATURE CITED

Abele, G. (1983) "Feasibility of Constructing a Snow Runway at the South Pole Station for C-141 Aircraft." Technical Note, Nov. 1983, prepared for Naval Civil Engineering Laboratory, by USA CRREL.

Abele, G. and Frankenstein, G. (1967) "Snow and Ice Properties as Related to Roads and Runways in Antarctica," USACRREL Technical Report 176.

Barber, M.J., Brown, R.L., and Lee S. (1989) "Improving Snow Roads and Airstrips in Antarctica," USACRREL Special Report 89-22.

Barber, M.J., Brown, R.L., and Lee S. (1989) "Binders for Snow Roads and Runways in Antarctica," *Journal of Cold Regions Engineering*, Vol. 3, No. 2.

Barber, M.J., Brown, R.L., and Lee S. (accepted) "Laboratory and In Situ Study of the Effect of Additives on Compaction Strength of Snow," *Journal of Ocean Engineering and Technology*.

Bowen, R.M. (1976) "Theory of Mixtures," *Continuum Physics III*, Eringen, A.C. ed.

Coleman, B.D. and Gurtin, M.E. (1967) "Thermodynamics with Internal State Variables," *Journal of Chemical Physics*, Vol. 47, No. 2.

Edens, M. (1989) "Determining the Change in Snow Microstructure During Large Deformation Processes by the Method of Quantitative Stereology," Masters Thesis, Montana State University.

Gow, A.J. (1965) "Snow Studies in Antarctica." USA CRREL Research Report No. 177.

Hansen, A.C. (1985) "A Constitutive Theory for High Rate Multiaxial Deformation of Snow," Ph.D. Thesis, Montana State University.

Hansen, A.C. (1989) "Reexamining Some Basic Definitions of Modern Mixture Theory," *Int. J. Engng. Sci.*, Vol. 27, No. 12.

Hansen, A.C., Crane, R.L., Damson, M.H., Donovan, R.P., Homing, D.T., Walker, J.L. (1991) "Some Notes on a Volume Fraction Mixture Theory and a Comparison with the Kinetic Theory of Gases," *Int. J. Engng. Sci.*, Vol. 29, No. 5.

Hansen, A.C., Walker, J.L., Donovan, R.P. (1991) "A Finite Element Formulation for Composite Structures Based on a Volume Fraction Mixture Theory," (to be published).

Lubliner, J. (1990) "Plasticity Theory," Macmillan Publishing Co., New York, New York.

Moser, E.H. (1963) "Navy Cold-Processing Snow-Compaction Techniques." In *Ice and Snow* Kingery, W.D. (ed), MIT Press, Cambridge, Mass., 459–484.

Segev, R. and Taragan, E. (1989) "Stresses in Mixture Theory," *Int. J. Engng. Sci.*, Vol. 27, No. 12.

Truesdell, C. and Toupin, R. (1960) "The Classical Field Theories," *Handbuch der Physik*, Vol III/3, Flugge, S. Ed.

Truesdell, C. (1984) Rational Thermodynamics, Springer-Verlag, New York, New York.

The Influences of Adjustable Tire Pressure (CTIS) and Anti Skid Devices When Driving In Snow

STURE BERNHARDSSON
Defense Material Administration, Mobility Directorate
Transport Behicles Division, Test Center
S-645 83 Strangnas, Sweden

Vehicles equipped with an arrangement to adjust the tyre pressure from the driver's seat (Central Tire Inflation System, CTIS) have been used for a long time in Eastern European States, mainly in the Soviet Union. The system was used in the West on certain special vehicles during the second world war. In the United States this method to improve passability on soft ground seems to have received an increased interest in the past few years. During the "Desert Shield" and "Desert Storm" a lot of experiences have proved the advantage of CTIS.

Different solutions of CTIS arrangements have been discussed and shown at previous conferences, among others, by Robert Kaczmarek.

I will here confine myself to tests which have been carried out at the Swedish Defence Materiel Administration's Test Center, and bring forward only results which fall within the theme of this conference.

In order to find out to what extent the CTIS influences a wheeled vehicles advancement, we have equipped a 4x4 vehicle, Volvo C3, (Mil = TGBIL 11), figure 1, with such a system, figure 2. Since a complete system was not available we had to put together components from what we could find. With a control at the driver's seat desired tire pressure can be selected and the pressure can be read on an indicator. All four wheels obtain the set air pressure. Normal air pressure for Volvo C3 is 170 kPa. The dimension of the tires are 280/85-16 and the load is about 850 kg/wheel.

How the surface contact area increases with reduced tire pressure appears from figure 3 and from the diagram in figure 4.

The strength of the surplus drawbar pull was measured in roughly 40 cm deep snow. The snow was mainly of hardness class 1, with a layer of 5 cm thick frozen crust on top of about 20 cm of old coarse grain snow. The results are shown in the bar diagram, figure 5. This diagram shows that the drawbar pull increases by roughly 2.5 times when the tire pressure is reduced from 200 kPa to 50 kPa.

With the type of wheel used, there is a danger of skidding between the rim and the tire at very low air pressure. The type of emergency driving equipment you find on heavier cross-country trucks of the Swedish Defence Forces assures that the tires remain attached to the rim even at low air pressure. Figure 6; cut through wheel with bead clamps.

Returning to the diagram (figure 5), we pass directly onto my next report, concerning driving with snow chains, or anti-skid devices as we prefer to call them in the Swedish Defence, and the reason for that is that we use the chains all the year round on slippery ground (clay, wet stones). The results from draw bar pull tests in identical snow conditions show that with normal tire

Figure 1. Terrängbil 11 (Volvo C3).

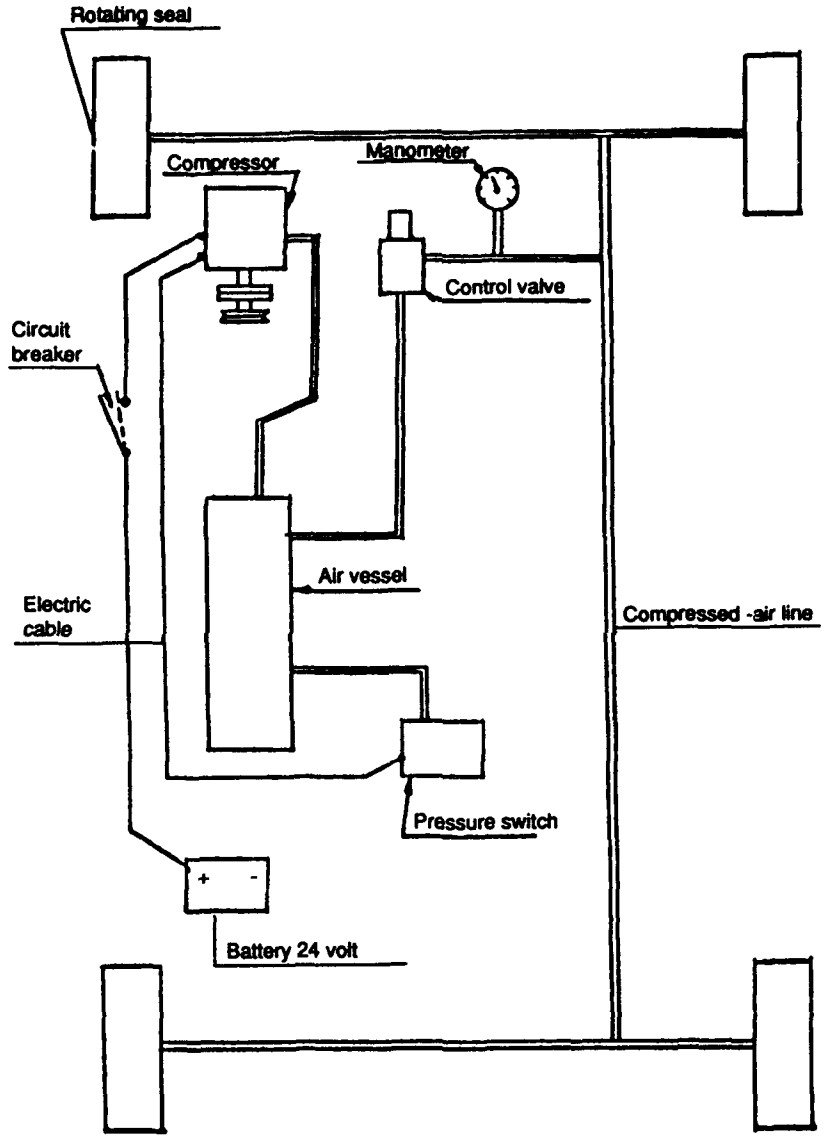

a. Circuit diagram TGB 11.

Figure 2. Central tire inflation system.

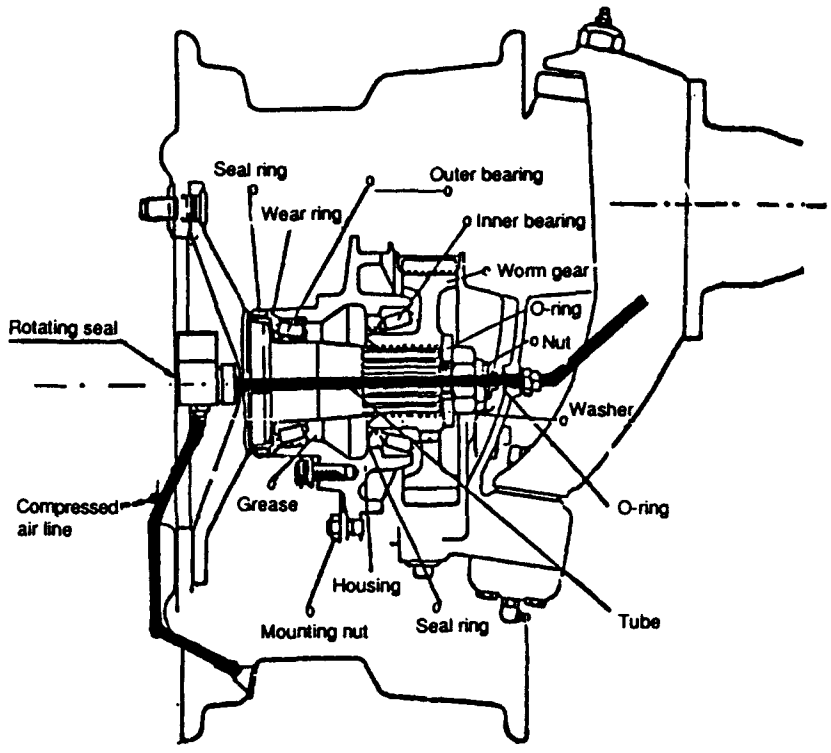

b. Front wheel gear TGB 11.

Figure 2 (cont'd). Central tire inflation system.

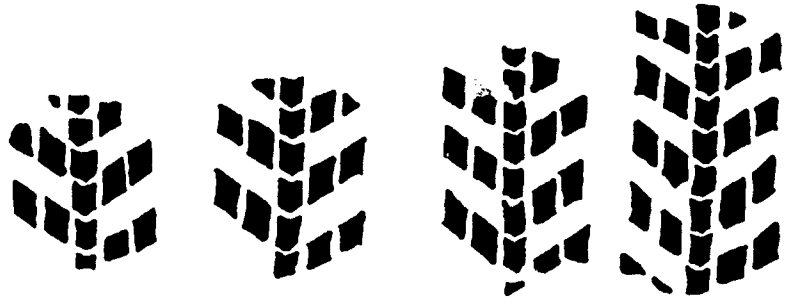

Kpa.	200	150	100	50
Area cm²	465	504	599	860
Kg/cm²	1.88	1.73	1.46	1.02

Figure 3. Rest surface on firmed ground, TGB 11, tyre - 280/85-16.

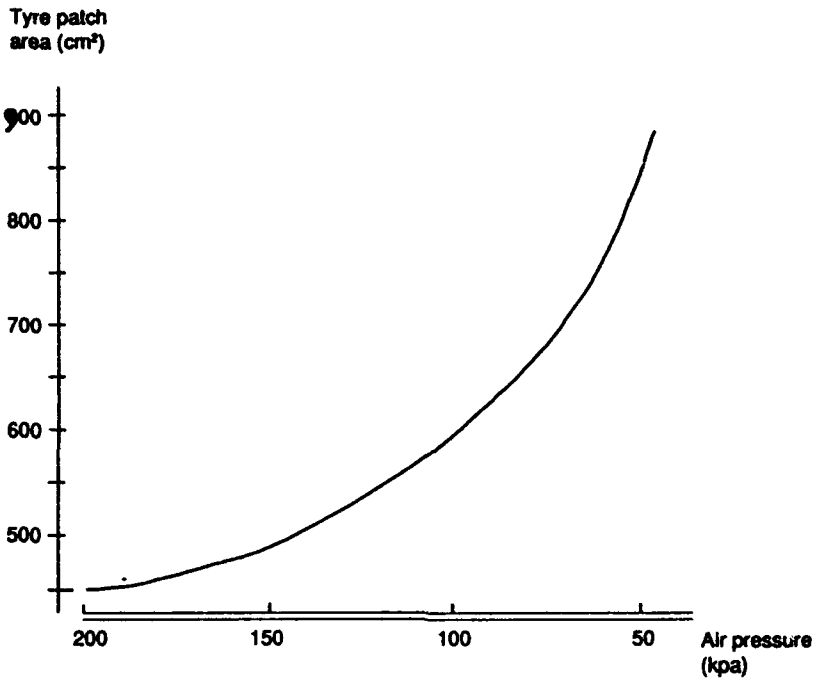

Figure 4. TGB 11, Goodyear 280/85-16.

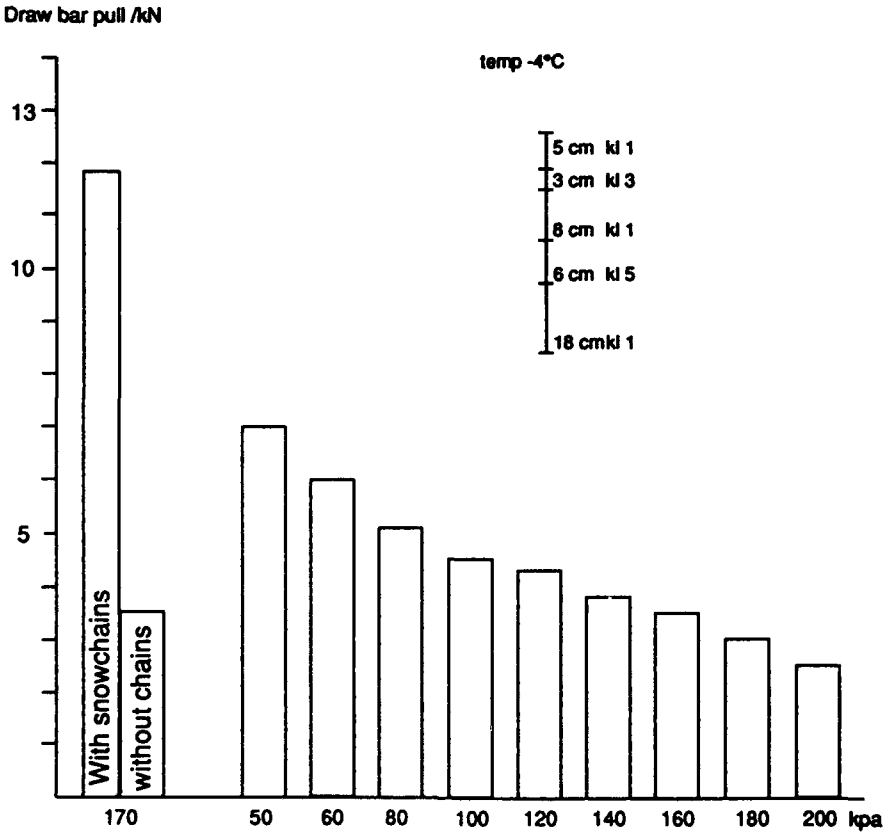

Figure 5. Adjustable tyre pressure TGB11 in 40 cm snow depth.

The tyre lasts longer and will not burst.
The Trelleborg Run Flat System is tubeless, which means longer life than normal as the tyre generates less heat. The tyre being tubeless, also implies that the risk of tube failure is eliminated.

Low weight.
Thanks to the simple construction, the system is light which assists the riding performance. The unsprung weight is low.

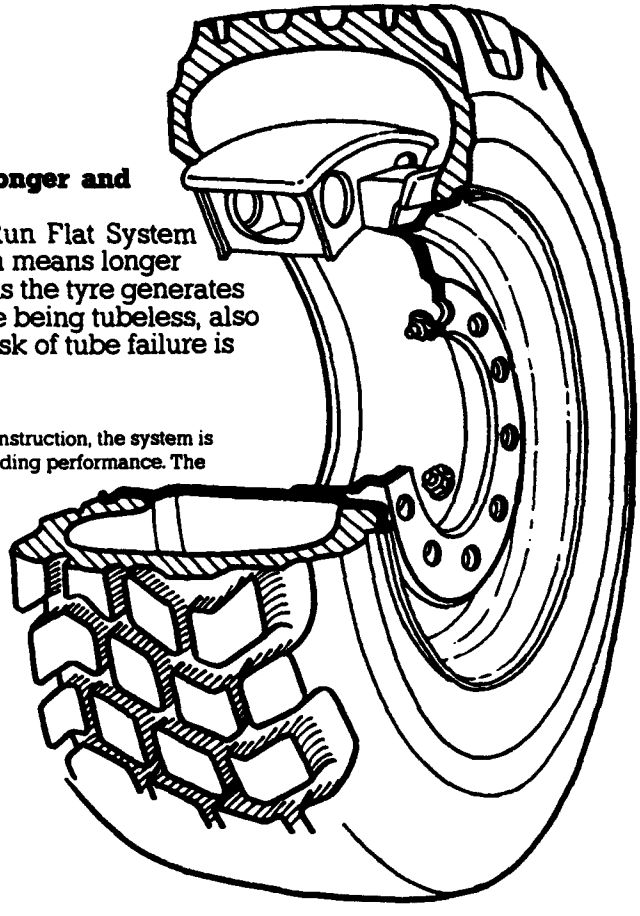

Figure 6. Trelleborg Run Flat System.

pressure and anti-skid devices, the draw bar pull increases considerably. All new cross-country trucks of the Swedish Defence (Volvo C3 4×4 6×6, Scania SBA 4×4 and SBAT 6×6) are at the delivery equipped with anti-skid devices. These have been developed by Gunnebo AB in close cooperation with the Defence Materiel Administration. At drawbar pull tests with SBAT 6×6 (Mil = TGBIL 40) in about 45 cm deep snow, we obtained the results shown in the bar diagram on figure 7. This diagram shows, that in exactly *these* snow conditions, the truck with all wheel drive and differential locks only has a surplus drawbar pull of 0.8 kN. Anti-skid devices on only the first bogie axle increase the pull to 6 kN and with another 2 or 4 anti-skid devices the pull increases moderately. This is one of the reasons why all 3-axle trucks are equipped with only 4 anti-skid devices at the delivery to troop.

The various designs of anti-skid device are not of major importance to the drawbar pull in snow.

Next figure (8) shows tests with different kind of chains on a wheeled tractor on hard, compact snow. The bar diagram shows that the old transversally linked standard chains increase the drawbar pull twice, while the recent special chains with square links or special grip studs respectively, only give a somewhat stronger pull.

When the design of anti-skid devices and their features are discussed the drawbar pull is often given

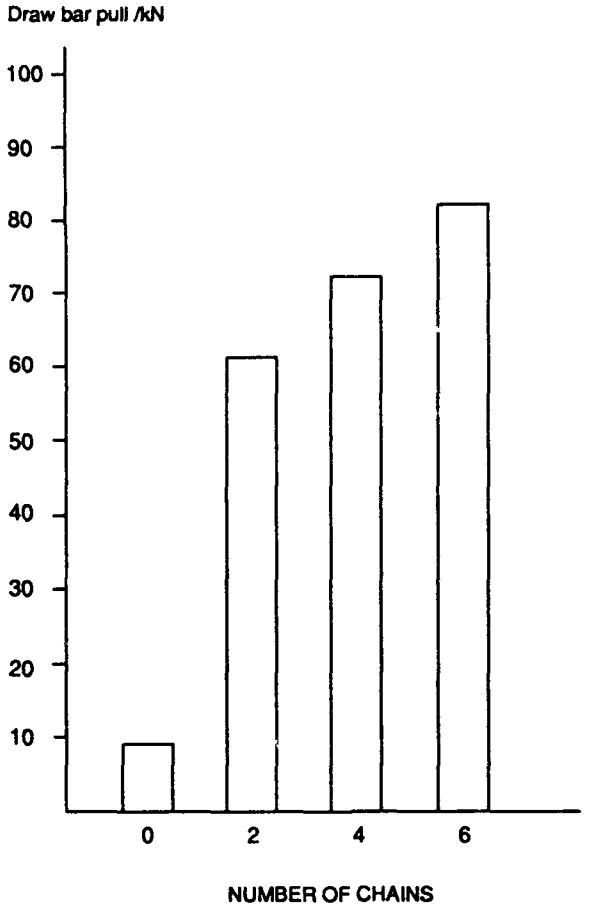

Figure 7. Drawbar pull with standard chains TGB 40 (snow depth 45 cm).

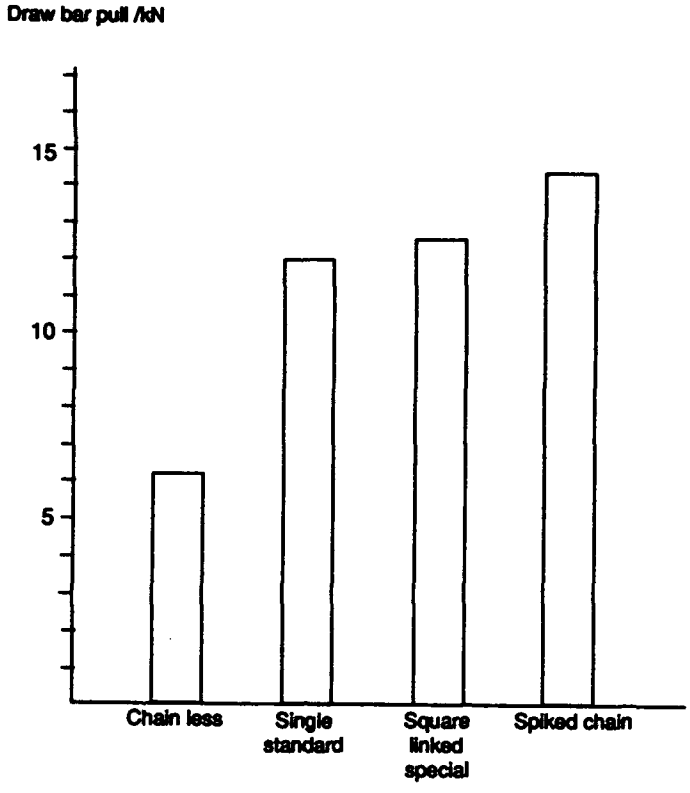

Figure 8. Drawbar pull with three types of chains (wheeled tractors). Hard packed snow on road.

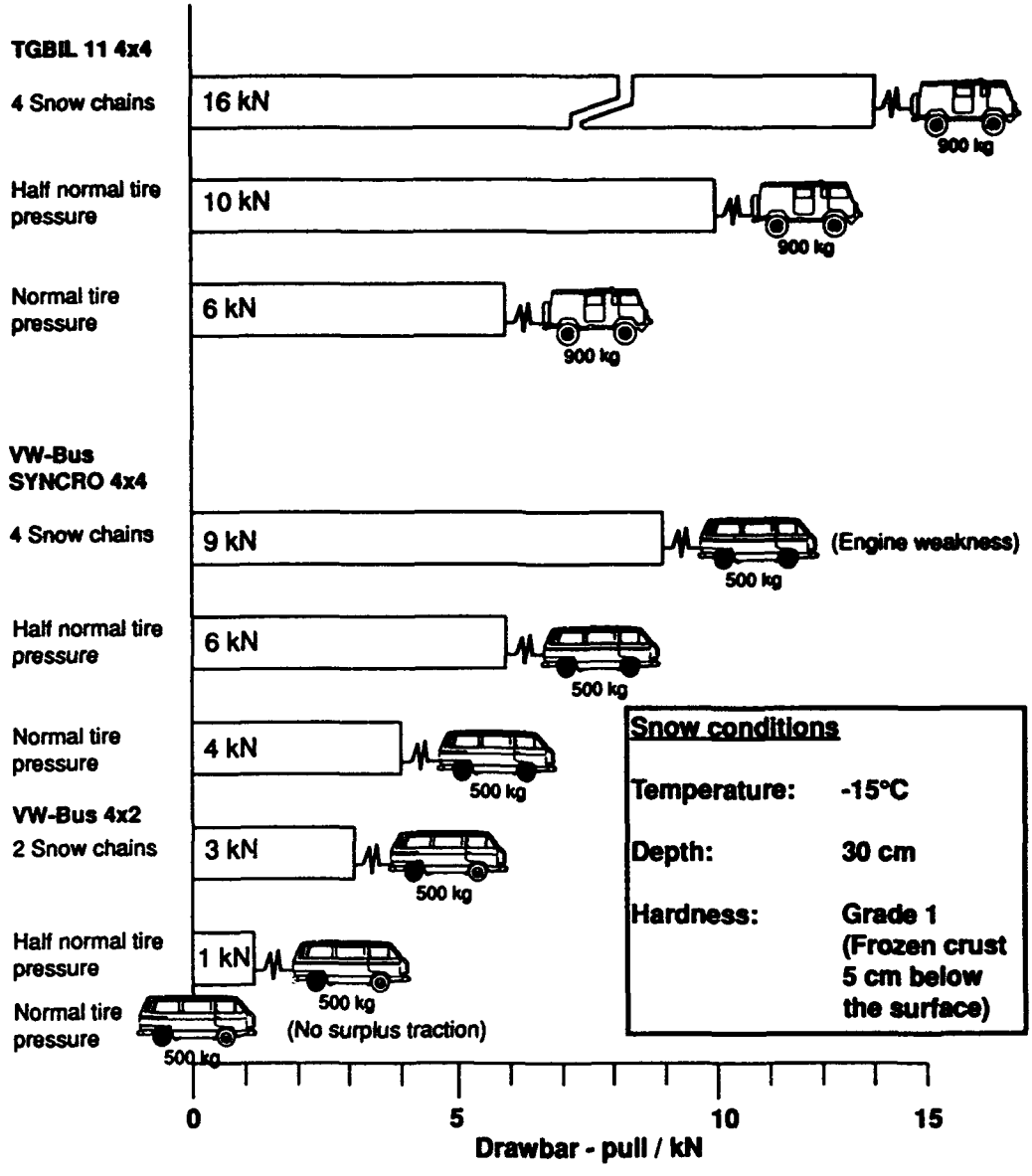

Figure 9. Drawbar pull. VW Bus 4×2, 4×4 Syncro and TGBIL 11 4×4.

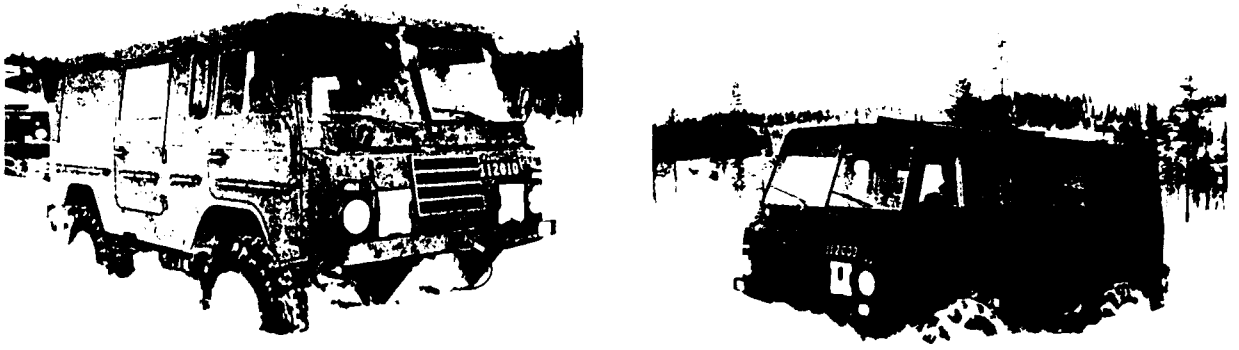

a. Reduced air pressure. *b. Normal air pressure and chains.*

Figure 10. "Floating" position in snow.

attention out of proportion. The following factors should be considered at the evaluation as well:

—Handling (easy to mount and demount)
—Durability (wearing qualities)
—Effects on the vehicle (vibration, wheel balance)
—Effects on the tires (risk of puncture)
—Riding quality (in curves, at braking)
—Contact against the tire (fit-up, throw out)
—Wear on the road
—Maintenance (damage frequency, spare parts, TTR)
—COSTS (LCC)

Comparison of different steps to increase traction (figure 9); We have compared Volkswagen Transporter/Bus 2×4, 4×4 Syncro and Volvo C3 4×4 at the same time and in the same snow conditions. Depending on different designs and different actions the drawbar pull has increased from 0 (zero) to 9 kN (Volkswagen) and from 6 to 16 kN Volvo C3 (TGBIL 11).

SUMMARY

The CTIS gives a skillful driver the possibility to use the wheel equipment in an optimal way on various ground conditions. In certain snow conditions it can give a better passability than anti-skid devices, since it gives the truck a higher floating position (figure 10). The anti-skid device *can not* be replaced by the CTIS. A combination of anti-skid device and CTIS does not work well. The driver should be able to adjust the tire pressure in such a way, that each pair of wheels has a tire pressure corresponding to each axle load.

The Negatively Buoyant Jet/Plume With Applications to Snow Plow Exit Flow Behavior

WILLIAM R. LINDBERG AND JOSEPH D. PETERSEN
Department of Mechanical Engineering
University of Wyoming
Laramie, Wyoming 82071

ABSTRACT

This paper presents the initial findings of an ongoing study of negatively buoyant jet/plume behavior. The motivation for this research is to quantify the dynamics of the exit snow plume from displacement and rotary snow plows. The effects of injection angle and cross flow on the jet/plume behavior have been of particular interest in this phase of the study.

A water tow tank was used for the experiments, where the exit jet was towed through quiescent water at a constant velocity. Photographic records of the jet/plume structure were used to measure the jet/plume dimensions. Dimensional reasoning yielded a set of dimensionless parameters which correlated the jet/plume length scales over a wide range of the experimental parameters.

Three flow regimes have been identified, which depend on the cross flow Froude number, F_o:

$F_o \ll 1$: negligible cross flow,
$0 < F_o < 1$: weak cross flow,
$F_o > 1$: strong cross flow.

where: $F_o = U_o/(g'r_o)^{1/2}$, U_o is the cross flow velocity, g' is the reduced gravity and r_o is the jet radius. Correlations of the measured length-scales with F_o were determined for all three flow regimes.

1. INTRODUCTION

An important aspect of the performance of snow plows is the behavior of the snow after it exits from the moldboard. The exiting snow experiences a very different dynamic environment than the flow conditions along the moldboard itself. At the exit plane, the flow has acquired considerable momentum in the transverse direction (i.e. normal to the plow motion). The flow then persists as a free jet whose trajectory depends on this momentum and the modifying external forces. The forces on this exit fluid include gravity and a complex three-dimensional interaction with the surrounding air, in the forms of entrainment and drag.

Knowledge of the exit plume flow for a variety of operational conditions is viewed as an important element in understanding plow performance, including cast distances, plume trajectories and dilutions, visibility and the potential for altering these characteristics via plow design and operator control.

Very little prior work applicable to exit plume behavior has been reported. In order to begin to address this shortcoming, a laboratory program was initiated to systematically examine the characteristics of negatively buoyant jets/plumes subjected to a cross flow. A very fundamental approach to this study has been adopted, where the full complexity of the problem is initially reduced in order to focus on the basic flow phenomena. Additional parameters may then be introduced and their effects placed in the context of previous observations. This paper summarizes the initial results of this research program.

2. BASIC CONSIDERATIONS— THE NEGATIVELY BUOYANT PLUME

The wide variety of circumstances where knowledge of the behavior of a jet or plume whose density is different than its surroundings has stimulated research on this topic for decades. The majority of this work has centered on the positively buoyant case, where the density deficit of the jet or plume provides a body force in the same general direction as the initial injection direction (i.e. a light fluid injected upward, or a heavy fluid injected downward). Examples of this positively buoyant jet/plume include a cumulus cloud, an industrial smoke-stack or the rising column of smoke from a campfire.

A negatively buoyant jet/plume has a body force in the opposite direction as the vertical component of the injection velocity. In this case, equilibrium heights or flow reversals are always present. The term "vertical component of the injection velocity" is used because these jets can be aligned at an angle to the vertical. Examples of this type of flow include the vertical injection of a dense gas into the atmosphere, the introduction of saline water into a lake or river and for present interest, the behavior of a plume of snow particles after exiting from a snow-plow blade.

A distinction is made between a jet and a plume. A jet is a flow which is due to a source of concentrated momentum such as the flow induced by the discharge from a pipe or orifice. The driving force for a plume is the body force or buoyancy of the plume itself. As an example of this distinction, an initially buoyant jet will expand, slow down and dilute with increasing downstream distance. Eventually, the momentum of the fluid will decrease to the same order as the fluid buoyancy. At this point, the jet becomes plume-like, as buoyancy begins to dominate the flow dynamics, and different behavior would be expected. The same processes are present for a negatively buoyant jet/plume, with the distinction of the reversed body force for the plume, which retards upward motion and ultimately reverses the vertical motion.

The presence of an ambient cross-flow further complicates this process. This external flow can have the effect of turning the jet/plume flow toward the downstream direction and will also alter the internal flow behavior of the jet/plume itself.

Laboratory studies of turbulent jets and plumes have proven to be very useful in applications where the prototype and laboratory scales are considerably different. Dimensional and dynamic similarity arguments are insufficient to justify this success without the underlying premise of Reynolds number independence in these turbulent shear flows. It has been observed that the large-scale turbulent motions are dynamically similar for flows with widely differing Reynolds numbers. It is the large-scale motions which dominate such processes as entrainment, momentum transfer and mixing. All of these processes are central to the dynamical behavior of jets and plumes. Laboratory studies where the basic shear flow is turbulent may then be used to simulate flows whose Reynolds numbers are different, but whose basic behavior is similar.

A dimensional analysis of jets and plumes may be performed to identify the basic parameters of these flows. Figure 1 provides a schematic of the geometry of the negatively buoyant jet/plume in an ambient flow. The jet, of density ρ_j, exits the nozzle, of radius r_o, at a velocity of U_j, into ambient fluid surroundings of density ρ_a. The ambient flow velocity is U_o. For the studies to be reported in this paper, the axis of the jet is inclined an angle θ from the horizontal in a plane perpendicular to the ambient flow direction.

The two most important dynamical parameters of the initial jet are the jet momentum (M) and buoyancy (B) fluxes (normalized with jet exit density):

$$M = \pi r_o^2 U_j^2$$

$$B = \pi r_o^2 U_j \left[(\rho_j - \rho_a)/\rho_j\right] g$$

where g is the gravitational acceleration.

The desired observable geometric parameters include $\mathbf{X_m}$, $\mathbf{W_m}$, $\mathbf{X_t}$ and α, where $\mathbf{X_m}$ is the (x,y,z) length scale triad when the jet is at its maximum height, $\mathbf{W_m}$ is the jet width ($\mathbf{W_y}$, $\mathbf{W_z}$) at the same location, $\mathbf{X_t}$ is the (x,y) length scale for the return of the jet/plume centerline to the original height of the jet and α is the spread-rate parameter (dW_y/ds, dW_z/ds, where s is directed along the jet/plume centerline). Dynamic parameters such as velocity scales and dilution rates are also of importance, but have not been measured in these studies.

A dimensional analysis, using the defined parameters, yields the following functional set of dimensionless parameters:

$$\mathbf{L^*} = F_j\, \mathbf{f}\left[F_o,\ Re_j,\ \theta\right] \qquad (1)$$

where $\mathbf{L^*} = \mathbf{L}/r_o$ (or α)

L = dimensional length scale (i.e. $\mathbf{X_m}$, $\mathbf{W_m}$ or $\mathbf{X_t}$)

$F_j = U_j/[g' r_o]^{1/2}$ (the jet Froude number)

$F_o = U_o/[g' r_o]^{1/2}$ (the cross-flow Froude number)

$Re_j = 2U_j r_o/\nu$ (the jet Reynolds number)

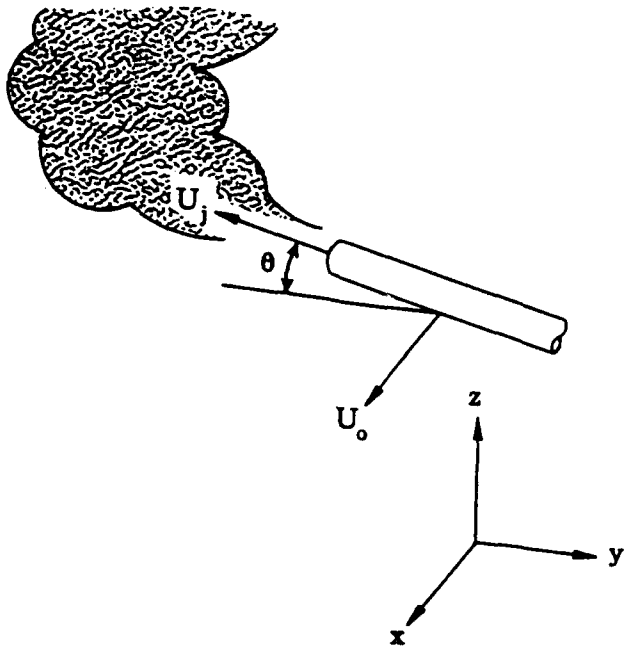

Figure 1. Basic geometry of the negatively buoyant jet/plume which is translating relative to the ambient fluid.

$g' = [(\rho_j - \rho_a)/\rho_j]\, g$ (the reduced gravity)

ν = kinematic viscosity.

The assumption of Reynolds number independence for sufficiently large Re_j ($Re \gtrsim 500$), reduces the number of independent parameters to three: Fj, Fo and θ:

$$L^* = F_j\, f\,[F_o, \theta]. \tag{2}$$

It is in this form that all the present experimental data will be presented.

Three vertical length-scales for this flow may be identified [Lindberg and Petersen (1990), Fischer et al. (1979)]. These length-scales are based on the vertical scale where there is a dynamical balance of the various forces acting on the jet/plume:

$$\ell_b = (M \sin\theta)^{3/4} / B^{1/2} \tag{3a}$$

$$\ell_m = M^{1/2} \sin\theta / U_c \tag{3b}$$

$$\ell_p = B \sin\theta / U_o^3. \tag{3c}$$

These length scales represent the vertical transition points between various modes of the jet/plume behavior:

$z \sim$ lb: jet-plume transition (for negligible ambient flow),

$z \sim \ell_m$: transition point for bent-over jet in an ambient flow,

$z \sim \ell_p$: transition point for bent-over plume in an ambient flow.

Not all of these length-scales are independent, as:

$$Fo \sim (\ell_b/\ell_p)1/3 \sim (\ell_b/\ell_m). \tag{4}$$

We may then characterize the effect of the ambient cross-flow in terms of the magnitude of Fo as:

$Fo \ll 1$: negligible cross flow,

$Fo < 1$: weak cross flow,

$Fo > 1$: strong cross flow.

Additionally, the ratio of ℓ_b to ro is proportional to Fj:

$$\ell_{b/ro} = (\pi \sin\theta)3/4\ Fj$$

Since there is a transition region of approximately 10 jet diameters for the basic jet shear flow to develop, small values of Fj would indicate that the flow was still

developing when the buoyancy forces were beginning to be important. Low values of Fj were avoided.

At this point it is appropriate to point out those parameters which have not been included in this study. The four most important parameters are the cross-flow Reynolds number, Reo, the fluid density ratio, Sr, the azimuthal jet angle, f, and the nozzle geometry, where

Reo = $Uo\ell_s/\nu$
Sr = ρ_j/ρ_a,
ℓs = transverse length scale of the jet/plume,
ϕ = the jet angle in a vertical plane relative to the plane normal to the cross-flow direction (identical to a spherical coordinate system).

Studies have clearly shown that cross flows directly alter the internal dynamics of jet/plume flows, but the resulting flow behavior is relatively insensitive to variations in Reo, provided Reo is sufficiently large.

For the present experiments, the flow is approximately Boussinesq [i.e. Sr ~ O(1)], so these experimental results should be adequately modeled without the inclusion of S_ρ as an independent parameter. It should be noted that the density ratio is incorporated in the buoyancy flux parameter, B, as it is defined in this paper, which does reflect non-Boussinesq effects.

As was discussed in the Introduction, this study was intended to provide the benchmarks for comparison to other studies incorporating such effects as large density ratios, azimuthal injection angles and non-circular exit jet geometries. At present, the importance of these effects remains unresolved.

3. RELATED STUDIES

A very limited amount of study of snow plow plume behavior has been performed. As has been pointed out by Minsk (1981), the cast distance (Y_{max}) for a snow plow has historically been modeled by equations of the form:

$$Y^* = h_d\, g(q,f)\, (hF_o)2, \qquad (5)$$

where: $\eta\delta$ = dynamic efficiency,
$g(\theta,f) = \sin 2q \sin f$
η = moldboard efficiency (~Uj / Uo).

This functional form of the cast distance has its theoretical origin in simple particle trajectory analysis. The effects of drag, entrainment, turbulence and density are accounted for in the dynamic efficiency parameter, η_d. For example, Vinnicombe (1968) reports η_d to range from 0.53 to 0.68. Shalman (1973) cites the following form for η_d:

hd = Tanh[ao (Hrs)1/2]

where: ao = 6.2 [cm^3/gm m]1/2,
H = undisturbed snow depth [m],
ρs = undisturbed snow density [gm/cm^3].

Such a formulation is probably most appropriate for wet, cohesive snow, where the plume entrains little, if any, surrounding air, similar to the behavior of a water jet. The appropriateness and/or the limitations of this type of approach is not at present resolved.

In contrast, an exit plume composed of dry, cohesionless snow will behave as a heavy fluid, characterized by strong entrainment, drag and mixing with the surrounding fluid. It is this situation which is most appropriately modeled by the approach of the present research.

The fluid dynamical modeling of snow avalanche motion using water tanks has been discussed by Hopfinger and Beghin (1980) and Hopfinger (1983). They were successful in properly scaling many of the observed features of avalanche behavior in the laboratory. The non-boussinesq effects of $S_\rho > 1$ were examined and found to be relatively minor up to $S_\rho \sim 10$.

Studies of negatively buoyant jet/plumes are quite limited. In particular, only a few laboratory studies of these flows have been reported [Bodurtha (1961), Turner (1966), Holly and Grace (1972), Pincince and List (1973), Hoot, Meroney and Paterka (1973) (see also Hoot and Meroney, 1974), Anderson et al. (1974), Chu (1975) and Badr (1984)].

An experimental study of a vertically injected dense jet in a water tank was reported by Turner (1966), for the case of no cross-flow. Unfortunately, Turner incorrectly reported his correlated results, and the error has been propagating in the literature since that time. The correct result for the maximum rise height of the vertically injected dense fluid is:

$$Z^*max = 4.17\ Fj \qquad (6)$$

This result is consistent with the dimensional arguments of the previous section [Eq (2)].

The work of Hoot, Meroney and Peterka (1973) [also Hoot and Meroney (1974) and Meroney (1980)] is of particular significance, both in its scope and in the quality of the experimental measurements. They report on wind tunnel studies of dense gases injected vertically in a low turbulence flow. Their quiescent flow studies were in complete agreement with Eq (6). Density ratios,

S_p, of between 1.5 and 3 were used. An integral analysis for the case of a cross-flow was performed and compared to their experimental results. The functional agreement was excellent, and their data correlate well with the following relationships:

$$\frac{\dot{Z}_{CL}}{F_j} = 2.1\, F_o^{-\frac{1}{3}}\, S_p^{\frac{1}{3}} \qquad (7)$$

$$X^*max/Fj = Fo \qquad (8)$$

where $\dot{Z}_{CL} \equiv \dot{Z} = Z_{CL} / r_o$ (*at the plume centerline*). Other measurements, including concentration distributions and longitudinal touchdown distances, were also reported.

Based on a very brief review in Ooms and Duijm (1984), it would appear that the work of Anderson, Parker and Benedict (1973) is of direct relevance. Unfortunately, the work was never published and a copy of their report has not been obtained. They used a water flume and varied θ between 45° and 90°.

The response of a neutrally buoyant jet in a cross-flow has been studied extensively. A summary to 1981 has been given by Crabb, et al. (1981). The characteristics of the jet deflection entrainment rates, mean turbulent flow properties have all been measured and documented. The observation of a double vortex structure in the downstream portion of the jet has intrigued investigators for years [see Abramovich (1963), Chapt. 12, Keffer and Baines (1963)]. The interest lies both in the mechanism of generation and in the subsequent influence on the jet's boundary shape, trajectory and entrainment rate.

In terms of numerical/analytical models of negatively buoyant jet/plume behavior, the survey by Hanna and Drivas (1987), the volume edited by Britter and Griffiths (1982) and the brief review by Ooms and Duijm (1984) represent most of the currently available models and provide a comparative assessment of these models to the fairly small experimental data base.

4. DESCRIPTION OF THE EXPERIMENT

A tow-tank was used to simulate the ambient flow. A round tube (the jet source) was towed through the tank at a constant velocity. The use of a towing facility insures a very uniform, repeatable and low turbulent mean flow (as seen by the jet/plume). The working fluid in the tow tank is water where the tank dimensions are 394 cm long × 40.6 cm wide and 50.8 cm deep. Salt water of various densities was used for the injection fluid. The water jet is mounted 10 cm above the bottom of the tank so that multiple test runs may be made with the same ambient fluid. The water jet is attached to a tow carriage which may be moved at a constant velocity along the tank's horizontal axis. The speed of the carriage may be varied between 0 and 12.4 cm/s. The jet flux is controlled by a valve located between a constant head tank and the jet nozzle. The flow rate is measured by a tapered tube flowmeter (calibrated for the variation in the fluid density). The resulting jet behavior is recorded photographically with two cameras, located at the side and end of the tank. The side camera uses a shadowgraph technique to record the projected image of the jet/plume density structure on an opaque grid surface. The end camera records an illuminated slice of the jet which is produced by directing a sheet of light from the side of the tank and using a small amount of white tempera paint in the jet solution. Examples of the images recorded by this technique are shown in Figures 2, 3 and 4.

The experimental program consisted of 260 separate tests. Table 1 lists the range of the experimental parameters used in these studies.

A typical experiment began with the installation of a selected nozzle at a predetermined angle setting. The tow tank was then filled and allowed to reach thermal equilibrium with the laboratory overnight. The vertical temperature structure was measured prior to testing. Thermal stratification within the tank never exceeded 2°C/m, so that internal wave motion and stratification within the tank was not important. Approximately 2 liters of water at the tank temperature was placed in the constant head tank. Sodium chloride was added to the water in this supply tank until the desired jet density was reached. Density was determined with a hand-held refractometer. A small amount of white tempera paint was then added to the mixture in negligible amounts to affect the density. A series of tests at various towing speeds and jet velocities were then made, without the necessity to drain the tank. The tow tank density was monitored during these tests to insure that the tank density above the level of the jet remained unstratified.

Photographic enlargements of the side and end views were made for each run. Measurements of the various length-scales were then made from the photographs. A single operator performed all of the measurements. In order to provide a check on any bias this procedure may have imposed, random tests were chosen and independent measurements of the length scales were made by a second observer. There was good agreement between the two estimates of these length scales.

A summary of the experimental uncertainties in these measurements is included in Table 2. However, the major source of scatter in the data is the inherent convoluted shape of the instantaneous boundary of the

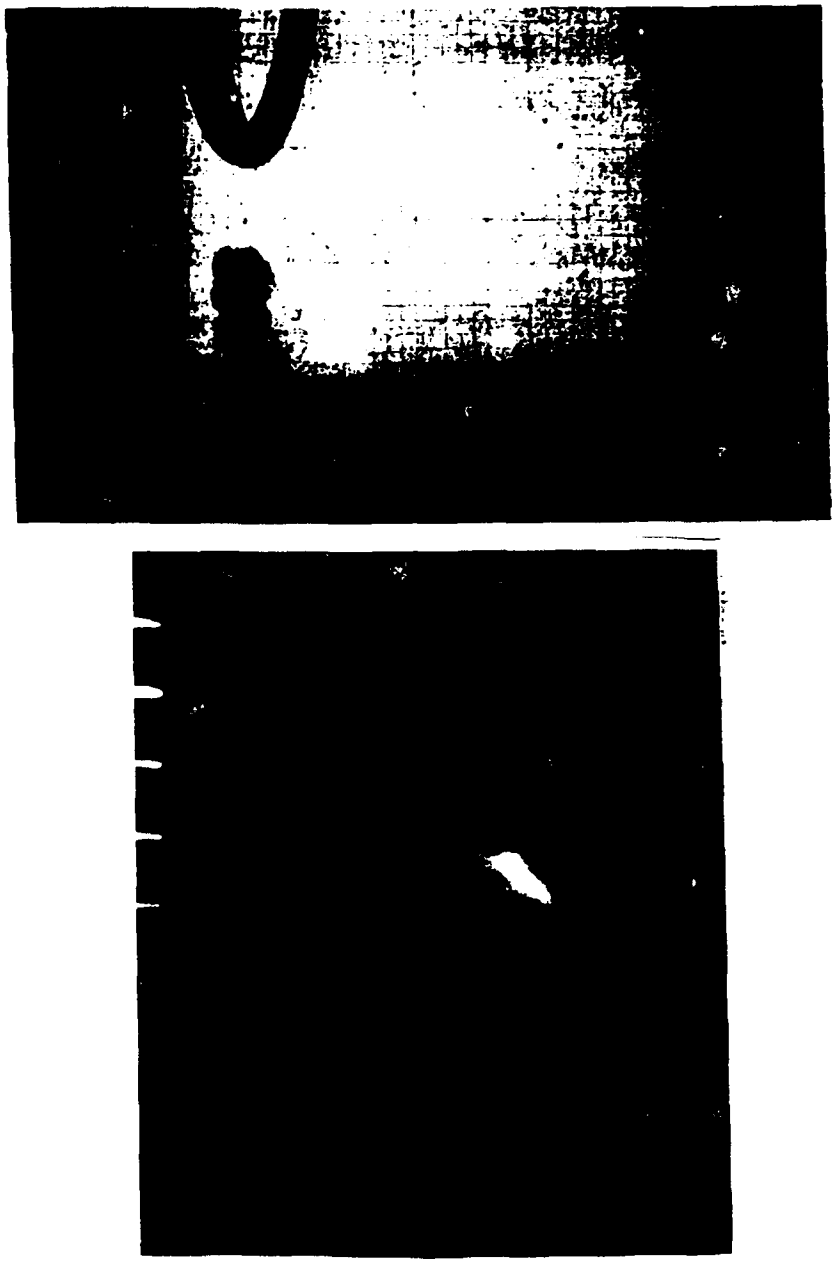

Figure 2. Side and end views of a jet/plume for the case of negligible cross flow; $F_j = 25.2$, $F_o = 0$, $Y^* = 67.2$, $Z^* = 60.2$, $\theta = 60°$. The grid in the side (shadowgraph) image is 1 cm square.

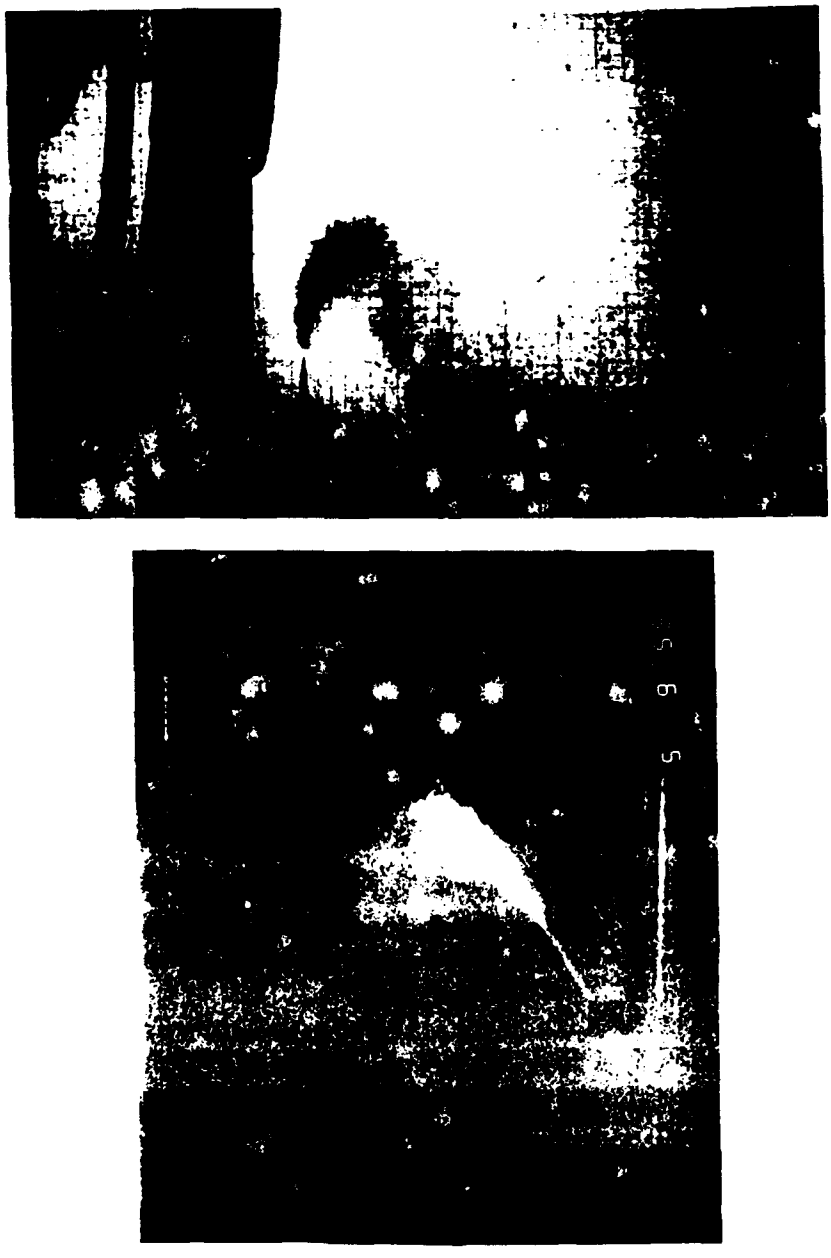

Figure 3. Side and end views of a jet/plume for the case of weak cross flow; $F_j = 28.9$, $F_o = 0.51$, $X^* = 34.9$, $Y^* = 54.6$, $Z^* = 81.3$, $\theta = 60°$.

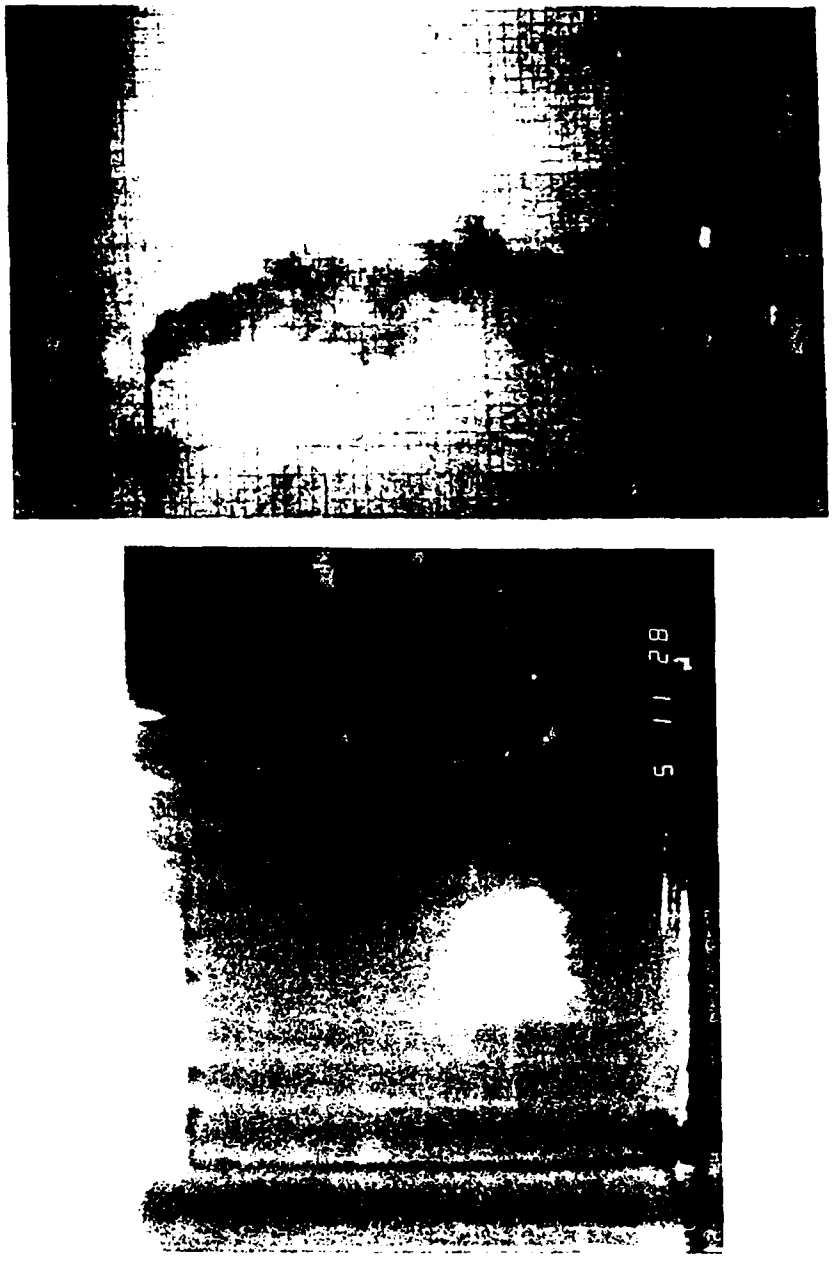

Figure 4. Side and end views of a jet/plume for the case of strong cross flow; $F_j = 84.5, F_o = 5.5, X^* = 179.0, Y^* = 67.0, Z^* = 95.0, \theta = 60°$.

Table 1. Ranges of experimental parameters.

Parameter	*Range of values*
V_j	80–280 cm/s
U_o	0–12.4 cm/s
θ	30°∠90°
$\Delta\rho/\rho_j$	0.01–0.20
r_o	0.046–0.24 cm
Re_j†	870–9220
Re_o†	0–700
F_j	12–170
F_o	0–15

†Based on jet diameter.

jet/plume. It is the instantaneous structure which is captured in the photographs, whereas, the average boundary shape would require averages over a number of observations.

5. EXPERIMENTAL RESULTS AND OBSERVATIONS

5.1 Observations

A complete photographic record of all tests has been obtained. Examples of these photographs are given in Figures 2, 3 and 4. These three photographic pairs are for the three ranges of F_o applicable to negligible, weak and strong cross-flows, respectively.

The observed variability in all length scales increased at low F_o and the higher values of θ. At these conditions, the plume length scales were observed to fluctuate with time around a mean value. These fluctuations were of the order of ±20% of the mean length scales, while at the same time, the jet flow rates were observed to be very constant. These low frequency fluctuations are then a result of the interaction of the jet/plume with the column of fluid which is falling back around the upward directed flow. At the lower angles and higher values of Fo, this interaction was not as pronounced, or did not occur, and the variability in these length scales was much smaller. The highly convoluted entraining interface of these jet/plume flows is also quite apparent in these photographs, where the large scale turbulent motion imposes a highly irregular boundary between the jet/plume fluid and the surrounding lower density fluid. The difficulty of determining the mean interfacial length scales from a single photograph is apparent, and the scatter of the measurements is predominantly due to this very convoluted structure.

The double vortex structure mentioned in Section 3 is illustrated in the photograph in Figure 5. This was for a strong cross flow situation ($F_o > 1$). The darker fluid

Table 2. Composite uncertainties of dimensionless parameters.

Parameter	*Uncertainty (%)*
F_j	9.1
F_o	2.4
L^*	9.6
L^*/F_j	13.3

on the inside of the double vortex is unmarked external fluid which is being entrained in a very preferential way by this vortical structure. The photograph also illustrates the elliptical cross-sectional shape of the plume, whose minor axis is aligned in the same general direction as the initial jet angle. The entrainment processes observed are in sharp contrast to the turbulent interfacial entrainment processes of negligible or weak cross flow jets and plumes.

5.2 Quantitative results

5.2.1. Comparisons with previous work

The special case of $\theta = 90°$ has, as has been noted, some limited prior research history. Turner's (1966)

Figure 5. Double vortex structure, as seen from an end view; $F_j = 51$, $F_o = 4.0$, $\theta = 60°$.

work, for $F_o = 0$, has been discussed, where a principal result of this work is Eq (6). Figure 6 shows the data for $\theta = 90°$ and $F_o = 0$, for the present study, along with Eq (6). The best fit line for this data (based on 8 tests) is:

$$Z^* = 3.7\, F_j\,, \qquad (9)$$

which is 11% lower than that predicted by Eq (5) or the results of Hoot et al. (1973). The observed fluctuations of the plume for high θ and low F_o provide some explanation for this discrepancy. The maximum plume height excursion was not recorded (unless by chance), and a small number of instantaneous photographs were obtained. This procedure results in effective plume heights which vary over the range of instantaneous plume heights. Given a sufficiently large set of observations, the data would then reflect the *average* plume height, rather than the maximum observed height. For these observations, a consistently lower value by 10% would then be expected. For the case of finite F_o, some visual averaging of the photographs was performed, to remove some of the instantaneous large-scale excursions from the data. This procedure is in contrast to the time-lapse photographs used by Hoot et al. (1973). The effect of such a procedure would be to record the maximum excursion over the time duration of the photograph.

A direct comparison to the data of Hoot et al. (1973) for the case of finite F_o is also possible. This comparison is made in Figure 7, where the present data are shown along with Eq (7) over the range of the experimental data used to obtain the correlation. The low F_o data of Hoot et al. was consistently below their reported asymptotic curve, in agreement with the present notion of a transition for $F_o = 1$, as is discussed below.

5.2.2. Data correlations

We shall discuss in some detail the measurements of the maximum vertical excursion of the plume, Z^*, as a function of F_j, F_o and θ. Many of the features of the jet/plume behavior are apparent from these observations alone. The other scales will then be presented and briefly discussed.

Maximum Plume Rise, Z^*. There is an ambiguity in the interpretation of the definition of maximum plume rise when F_o is varied continuously from 0 to values of the order of 15. For very weak (or negligible) cross flows ($F_o < 1$), the only observable is the maximum

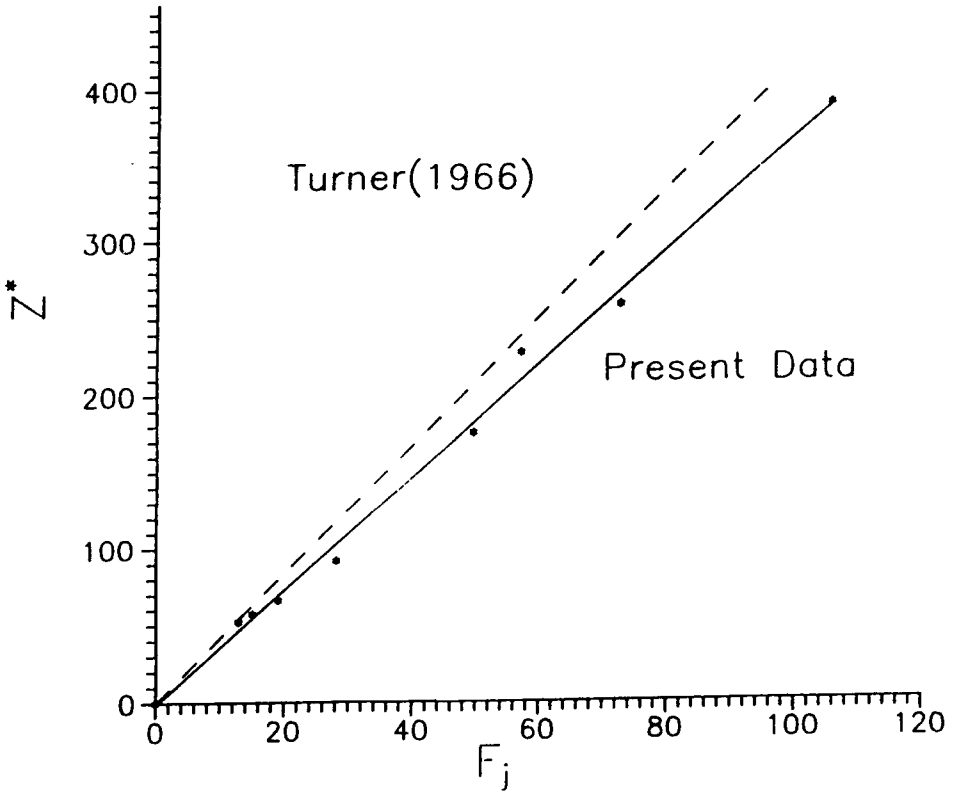

Figure 6. Comparison of vertical jet/plume behavior for no cross flow, with the results of Turner (1966).

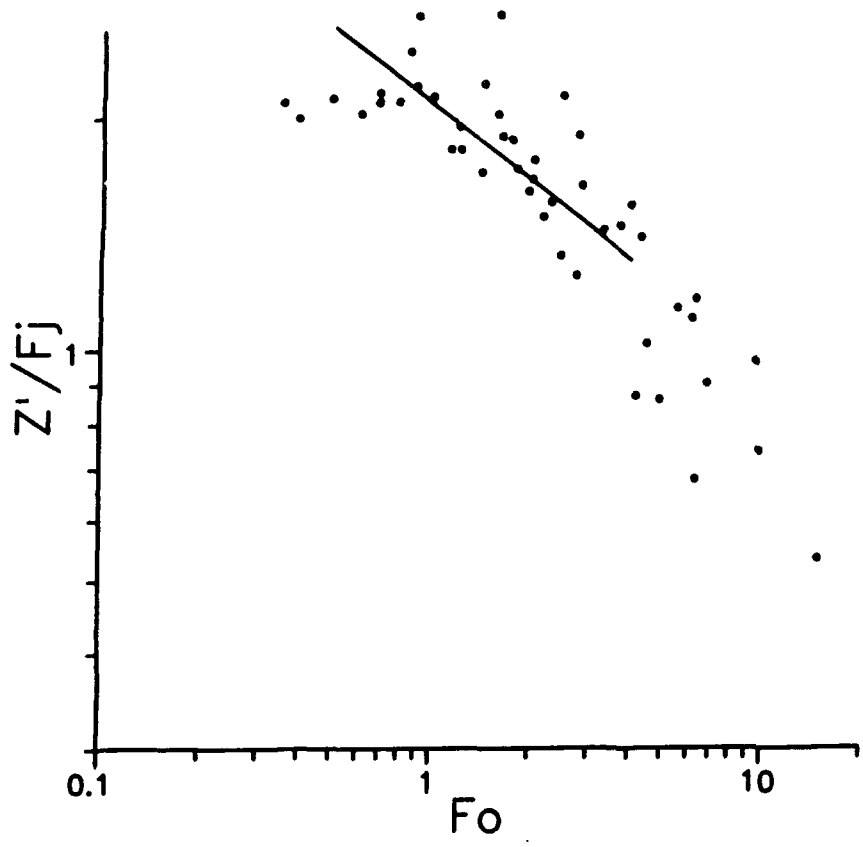

Figure 7. Comparison of vertical jet/plume behavior in a cross flow with the results of Hoot et al. (1973). Equation (7) is shown as a solid line, over the limits of the experimental data of Hoot et al.

plume "top," as the plume descends in the near vicinity of the initiating jet. This definition of plume rise was used in the previous subsection for the $F_o = 0$ case study. For strong cross flows (i.e. $F_o > 1$), the plume is advected in the downstream direction, so that a plume center-line may be considered. The example comparison study for finite F_o in the previous section used such a definition. The two ways to define Z_{max} are not consistent, but may be related as

$$Z' \equiv Z_{max,CL} = Z_{max,top} - W/2 ,$$

for $F_o > 0$. For negligible cross flows, the exact interpretation of $Z_{max,CL}$ is not clear, since the internal dynamics of an ascending jet/plume and the subsequent annular descending flow is not easily reduced to a single vertical length scale. The choice of the definition of Z_{max} for the data to be presented is:

$$Z_{max} = Z_{max,top} .$$

This choice was for reasons of consistency, where Z_{max} is defined the same way for $F_o < 1$ and for $F_o > 1$. Additionally, the experimental techniques used require separate determinations of both $Z_{max,top}$ and W_{max}. The increased uncertainty of combining these measurements is avoided by this choice. (Such increased experimental uncertainty is in evidence in Figure 7 of the previous section.)

Logarithmic plots of Z^*/F_j versus F_o are shown in Figure 8(a–d). The dimensional arguments leading to Eq (2) are seen to be valid representations of the processes involved, as the data is reasonably well correlated. There is a definite change in the functional behavior of Z^*/F_j in the neighborhood of $F_o \sim 1$, which marks the transition between a weak cross flow and a strong cross flow.

For the $F_o = 0$ cases, $Z^*/F_j = f_{z,o}(\theta)$. The values of this angular dependence for $F_o = 0$ were determined from a regression analysis of Z^* versus F_j, as was done in Figure 6. The linear dependence of Z^* on F_j was very

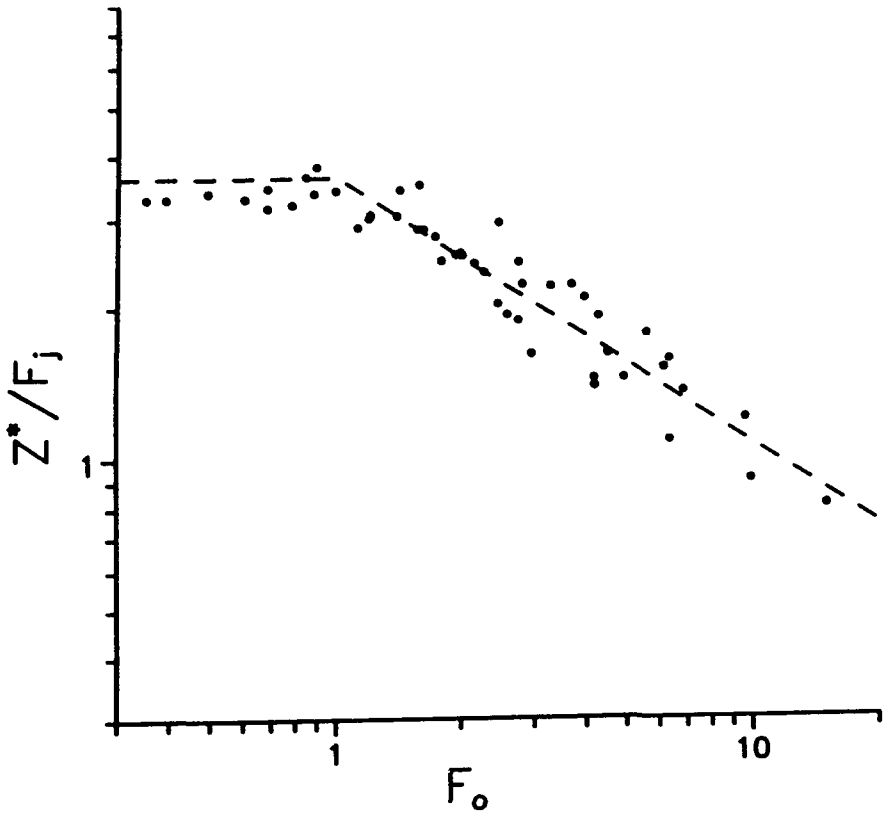

Figure 8a. Dimensionless maximum plume rise, Z^*/F_j, in a cross flow as a function of cross flow Froude number, F_o; (a) $\theta = 90°$, (b) $\theta = 60°$, (c) $\theta = 45°$ and (d) $\theta = 30°$.

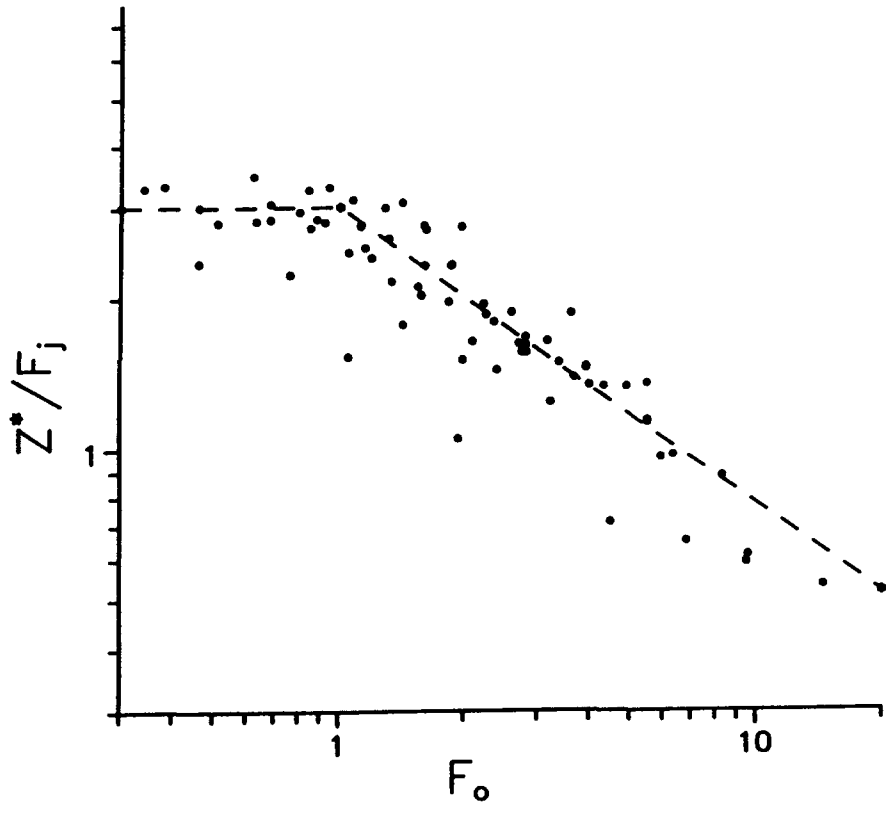

Figure 8b. Dimensionless maximum plume rise, Z^*/F_j, in a cross flow as a function of cross flow Froude number, F_o; (a) $\theta = 90°$, (b) $\theta = 60°$, (c) $\theta = 45°$ and (d) $\theta = 30°$.

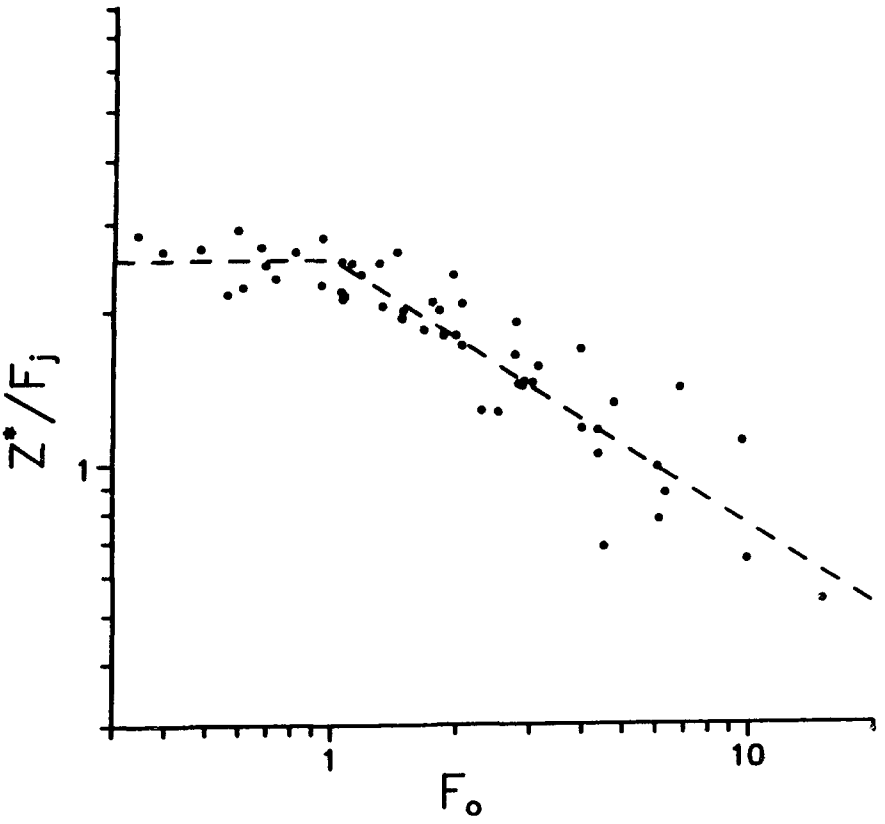

Figure 8c. Dimensionless maximum plume rise, Z^*/F_j, in a cross flow as a function of cross flow Froude number, F_o; (a) $\theta = 90°$, (b) $\theta = 60°$, (c) $\theta = 45°$ and (d) $\theta = 30°$.

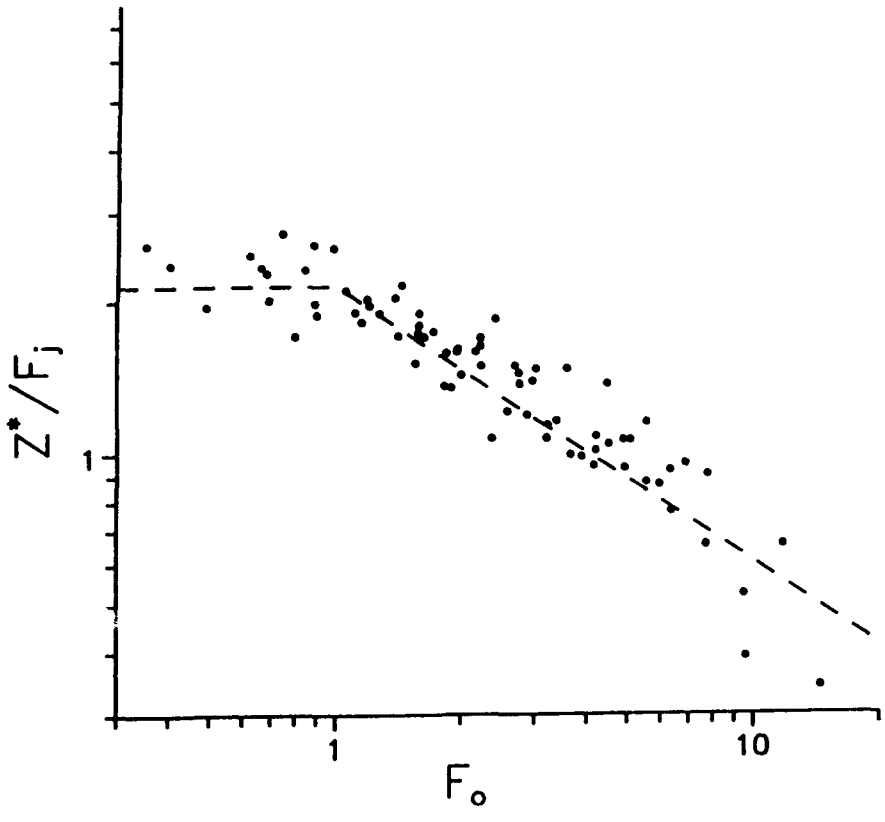

Figure 8d. Dimensionless maximum plume rise, Z^*/F_j, in a cross flow as a function of cross flow Froude number, F_o; (a) $\theta = 90°$, (b) $\theta = 60°$, (c) $\theta = 45°$ and (d) $\theta = 30°$.

Table 3. Linear regression analysis results for Z* behavior.

Initial jet angle, θ	$f_{z,o}(\theta)$	$f_z(\theta)$	n_z
90°	3.70	3.61	–0.53
60°	2.46	3.01	–0.59
45°	1.76	2.53	–0.53
30°	1.47	2.14	–0.50

consistent for all cases. The weak cross flow ($F_o < 1$) behavior is essentially $Z^*/F_j \sim f_z(\theta)$, which is consistent with the scaling arguments leading to Equation (2). For $F_o < 1$, $\ell_b < \ell_m$, so the transition to a pure plume would be expected before the effects of a cross flow became important. For $F_o > 1$, the slope of the data in the form:

$$Z^*/F_j = f_z(\theta)F_o^n \qquad (10)$$

was also determined from a regression analysis. A summary of the results of these correlations is given in Table 3.

A comparison of the values of $f_{z,o}(\theta)$ and $f_z(\theta)$ indicate that as θ decreases from 90°, the value of $f_{z,o}(\theta)$ decreases much faster than $f_z(\theta)$. A plausible explanation for this behavior is the observed change in the interaction of the descending fluid with the rising central column of fluid. Comparison photographs of this process indicate that the interference of the descending fluid on the jet/plume decreases for $F_o > 0$, where the low momentum descending fluid is advected by the cross flow. Without this sweeping away of this descending fluid, the rising/falling fluid interaction is stronger, both by increasing the mixing rate within the plume and by an increased momentum exchange between the two flows.

The asymptotic analysis of Lindberg and Petersen (1990) yielded a scaling for Z*/Fj for the case of a jet with weak cross flow (i.e. $F_o < 1$) and θ <90°. The experimental values of $f_z(\theta)$ agree with the following equation to within 4%:

$$Z^*/F_j = f_z(\theta) = 2.3[\sin\theta(1 + \sin^{1/2}\theta)]^{1/2}. \qquad (11)$$

As would be expected, the values of $f_{z,o}(\theta)$ do not correlate well with this expression, where it is noted that the entrainment hypothesis used in the analysis is only consistent with a weak cross flow behavior.

*Transverse Distance, Y**. We define Y* as Y_{max}/r_o, where Y_{max} is the measured maximum transverse distance of the jet/plume at the same location as Z_{max}. Figure 9(a–c) shows the measured Y^*/F_j values as a function of F_o. The asymptotic behavior of Y^*F_j with F_o is very similar to the Z^*/F_j data of Figure 8. Adequate representations of this data are thus:

$$Y^*/F_j = \begin{cases} f_{y,o}(\theta) & : F_o = 0 \\ f_y(\theta) & : 0 < F_o < 1 \\ f_y(\theta)F_o^n & : F_o > 1 \end{cases} \qquad (12)$$

A data correlation summary, similar to Table 3, is given in Table 4.

With the exception of $f_{y,o}(45°)$, both $f_{y,o}$ and f_y increase with decreasing θ. The dependence of Y^*/F_j on F_o continues to have an approximate $F_o^{-1/2}$ behavior, although the calculated slopes are even more negative.

Analysis of end-view photographs of plume behavior subsequent to the maximum plume rise location indicates that Y does not appreciably increase further downstream. The initial y-momentum has become so diffuse, through entrainment, at this point that further transverse transport is small. For the present, then, we may take Y* to be indicative of the maximum transverse plume distance, at least for $F_o > 1$.

*Longitudinal distance, X**. The downstream location where Z_{max} occurs is defined as X_{max}. The scatter in the X* data is significant for $F_o > 1$ and illustrates the difficulty of determining X_{max} when the irregular plume boundary is essentially horizontal for a finite distance downstream. Within the limits of the data, an asymptotic equation of the form:

$$X^*/F_j = f_X(\theta)\, F_o^{n_X} \qquad (13)$$

correlates the data for $F_o > 0$. Table 5 summarizes the linear regression analysis for this data. We should note that $X_{max} = 0$ for $F_o = 0$.

From Table 5, the variations of $f_x(\theta)$ are not significant, however the comparison of n_x for θ = 90° and all other angles is to be noted. The asymptotic theory of Hoot et al. (1973) and Lindberg and Petersen (1990), for θ = 90°, predict that $X^*/F_j \sim F_o$ [Eq (8)], in agreement with the measurements. For θ < 90°, this exponent, n_x, decreases by as much as a factor of two. A more detailed analysis will be necessary to clarify this observation, however it is clear that the nature of the downstream plume trajectory changes when the initial jet angle is not vertical.

*Plume width scale, W**. Observations of the plume width scale, W*, were made at the Z_{max} location. These measurements were made from the side, shadowgraphic images, so they represent the total vertical width of the plume at that location. Due to the elevation of the injection jet above the bottom of the tow tank, some measured widths exceed Z_{max}, however, these data were retained.

Table 6 summarizes the regression analysis for the

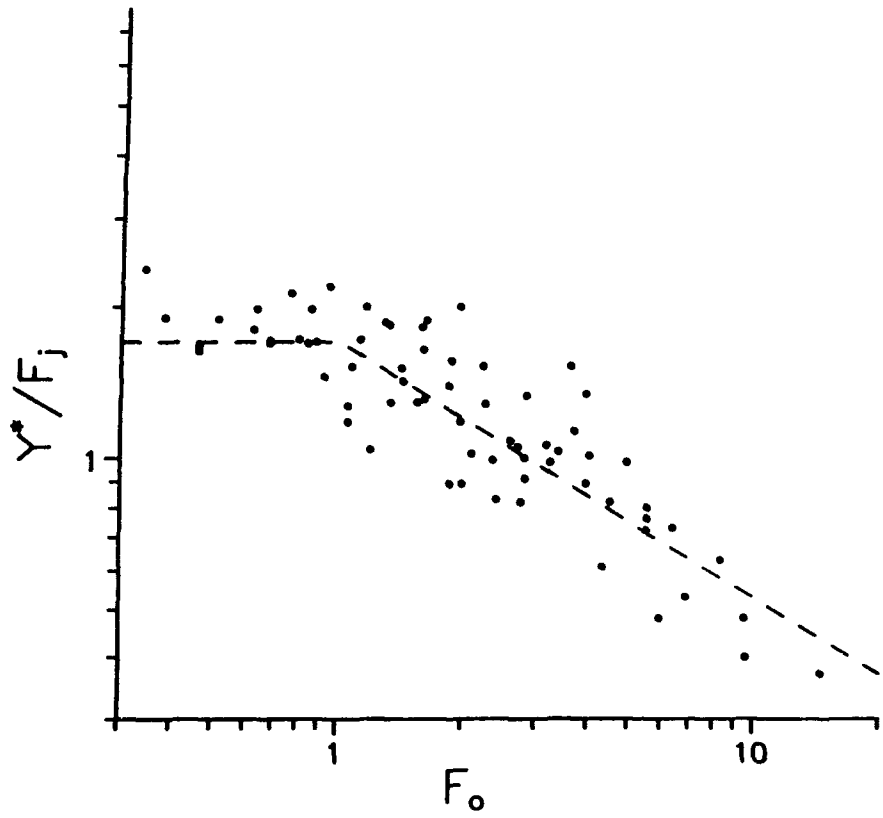

Figure 9a. Dimensionless transverse length scale, Y^*/F_j, in a cross flow as a function of cross flow Froude number, F_o: (a) $\theta = 60°$, (b) $\theta = 45°$ and (c) $\theta = 30°$.

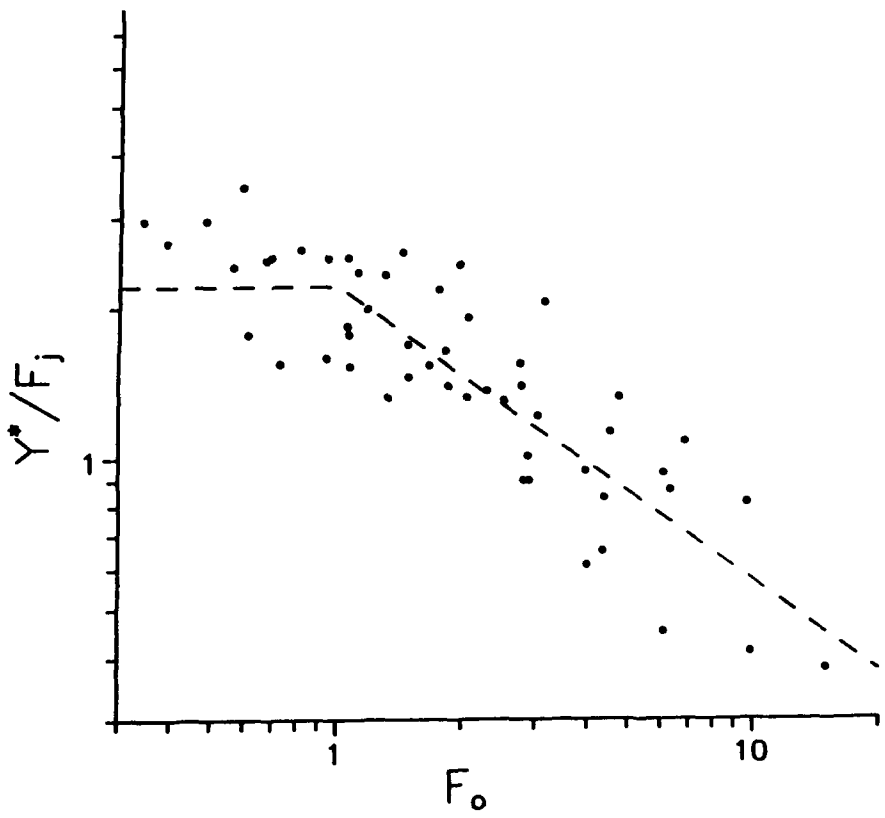

Figure 9b. Dimensionless transverse length scale, Y^*/F_j, in a cross flow as a function of cross flow Froude number, F_o: (a) $\theta = 60°$, (b) $\theta = 45°$ and (c) $\theta = 30°$.

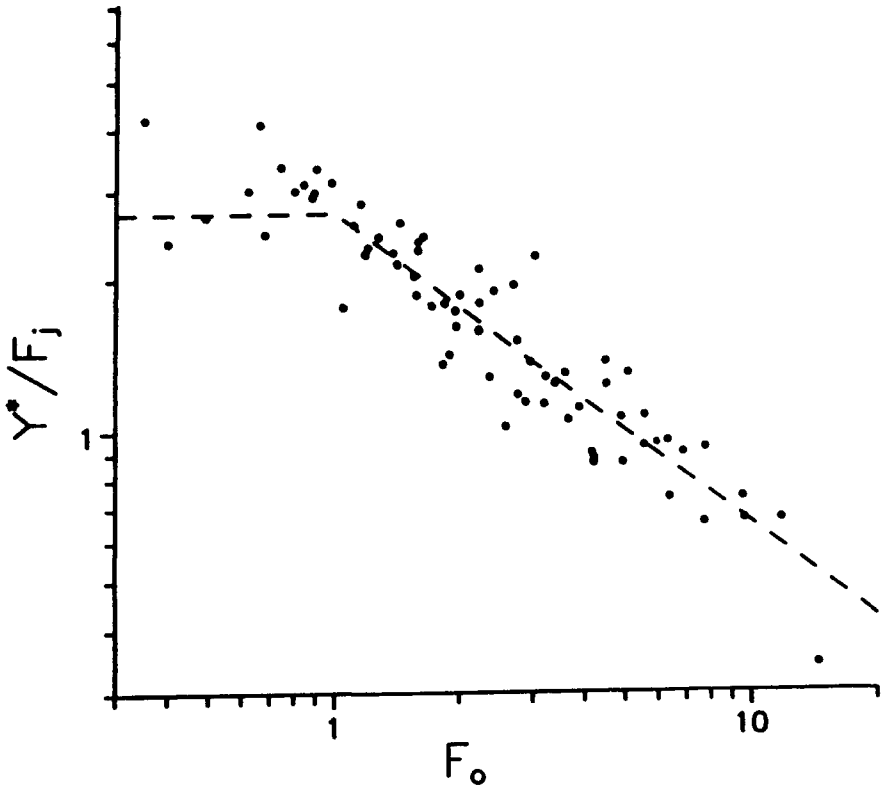

Figure 9c. Dimensionless transverse length scale, Y^*/F_j, in a cross flow as a function of cross flow Froude number, F_o: (a) $\theta = 60°$, (b) $\theta = 45°$ and (c) $\theta = 30°$.

four angles for $F_o > 1$, for the same asymptotic forms as Equation (12). The similar values of $f_w(\theta)$ and n_w for the various injection angles indicate that the vertical plume widths, for all injection angles, are very similar. If a conceptual elliptical shaped plume in the downwind direction is used, the lower injection angles have a smaller Z_{max}, but a larger projected plume width, due to the tilting of the ellipse.

6. APPLICATION TO SNOW PLUME BEHAVIOR

In terms of predicting snow plume cast distance or plume height for snow plow applications, we may re-write equation (12) as:

$$L^*_i = \eta\, f_i(\theta)\, F_o^{ni+1} \qquad (14)$$

for values of $F_o > 1$, which is appropriate for most displacement plowing operations. Note that the length scales depend linearly on the moldboard efficiency, η.

Since nominal values of n_i for Y^* and Z^* are of the order of –0.5, the exponent on F_o in the above equation is of the order of +0.5, in sharp contrast to the squared exponent of Equation (5). The characteristic length-scale for these laboratory studies has been the nozzle radius, r_o. An equivalent circular length-scale for the case of a snow plume yields the following scale:

$$r_{o,e} = [A_{exit}/\pi]^{1/2} = [bH/\pi\eta\alpha]^{1/2},$$

Table 4. Linear regression analysis results for Y* behavior.

Injection angle, θ	$f_{y,o}(\theta)$	$f_y(\theta)$	n_v
90°	*	*	*
60°	1.7	1.7	–0.51
45°	1.6	2.2	–0.59
30°	3.0	2.7	–0.62

* $-Y^*$ is zero for $\theta = 90°$.

Table 5. Linear regression analysis results for X* behavior [for all values of $F_o > 0$].

Injection angle, θ	$f_x(\theta)$	n_x
90°	1.20	0.92
60°	1.61	0.55
45°	1.43	0.48
30°	1.58	0.46

Table 6. Linear regression analysis results for W* behavior [for $F_o > 1$].

Injection angle, θ	$f_w(\theta)$	n_w
90°	2.5	-0.54
60°	2.2	-0.61
45°	2.2	-0.55
30°	2.2	-0.55

where b,H are the width and depth of the plowed snow, and α is the ratio of the final to initial snow densities. This equivalent scaling is limited to plow flow exit areas which are approximately circular (or elliptical).

Example predictions of cast distance, Y_{max} and maximum cast height, Z_{max}, using Equation (14), are shown in Figures 10 and 11. The assumed parameters for these calculations are:

snow depth, H = 0.20 m,
plow width, b = 3.3 m,
snow density, ρ_S = 100 kg/m^3,
plow efficiency, η = 1.0,
plow angle, φ = 0°,
effective exit radius, $r_{o,e}$ = 0.46 m.

Figure 10 also shows the prediction of cast distance using Equation (5) with the estimate of η_d as suggested by Shalman (1973), for the case of θ = 45°.

The calculations are presented to illustrate the potential benefit of the current research in exit plume behavior. It should be kept in mind the current limitations on the parameters examined to date.

7. SUMMARY AND CONCLUSIONS

The results of an experimental research program on the behavior of negatively buoyant jets/plumes are summarized in this paper. The effects of initial jet angle and cross-flow have also been investigated.

Plume trajectory behavior, in the form of coordinate length-scales at the location of maximum plume height,

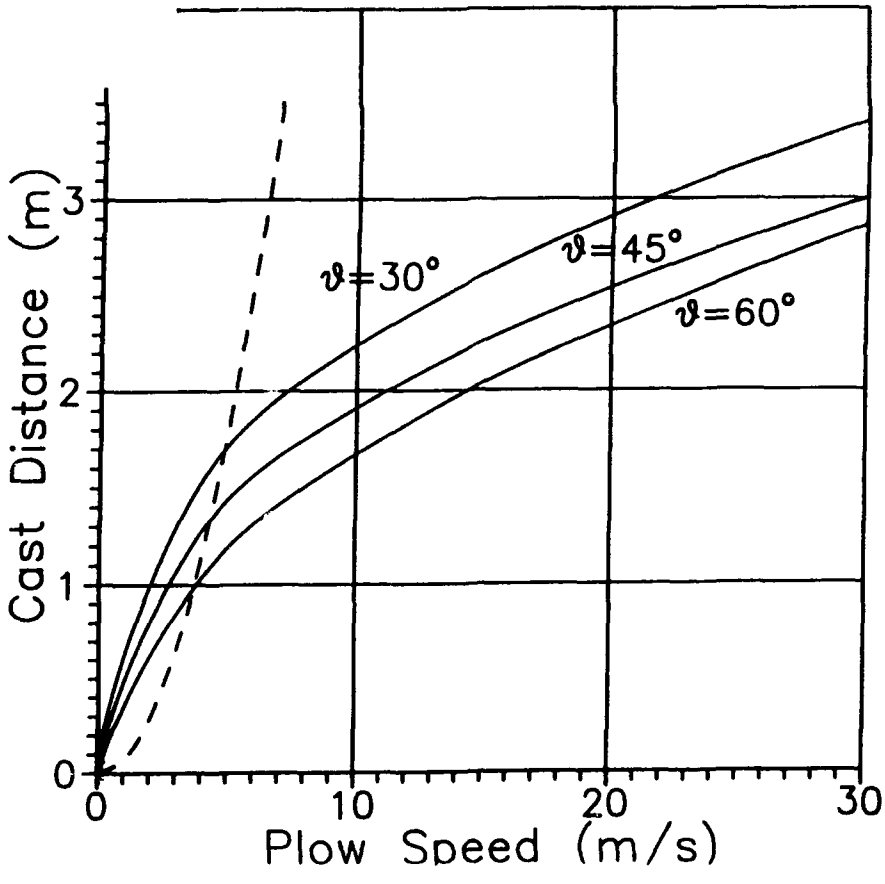

Figure 10. Predicted cast distance as a function of plow speed and initial moldboard exit angle, θ. The example parameters are summarized in the text. The dashed line is Equation (5), for θ = 45°.

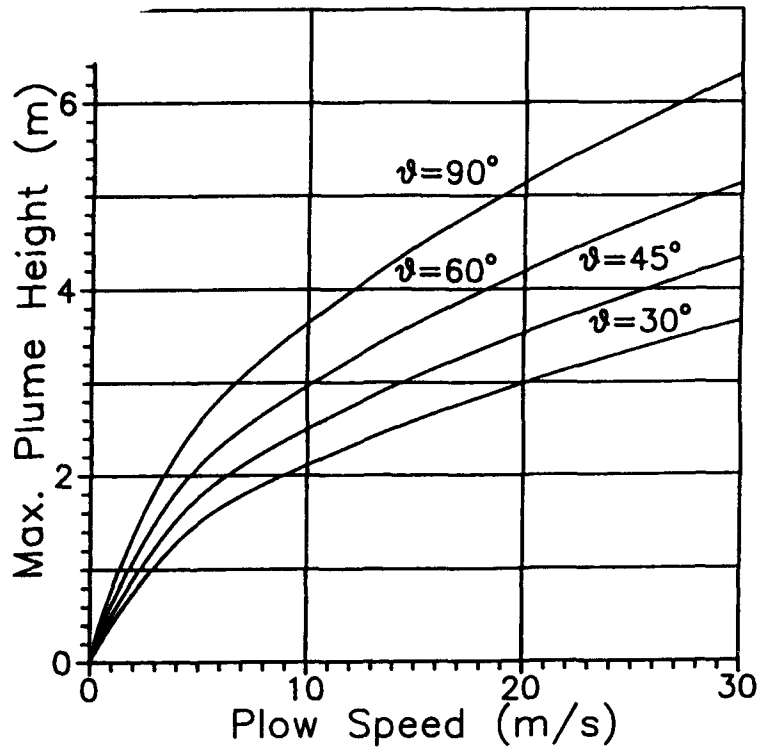

Figure 11. Predicted snow plume cast height for the same parameters as Figure 10.

was determined from photographs of the visualized plumes. These length-scales are seen to be functions of jet angle, θ, and the two Froude numbers: F_j and F_o. To the accuracy of the observations, the results have been correlated to an asymptotic power law as a function of flow regime in the form of:

$$L^*/F_j = \begin{cases} f_{o,i}(\theta) & ;F_o = 0 \\ f_i(\theta) & ;0 < F_o < 1 \\ f_i(\theta)F_o^{ni} & ;F_o > 1 \ (F_o > 0 \text{ for } X^*) \end{cases} \quad (15)$$

The flow regimes of $F_o = 0$ (no cross-flow), $0 < F_o < 1$ (weak cross-flow) and $F_o > 1$ (strong cross-flow) exhibit significantly different dynamical behavior, as is seen in the experimental observations and in the length-scale results.

This study has successfully demonstrated the usefulness of using a water tow-tank for the present jet/plume research. The range of parameters attainable in this facility has allowed for a clarification of the distinct flow regimes which have been discussed. Observations and photographic records have revealed much of the detail of these jet/plume flows from a variety of view angles.

At the outset of this phase of the study, the primary objectives were to:

- examine the effects of injection angle and cross flow on jet/plume behavior and relate the observations to previous work,
- attain a wide range of parameter values to demonstrate the validity of the scaling analysis of Section 2,
- determine the parameter space which may be identified with the various asymptotic flow regimes.

Within the limits of a photographic study, a large range of parameter space and a relatively small number of tests, the objectives of the study have been met.

Further laboratory study will be directed toward the following objectives:

- study the effect of changes in the exit jet geometry on jet/plume behavior, with emphasis on the strong cross flow regime,
- include the azimuthal angle to study the effect of both fore and aft injection angles,
- investigate the non-Boussinesq effect of S_ρ significantly different than one, by using different solutes and suspensions,
- examine the interaction between adjacent objects and the downstream plume behavior, including

the incorporation of flow control devices attached to the adjacent structures,

- compare jet/plume behavior in a quiescent flow to a turbulent environment,
- extend the analytical work to include higher level numerical models, primarily integral-based models.

ACKNOWLEDGMENTS

The research described herein was supported by the Strategic Highway Research Program (SHRP). SHRP is a unit of the National Research Council that was authorized by section 128 of the Surface Transportation and Uniform Relocation Assistance Act of 1987. The authors would like to express their appreciation to Wayne Foslien, Jeff Rogers and Roland Miller for their help with the data reduction and to Dr. R.N. Meroney of Colorado State University.

This paper represents the views of the authors only, not necessarily reflective of the views of the National Research Council, the views of SHRP, or SHRP's sponsors. The results reported here are not necessarily in agreement with the results of other SHRP research activities. They are reported to stimulate review and discussion within the research community.

LITERATURE CITED

Abramovich, G.N. (1963) *The Theory of Turbulent Jets*. MIT Press, Cambridge, MA.

Anderson, J.L., F.L. Parker and B.A. Benedict (1973) Negatively buoyant jets in a cross flow. *EPA-Report No. 660/2-73-012*, (as referenced by Ooms and Duijm, 1984).

Badr, A. (1984) Temperature measurements in a negatively buoyant round vertical jet issued in a horizontal cross flow. In: *Atmospheric Dispersion of Heavy Gases and Small Particles*, G. Ooms and H. Tennekes, Eds., Springer-Verlag, pp. 167-176.

Bodurtha, F.T. (1961) The behavior of dense stack gases. *J. Air Pollution Control Association*, Vol. 11, pp. 431-437.

Britter, R.E. and R.F. Griffiths (1982) *Dense Gas Dispersion*. Elsevier Scientific Pub. Co., [a bound collection of papers which constitute *J. of Hazardous Materials*, Vol. 6, parts 1 and 2].

Chu, V.H. (1975) Turbulent dense plumes in laminar cross flow. *J. Hydraulic Research*, Vol. 13, No. 3, pp. 263-279.

Crabb, D., D.F.G. Duraõ and J.H. Whitelaw (1981) A round jet normal to a crossflow. *J. of Fluids Engineering, Trans. ASME*, Vol. 103, pp. 142-153.

Fischer, H.B., E.J. List, R.C.Y. Koh, J. Imberger. N.H. Brooks (1979) *Mixing in Inland and Coastal Waters*, Academic Press, New York, Chapter 9.

Hanna, S.R. and P.J. Drivas (1987) *Guidelines for Use of Vapor Cloud Dispersion Models*. American Institute of Chemical Engineers.

Holly, F.M. and J.L. Grace (1972) Model study of dense jets in flowing fluid. *J. Hydraulics Div., Proc. ASCE*, Vol. 98, No. 9365, pp. 1921-1933.

Hoot, T.G., R.N. Meroney and J.A. Peterka (1973) *Wind tunnel tests of negatively buoyant plumes*. Fluid Dynamics and Diffusion Laboratory, College of Engineering, Colorado State University, Report No. CER73-74TGH-RNM-JAP-13.

Hoot, T.G. and R.N. Meroney (1974) The behavior of negatively buoyant stack gases. *Proc. 67th Annual Meeting, APCA*, Denver, Colorado, Paper No. 74-210.

Hopfinger, E.J. (1983) Snow avalanche motion and related phenomena. *Ann. Rev. Fluid Mech.*, Vol. 15, pp. 47-76.

Hopfinger, E.J. and P. Beghin (1980) Buoyant clouds appreciably heavier than the ambient fluid on sloping boundaries. *Proc. 2nd Int. IAHR Symp. Stratified Flows*. Trondheim, pp. 495-504.

Keffer, J.F. and W.D. Baines (1963) The round turbulent jet in a cross wind. *J. Fluid Mechanics*, Vol. 15, pp. 481-496.

Lindberg, W.R. and J.D. Petersen (1990) *The negatively buoyant jet/plume in an ambient cross flow*. Fluid Mechanics Technical Report. FMTR-90-1, Department of Mechanical Engineering, Univ. of Wyoming.

Meroney, R.N. (1982) Wind tunnel experiments on dense gas dispersion. *J. Hazardous Materials*, Vol. 6, nos. 1-2, pp. 85-106.

Minsk, L.D. (1981) Snow removal equipment. In *Handbook of Snow*, D.M. Gray and D.H. Male, eds., Pergamon Press, New York, pp. 648-670.

Ooms, G. and N.J. Duijm (1984) Dispersion of a stack plume heavier than air. In *Atmospheric Dispersion of Heavy Gases and Small Particles*. G. Ooms and H. Tenekes, Eds. Springer-Verlag, New York, pp. 1-23.

Pincince, A.B. and E.J. List (1973) Disposal of brine into an estuary. *J. of the WPCF*, Vol. 45, No. 11, pp. 2335-2344.

Shalman, D.A. (1973) *Snowplows, Construction, Theory and Design, 2nd Ed.* (in Russian). "Mashinostroenie," Leningrad.

Turner, J.S. (1966) Jets and plumes with negative or reversing buoyancy. *J. Fluid Mech.*, Vol. 26, pp. 779-792.

Vinnicombe, G.A. (1968) Comparative tests on model vee snow ploughs. *Rept. LR 180, Road Res. Lab.*, Crowthorne, U.K..

5. MATERIALS PROPERTIES

Viscosity Measurements on Very Wet Soils

SALLY SHOOP
U.S. Army Cold Regions Research and Engineering Laboratory
Hanover, New Hampshire 03755-1290

ABSTRACT

Springtime and intermittent thaws are often accompanied by soft, wet ground conditions and thaw weakening of the soil. Water added during snow melt and spring rain accumulates in the thawed layer because drainage is limited by the relatively impermeable frozen soil below. This added water decreases the strength of the thawing soil even further. For these very wet soil conditions the soil can be considered a non-Newtonian viscous fluid. Information from viscosity tests can then be used in analytical or numerical models where the thawing soil is modeled as a semi-viscous fluid for determination of the drag resistance of wheels in viscous mud.

This paper describes apparent viscosity measurements on three soil types—sand, silt and clay— chosen to cover a wide range of grain sizes. Extensive mobility test data and supporting information, such as shearing resistance, grain size and Atterberg limits, were also readily available for each of the soils tested. Six to eight soil-water mixtures, ranging in consistency from a paste to a slurry, were tested for each soil type.

The viscosity was found to be strongly influenced by water content, as expected. Below the liquid limit, when the soil samples were paste- like, the viscosity was very high (39 to 85 Pa•s), and was difficult to measure because the soils behaved as a semi-solid. At or near the liquid limit, the viscosity of all the soil types was approximately 40 Pa•s. As the percentage of water increased beyond the liquid limit, the viscosity decreased dramatically and then steadily declined as additional water was added. The lowest viscosity value measured, for the very wet clay (over 100% water content), was approximately 0.07 Pa•s. In general, the values obtained in this study extend smoothly beyond the range of previously published data.

INTRODUCTION

Thawing soil is primarily a two-layer configuration, where a soft and wet soil layer overlies the hard frozen ground (Figure 1). Because the frozen ground can form a relatively impermeable barrier, any moisture added to the system during thawing, such as rain and/or snow melt, becomes trapped in the thawing layer, making it exceptionally wet and weak. Under these very wet conditions, the soil can be considered as a viscous fluid (Shoop, 1990). These kinds of conditions can be very difficult for vehicle mobility. Vehicle traffic is often restricted on secondary roads and may be impossible on unpaved roads and off-road. In addition, when vehicles can pass, they may leave excessive ruts, causing severe road or terrain damage and subsequent erosion.

In the study of vehicle mobility on thawing ground, when the thawing soil is very wet it can be modeled as a viscous fluid. For a Newtonian (perfectly viscous) fluid the shear stress, τ, is proportional to the rate of shear, $\dot{\gamma}$:

$$\tau = \mu\dot{\gamma} \tag{1}$$

where the proportionality constant, μ, is the viscosity. A Bingham plastic fluid also behaves as a linear function of the rate of shear but requires an initial yield stress, τ_y, to cause displacement:

$$\tau = \tau_y + \mu\dot{\gamma}. \tag{2}$$

The behavior of viscous soils (and mud) has been observed to be somewhere between these two, as shown in Figure 2.

Dynamic or absolute viscosity can be expressed in several different units. Historically, viscosity has been

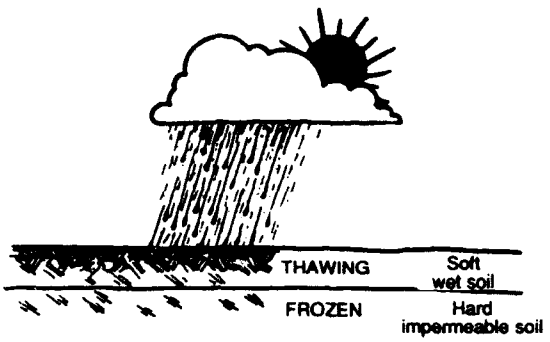

Figure 1. The nature of thawing soils.

expressed in units of poise (from Poiselle). The official SI unit is Pascal seconds:

1 Pa•s = 10 poise = 1000 cp (centipoise).

Kinematic viscosity, v, in units of length squared per second, is related to absolute viscosity as follows:

$$v = \mu/\rho \qquad (3)$$

where ρ is the fluid density. The viscosity measurements discussed in this paper are absolute, or dynamic, viscosity and are also apparent viscosity since the fluid is non-Newtonian.

If thawing soil is considered as a viscous fluid, then the movement of a tire through the soil can be calculated as the viscous drag on the tire. The equation to calculate the drag force on a tire (after Rowe and Hegedus, 1959) can be expressed as

$$F_D = 2\mu V A_1/\delta + \delta z b/2 + \rho V^2 A_2/2 \qquad (4)$$

where D = drag force
μ = viscosity
V = relative velocity
γ = specific weight
A_1 and A_2 = tire contact area
δ = boundary layer thickness
z = thaw depth
b = tire width
ρ = fluid density.

The velocity of the tire and the soil's density, specific weight and thaw depth can be easily measured, along with the contact area and object width. The boundary layer thickness can be estimated from the literature, so the viscosity of the mud is the primary unknown.

Not much data for viscosity of mud exist in the published literature. In the late fifties, Hegedus (1958) and Rowe and Hegedus (1959) performed viscous flow experiments on a tire moving through bentonite clay. In addition, the Asia/Pacific mobility researchers sometimes use fluid flow theory to simulate vehicle movement through puddled rice paddy fields (Xie and Shoa, 1988). Another subject area that considers soil as a viscous fluid is that of massive mudslides and landslides (Maa and Mehta, 1988). Sewage treatment engineering has also considered the viscosity of soil and sludge mixtures (Vesilind, 1975). These published values, as well as those of other common materials, are listed in Table 1.

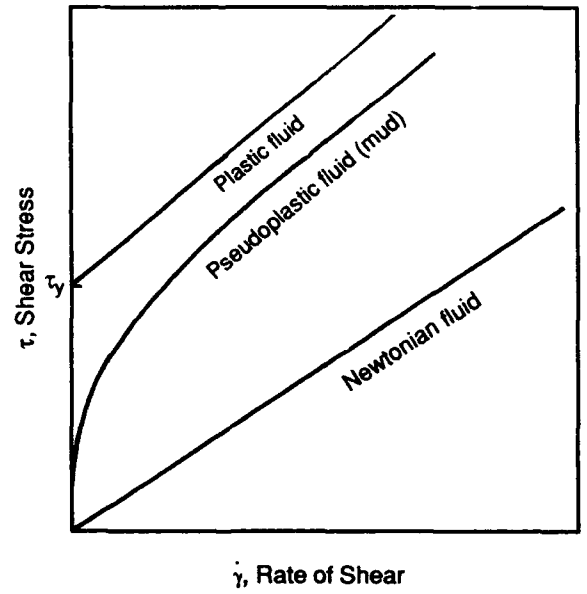

Figure 2. Shear stress vs shear rate for Newtonian and non-Newtonian fluids and mud.

Table 1. Viscosity of selected materials.

		Pa•s	*Reference*
Air (20°C)		1.86×10^{-5}	Jaeger (1962)
Water (20°C)		1.0×10^{-3}	Jaeger (1962)
Mercury (20°C)		1.56×10^{-3}	Jaeger (1962)
Castor oil (20°C)		0.72	Jaeger (1962)
Pitch (15°C)		2×10^{10}	Jaeger (1962)
(50°C)		2×10^{6}	Jaeger (1962)
Glass (20°C)		10^{21}	Jaeger (1962)
(575°C)		1.1×10^{12}	Jaeger (1962)
Lava flow		4×10^{3}	Jaeger (1962)
Sludges: Raw primary		0.028	Vesilind (1975)
Mixed digested		0.092	Vesilind (1975)
Activated	A	0.006	Vesilind (1975)
	B	0.005	Vesilind (1975)
	C	0.007	Vesilind (1975)
Mud: Bentonite		4.5 → 17	Hegedus (1958)
Coastal, clayey		60 → 300	Maa and Mehta (1988)
Clay, loam		0.002 → 4	Xie and Shao (1988)

Because of the wide range in the published values of soil viscosity, I decided to measure the viscosity of specific soils which had been used in our vehicle mobility test program. These values will be used in predictive calculations (like equation 4) to check the theoretical results against mobility test data.

Table 2. Atterberg limits.

	PL	*LL*	*PI*
Lebanon Sand	—	20	—
MoultonPit Silt	26	27	1
LeTourneau Clay	23	32	9

EXPERIMENTAL METHOD

Three soil types were chosen for viscosity testing: a sand, a silt and a clay. The soils were chosen to cover a range of grain sizes and also because of the existence of data from mobility testing and strength testing in the lab and field. Lebanon Sand is a fine-grained silty sand obtained from the banks of the Connecticut River in Lebanon, New Hampshire. Moulton Pit Silt is a clayey silt, also from Lebanon. LeTourneau Clay is a low plasticity clay from just south of Vicksburg, Mississippi. Their grain size distribution curves are shown in Figure 3 and the Atterberg limits are listed in Table 2.

Six to eight samples of each of the soils were prepared to cover a wide range of consistencies from a very wet slurry to a dry paste. I tried to test at least one sample that was below the liquid limit from each soil type but this was difficult as the soil behaves more as a solid at these water contents and is difficult to test in the viscometer.

A suite of ASTM viscosity standards, covering a wide range of viscosities, were measured to determine the relationship between the viscometer output voltage and viscosity. All samples and standards were set in a constant temperature bath for approximately 30 minutes in order to equilibrate at a temperature of 20°C. Each soil mixture was then tested for viscosity, weighed, and placed in an oven to dry. The dry weights of the mixtures were used to calculate the moisture content of each sample.

The viscosity of the samples was measured using a Brookfield Viscometer (Figure 4) according to ASTM Standard D 2196-86, Test Method A for Apparent Viscosity. The viscometer measures the torque required to rotate a spindle within the specimen at a constant speed set with an adjustable-speed motor. The viscosity of the sample causes a torque on the spindle, which is converted to voltage using an electronic pressure transducer. Output voltage was recorded on a strip chart recorder. The viscometer can be set so that the spindle constantly moves up and/or down within the sample by using the helipath stand. This causes the spindle to cut a helical path through the sample, always cutting into fresh material and eliminating problems with channeling or

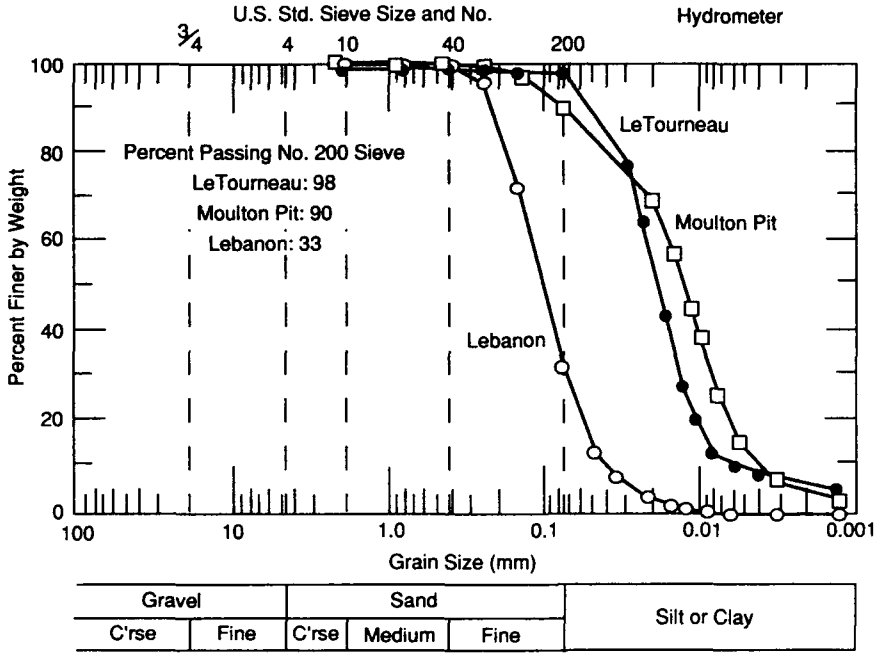

Figure 3. Grain size distribution curves for Lebanon Sand, Moulton Pit Silt and LeTourneau Clay.

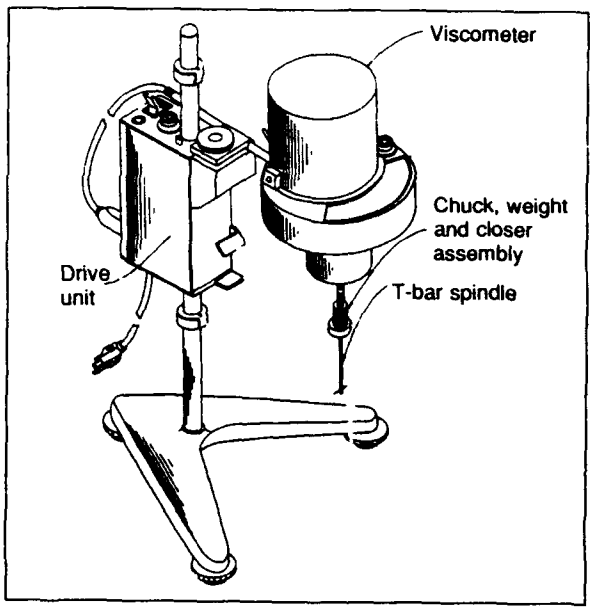

Figure 4. Brookfield viscometer.

settling of the material. The viscosity can also be measured at a constant level within the sample.

Because of the effect of speed on viscosity for non-Newtonian or pseudo-plastic fluids, the spindles and settings of the viscometer were held constant for all samples, including the standards. Spindle F (a T-shaped bar with a crosspiece diameter of 1.09 cm) was chosen and rotated at a constant speed of 100 rpm. This configuration was chosen because of the high viscosities expected for the soil pastes. However, since the speed at the outside edge of the crosspiece (0.05 m/s) is less than the speed used in running the mobility tests (1.34 m/s), the viscosity values may be different than those encountered in the field situation.

RESULTS

The apparent viscosities were calculated by measuring the voltages recorded on the chart and comparing them to the voltages obtained from standards of known viscosity. Six different standards of a wide range of viscosities were measured (Figure 5). Because the relationship between the viscosity and voltage is not linear within the wide range of viscosities tested, a polynomial

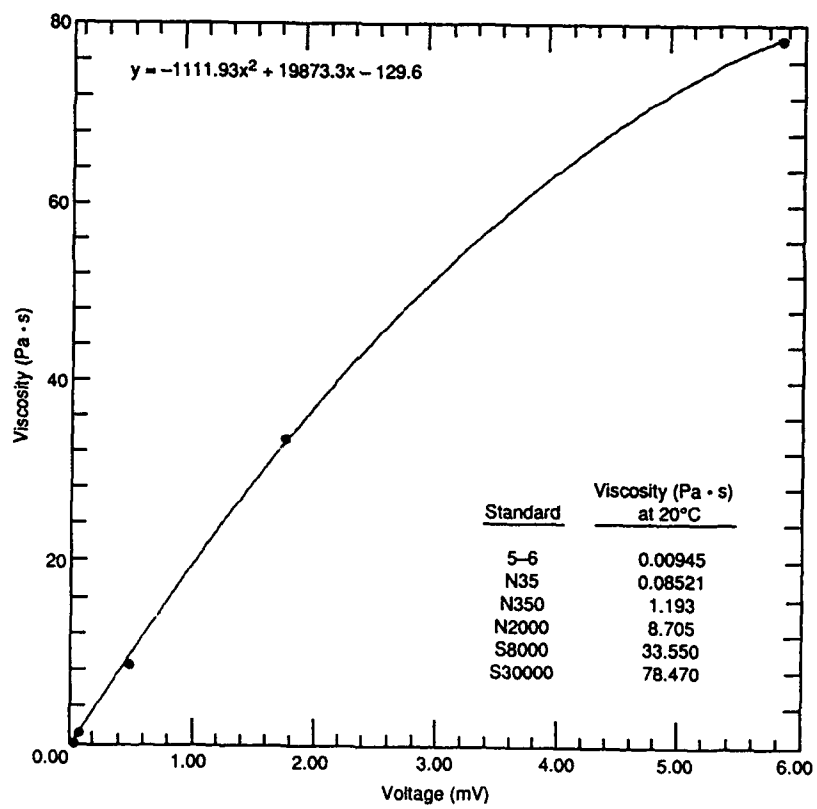

Figure 5. Curve fit of the viscosity standards to viscometer output voltage.

Table 3. Soil viscosity values.

Moisture content (%)	*Apparent viscosity (Pa•s)*
Lebanon Sand	
19	38.761
23	4.713
26	2.604
29	2.604
32	2.178
35	1.003
Moulton Pit Silt	
32	40.332
37	24.291
42	16.502
46	7.826
47	5.550
71	0.574
LeTourneau Clay	
29	84.807
31	82.599
33	41.162
40	7.756
44	3.412
47	1.256
63	0.168
101	0.069

regression was fitted to the data to be used for calculating the unknown viscosities of the soil mixtures. The second-order polynomial shown in Figure 5 fits the standards very well. The viscosities of the soil mixtures, calculated using this equation, are listed in Table 3 along with the corresponding moisture contents.

DISCUSSION

The apparent viscosity of each of the mixtures was compared to the water content and is plotted in Figure 6 for each of the soil types. In general, decreasing the water in the sample increases the viscosity, as expected. Starting with the highest water content and decreasing the water, the increase in viscosity is gradual until the water content is near the liquid limit; viscosity then increases rapidly. This trend was consistent between two of the samples, but for the silt the increase in viscosity (with decreasing water content) was more gradual, and water contents below the liquid limit were not tested. For non-plastic soils (the sand and silt) at moisture contents below the liquid limit, the soil behaves like a solid and the viscosity measurements are both difficult and not particularly applicable. For the slightly plastic clay, additional measurements were possible between the liquid limit and the plastic limit, and yielded viscosity values upwards of 80 Pa•s.

Near the liquid limit the soil viscosity of all the soils is similar (Lebanon Sand is 38.8 Pa•s, Moulton Pit Silt is 40.3 Pa•s, and LeTourneau Clay is 41.2 Pa•s). At these moisture conditions, viscosity may be independent of the soil type. This would agree with Casagrande's (1932) discussion of the physical significance of the Atterberg limits, which states that the shear resistance at the liquid limit is a constant value (20 to 25 g/cm^2; Seed et al., 1964) for all soil types. The liquid limit test is primarily a measure of the shear resistance of the soil, and viscosity is also a measure of shear resistance. Thus, at the liquid limit, shear resistance and viscosity can be expected to be the same value for every soil type. It should be noted that while Casagrande's work referred primarily to cohesive soils, these data suggest similar results for non-cohesive soils or soils with very low cohesion.

To compare the three soil types, the results were plotted on a single log-log plot (Figure 7). The results for the silt and clay are very similar (as are their grain size distributions), while the sand is offset. This is likely because of the coarser particles in the sand sample settling out of suspension.

The results of these experiments are plotted alongside data presented in Xie and Shoa (1988) in Figure 8. The soil types are similar to the soils I tested and are listed in the legend. (Note that the soils I used are named based on the Unified Soil Classification System, whereas Xie and Shoa used an agricultural soil classification system.) The water content of my samples ranged from 19% to 101%, and the water contents of their samples ranged from 50% to 800%. Since they were working with paddy soils they were naturally more interested in the extremely wet conditions when the fields are flooded. However, both data sets overlap within the same range of moisture contents and my data extend smoothly, following the same trend into the range of lower water contents.

SUMMARY AND CONCLUSIONS

Thawing soils can create severe problems for vehicle mobility; roads are often closed or restricted and off-road travel becomes nearly impossible. When passage is possible, the resulting rutting can cause extensive environmental damage and subsequent erosion. Moisture from snow melt and spring rains accumulates in the surface layer of thawing ground, creating a very wet and weak soil layer over the strong frozen ground below. This wet soil can behave as a viscous fluid and, therefore, vehicle mobility can be simulated using the equa-

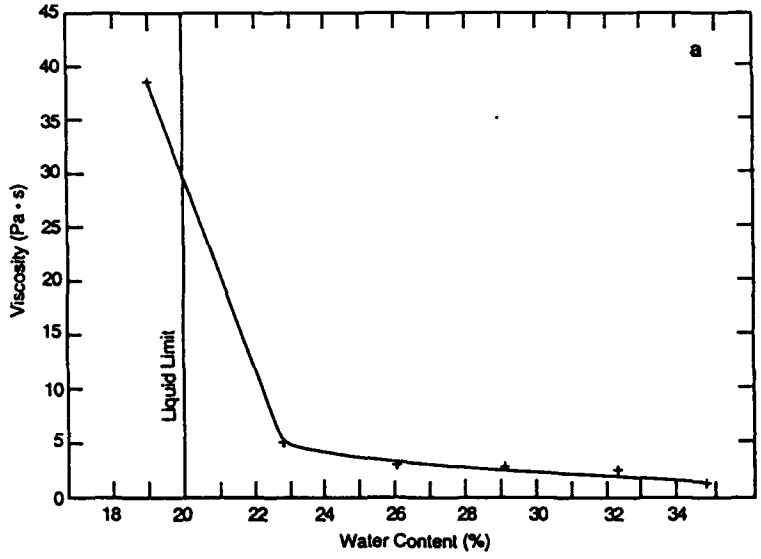

a. Lebanon Sand.

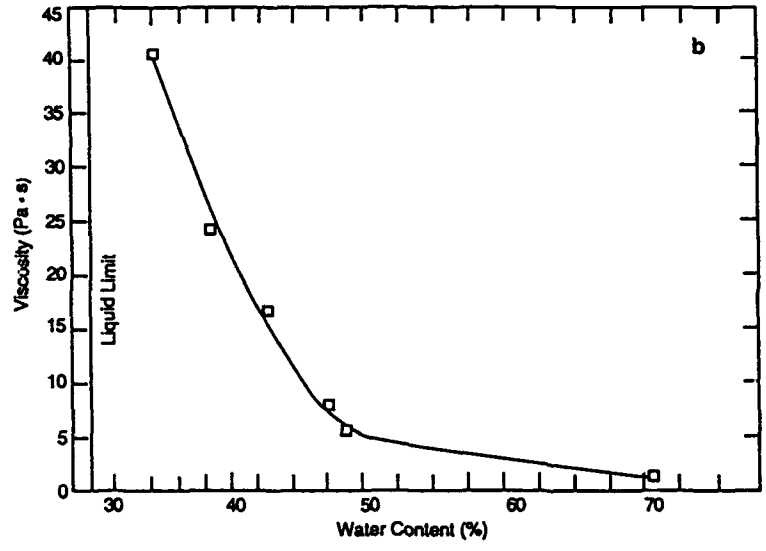

b. Moulton Pit Silt.

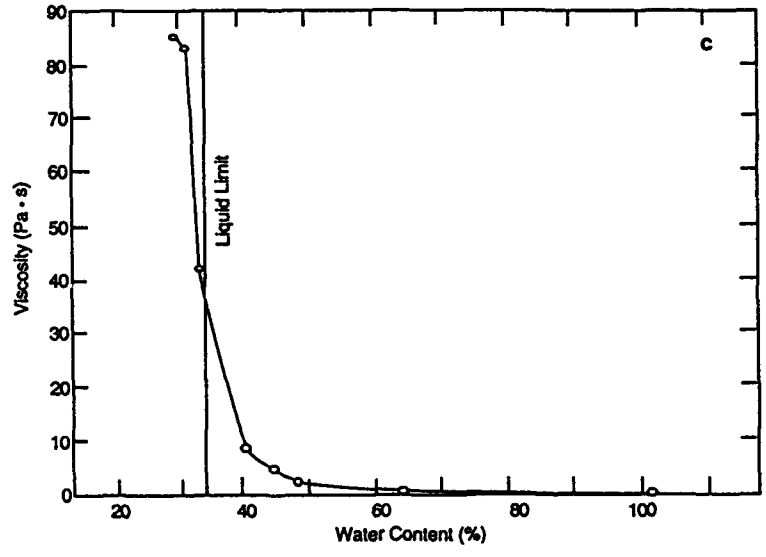

c. LeTourneau Clay.

Figure 6. Viscosity vs water content. The value of the liquid limit is shown by the vertical line.

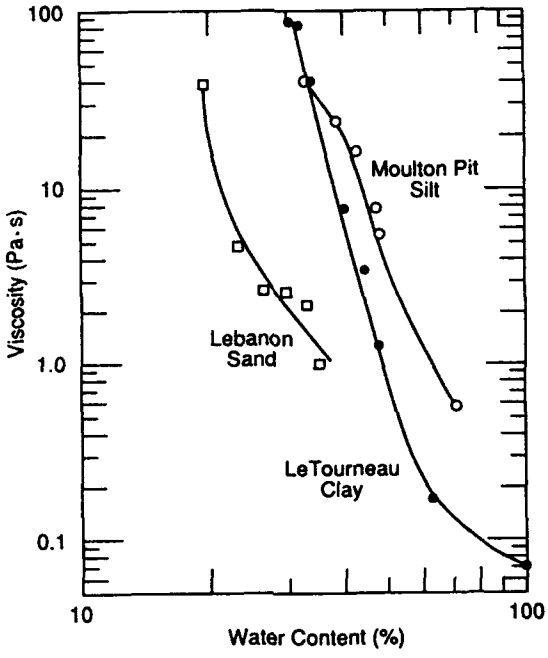

Figure 7. Log-log plot of viscosity vs water content for the three soil types tested.

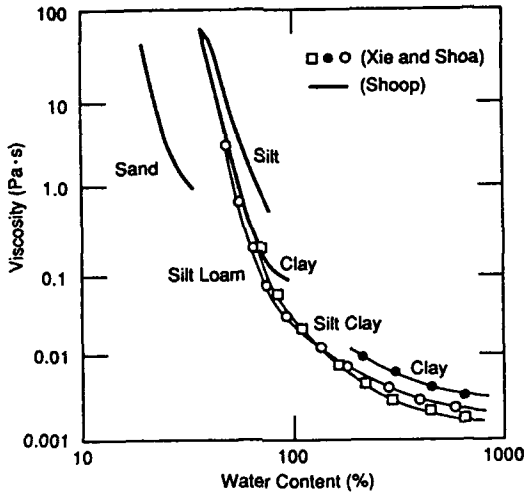

Figure 8. Comparison of viscosity data for the three soil types with results of Xie and Shoa (1988).

tions of viscous drag from fluid flow theory.

The apparent viscosity of three soil types—a sand, a silt and a clay—was measured using a Brookfield Viscometer. The soils were chosen to cover a wide range of grain sizes and also because of existing mobility data, strength data and other basic soil behavior information on these particular soils.

Six to eight samples of each of these soil types were prepared to cover a range of moisture contents and soil consistencies ranging from a paste to a slurry. In general, the viscosity is strongly dependent on water content, particularly near the value of the liquid limit. At water contents below the liquid limit, the soils behave as a solid or plastic, making the validity of the technique limited. Near the liquid limit, the viscosity values of each of the soil types is similar (approximately 40 Pa•s), as expected since the shear resistance for all soils is equal at the liquid limit. Beyond the liquid limit, the viscosity decreases rapidly as water is added to the soil, dropping as low as 0.07 Pa•s for the clay slurry at a water content of 101%.

Knowing the viscosity of the soil as a function of water content, the motion resistance of a tire moving through the viscous soil can be calculated based on the equations of fluid flow. These calculations can be checked against measured motion resistance to evaluate the success of the prediction and either validate or modify the theory.

ACKNOWLEDGMENTS

The author thanks Mr. Alan Tice, Dr. Vincent Janoo and Mr. Stephen Bowen for their thoughtful reviews of this paper and Mr. Alan Tice and Dr. Patrick Black for their technical assistance in setting up the experiments.

LITERATURE CITED

Casagrande, A. (1932) Research on the Atterberg Limits of Soils. Public Roads, Vol. 13, Oct, p. 121–136.

Hegedus, E. (1958) Drag Coefficients in Locomotion over Viscous Soils, Part I. U.S. Army, Land Locomotion Laboratory Report No. 25, AD 201 183.

Jaeger, J.C. (1962) *Elasticity, Fracture and Flow*. John Wiley and Sons, Inc., New York, 208 p.

Maa, J. P.-Y., and A.J. Mehta (1988) Soft Mud Properties: Voight Model. Journal of Waterway, Port, Coastal and Ocean Engineering, Vol. 114, No. 6, November, p. 765–770.

Rowe, R.S. and E. Hegedus (1959) Drag Coefficients of Locomotion over Viscous Soils, Part II. U.S. Army, Land Locomotion Laboratory Report No. 54. AD 235 703.

Seed, H.B., R.J. Woodward, and R Lundgren (1964) Fundamental Aspects of the Atterberg Limits. J. of the Soil Mechanics and Foundation Division of the ASCE, Vol. 90, No. SM6, November, p. 75–105.

Shoop, S. (1990) Mechanism Controlling Vehicle Mobility on Thawing Soils. Proceedings of the 10th International Meeting of the International Society of Terrain Vehicle Systems, Kobe, Japan, August, Vol. I, p. 301–311.

Vesilind, P.A. (1975) Treatment and Disposal of Wastewater Sludges. Ann Arbor Science Publishers, Inc., Ann Arbor, Michigan.

Xie, X.Y. and Y.J. Shoa (1988) Analysis on the Pressure–Sinkage Relationship and Viscosity of Top Layer Paddy Field Soil. Proceedings of the 2nd Asia/Pacific Conference of the International Society of Terrain Vehicle Systems, Bangkok, Thailand, Dec. 6–10, p. 79–88.

The Relationship Between the Microstructure and Mechanical Properties of Snow

MICHAEL Q. EDENS AND ROBERT L. BROWN
Civil/Ag Engineering Department
Montana State University
Bozeman, Montana 59717

ABSTRACT

The mechanical properties of snow are determined by the properties of the matrix material (ice) and the microstructure of the material itself. Microstructure is defined to include such factors as grain size, pore size, bond size, neck length, grain shape and three-dimensional coordination number (number of bonds per grain). This set of microstructural relations from quantitative stereology theory are presented along with relations and techniques required for numerical evaluation of these variables. An experimental investigation is carried out to determine changes in these variables for snow subjected to large compressive deformations. Measurements at several stages of deformation are used to evaluate the changes in the microstructure as functions of deformation. Grain size and bond radius were found to go through finite changes during compression. The coordination number and specific free surface area were found to go through large changes during compression. No discernible patterns of change in neck length could be found in the experiments. A close relationship between some of the microstructural variables and the stress response of the material were observed. These results serve to contribute to the presently available data and understanding of the microstructural behavior of snow.

INTRODUCTION

One of the most commonly observed features of snow is its compressibility. It can undergo large volumetric deformations when subjected to moderate bulk stresses. Snow's ability to undergo large deformation is due in large part to its porosity. In a natural state snow exhibits a wide range of grain shapes and densities. Abele and Gow (1975 and 1976) demonstrated the effect snow's initial density has on its load bearing ability. From their experiments it was clearly demonstrated that if undisturbed snow with densities from 100 to 300 kg/m^3 is subjected to high rate deformation, then the smaller the initial density, the smaller the final density that is attained for a given final stress state. This was attributed to the irregular shaped grains found in low density snow and to the more uniform rounded nature of higher density material. It was found that the initial density was a significant factor for final stresses < 1 MPa. The effects of higher initial density became less obvious for loadings above 1 MPa. Their studies also demonstrated the rate dependent nature of snow's load bearing ability. These results have also been verified with a constitutive theory developed by Brown (Brown 1979, 1980).

Microstructural parameters are now being included in many modern constitutive theories. Among the parameters being included are bond radius, neck length, grain size, and three dimensional coordination number. A grain bond intercepted by the section plane will appear as a line joining two opposite edges of the ice in the plane. To identify this line as a bond, three criteria must be met. First, there must be a minimum constriction of the ice in the section plane. Secondly, the

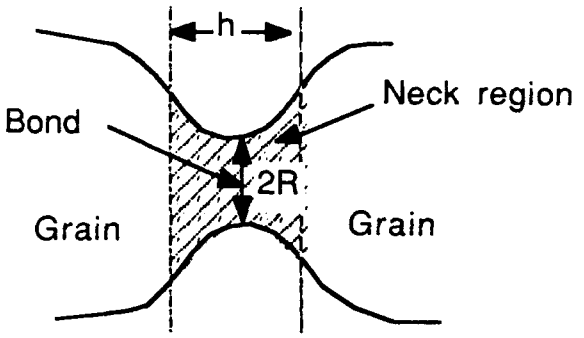

Figure 1. Schematic of neck and bond as they appear in a surface section.

constriction must be present on both edges of the ice. Finally, the constrictions must point approximately towards each other (Kry 1975a). These are shown in Figure 1.

A neck is assumed to begin at the point where the surface curvature changes from convex outward to concave outward as viewed in a surface section. In cases where a sharp change in surface slope exists, this is used to define the juncture of the neck and grain. Figure 1 illustrates a neck connecting two grains and Figure 2 illustrates a surface section with a number of grains with their bonds shaded gray. Admittedly, the definition used here to define the neck contains a degree of subjectivity and at times is difficult to implement. The three-dimensional coordination number is the average number of bonds per grain in the material.

A volumetric constitutive law based on a neck growth model was developed by Brown (1980). This model included structural parameters for change in neck radius, neck length, grain radius and coordination number. The resulting equation described qualitatively the behavior of snow subjected to arbitrary deformation histories for a range of initial densities. To obtain an accurate quantitative description of the strains requires empirical adjustment. A more general constitutive law, based upon nonequilibrium thermodynamics and the mechanical properties of ice, has been developed by Hansen and Brown (1988) for snow subjected to high rate multiaxial deformations. The microstructural properties of snow in this theory are included in the form of internal state variables. This theory was shown to predict behavior such as rate dependence, stress relaxation, and strain recovery. Over the past ten years other investigators have formulated constitutive relations with the use of microstructural variables. These include Maeno and Ebinuma (1983), Ebinuma and Maeno (1985), Wilkinson (1988), Alley (1987), and others.

Accuracy of any constitutive relation is dependent upon understanding the behavior of the microstructural variables included in the theory. Most constitutive laws based on microstructural parameters are too complicated to be of use in practical applications. Simplifications of these constitutive laws for special situations are

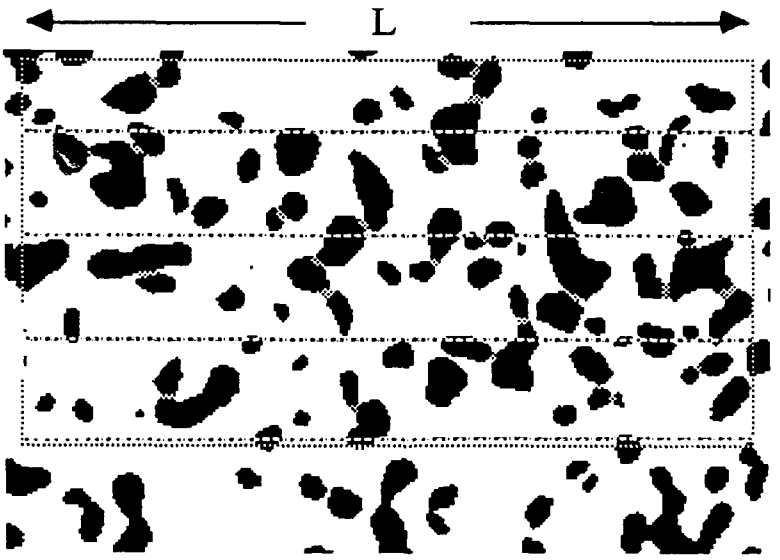

Figure 2. A typical digitized surface section is shown with selected measurement and a series of test lines. Within this rectangle measured bonds are shaded gray region.

best accomplished with knowledge of which parameters can be eliminated. At the present time little or no data on microstructural behavior exists for snow densified by large deformation to the 500 to 650 kg/m^3 density range. The work of Abele and Gow (1975, 1976) provides a strong basis for understanding bulk behavior of snow, subjected to high deformation rates and large strains, but, little or no data was obtained relating the microstructure to the deformation. Gubler (1978a, 1978b) and Kry (1975a, 1975b) carried out extensive microstructural evaluation in their work but these studies were generally confined to final densities below 500 kg/m^3 and to small deformations.

It was the major purpose of this investigation to evaluate the changes in microstructural variables that result from large deformations. In addition, it was intended to measure microstructural variables which to the present have not been adequately measured and mathematically described.

EXPERIMENT AND RESULTS

A series of confined compression tests were run at Montana State in which values of several microstructural parameters were measured. For these tests freshly fallen snow was collected and stored in a cold room at −10°C. Original sample volumes decreased by nearly 50% during the first two months in storage; volume changes occurring after this generally were small. The main test apparatus configuration is depicted in Figure 3. This setup was then placed in an environmental chamber maintained at −10°C and the snow compressed, until a predetermined loading was attained, at a nominal strain rate of 2.75×10^{-3} s^{-1}. Maximum loads used were 44.8 kN, 22.4 kN, or 11.2 kN, corresponding respectively to Cauchy stresses of 1.55 MPa, 0.77 MPa, and 0.39 MPa deformation, a $2.5 \times 2.5 \times 1.5$ cm^3 section of the sample was removed. This was prepared for surface sectioning by saturating it with a mixture of Dimethylthalate-Methyl Blue, precooled to −3°C, then allowed to freeze solid. The frozen snow-Dimethylthalate-Methyl Blue was then microtomed and the resulting surface polished with lampblack to prepare it for photographing (Perla 1982). A similar procedure was followed to obtain surface sections for the compressed samples.

Each surface section was photographed and prints were made with image magnifications ranging between 10× and 20×. These prints were digitized and run through filtering software supplied with the Thunder Scanner digitizer on a Macintosh computer. The filter-

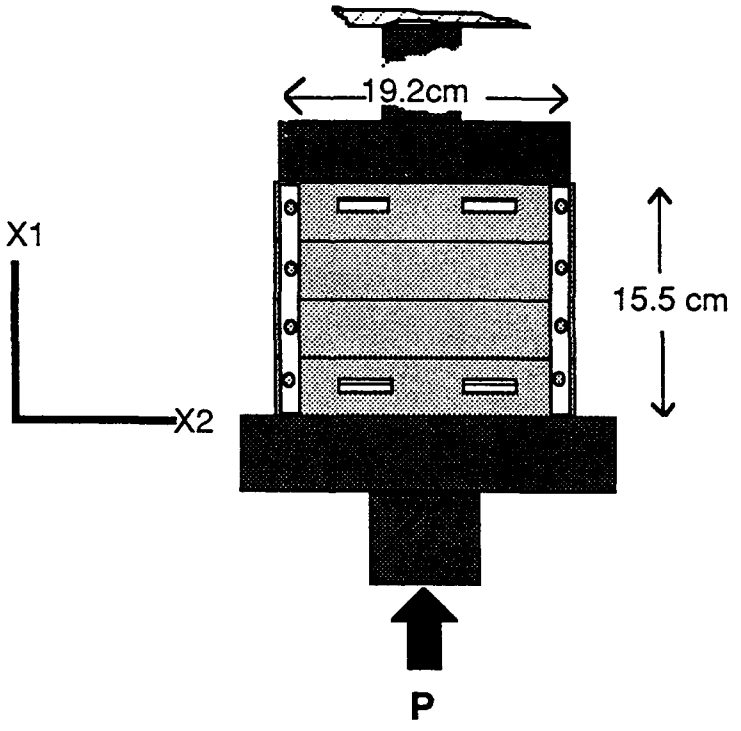

Figure 3. Schematic of compression ring with upper and lower platens.

ing process was used to remove blemishes and maximize contrast. Resolution of the digitized images was better than 0.033 mm/pixel.

The snow was considered to be a three phase mixture with air, necks and ice grains taken as the three phases (Hansen 1985). The subscripts representing each phase were respectively "a," "b" and "g." The variables used to represent surface section measurements were:

N_{gL}: number of grains intercepted per unit length of test line

N_{bA}: number of bonds per unit area

N_{gA}: number of grains per unit area

A_{aA}: area fraction of air phase appearing in the surface section.

A_{bA}: area fraction of neck phase in the surface section.

A_{gA}: area fraction of ice grain phase in the surface section.

D_{2i}: ith two dimensional bond diameter

f0: fraction of grains with 0 bonds appearing in the section plane

f1: fraction of grains with 1 bond appearing in the section plane

f2: fraction of grains with 2 bonds appearing in the section plane

f3: fraction of grains with 3 bonds appearing in the section plane.

Measurements of these parameters were then used to evaluate the following variables:

$$\alpha = \frac{1}{A_{gA} + A_{bA}}$$ ratio of ice to snow density, ρ_i/ρ_s (Underwood 1970) (1)

$$E = \frac{1}{N} \sum_{i=1}^{N} \frac{1}{D_{2i}}$$ harmonic mean of bond diameter (Fullman 1953) (2)

$$R_3 = \frac{\Pi}{4E}$$ mean three dimensional bond radius (Fullman 1953) (3)

$$h = \frac{A_{bA}}{N_{bV} \Pi r^2}$$ mean neck length (Hansen 1985) (4)

$$\lambda = \frac{\alpha - 1}{\alpha N_{gL}}$$ mean pore diameter (Fullman 1953) (5)

$$N_{bv} = \frac{8E\, N_{bA}}{\Pi^2}$$ mean number of bonds per unit volume (Fullman 1953) (6)

$$L_3 = \frac{A_{gA} + A_{bA}}{N_{gL}}$$ mean grain length (Underwood 1970) (7)

$$S_V = 4\, N_{gL} - 2\, \Pi\, R^2\, N_3\, N_{gV}$$ mean grain surface area (Hansen 1985) (8)

$$V = \frac{A_{gA} + A_{bA}}{N_{gV}}$$ mean grain volume (Hansen 1985). (9)

Two distinct ranges of grain size existed among the snow tested. Large grains corresponding to number 1 samples had average grain lengths, L_3, ranging from .34 to .39 mm in the uncompressed state. Small grained number 2 samples ranged from .19 to .22 mm. The initial densities of the samples were all between 250 kg/m^3 and 320 kg/m^3 so there was not a wide spread, in this variable, among the samples tested. The notation used for identifying samples was:

1) maximum load to which a sample would be subjected is indicated by the first four terms (2k50, 2500 lbs (11.2 kN))
2) p or f indicates if the sample is precompressed or in its final compressed state
3) 1 or 2 indicates if the sample was tested in the first or second year, respectively.

In what follows, an "o" subscript indicates initial or predeformation values and $\Delta\rho = \rho - \rho_o$ is the resulting change in density. The ratios of compressed to uncompressed mean grain length, L_3/L_{3o} vs. $\Delta\rho/\rho_o$, are plotted in Figure 4 and show a gradual decrease in grain size with increasing density. Since the strain rates used in these tests were large, some apparent grain fracture did result. The straight line is the linear regression curve and the vertical bars represent the entire range of the data scatter.

The mean pore length, λ, is the mean distance across a pore from grain surface to grain surface. Values for this parameter are listed in Table 1. Equations (1), (5) and (7) were combined, resulting in the equation

$$\lambda = L_3 (\alpha - 1) \qquad (10)$$

The solid curves in Figure 5 were generated using (10) and by holding L_3 constant over the entire density range. For the large grain curve, L_3 = .39 mm (10k01p) and L_3 = .22 mm (5k002p) for the small grain curve. The data points lie close to their respective curves, implying that little or no bond breakage occurred during the deformations.

The ratio of λ/L_3 for the compressed samples de-

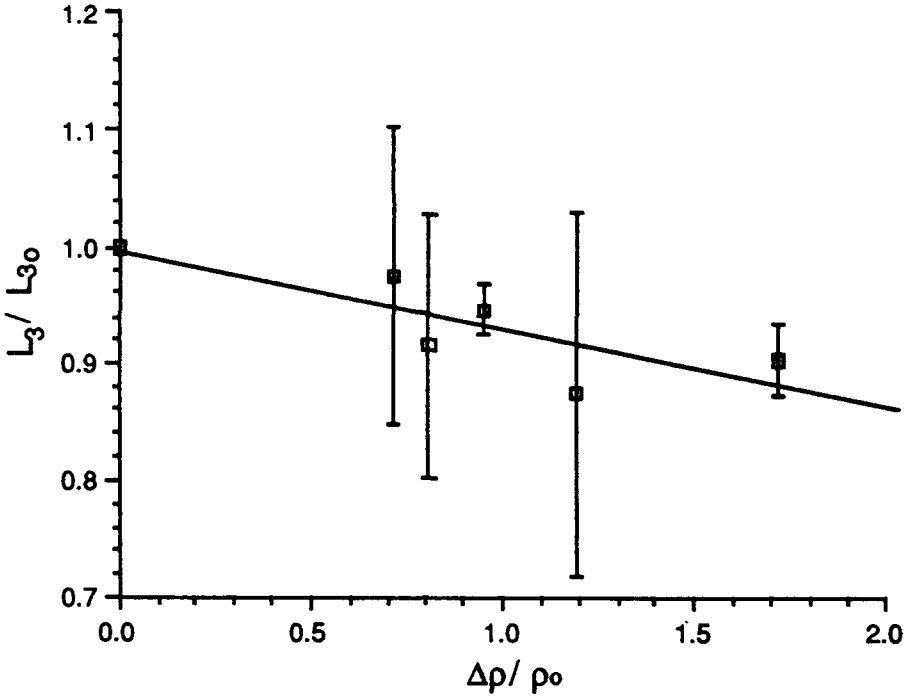

Figure 4. Normalized grain length plotted against the corresponding relative change in density. This figure indicates that some grain breakage may have occurred during the large deformation testing.

creased from 0.99 to 0.62 mm while the corresponding final loads increased from 11.2 kN (.387 MPa) to 44.8 kN (1.55 MPa). This demonstrates that the load bearing ability is closely tied to the mobility of the grains, and, as would be expected, the decrease in grain mobility corresponds to an increase in load bearing capability.

The factors which collectively govern the change in neck length are fairly complicated thus predicting neck length change is difficult. It suffices to say that for the densifications considered here, as can be seen for the values of h in Table 1, no definite trends in neck length could be unambiguously determined.

Two and three dimensional bond diameters and radii are given in Table 2. The two dimensional bond diameters D_2 and three dimensional bond diameters R_3 both show a definite decrease corresponding to deformation. This indicates that for large deformation, bond growth is less significant than bond fracture and new bond formation as few of the bonds found in the uncompressed state appear to survive the deformation process. There

Table 1. Mean intercept length, mean pore length and mean neck length.

Sample	*L_3 (mm)*	*λ (mm)*	*h (mm)*
10k01p	0.3987 ± 3.5%	0.8850 ± 7.7%	0.0958 ± 14.6%
10k01f	0.3405 ± 13.8	0.2114 ± 7.1	0.0708 ± 7.8
5k001p	0.3506 ± 8.0	0.6987 ± 8.5	0.0713 ± 13.3
5k001f	0.3209 ± 3.2	0.2612 ± 12.8	0.0877 ± 2.9
5k002p	0.2190 ± 1.3	0.6106 ± 4.1	0.0650 ± 11.9
5k002f	0.1977 ± 2.2	0.1703 ± 12.6	0.0621 ± 5.1
2k501p	0.3501 ± 8.5	0.8022 ± 7.6	0.0667 ± 6.7
2k501f	0.3416 ± 3.4	0.3112 ± 4.0	0.0607 ± 6.5
2k502p	0.1922 ± 0.8	0.5053 ± 3.4	0.0535 ± 8.9
2k502f	0.1820 ± 1.4	0.1796 ± 9.0	0.0588 ± 4.2

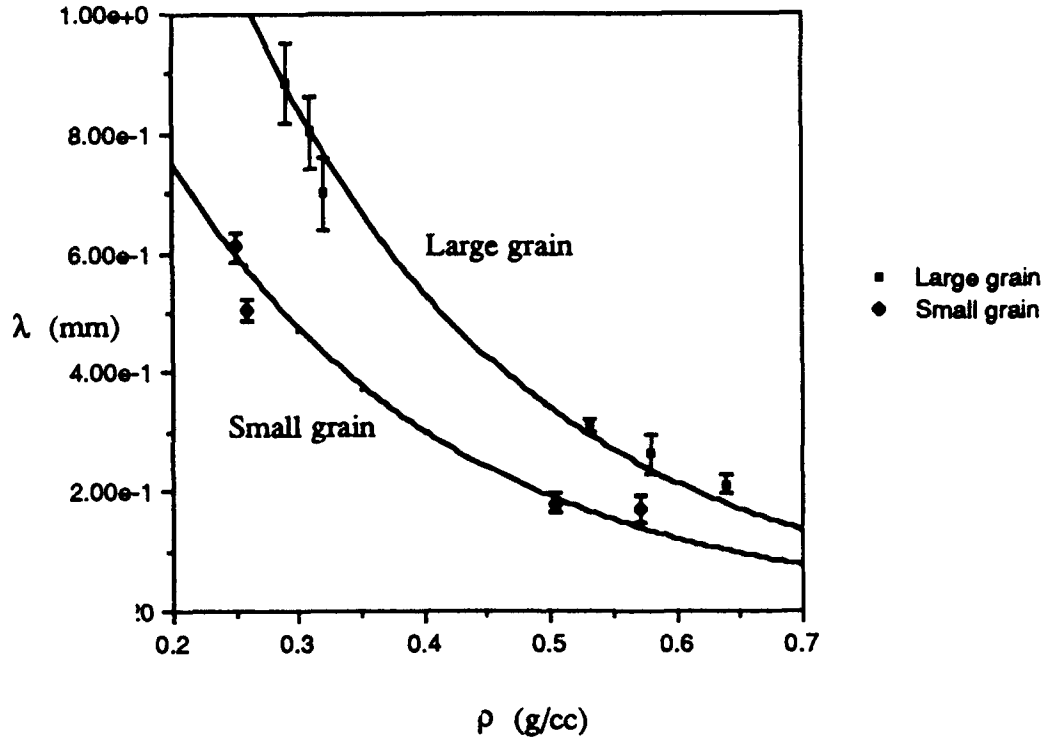

Figure 5. Shown are the curves for large and small grain groups using equation 10 and along with the experimentally determined data. Error bars represent range of data scatter.

should be a point corresponding to decreased grain mobility at which the average bond radius ceases to decrease as a result of bond breakage and where the average bond radius begins to increase. Some indication of this can be seen in Figure 6 for the largest fractional density change.

Complementary to the grain bond size is N_{bV}, the number of bonds per volume. This along with the bond radius will strongly influence the stress concentration at each bond. Over the range of loading conditions in this study, N_{bV} showed a 2.5 fold increase relative to the undeformed state at the 11.2 kN load (0.387 MPa) to a 6.9 fold increase at the 44.8 kN load (1.55 MPa). The values of N_{bV} are shown in Table 4.

The values of N_3, the mean three dimensional coordination number, N_{gV}, the mean number of grains per unit volume, V, the mean grain volume and S_V, the mean grain surface area to volume ratio, obtained for

Table 2. Values obtained directly from measured 2-D bonds in the plane.

Sample	D_2 *(mm)*	E *(mm^{-1})*	R_3 *(mm)*	D_{2min} *(mm)*
10k01p	0.1692 ± 2.1%	07.2841 ± 3.7%	0.1080 ± 3.7%	0.0652 ± 14.3%
10k01f	0.1299 ± 0.2	09.2088 ± 0.1	0.0853 ± 0.1	0.0434 ± 4.5
5k001p	0.1488 ± 3.9	08.0084 ± 5.6	0.0984 ± 5.6	0.0895 ± 5.0
5k001f	0.1420 ± 5.1	09.5567 ± 6.6	0.0826 ± 6.6	0.0413 ± 0.9
5k002p	0.0899 ± 5.7	15.6394 ± 3.4	0.0503 ± 3.4	0.0178 ± 21.9
5k002f	0.0693 ± 0.4	19.5801 ± 3.1	0.0402 ± 3.1	0.0118 ± 2.5
2k501p	0.1485 ± 3.1	07.8755 ± 0.8	0.0998 ± 0.9	0.0859 ± 0.5
2k501f	0.1315 ± 9.5	08.5692 ± 10.1	0.0926 ± 10.1	0.0703 ± 9.8
2k502p	0.0808 ± 1.9	15.3586 ± 0.8	0.0512 ± 0.9	0.0270 ± 9.1
2k502f	0.0677 ± 0.8	18.8240 ± 2.0	0.0417 ± 2.0	0.0196 ± 42.9

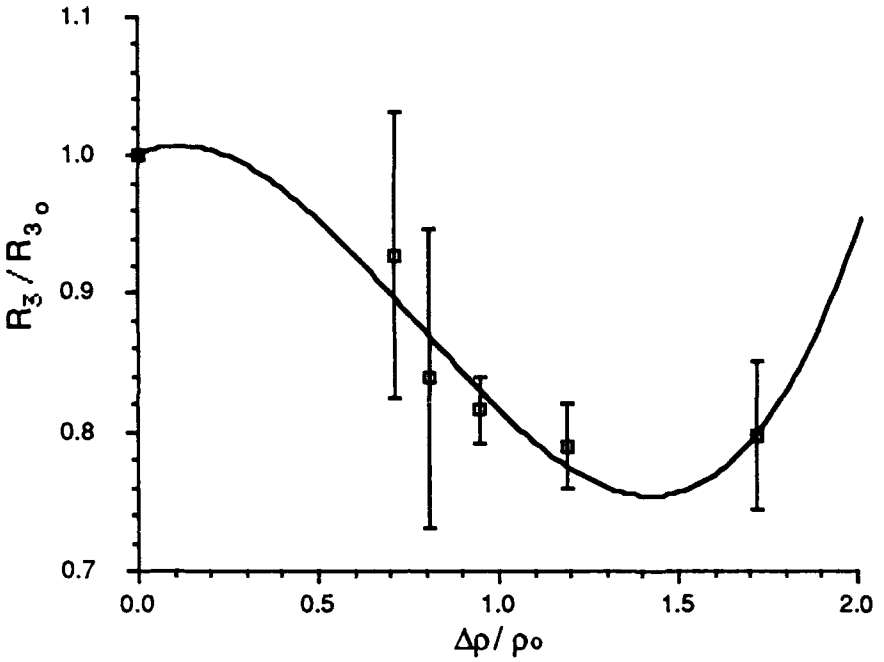

Figure 6. Normalized three dimensional radius versus the relative change in density. The error bars represent the range of data scatter.

each of the five precompressed samples, are shown in Table 3. These could not be obtained directly from the section measurements as they generally require knowledge of a grain shape factor. As alpine snow is irregularly shaped characterizing it by shape factor may not be a valid generalization. Work done in Switzerland by Gubler (1978a) and later modified by Hansen and Brown (1976) provided a method to obtain the mean coordination number N_3 and mean grain volume V without requiring assumptions about a grain shape factor other than for an initial guess. Edens and Brown (in publication) found it necessary to modify the method further. Good results were then obtained for N_3, V and correspondingly N_{gV}, and S_V for the uncompressed samples.

The mean coordination number, N_3, ranged from 2.28 bonds/grain to 2.67 bonds/grain. It appears that N_3 is independent of the mean grain size. N_{gV} for the compressed samples was obtained by using the following equation to obtain a first estimate,

$$N_{gVf} = \frac{\rho_f}{\rho_i} N_{gVi}, \qquad (11)$$

where the subscripts f and i refer to initial and final respectively and where ρ is the density. Figure 6 demonstrates the variation of the three-dimensional coordination number, N_3, for the density ranges covered in the testing program reported here.

Values of S_V in Tables 3 and 4, indicate an increase in the surface area per unit volume. This is shown in Figure 7. As would be expected, S_V increases steadily for much of the deformation where bond breakage is frequent and where there is some grain fracturing. It then levels out as the density approaches 600 kg/m^3

Table 3. N_3, N_{gV}, V and S_V for the precompressed samples.

Sample	N_3 *(bonds/grain)*	N_{gV} *(mm^{-3})*	V *(mm^3)*	S_V *(mm^{-1})*
10k01p	2.28 ± 10.7%	02.09 ± 4.8%	0.15 ± 4.6%	2.80 ± 17.5%
5k001p	2.41 ± 7.1	02.8º ± 5.6	0.12 ± 5.4	3.41 ± 6.8
5k002p	2.64 ± 3.4	12.19 ± 3.9	0.02 ± 6.1	4.31 ± 8.5
2k501p	2.58 ± 10.6	03.05 ± 2.9	0.10 ± 2.8	3.00 ± 13.2
2k502p	2.36 ± 9.3	19.22 ± 6.5	0.01 ± 6.1	5.01 ± 2.6

Table 4. N_3, N_{gv}, V and S_V for the compressed samples.

Sample	N_3 (bonds/grain)	N_{gv} (mm^{-3})	V (mm^3)	S_V (mm^{-1})
10k01f	7.14 ± 19.6	04.74 ± 13.6	0.14 ± 4.6	5.83 ± 13.6
5k001f	5.85 ± 8.0	05.24 ± 6.0	0.11 ± 5.4	5.60 ± 7.20
5k002f	5.72 ± 6.6	27.69 ± 4.1	0.02 ± 3.7	9.32 ± 7.10
2k501f	4.17 ± 16.8	05.22 ± 3.0	0.10 ± 2.8	4.99 ± 6.10
2k502f	3.89 ± 11.9	37.48 ± 7.0	0.01 ± 6.1	9.49 ± 10.2

($\Delta\rho/\rho_o$ approaches 1.75–2.0). At densities which are higher than those studied here this ratio should begin to decrease as bond breakage all but ceases and bond mobility approaches zero.

One should not confuse the results shown in Figure 8 with what one would expect with thermodynamic consolidation of snow. Here we are studying the large scale compaction of snow at large enough rates to fracture grain bonds as well as grains. As a consequence new surface area is exposed due to the fracturing at high deformation rates. This is in contrast to the slow consolidation of snow as it attempts to reduce its free surface energy by grain growth and densification. In this case deformations are so slow that no fracturing occurs and a gradual reduction of free surface area results.

DISCUSSION AND CONCLUSIONS

At the maximum density attained, there was approximately a 3.5 fold increase in coordination number. The increase in coordination number is not very rapid until densities of 500 kg/m^3 are reached. This corresponds to strains of approximately 33% and occurs at the point where the stress response begins increasing rapidly during the compression. The stress is about 0.1 MPa at this point. At the maximum stress the density (639.4 kg/m^3) represents a 25% increase over that at 0.1 MPa (500 kg/m^3). In this interval the axial stress increased 16 fold and the coordination number was doubled. There is approximately a 60% decrease in the grain mobility as indicated by λ/L_3 at 500 kg/m^3 and at 639.4 kg/m^3 (Figure 9).

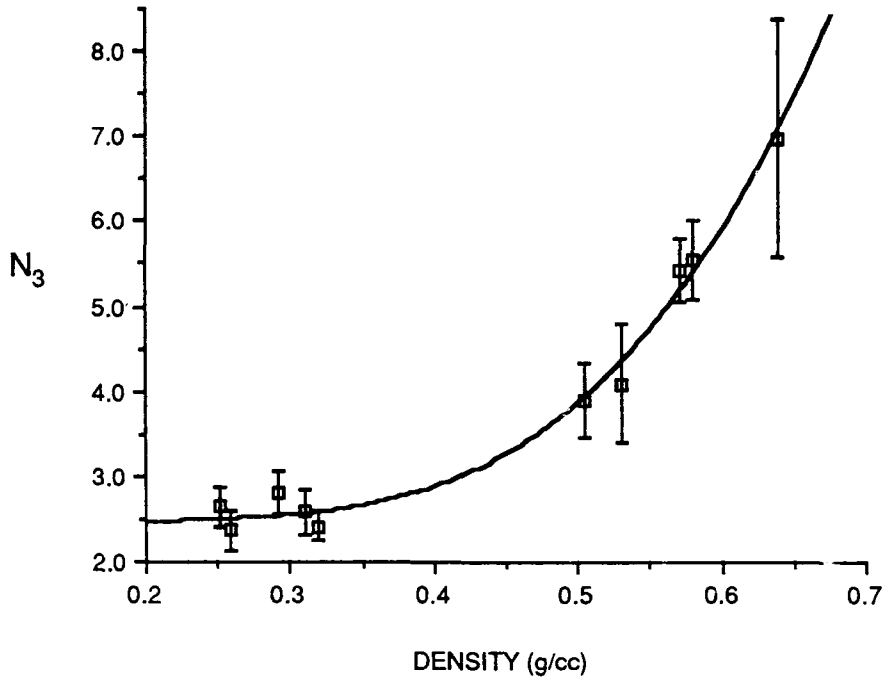

Figure 7. Density versus the three dimensional coordination number. Error bars are for range of data scatter.

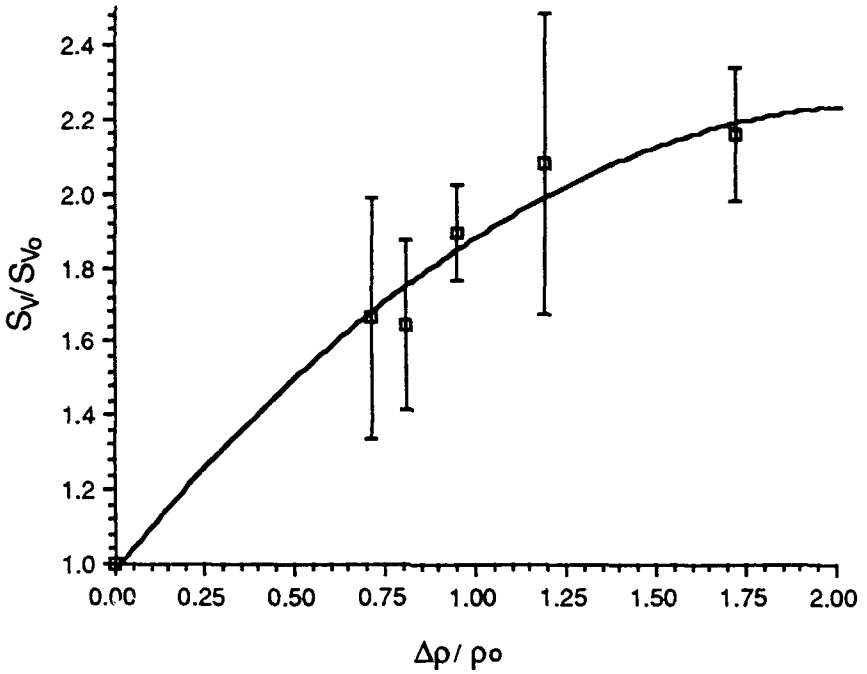

Figure 8. Normalized surface area to volume ratio versus relative density change.

The largest relative decrease in bond radius (22%) occurs at this maximum stress. This is a 38% reduction in original bond area, but is countered by an increased coordination number and a factor of 1.9 increase in bond area by over the entire deformation process. The material stiffness is not a linear function of total bond area, since the structural rigidity of the ice matrix is strongly influenced by the coordination number, in the sense that a structurally indeterminant structure is much stiffer than one that is structurally determinant. Therefore the

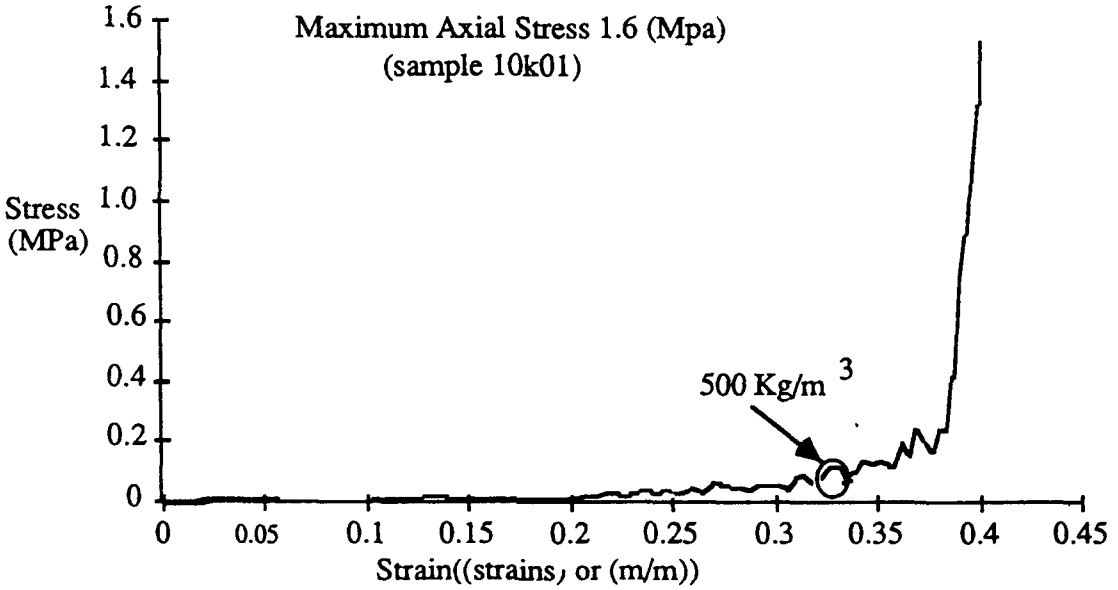

Figure 9. Raw data for axial stress versus Lagrangian strain. The approximate location of the point corresponding to the 500 kg/m^3 density is shown.

coordination number is a dominant factor determining the material stiffness and strength.

This discussion indicates the effect that relatively small order of magnitude changes in the microstructure have in increasing the load bearing ability of snow. As indicated by Brown (1979), the effects of reduced grain mobility due to pore collapse may account for much of this at high densities.

The neck length parameter (h) has not been described in a satisfactory manner in this study. The results of the testing program and image analysis gave an erratic behavior, as illustrated in Table 1. In some cases the neck length is seen to increase in value, while in other instances the results showed the neck length decreasing. It was expected that the neck length would decrease with compressive deformation, since compressive stresses on the necks would shorten them. Formation of new bonds (and subsequently new necks) during densification would also serve to cause the mean neck length to decrease since necks with nearly zero length would be added to the averaging process. There are a number of possible explanations for this apparent discrepancy. One could be that an image analysis system with a better resolution is needed to provide a more accurate measurement of the neck length. Also the definition of the neck length is difficult to implement and leads to a subjective criterion for measuring h. Changes in the sign of the surface curvature as seen in the surface sections is difficult to determine with the system used.

There are several experimental results that would complement this study. Values of L_3 for density changes of 25, 50, 150 and 200% will help verify any trends in grain size change that are occurring (Figure 4). It appears that the average grain bond radius may begin to increase at a density change of 150% (Figure 6). Measurements of R3 at 130, 150 and 200% are needed to confirm this. The other measurement needed is for the coordination number at a final density of 450 kg/m^3. This should be sufficient to define the point of transition from low to high coordination numbers. In addition, the methods presented here can also be applied to evaluation of changes in microstructure of snow due to thermodynamic sintering and also for low strain rates where grain and bond fracturing is much less significant.

ACKNOWLEDGMENTS

The work reported here was supported by the Army Research Office (Grant No. DAAG29-85-K-0259). The authors wish to express their appreciation of the support by the Geosciences Program in the Army Research Office.

LITERATURE CITED

Abele, G., and Gow, A.J. (1975) Compressibility characteristics of undisturbed snow, CRREL Research Report 336.

Abele, G., and Gow, A.J. (1976) Compressibility characteristics of compacted snow, CRREL Report 76-21.

Alley, R.B. (1987) Firn densification by grain boundary sliding: a first model, Journal de Physique, Vol 48, (Colloque CI, Supplement au No. 3).

Brown, R.L. (1979) A volumetric constitutive law for snow subjected to large strains and strain rates, CRREL Report 79-20.

Brown, R.L. (1980) A volumetric constitutive law based on a neck growth model, Journal of Applied Physics, Vol. 51, No. 1, 161-165.

Ebinuma, T. and Maeno, N. (1985) Experimental studies of densification and pressure sintering of ice, Annals of Glaciology, Vol. 6, 83-86.

Edens, M.Q. and Brown, R.L. (in publication). Changes in microstructure of snow under large deformations, Journal of Glaciology.

Fullman, R.L. (1953) Measurement of particle sizes in opaque bodies, AIME, Vol. 197.

Gubler, H. (1978a) Determination of the mean number of bonds per snow grain and of the dependence of tensile strength of snow on stereological parameters, Journal of Glaciology, Vol. 20, No. 83, 329-342.

Gubler, H. (1978b) An alternate statistical interpretation of the strength of snow, Journal of Glaciology, Vol. 20, No. 83, 343-358.

Hansen, A.C. and Brown, R.L. (1986) The granular structure of snow: An internal state variable approach, Journal of Glaciology, Vol. 32, No. 112, 434-438.

Kry, P.R. (1975a) Quantitative stereological analysis of grain bonds in snow, Journal of Glaciology, Vol. 14, No. 72, 467-478.

Kry, P.R. (1975b) The relationship between the viscoelastic properties and structure of fine-grained snow, Journal of Glaciology, Vol. 14, No. 72, 479-500.

Maeno, N. and Ebinuma, T. (1983) Pressure sintering of ice and its implication to the densification of snow at polar glaciers and ice sheets, The Journal of Physical Chemistry, 1983, 87, 4103-4110.

Perla, R. (1982) Preparation of section planes in snow specimens, Journal of Glaciology, Vol. 28, No. 98, 199-203.

Underwood, E.E. (1970) Quantitative Stereology, Addison-Wesley, Reading, Massachusetts.

Wilkinson, D.S. (1988) A pressure sintering model for the densification of polar firn and glacier ice, Journal of Glaciology, Vol. 34, No. 116, 40-45.

Short Term Settlement of Footing On Snow Foundation

PUNEET MAHAJAN AND R.L. BROWN
Mechanical Engineering Department
Montana State University
Bozeman, Montana 59715

ABSTRACT

A constitutive theory for snow, developed by the authors, is applied to solve for the short term settlement of a footing on a snow foundation. The constitutive law used in the study is a microstructurally based formulation which includes the effects of bond deformation and fracture. It also includes transient creep effects and strain hardening of snow.

The foundation problem is solved for stress and displacement distribution, with two different loads of 0.008 MPa and 0.1 MPa distributed uniformly over a part of the top face. The stress distribution matches closely with the existing theoretical results. The results presented here have shown that the constitutive theory can be used to solve practical problems such as the foundation settlement problem. With some additional development the theory could be used to evaluate situations where high rates of loading occur, such as in vehicle mobility problems.

INTRODUCTION

Snow is a porous viscoelastic granular material capable of undergoing large deformations. Any object placed on a surface of snow settles as a result of combined effect of natural densification of snow and penetration of the object. The differential settlement due to the penetration of object can impose severe stresses in structural elements and is of primary interest to design engineers.

In soils the settlement is kept within definite limits to ensure against abrupt failure by plastic yielding or rupture. In snow the settlement of foundations can continue indefinitely, and under constant load gradual consolidation of snow may lead to ultimate collapse. If, however, the loading is sufficiently low compaction alone may not lead to complete failure of material, since moderate penetration is accompanied by an increasing resistance as the snow compact deforms (Dandekar and Brown, 1985).

For snow foundations, the grain size, neck length, bond diameter and coordination number all influence the settlement rate. The size of intergranular bonds, developed during sintering of particles, is an important factor in determining the deformation resistance of snow. The grain size and shape and the bond size are determined by the type of metamorphism snow undergoes.

Kerr (1962) treated the problem of foundation settlement rate on snow by representing the snow mass in the form of elastic and viscous elements. Dandekar and Brown (1985) used a modified version of a constitutive law developed by Brown (1979) to model long term settlement of a footing on snow. The transient creep effects were not included in this model.

In this paper we model the short term settlement of a snow foundation, subject to loads low enough so that no collapse of the snow structure takes place. The constitutive law used here is one developed by Mahajan and Brown (1990) for snow formed under equitemperature metamorphism. This constitutive law is based on the microstructure of snow and takes into account a number of intergranular deformation processes. It also includes the effects of transient creep. This constitutive theory is discussed in the following section.

CONSTITUTIVE THEORY

Snow which has existed under equitemperature conditions is made of spherical ice granules connected by bonds or necks. The constitutive behavior of snow is

determined by the size of the ice particles and the geometry of bonds connecting the grains. Because of their smaller cross section, the necks which connect the grains are subjected to much higher stresses when compared to the ice particles and therefore undergo large deformations. It is the straining of necks which is responsible for deformation of snow, particularly at low stresses. At higher stresses the necks undergo fracture, and interparticle slip becomes a significant deformation mechanism. It is this relative displacement between the particles which is responsible for strains in snow at large stresses. At these stresses snow behaves somewhat like other granular materials. The deformation of snow is therefore an averaged effect of the deformation of the unbroken necks and of relative sliding between particles with broken necks.

A constitutive theory taking into account these deformation mechanisms has been suggested by Mahajan and Brown (1990). The stresses at the points of contact of a representative particle, are calculated using the variational approach suggested by Kanatani (1981). Next, the strains in the necks are calculate using equations developed for constitutive behavior of ice. If fracturing of necks takes place, empirical relations are developed to model the intergranular motion due to the relative sliding between ice particles. The strains are then averaged, over the representative particle to obtain the strains in snow.

Consider now a typical ice grain and the necks or bonds which connect it to other grains. To calculate the stresses in the necks, a local coordinate system, as illustrated in Figure 1, is set up at the contact point. The stress vector at the contact point or the ice neck is resolved into three components along the coordinate axis of this local coordinate system. The unit vectors for this coordinate system are

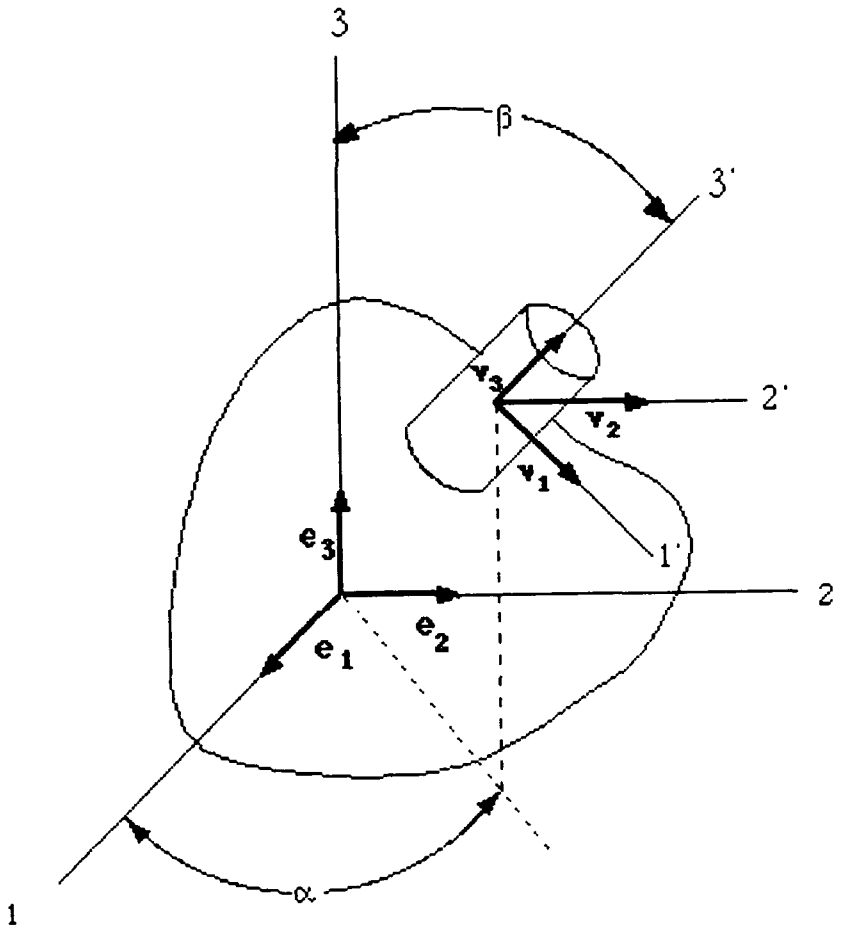

Figure 1. Coordinate system. 1-2-3 global coordinate system centered at the ice particle center. 1'-2'-3' neck coordinate system centered at the center of neck.

$$\nu_1 = \cos\alpha\cos\beta\, e_1 + \sin\alpha\sin\beta\, e_2 - \sin\beta\, e_3$$
$$\nu_2 = -\sin\alpha\, e_1 + \cos\alpha\, e_2 \qquad (1)$$
$$\nu_3 = \cos\alpha\sin\beta\, e_1 + \sin\alpha\sin\beta\, e_2 + \cos\beta\, e_3.$$

The stress vector in the necks, on the face with normal **n**, is given by

$$\sigma^n A_T P = \frac{a^2}{\gamma} t^n. \qquad (2)$$

The vector **n** is same vector as ν_3 in equation (1) above. A_T is the contact area (neck cross sectional area), a is the grain radius, γ is the solid volume fraction, and P is the probability function which determines the probability that a point on the surface of a grain is also located on a neck.

The components of stress on the face with normal **n** are given as:

$$\sigma_{i3} = \nu_i \cdot \sigma^n \qquad (3)$$

If averaging is done over the contact area lying between the solid angle imbedded by angles α to $\alpha+\Delta\alpha$ and β to $\beta+\Delta\beta$, we obtain

$$(\sigma_{i3})_{av} = \frac{\int_\beta^{\beta+\Delta\beta}\int_\alpha^{\alpha+\Delta\alpha} t^n \cdot \nu_i \frac{a^2}{\gamma}\sin\beta\, d\alpha\, d\beta}{\int_\beta^{\beta+\Delta\beta}\int_\alpha^{\alpha+\Delta\alpha} A_T \cdot P \sin\beta\, d\alpha\, d\beta}.$$

A constitutive law for ice is now needed in order to find the strain in these necks. This constitutive law is based on the theory developed by Szyszkowski and Glockner (1987) and are given by the following relations

$$\dot{e}_{ij} = \frac{(1+\nu)}{E}\dot{\sigma}_{ij} - \frac{\nu}{E}\dot{\sigma}_{kk}\delta_{ij} + \frac{1}{\nu_1}\frac{d}{dt}\int_0^t \left[\tilde{\sigma}_{ij}(\tau)\right]^n j(t-\tau)\,d\tau + \frac{\tilde{\sigma}_{ij}^n}{\nu_2} \qquad (4)$$

where

$$\tilde{\sigma}_{ij} = s_{ij}\left\{1.5\left|\frac{S}{s_{ii}}\right|^{n-1}\right\}^{1/n}$$
$$S^2 = 1.5\, s_{ij}s_{ij}. \qquad (5)$$

In equation (4) ν is the Poisson's ratio, E is the Young's modulus, j is the creep compliance, and ν_1 and ν_2 are material constants. s_{ij} is the deviatoric stress. The strain rate is decomposed into elastic, recoverable creep and plastic components, denoted as:

$$\dot{e}_{ij} = \dot{e}_{ij}^{\,e} + \dot{e}_{ij}^{\,c} + \dot{e}_{ij}^{\,p} \qquad (6)$$

The expressions for the various components as observed from equation (4) are

$$\dot{e}_{ij}^{\,e} = \frac{(1+\nu)}{E}\dot{\sigma}_{ij} - \frac{\nu}{E}\dot{\sigma}_{kk}\delta_{ij} \qquad (7)$$

$$\dot{e}_{ij}^{\,c} = \frac{1}{\nu_1}\frac{d}{dt}\int_0^t \left[\tilde{\sigma}_{ij}(\tau)\right]^n j(t-\tau)\,d\tau \qquad (8)$$

$$\dot{e}_{ij}^{\,p} = \frac{\tilde{\sigma}_{ij}^n}{\nu_2}. \qquad (9)$$

Instead of directly solving the integral in equation (8), Szyszkowski and Glockner (1987) have approximated the equations (8) and (9) by a generalized Kelvin body in series with a nonlinear dashpot. The equations for the Kelvin body are written as

$$\dot{e}_{ij}^{\,c} = \frac{\left(\tilde{\sigma}_{ij}'\right)^n}{\nu_1} \qquad (10)$$

$$\left(\tilde{\sigma}_{ij}'\right)^n + c\,\tilde{\sigma}_{ij}'\left(\tilde{\sigma}_{ij}\right)^{n-1} = E_1 e_{ij}^{\,c} \text{ (no summation)} \qquad (11)$$

$$\tilde{\sigma}_{ij}' + \tilde{\sigma}_{ij}'' = \tilde{\sigma}_{ij}, \qquad (12)$$

where $\tilde{\sigma}_{ij}$ is the effective viscous stress tensor defined above, $\tilde{\sigma}_{ij}'$ is the component of effective stress in the spring and $\tilde{\sigma}_{ij}''$ is the component of effective stress in the dashpot. The value of the constants ν_1 and ν_2 depends on the stress in the necks. If the principal tensile stress in the neck is less than 0.7 MPa the constants ν_1 and ν_2 have values of 10.8 and 235, respectively. Otherwise, ν_2 is equal to 5040. The values of the constants for two cases are different because the deforming mechanisms, as explained in reference (1), are different. If the maximum principal stress in the necks is less than or equal to 0.7 MPa, superplastic deformation occurs, whereas for stress higher than this dislocation creep becomes predominant.

The strains in the ice necks are next transformed to the snow coordinate system by the equation:

$$E_{ij} = Q_{ir}^T e_{rs} Q_{sj}. \qquad (13)$$

Q is an orthogonal transformation matrix carrying the local coordinate system centered at the neck to the global coordinate system centered at ice particle center (Figure 1).

If the principal stress in necks is greater than 0.7 MPa and principal strain exceeds 5×10^{-3}, we assume the neck has lost the ability to carry principal tensile stress and therefore fractures. After the occurrence of fracture, deformations in snow are due to interparticle sliding. The tangential and normal velocities and displacements are calculated using the equation

$$\dot{\eta} = c_1(\tau)|\tau|^{n-1}\left(1/\delta^m\right) \tag{14}$$

$$\dot{\xi} = c_1(\sigma)|\sigma|^{n-1}\left(1/\delta^m\right)c_2, \tag{15}$$

where $\dot{\xi}$ and σ are respectively the velocity and the component of traction in the direction normal to the grain surface at the neck. $\dot{\eta}$ is the tangential velocity, τ is the component of traction in the shearing direction, and disp is the relative current displacement between the grains at a particular time. The expression $1/\delta$ appears because, as the sliding displacement increases, the particles form new contacts with other particles, and this impedes further relative displacement. This seems to account for much of the strain hardening in snow. The parameter m was obtained, using a regression fit, as a function of effective strain in snow. The constant c_1, in equations (14) and (15), has a value of 3.906×10^{-3}. The constant c_2 depends on the ratio of shear to compressive stress at the point of contact. If the absolute value of the ratio of shear to compressive stress is less than 0.5, then c_2 is equal to 0.3. Otherwise it has a value of 0.40. The constant n has a value of 1.8. The parameters c_1, c_2 and m have slightly different values for tensile stress states. For tension c_1 is 5.468×10^{-3} and c_2 is approximately 0.1. The strain rate is given by the expression

$$\dot{E}_{ij} = \frac{1}{a}\left(\frac{1}{2}\dot{\eta}\,(s_i n_j + s_j n_i) + \dot{\xi} n_i n_j\right). \tag{16}$$

s_i and n_i are components of the unit vectors **n** and **s**, where **n** is normal to the grain surface and **s** is in the direction of the shear stress τ. The strain in snow is the average of strain in all necks.

$$(E_{ij})_{av}\int_0^{2\Pi}\int_0^{\Pi}\sin\beta\,d\alpha\,d\beta = \int_0^{2\Pi}\int_0^{\Pi}E_{ij}\sin\beta\,d\alpha\,d\beta, \tag{17}$$

where $E_{ij}\sin\beta d\alpha d\beta$ on the right-hand side is obtained from equation (13) or (17), depending on whether it is a broken neck or a neck undergoing superplastic deformation. $(E_{ij})_{av}$ is the strain in snow averaged over the solid angle.

NUMERICAL SOLUTION OF THE FOUNDATION PROBLEM

It has been experimentally observed that for symmetrical loading, the vertical and horizontal extent of the deformation zone (pressure bulb) in a foundation extends to about two times the width of the footing (Reed, 1966). For simplicity we consider a rectangular area underneath the footing as shown in Figure 2. The dimensions of this rectangle are larger than the observed size of the pressure bulb. Plane strain has been assumed for this problem, and therefore a three dimensional state of stress exists. The method followed in solving this problems in a commonly used technique for solving problems involving creep of structures. This method is closely linked to the elastic solution procedure. This relation between creep and elastic solutions derives from the fact that, after initial loading, creep strains arising during the passage of time require that stresses change by elastic straining to accommodate these changes (Boyle and Spence, 1983).

The stress strain relation for an isotropic elastic material is

$$\sigma_{ij} = \lambda\epsilon_{kk} + 2\mu\epsilon_{ij},$$

where λ and μ are Lame's constants. We can write this last relation as

$$\sigma_{ij} = \lambda(e_{kk} - \epsilon_{kk})\,\delta_{ij} + 2\mu(e_{ij} - \epsilon_{ij}) \tag{18}$$

$$\sigma_{ij} = \lambda\left(\frac{\partial\mu_k}{\partial x_k} - \epsilon_{kk}\right)\delta_{ij} + \mu\left(\frac{\partial\mu_i}{\partial x_j} + \frac{\partial\mu_j}{\partial x_i} - 2\epsilon_{ij}\right).$$

Substituting this into the equilibrium equation we obtain the Navier's equation

$$\mu\left(\nabla^2 u_j\right) + (\lambda+\mu)\,\nabla_j\nabla_i u_i + \rho b_j = \lambda\frac{d\epsilon_{kk}}{dx_j} + 2\mu\frac{\partial\epsilon_{ij}}{\partial x_i}. \tag{19}$$

For the case of plane strain, the reduced Navier's equations are

$$G\left[\nabla^2 u_1 + \frac{1}{1-2\nu}\frac{\partial}{\partial x_1}\left(\frac{\partial u_1}{\partial x_1} + \frac{\partial u_2}{\partial x_2}\right)\right] + \rho b_1 \tag{20}$$

$$G\left[\nabla^2 u_2 + \frac{1}{1-2\nu}\frac{\partial}{\partial x_2}\left(\frac{\partial u_1}{\partial x_1} + \frac{\partial u_2}{\partial x_2}\right)\right] + \rho b_2$$

$$= \frac{E\nu}{(1+\nu)(1-2\nu)}\left(\frac{\partial\epsilon_{11}}{\partial x_2} + \frac{\partial\epsilon_{22}}{\partial x_2} + \frac{\partial\epsilon_{33}}{\partial x_2}\right) +$$

$$2G\left(\frac{\partial\epsilon_{22}}{\partial x_2} + \frac{\partial\epsilon_{12}}{\partial x_1}\right). \tag{21}$$

The boundary conditions are:
Top face:

$x_2 = 2.25$ m	$Q = Q_0$	$0 \le x_1 \le 0.45$ m
	$Q = 0$	$x_1 > 0.45$ m
	$t_{xy} = 0$	$0 \le x_1 \le 0.9$ m.

Using the above relations in the constitutive relation (equation 18) we have

$$Q = (\lambda + 2\mu)\left(\frac{du_2}{dx_2} - \epsilon_{f22}\right) + \lambda\left(\frac{du_1}{dx_1} - \epsilon_{f11}\right) - \lambda\epsilon_{f33}, \quad (22)$$

$$\left(\frac{\partial u_2}{\partial x_1} + \frac{\partial u_1}{\partial x_1}\right) = 2\epsilon_{f12}. \quad (23)$$

Axis of symmetry:

$$\frac{\partial u_2}{\partial x_1} = 0, \; u_1 = 0 \qquad 0 \leq x_1 \leq 0.9\,\text{m}, \; x_2 = 0. \quad (24)$$

Bottom and right vertical side:

$$u_1 = 0, \; u_2 = 0 \qquad \begin{matrix} 0 \leq x_1 \leq 0.9\,\text{m}, \; x_2 = 0 \\ \text{and } x_1 = 0.9\,\text{m}, 0 \leq x_2 \leq 2.25\,\text{m}. \end{matrix} \quad (25)$$

If we substitute the boundary conditions for the top face into equations 20 and 21, we obtain

$$G\left[\left(1 + \frac{1}{(1-2\nu)}\right)\frac{\partial^2 u_1}{\partial x_1^2} + \left(1 - \frac{1}{(1-2\nu)}\right)\frac{\partial^2 u_2}{\partial x_2^2}\right]$$

$$= \frac{E\nu}{(1+\nu)(1-2\nu)}\left(\frac{\partial \epsilon_{f11}}{\partial x_1} + \frac{\partial \epsilon_{f22}}{\partial x_1} + \frac{\partial \epsilon_{f33}}{\partial x_1}\right) +$$

$$2G\left(\frac{\partial \epsilon_{f21}}{\partial x_1} + \frac{\partial \epsilon_{f11}}{\partial x_2}\right) - \frac{2}{1-2\nu}\frac{\partial \epsilon_{f12}}{\partial x_2} \quad (26)$$

$$G\left[\left(1 + \frac{1}{(1-2\nu)}\right)\frac{\partial^2 u_2}{\partial x_2^2} + \left(1 - \frac{1}{(1-2\nu)}\right)\frac{\partial^2 u_1}{\partial x_1^2}\right] + \rho b_2$$

$$= \frac{E\nu}{(1+\nu)(1-2\nu)}\left(\frac{\partial \epsilon_{f11}}{\partial x_2} + \frac{\partial \epsilon_{f22}}{\partial x_2} + \frac{\partial \epsilon_{f33}}{\partial x_2}\right) +$$

$$2G\left(\frac{\partial \epsilon_{f22}}{\partial x_2} + \frac{\partial \epsilon_{f12}}{\partial x_1}\right) - \frac{2}{1-2\nu}\frac{\partial \epsilon_{f21}}{\partial x_1} \quad (27)$$

The symmetry boundary condition, on substitution into the equation 20, acquires the form

$$G\left[\left(1 + \frac{1}{(1-2\nu)}\right)\frac{\partial^2 u_2}{\partial x_2^2} + \frac{\partial^2 u_1}{\partial x_1^2}\right] + \rho b_2$$

$$= \frac{E\nu}{(1+\nu)(1-2\nu)}\left(\frac{\partial \epsilon_{f11}}{\partial x_2} + \frac{\partial \epsilon_{f22}}{\partial x_2} + \frac{\partial \epsilon_{f33}}{\partial x_2}\right) +$$

$$2G\left(\frac{\partial \epsilon_{f22}}{\partial x_2} + \frac{\partial \epsilon_{f22}}{\partial x_2}\right).$$

The above differential equations with boundary conditions are solved using the finite difference method. Central finite differences have been used throughout. A grid with mesh refinement near the top face has been used. The problem was solved for two different values of Q_0, namely, 0.008 MPa and 0.1 MPa.

Although not obvious, these equations are time dependent. The time dependence appears because the creep strains in the above equations change with time. The first step in solving these equations involves finding the elastic solution at time t = 0. For this the creep terms on the right-hand side are set to zero. The stresses from this elastic solution are then used to calculate the creep strain rates using the constitutive equation presented in the preceding section. Once the creep strains have been calculated from these creep rate equations, they are substituted in the above differential equations which are solved for displacements at end of time step. The new stresses at the end of time step are next calculated. Due to the rather complex nature of the creep equations, it is not possible to use implicit methods to integrate the creep strain rate equations, and explicit methods have to be used. This, unfortunately, poses a big limitation on the size of time step. The grain data reported by Hansen (1985) was used. For a compressive stress of 8×10^{-3} MPa with a time step of 120 seconds, a steady state of stress is not reached even after 300 time steps, although the rate of change of stress does exhibit a decreasing trend. For instance, the rate of change of the largest stress decreases from 1.5×10^{-4} MPa/hr at the beginning to 3×10^{-5} MPa/hr by the 300th iteration. Since this rate of change is small, it was decided to assume a steady state of stress after 300 time steps.

For Q equal to 0.1 MPa there are regions under the loading where stresses are high enough to cause the neck fracturing after a very small period of time. On the other hand, there are areas away from the loading region at which the stresses are low enough that, according to the theory developed, superplastic deformation should be taking place in necks. At the boundary of these two areas, there are regions where ice necks, at a particular solid angle, have a principal stress of, for example, 0.7 MPa at one grid point, and at the next grid point the principal neck stress, for the same solid angle, is 0.705 MPa. In the theory we have assumed that for stresses less than or equal to 0.7 MPa superplastic deformation takes place, whereas for stresses greater than this value deformation is due to sliding of particles. Therefore, at the first grid point the neck is undergoing a superplastic deformation whereas at the second grid point there is relative sliding between the particles. This results in discontinuous strain rates (because the strain rates for superplastic deformation and sliding are different) and also leads to a situation where regions of low stress have higher strain rates as compared to regions with higher

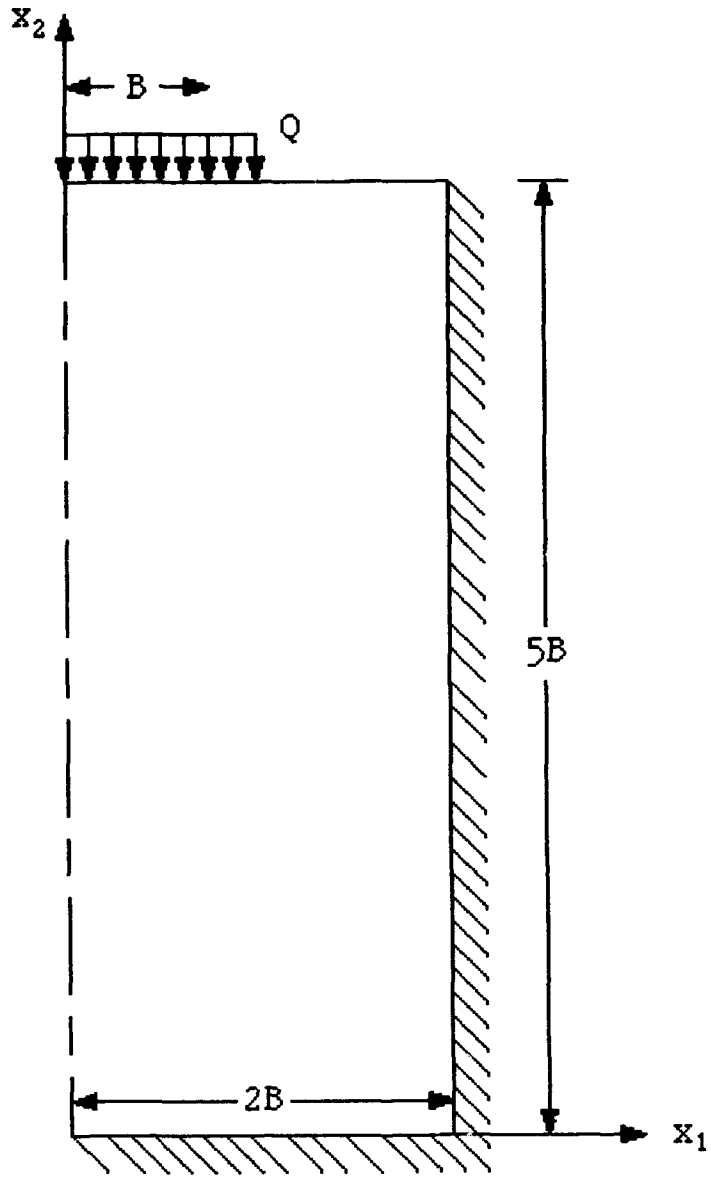

Figure 2. Foundation with a stress of Q MPa. B = .45 m. Symmetry with respect to x_1 allows only half of the foundation and snow cover region to be analyzed.

stress (superplastic strain rate at 0.7 MPa is higher than sliding rate at the same stress). To avoid this discontinuity in strain rates it was assumed that necks remain intact for the first fifty time steps, deforming according to the creep law for high stresses. After fifty time steps all necks were assumed to have broken, and relative sliding of particles was taken as the sole deforming mechanism for the whole problem. The solution becomes unstable rather quickly if this assumption is not made.

At this load it was found that with a step of 120 seconds the stresses continue to decrease, as was expected, for 150 time steps. However, after that the high stresses change negligibly, but the low stresses, instead of decreasing, begin increasing and the problem becomes unstable, as indicated by large changes in lateral stresses and a decrease in vertical displacement instead of an increase. It is possible that by use of a still smaller time step this problem can be remedied, but this would also result in increased computational time. This instability seems to be associated with the strain hardening in the constitutive equation becoming significant. Most multiaxial creep problems are solved using implicit methods, and even then a very short time step has to be used. So the instability with the use of the explicit method for strain hardening problem is not surprising. It was decided to take the stresses at the end of 150 time

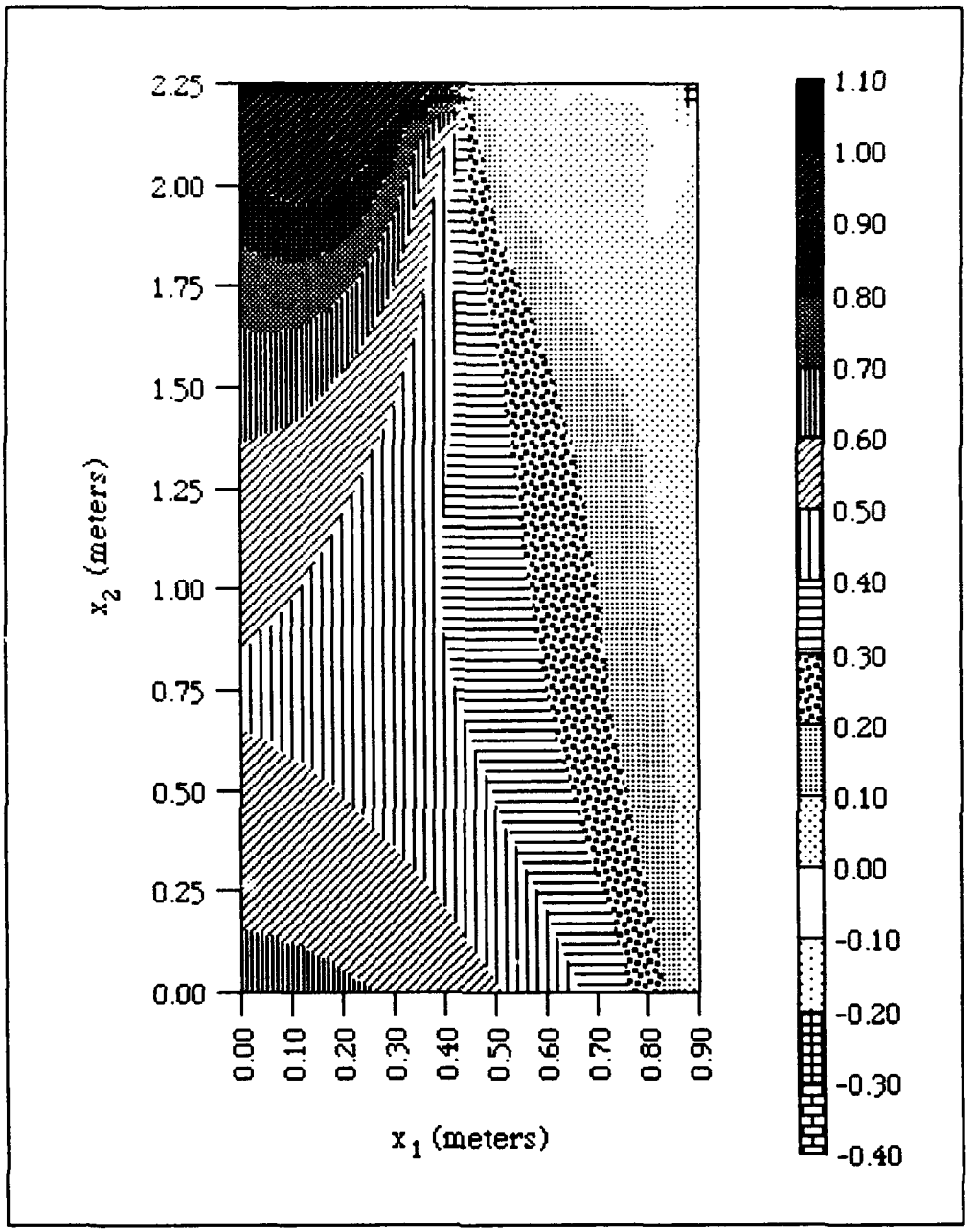

Figure 3. Normalized stress contours by seven hours for Q = 0.008 MPa. The stresses were assumed to have reached a steady value at this time.

steps as the stresses to be used for all future time steps. By imposing this restriction we are violating the equilibrium equation. However, the change in maximum stresses by the 150th time step are small and this assumption was considered to be reasonable.

For low compressive stress of 8×10^{-3} MPa the normalized vertical stress component (stress/(8×10^{-3})) contours are shown in Figure 3 and the displacement contours at the end of sixty hours are shown in Figure 4.

A steady state of stress was assumed to have been reached by seven hours. From these it becomes apparent the stresses are much higher closer to the axis of symmetry and fall to a very low value as one moves away from this axis. Also, the stresses beneath the loaded area at 1.8 m from the surface are about 65% of the stresses at 0.45 m from surface. Figure 5 illustrates the stress distribution along two vertical sections. For a section at the axis of symmetry the stresses first de-

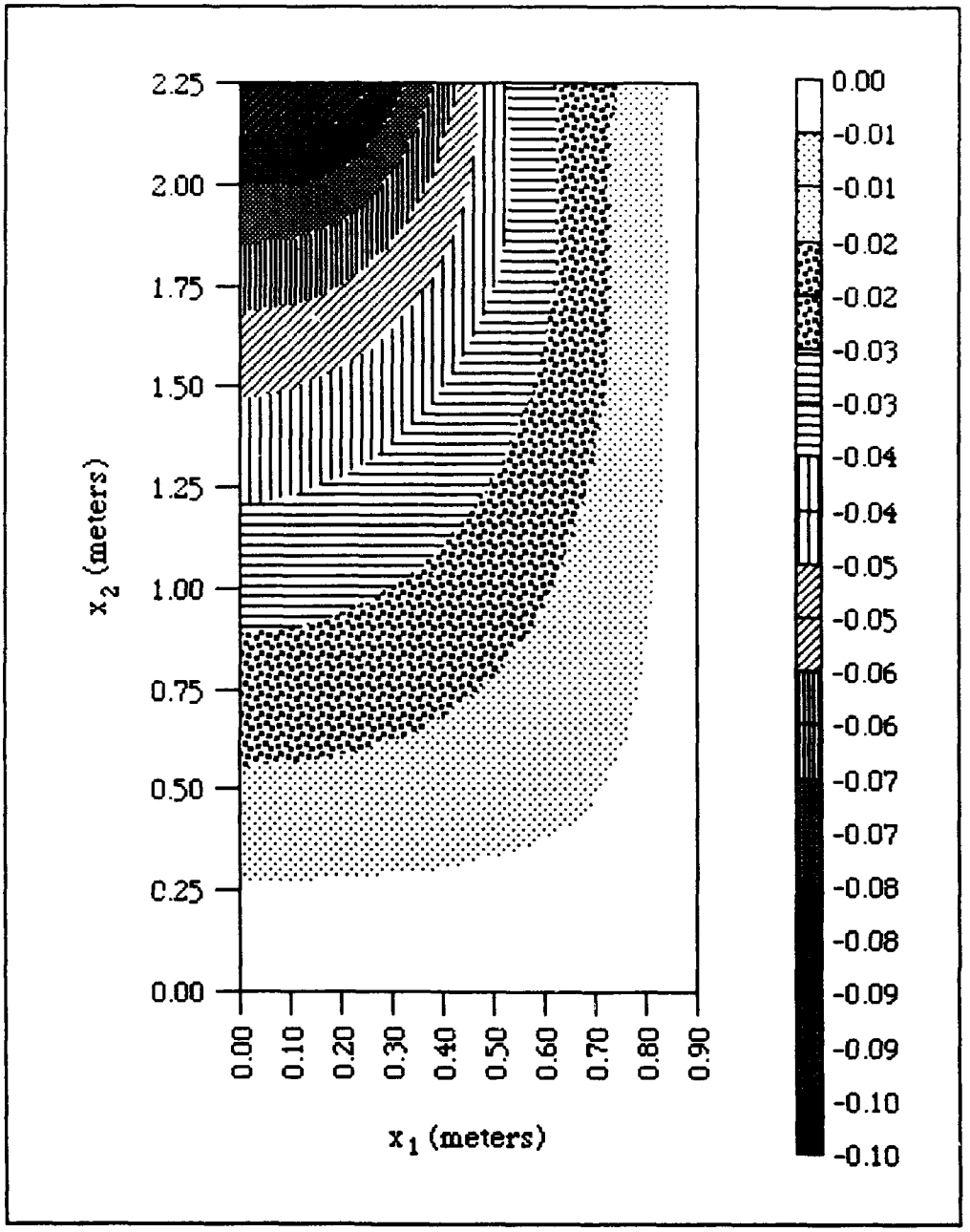

Figure 4. Displacement contours by sixty hours. Q = 0.008 MPa.

crease with height and then rise. The stresses begin increasing toward the bottom because the body force effect of gravity is almost half the value of the applied stress effect. Had the body forces not been taken into account, the stress at the bottom would have been much lower than stress at the top. At the section 0.5 m from the axis of symmetry Q is equal to zero. Here the stress at the bottom is only about 25% lower than that at a section along axis of symmetry, probably because the stresses here again are largely due to weight of snow. From Figure 4 it is seen that vertical displacements are highest right under the applied load. At the end of 60 hours the maximum vertical displacement is 0.1 cm. The maximum horizontal displacement is about one-fourth this value.

For Q equal to 0.1 MPa the gravity forces are insignificant compared to the external load. The normalized stress contours and displacement contours are shown in Figures 6 and 7 respectively. The stresses in the section right under the footing show a big drop

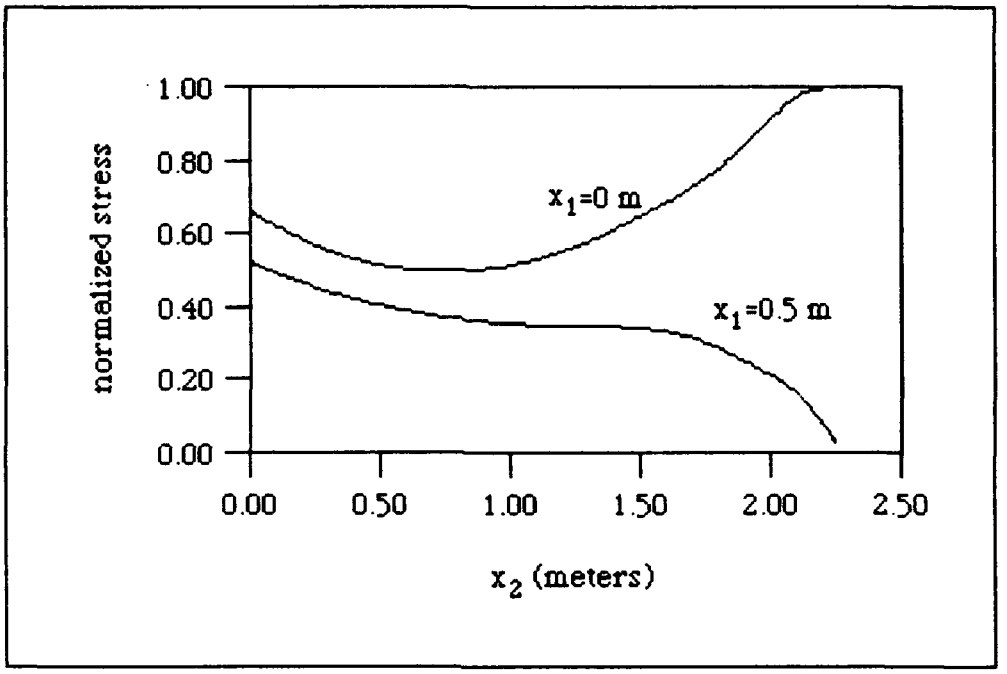

Figure 5. Stress distribution along vertical section at the center line and 0.5 m from the center line. Q = 0.008 MPa.

within the top 0.50 m. The stresses at 1.6 m are 20% of the value at the top. This is consistent with experimental data (Reed, 1966) according to which the pressure bulb extends to about two times the width of the footing. Since gravitational effects are insignificant compared to the applied load, the stresses at the bottom are less than 10% of the values at the top. This is in sharp contrast to values at the bottom for Q equal to 8×10^{-3} MPa, which were almost 75% of the values at the top. Figure 8 shows the stress distribution at a section 0.45 m from axis of symmetry. This shows a fairly constant value for stresses from top to bottom. The displacement contours in Figure 8 show that major displacements are largely restricted to about the top 0.9 m of the foundation. The gradients in vertical displacement were more gradual for 8×10^{-3} MPa than for 0.1 MPa. The maximum displacement at the end of 30 hours was 0.57 cm.

CONCLUSION

In this paper, a constitutive theory developed earlier was applied to solve for the settlement of a snow foundation subjected to a uniformly distributed load on a part of its top surface. The constitutive theory is based on the microstructure and the various constants used do not have to be changed when the grain size or bond size changes. The theory is also able to model strain hardening in snow due to increases in the 3-D coordination number with increasing strains. However, no attempt has been made to model strain hardening due to metamorphic processes which are active during deformation. Since we are concerned with short duration deformation, the latter may not be important.

Presently, there is not much data available for comparison with the example given here. The data presented by Reed (1966) and used by Dandekar and Brown (1986) for comparison of their results is for long term settlement of foundation. The general behavior of Dandekar's result was in agreement with the data presented by Reed. The stress distribution determined with the theory presented here matches closely to that presented by Dandekar and Brown.

The present theory does suffer from drawbacks of excessive computational time and instability of the solution once strain hardening becomes significant. This problem may be remedied, as has been suggested by Mahajan and Brown (1990), by the use of invariant theory. The data required for determining the various constants in the invariant theory can be obtained from the present theory.

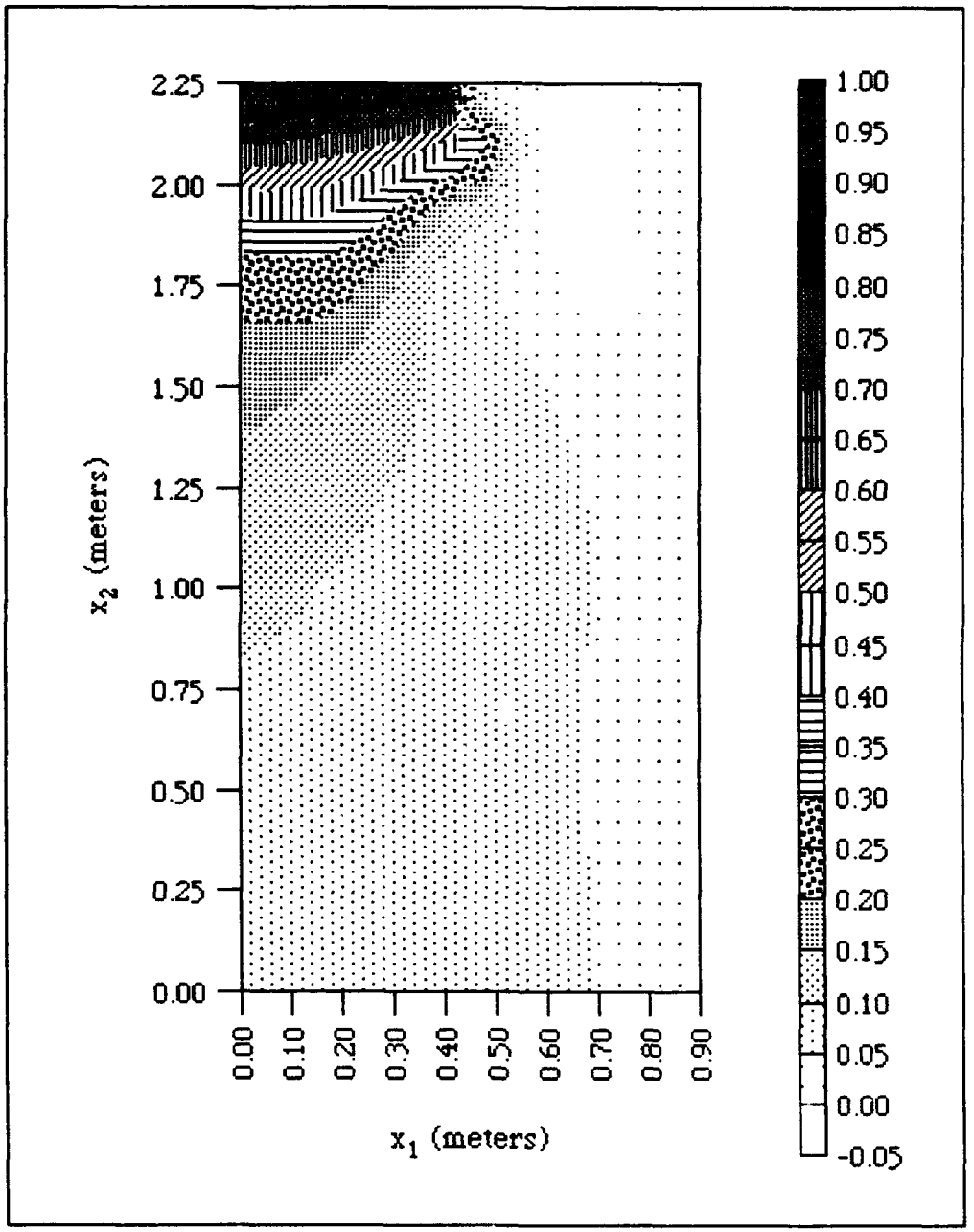

Figure 6. Normalized stress contours by five hours for Q = 0.1 MPa. The stresses were assumed to have reached a steady value at this time.

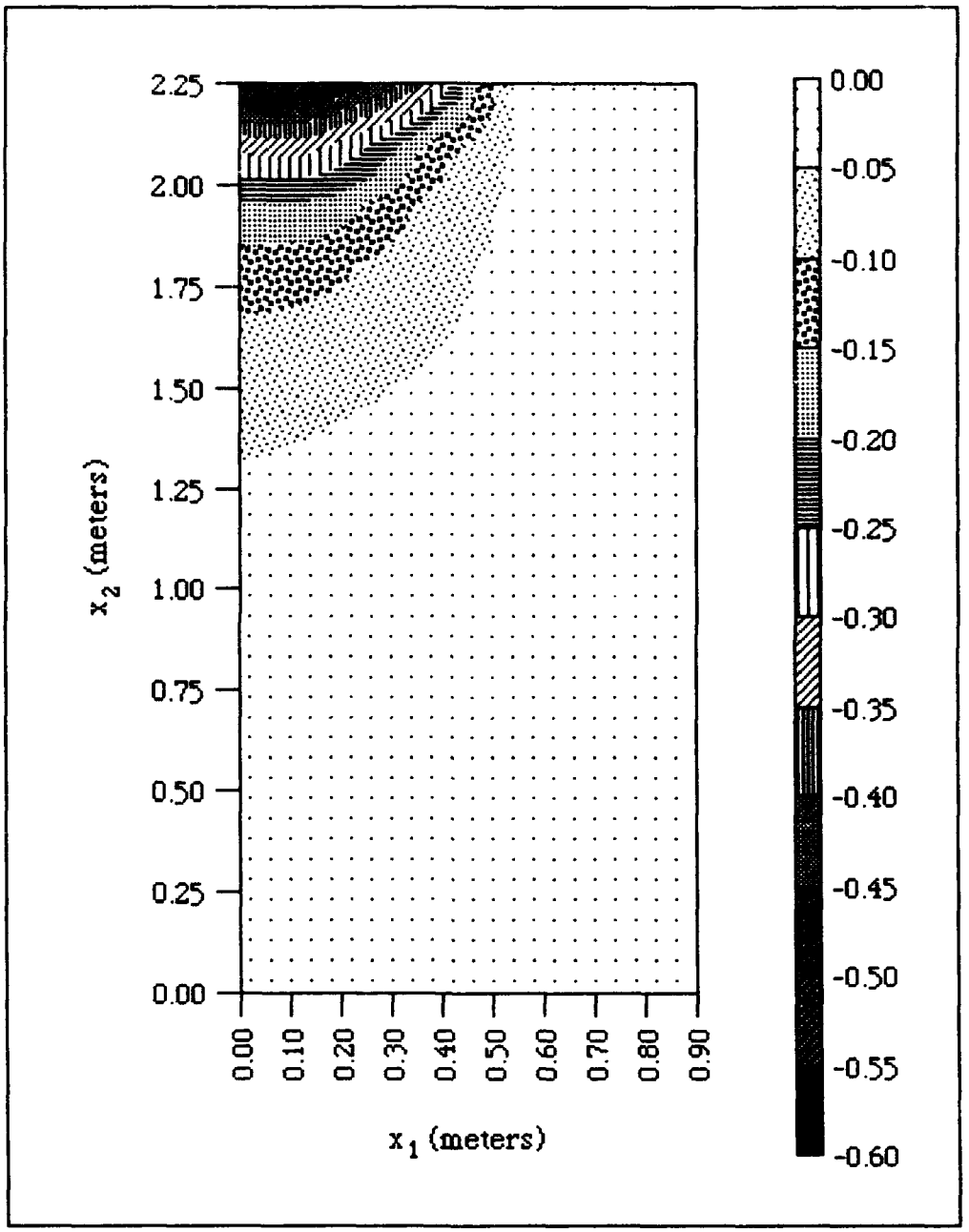

Figure 7. Displacement contours by thirty hours. Q = 0.1 MPa.

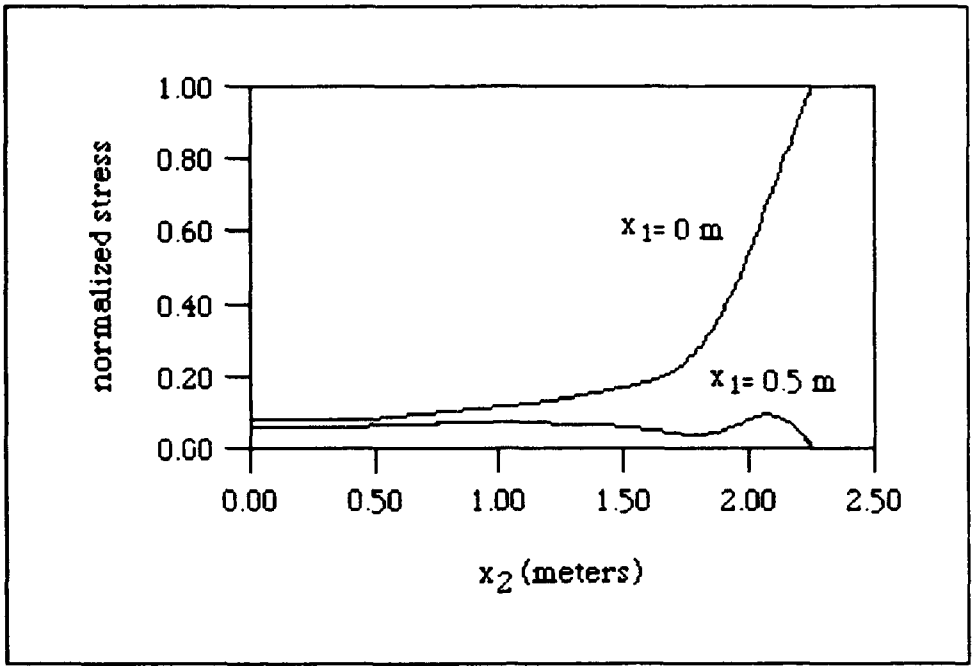

Figure 8. Stress distribution along vertical section at the centerline and 0.5 m from the centerline. Q = 0.1 MPa.

ACKNOWLEDGMENT

The work reported here was conducted under sponsorship of the Geosciences Program of the United States Army Research Office. The authors wish to express their appreciation of ARO's support.

LITERATURE CITED

Boyle, J.T. and Spence, J. (1983) *Stress Analysis for Creep*, Butterworths.

Brown, R.L. (1979a) A Volumetric Constitutive Law for Snow Subjected to Large Strains, CRREL Report 79-20.

Dandekar, B.W. and Brown, R.L. (1986) A Numerical Evaluation of Flexible Footing into Uniform Snow Cover, *Cold Regions Science and Technology*, Vol. 12, 131–138.

Kerr, A.D. (1962) Settlement and Tilting of Footing on a Viscous Foundation, CRREL Research Report 81.

Mahajan, P. and Brown, R.L. (1990) A Microstructure Based Constitutive Law for Snow, submitted for publication.

Kanatani, K. (1981) A Theory of Contact Force Distribution in Granular Material, *Powder Technology*, Vol. 28.

Mellor, M.A. (1974) A Review of Basic Snow Mechanics, in: *Proceedings of the Grindewald Symposium*, IAHS Publ. 114, Grindewald, Switzerland.

Reed, S.C. (1966) Spread Footing Foundations on Snow, CRREL Report TR-175.

Szyszkowski, W. and Glockner, P.G. (1987) Modelling the Mechanical Properties of Ice, in: *Proceedings of Sixth International Offshore Mechanics and Arctic Engineering Symposium*, ASME.

AD-A271 546 FIRST INTERNATIONAL CONFERENCE ON WINTER VEHICLE MOBILITY SANTA BARBARA CALIFORNIA JUNE 1991(U) COLD REGIONS RESEARCH AND ENGINEERING LAB HANOVER NH

UNCLASSIFIED G L BLAISDELL JUL 93 93-17 XA-CRREL NL

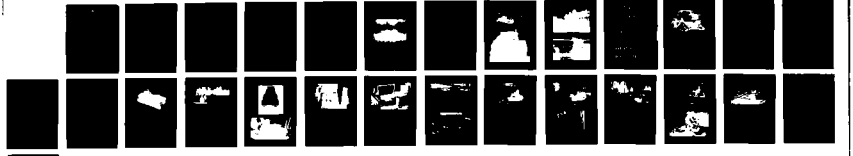

END
FILMED
DTIC

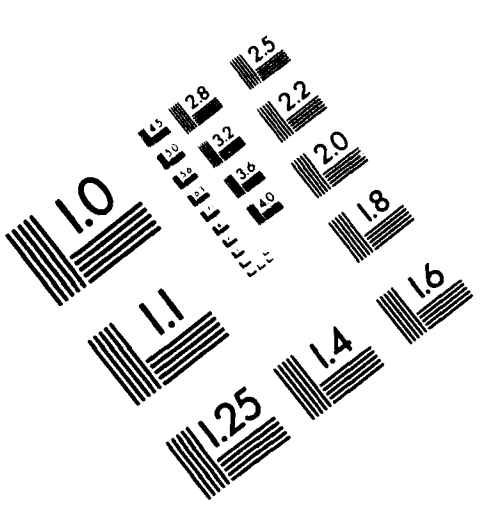

Association for Information and Image Management
1100 Wayne Avenue, Suite 1100
Silver Spring, Maryland 20910
301/587-8202

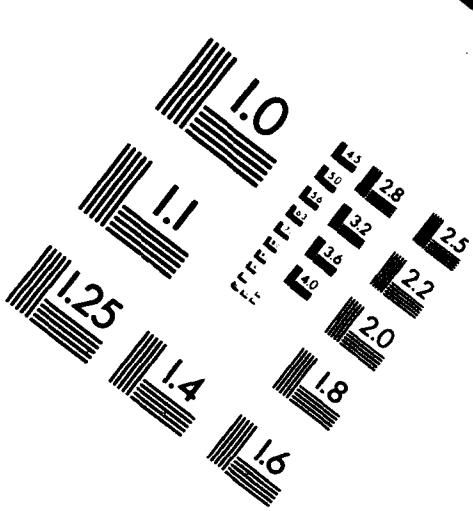

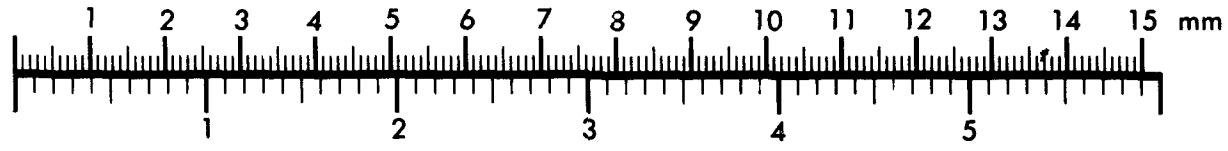

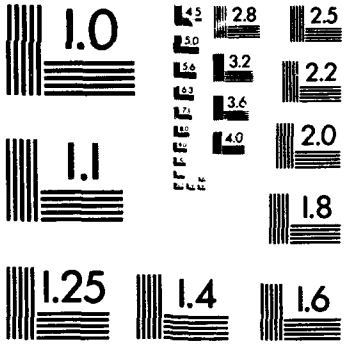

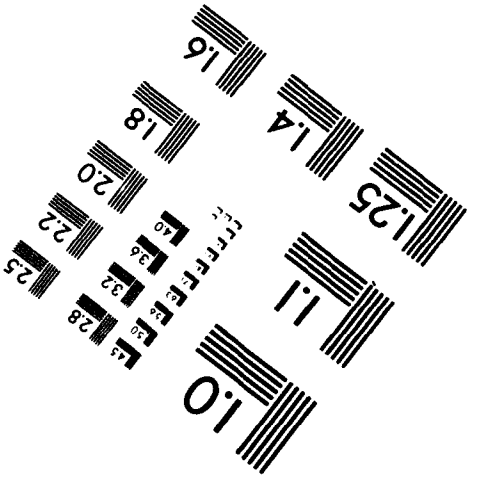

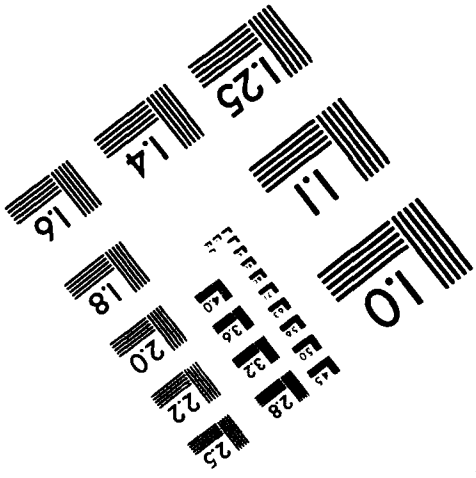

MANUFACTURED TO AIIM STANDARDS
BY APPLIED IMAGE, INC.

Snow Characterization for Traction Testing
A Survey of Techniques Used

SALLY SHOOP
U.S. Army Cold Regions Research and Engineering Laboratory
Hanover, New Hampshire 03755-1290

AND

RUSS ALGER
Institute of Snow Research
Houghton, Michigan 49931

ABSTRACT

A variety of techniques exist for the characterization of snow for vehicle mobility or tire traction testing. Snow surfaces that are used for testing are either natural or groomed and vary widely in strength and texture. To complicate the situation even further, tire testers perform their traction tests in a number of different manners.

Snow characterization methods are discussed and the various techniques presented. This paper is the start of what hopefully will become a broad survey of most of the testing and characterization methods used by the several tire testing companies that perform these tests on a routine basis.

This work is part of an ongoing effort between USACRREL and the Keweenaw Research Center.

1. INTRODUCTION

Commercial tire designers and the research community have been involved in the testing of rubber tires in winter environments for several decades. These tests have evolved into several measurement techniques that are used by each group by preference. Tests range from comparisons made by highly trained drivers in standard commercial vehicles to high tech instrumented vehicles designed to measure the traction characteristics of a given tire. These testing techniques are designed to optimize the traction afforded by a new design over a previously accepted one.

2. DESIRED OUTCOME

In order to make use of the data collected by the various testing and research groups it would be advantageous for a system of measurement for snow characterization to be standardized and used throughout the tire testing community. The system must be easily used but still offer enough information about the engineering properties of the snow test surface to make the final product useful to the entire group.

Since each group has a specific method for performing tests as well as preparing test surfaces, documentation is of primary importance. This is sometimes difficult, however, when working in a cold environment but must be carried out with diligence to make the results useful to all of the groups involved.

Finally, a willingness for all of the groups concerned to disseminate their results into the proper channels to allow it to be useful to both researchers and designers is a necessity. This is sometimes difficult, especially in the commercial world due to proprietary rights.

3. CHARACTERIZATION METHODS

The engineering properties of hard packed snow surfaces as well as virgin snow layers are documented

in many ways. Methods as simple as measuring temperature and density are probably used more than more sophisticated techniques such as bevameters and instrumented vehicles, although these have become more common in the past decade.

The various measurements that are commonly used and will be discussed briefly here are temperature, density, strength, hardness, grain size, structure, metamorphic state and free water content.

3.1 Temperature and density

These two parameters are probably the simplest of all to measure in the field and do not need to be elaborated upon to any degree. They do have their place as a representation of the characteristics of a packed snow surface, but do not by any means totally describe the test layer.

3.1.1 Temperature

Temperature can be measured by use of a simple probe or by use of a number of thermocouple or thermistor type meters and probes. The temperatures measured are normally done in a profile through the thickness of the layer. Temperature profiles can give an idea of the probable "wetness" of the snow surface and can also give a very crude relationship to strength when coupled with a density measurement. A minimum of air temperature and snow temperature should be taken for shallow snow, whereas a profile of snow temperature measurements may be required for deep snow.

3.1.2 Density

Density of comparatively soft snow layers can be measured using a number of commercial snow density kits which are marketed by several different companies. These kits range from large elaborate systems to small scoops and scales that can be carried in a fanny pack. Each is probably special in some way but all of them are used in essentially the same manner. A sample of a known volume is taken from the snow and the weight measured on a scale.

In very hard surfaces a cut section is used to determine the density. For this method a sample of snow is cut from the surface using a small saw or knife. This sample is then trimmed using one of these tools or possibly a plane to some measured dimension and weighed. This method is somewhat difficult, however, because it is often not easy to cut and measure a *perfect* block of snow.

Density can give a crude indication of strength and or hardness of the hard packed layer and when used with temperature is better than taking no measurements at all.

3.2 Free water content

Until recently the measurement of free water content was a cumbersome and time consuming process. Liquid water content was determined visually or measured using one of two different types of calorimeters.

3.2.1 Visual observation

The relative amount of liquid water present in a snow pack can be observed grossly by simply picking up a handful of snow and attempting to pack it into a snow ball. If the snow is dry it will not form into a ball. Snow of medium wetness will hold together loosely and very wet snow will form readily into an ice hard ball.

A second method used to visually determine the relative wetness is to sprinkle the snow with Fushin (Rosanalin Hydrochloride) powder which is a dark color when dry but turns a bright pink when it comes in contact with liquid water.

3.2.2 Freezing calorimetry

Freezing calorimetry is used in some instances, but is probably the most cumbersome of all methods. A calorimeter bottle with a temperature probe installed is filled with a fluid such as silicon oil at a temperature in the range of –75°C. Dry ice must be used to keep the oil at this temperature. A sample of snow is added to the cold fluid and the temperature of the mixture is recorded over a period of time long enough to ensure that all of the free water present has frozen.

From the temperature measurements, the amount of energy removed by the mixture and thus the amount of free water frozen can be calculated.

3.2.3 Melting calorimetry

In recent years, melting calorimetry has become more popular due to the fact that the equipment needed is much more compact and is easier to use.

Melting calorimetry works much along the same lines as freezing methods. The difference is that the energy taken out by the mixture is used to melt the ice present instead of freezing the water. Alcohol is the fluid that is normally used for this process. Tests are run at the freezing point of water and therefore no special provisions need to be made to keep the alcohol extremely cold. A simple water bath suffices for this purpose

3.2.4 Moisture meter

The newest method of determining the liquid water present in snow is a capacitance meter that is easily operated and quite accurate (Boyne and Fisk, 1990). This gauge consists of a plate that is placed on the snow and a small meter used to measure the capacitance. By

taking a reading in the air and one on the snow surface, the free water content can be easily determined. This method does not require any special fluids or bulky equipment and could easily be carried in a back pack.

3.3 Crystal structure and metamorphic state

3.3.1 Crystal size and shape

The size and shape of the ice grains that make up a snow pack have an influence on how the pack acts as a whole. Large rounded crystals tend to roll past each other while small angular crystals tend to pack tightly together when loaded. These properties have a marked influence on results during mobility exercises.

Crystal size and shape can be easily documented by use of a standard magnifying glass and ruler. Small lenses with measurement grids are also available commercially for this purpose.

3.3.2 Metamorphic state

The stage of metamorphic change that a snow pack has achieved can have an influence on how it will react when trafficked. Freeze thaw cycling for instance can change the strength characteristics of the snow considerably throughout a very short period of time. Metamorphism affects the shape, size and bonding of the crystals and therefore affects the strength characteristics as well. Ice lenses within a virgin pack can also markedly increase the strength of the system.

Determination of the metamorphic state is a science in itself and cannot be explained in detail here. It is sufficient to say, however, that there are several different guides and manuals available to make it easy to make the necessary characterizations (see Colbeck et al 1990).

3.4 Strength indices

The strength characteristics of a snow pack are probably the most important parameters that can be measured during a mobility test. As they are very important to the outcome of a test, this measurement is also the most difficult to obtain with any degree of accuracy and is probably the area of most disagreement between members of the snow testing community. Some of the problems associated with this measurement include the question of what rate to perform the test at, what size probes or plates are optimum and how to perform a measurement that takes into account the slipperiness of the surface.

Since there are a number of manuals and references to each of these methods of measurement, each will only be discussed briefly here. The list presented here is not intended to be a complete overview of *all* of the techniques available but more a listing of the more common methods.

3.4.1 Cone penetrometer

The cone penetrometer is a probe that was designed originally for use in soils as a tool to measure mobility properties. It was designed by the U.S. Army as a tool that could be used easily in the field and would give an indication of the trafficability of a soil. The instrument is generally composed of a 30° cone with a cross-sectional area of 1/2 in^2. This cone is pushed into the medium at a constant rate and loads are read from a proving ring at a constant interval that is usually the depth of penetration. There have been some variations of this device, namely changes in size of the cone to account for different material stiffnesses.

Several indices are obtained from the use of the cone that can be related to the characteristics of the medium. The cone has been used in snow for several years and is used in the same manner as in soil. Although it was originally designed for use in soils it has had success in some types of snow packs.

3.4.2 Rammsonde

The rammsonde is a cone device similar to the cone penetrometer although the standard ramm cone is much larger than the cone on the cone penetrometer. The major difference between the two devices is that while the cone is pushed into the material the ramm is driven using a drop hammer. Generally a complete ramm set-up will have two different sized hammers along with a hammer slide and several lengths of rod that connect to the ramm cone for use in deep snow packs. To perform a measurement the hammer size and drop height are determined according to material hardness. The cone is then placed on the surface and the hammer is dropped a measured distance. The penetration is then measured and the process repeated until the desired profile depth is obtained.

For the most part, this instrument has been used in deep packs such as in avalanche zones and in the Arctic and Antarctic to obtain hardness profiles through deep layers of snow.

3.4.3 Canadian hardness gauge

The Canadian Hardness Gauge is a small plate sinkage type device that is designed to be carried in a pack in the field. Its major use has been in the area of avalanche prediction and is best used in hard virgin snow. Plates of various sizes can be attached to the instrument and pushed into the snow. The resistance to penetration is measured on a gauge that is built into the instrument handle.

3.4.4 Plate sinkage

The plate sinkage test is used to measure the bearing capacity and compaction due to loading of a snow pack.

Plates of various diameters are pushed, normally hydraulically, into the snow and the load and sinkage measured constantly throughout the test.

The plate sinkage test is most commonly used in conjunction with an annular shear test. These two tests comprise the bevameter and result in the "Bekker" values used in mobility analysis.

3.4.5 Shear tests

Shear strength of snow is measured in a number of different ways. The shear annulus generally associated with a bevameter is used to measure parameters that relate to the shear strength. This device is normally used with either a rubber faced annulus or a grousered annulus. The rubber annulus gives an indication of shear force afforded by the surface snow crystals to a rubber surface. This value gives an idea of the interface shear between a rubber element such as a tire and the snow surface. The grousered annulus is used to measure the inter-granular shear that is present when shearing takes place within the snow pack (Alger, 1989).

Other types of devices have been used to measure shear strength with limited success. These include the vane and the vane cone.

3.4.6 Instrumented vehicles

There are several different types of instrumented vehicles that are used by researchers and tire testers throughout the tire testing community. Some of these instrumented vehicles are trailers that are towed by a vehicle while others are trucks or cars that have been modified to measure the desired parameters. Most of these systems have been equipped with onboard computers, various load and torque measuring devices and tire and ground speed measurement devices.

The Society of Automotive Engineers have developed a standard for the evaluation of dynamic tire traction in snow that is followed, at least to some extent by most commercial tire testers. This standard requires the use of a standard reference tire. In the case of snow testing, this tire is referred to as a snow monitoring tire or SMT. This tire is used as the reference for performance of all other tires tested. The performance of this SMT in a given snow condition is used as the primary means of characterizing the test surface.

Several different measurement devices and systems are used in conjunction with the SMT. As mentioned earlier, these can consist of tow behind trailers or dynamometers and instrumented vehicles.

The follow on work to this paper will be a study of the common devices used in the industry and by researchers. This work has been done in the past, but with recent advancements in measurements and techniques, an update should be of interest to the testing community.

REFERENCES

1. **R.G. Alger (1989)** Shear and compressive strength measurements of snow using the bevameter. In *First International Conference on Snow Engineering*, Cold Regions Research and Engineering Laboratory, Special Report 89-6.

2. **M.G. Bekker** (1969) *Introduction to Terrain Vehicle Systems.* The University of Michigan Press, Ann Arbor, Michigan.

3. **M.G. Bekker** (1956) *Theory of Land Locomotion.* The University of Michigan Press, Ann Arbor, Michigan.

4. **H.S. Boyne and D.J. Fisk (1990) A** *Laboratory Comparison of Field Techniques for Measurement of the Liquid Water Fraction of Snow.* Special Report 90-3, Cold Regions Research and Engineering Laboratory.

5. **S.C. Colbeck, et al.** (1990) *The International Classification for Seasonal Snow on the Ground.* Technical Report MP 2794, International Commission on Snow and Ice of the International Association of Scientific Hydrology and the International Glaciological Society.

6. **J.Y. Wong** (1978) *Theory of Ground Vehicles.* John Wiley & Sons, New York.

7. **R.N. Yong, E.A. Fattah and N. Skiadas (1984) Vehicle** *Traction Mechanics.* Elsevier, New York.

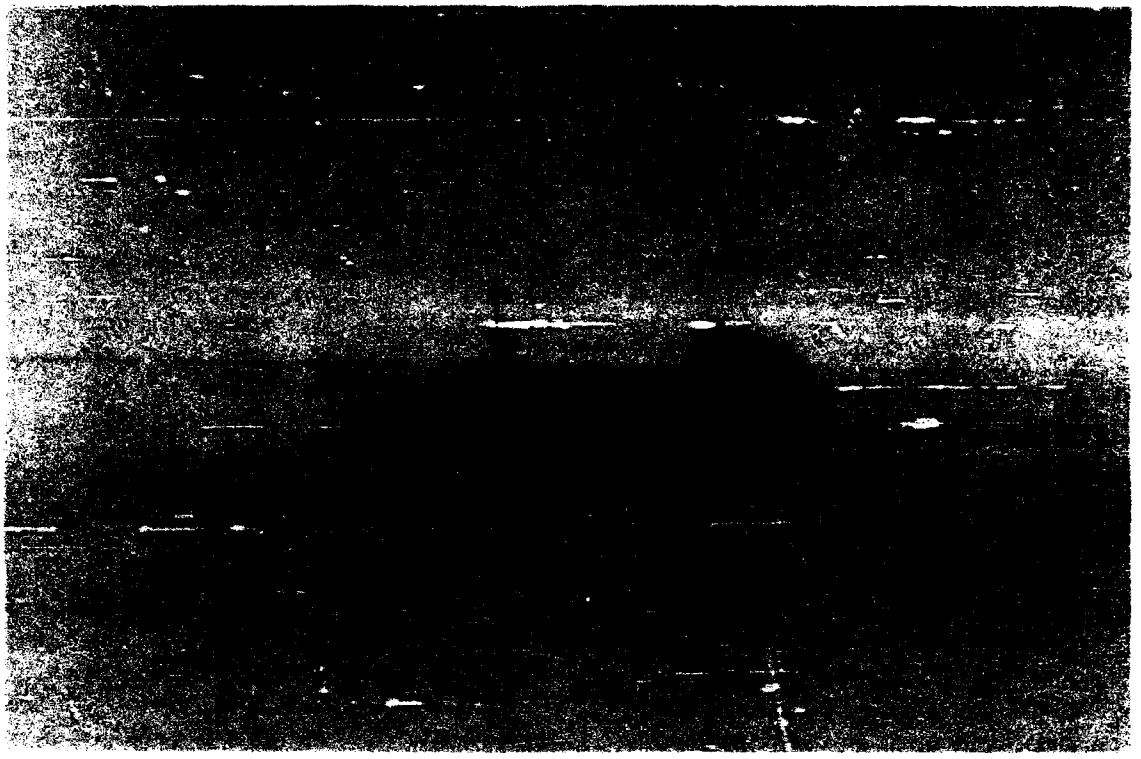

6. NOVEL DESIGNS

Caterpillar Mobil-Trac System's Application To Cold Regions Mobility Problems

DALE STEINKE
Defense Products
Caterpillar, Inc.
Peoria, Illinois 61629

This paper is designed to give you a quick rundown on Caterpillar's Mobil-Trac system, and the mobility advantages it offers cold regions users. Particular emphasis will be given to the CAT challenger tractor...A vehicle purposefully designed to take maximum advantage of the Mobil-Trac system.

First, it's important to understand what Mobil-Trac is. Although it's been out in the marketplace for several years now, we still find people who think it's just another rubber track. That...it definitely is not!

Caterpillar has long been a leader in the development of elastomer or rubber products. This surprises a lot of people, but the fact is most of the equipment we sell runs on rubber, not track.

For example, Caterpillar has become the world's largest manufacturer of high pressure hydraulic hose. We manufacture over 2500 miles of the stuff every year. We got into the business because of all the downtime our customers were experiencing due to hose failures. You might wonder what hydraulic hose has to do with mobility, but bear with me a minute.

CAT XT hose is uniquely superior due to the way layer upon layer of metal wire is bonded into the rubber. The manufacturing technology has remained a closely guarded secret. The wire provides tremendous strength while permitting a high tolerance for flexing under load. Perhaps predictably, someone eventually wondered: "gee, what if we made this stuff into a track belt?"

The Mobil-Trac belt that developed is shown in Figure 1. In a cut away you could clearly see how the composition is similar to the XT hydraulic hose. It's very tough stuff. The advantage of this track is plain to see: it opens the way to enjoy the advantages of both track and wheels, all in one neat system. As you probably know, track gives you low ground pressure, stability, high drawbar pull, low forward motion resistance, and obstacle bridging. Wheels give you high speed and mobility over hard, abrasive surfaces.

These qualities make the Mobil-Trac system an ideal combination for cold regions with their challenging set of unpredictable underfoot conditions: tundra, muskeg, ice, snow, rocks, logs, adverse grades, and bare ground.

So how come, you may be wondering, I don't see Mobil-Trac zooming all over the Arctic? One reason is that Caterpillar looked for the biggest sales opportunity to get started in. It was agriculture. Low ground pressure meant earlier tillage and less root compaction for higher crop yields per acre. And the combination of high speed and drawbar pull reduced fuel consumption and other operating expenses. The farmers love it!

The other reason—I think—is that operations in the remote cold regions where Mobil-Trac will really shine tend to be governmental in one form or another. Procurement lead times are often very long, and frustrating for vendors.

Over the past few years, Mobil-Trac has accumulated millions of hours in the field, mostly on the Challenger where some farmers are still using their original belts after 20,000 miles.

The Challenger 65B (Figure 2) is a 285 HP tractor weighing about 32,000 pounds bare. Fully equipped for arctic service (Figure 3) with dozer blade, winch, power train guards, and heavy duty, studded belts, etc., it'll weigh close to 36,000 lbs (close to the weight of a CAT D6 dozer). It has a 10-speed, powershift transmission and can travel over 18 mph. It's amazingly simple to operate. If you can drive a truck with an automatic transmission, you can hop on a Challenger and drive away. It even has a conventional steering wheel.

An important feature of the Challenger is the fact that it steers differentially. This means that live power is maintained to both tracks at all times during turning

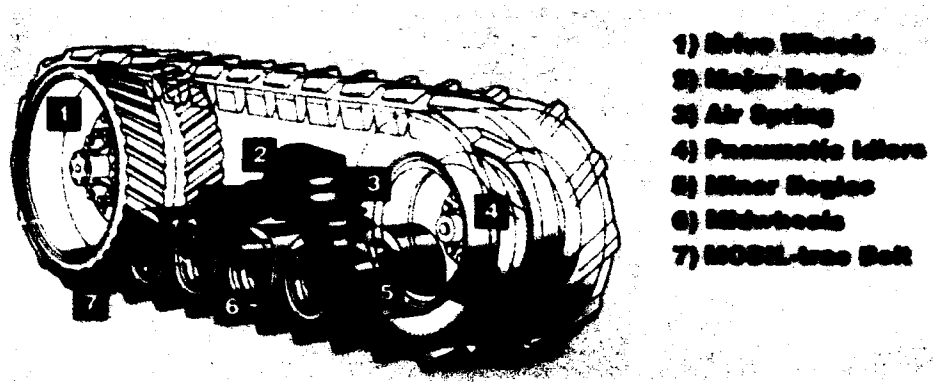

Figure 1. Detail of Mobil-Trac system.

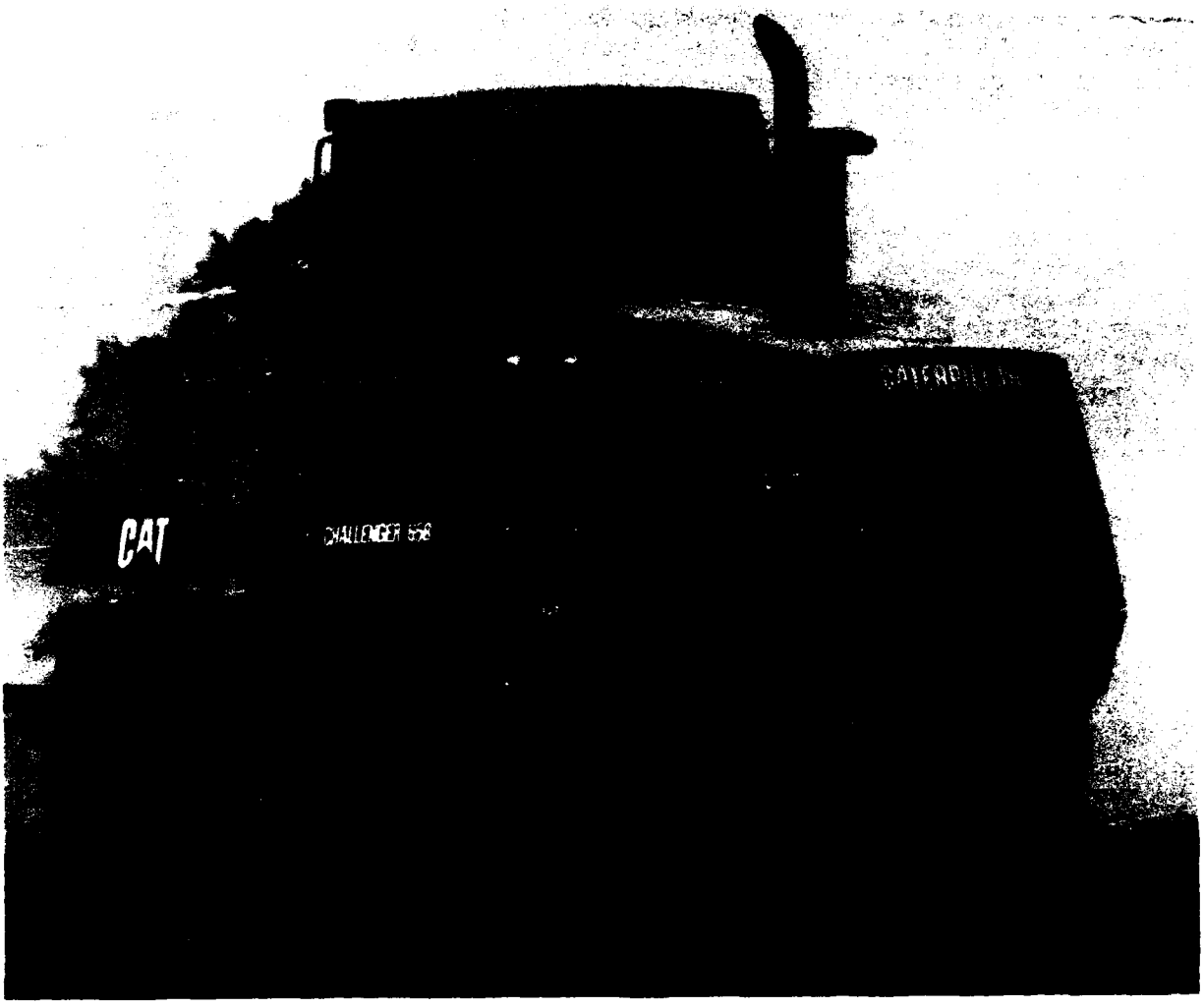

Figure 2. Standard Challenger tractor.

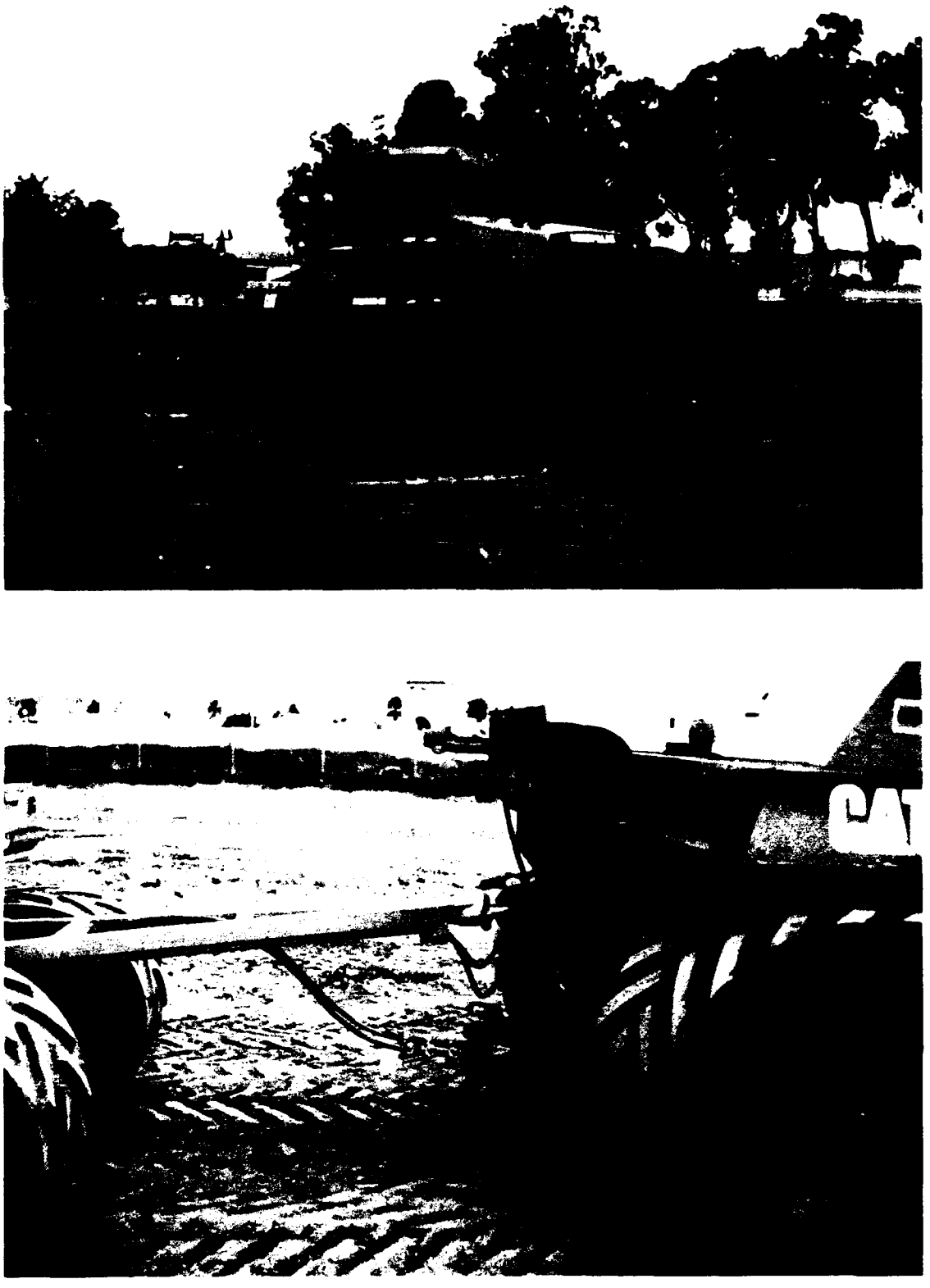

Figure 3. Over snow model Challenger.

THIS
PAGE
IS
MISSING
IN
ORIGINAL
DOCUMENT

195/198

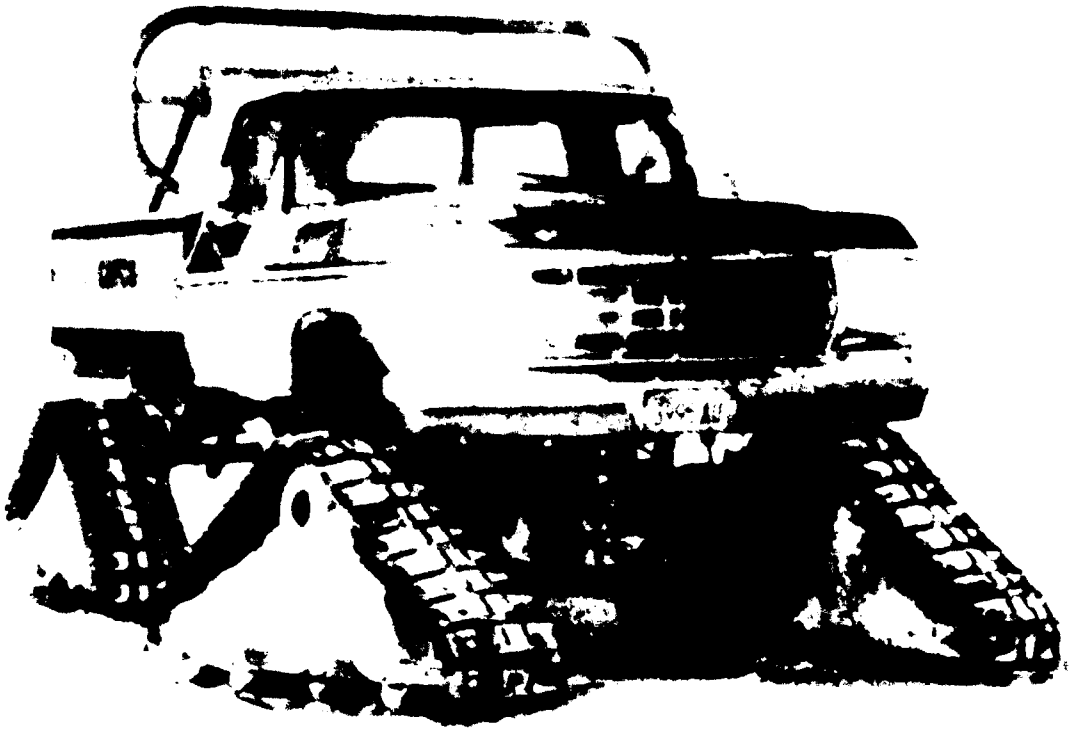

Figure 1. Ultra-Track installed on a conventional pickup truck operation on the north slope of Alaska.

and highways during weekdays and go off-road on the weekends.

"People get the cost benefit of buying a standard, mass-produced vehicle," Barbieri said. "Somebody building a special purpose tracked vehicle does not have that economy of scale."

Imagineering has painstakingly developed and tested the Ultra Track during the past five years. Now that the track's performance and durability are assured, the Seattle company is ready to begin manufacturing the units on a production basis. "People can buy the Ultra Track in kit form or as a complete unit," Barbieri said.

The full assembly from the factory includes a spring package for raising the height of the vehicle so that there is proper clearance between the tracks and vehicle fenders. Also included is a step for each side of the raised cab. A list of off-the-shelf hardware and a detailed set of assembly prints can be purchased from Imagineering.

Once the kit is assembled into four track units which adapts to most 3/4-ton and one ton four wheel drive vehicles, it has an unloaded ground pressure as little as one and one half pounds per square inch, depending on vehicle size and make. As a result, a track-equipped vehicle, even on snow, sand, or mud has the same payload capability as a vehicle running on wheels.

Because each revolution of a track's sprocket moves a vehicle ahead 60 inches, the vehicle with Ultra Track units has a two-to-one mechanical advantage over wheels. This means there is twice as much power from the engine and less wear on the drive train.

The Ultra Track has many applications. A four-wheel-drive vehicle equipped with these novel units can be used for:

- — Weekend Recreation. Off-road enthusiasts can head for the hills or make a beeline for the beach and simply switch from tires to tracks when they leave the roadway.
- — Ranching and Farming. An Ultra Track pickup can carry livestock feed, fence-mending supplies and the like across all terrain and in all weather.
- — The Oil and Gas industry. Surveying, pipeline maintenance and ferrying men and supplies to oil pumping stations and drilling platforms are easily performed with Ultra Track units.
- — Construction Work. Construction in rugged, remote areas is simplified when workers and sup-

plies can be delivered in cost-saving, conventional pickups rather than special purpose, limited-use vehicles.

— Ski Resorts and Parks. Ultra Tracks can be used for transporting personnel, grooming lower slopes, planting slalom flags and performing search and rescue work.

— Road Maintenance. A four-wheel-drive vehicle equipped with Ultra Track units can keep highways and back roads open by plowing through snow.

— Military Missions. An Ultra Track vehicle can carry men, supplies and equipment in support of various field exercises and deployment.

Barbieri said Imagineering has received several military and commercial application inquiries from around the world where remote areas and rough terrain are in abundance. Getting supplies to gold mines is one prospective use in Alaska as well as Canada.

APPLICATION TO THE MILITARY HMMWV

Versatility

The AM General HMMV has been designed to accommodate 26 configurations and can be adapted to mount a variety of electronics and communications systems to support various (command, control, communications and intelligence) functions. With the addition of the Ultra Tracks, one more configuration has been added to the expanding list.

Weapons Systems

AM General designed the basic vehicle as a platform which can be readily adapted to a wide range of weapons systems to meet specific military requirements.

Transportability

The low 5,400 pound curb weight of the 1 1/2 Ton HMMV with attached tracks can be airlifted to tactical heliborne operations. The C-130 transport holds three HMMVs, the C141B holds six and the C-5A holds fifteen. In tactical strikes, the tracked HMMV vehicle can be transported by the UH60A, the CH-47 and the CH-53 helicopters. The AM General HMMV can also be air dropped by using the low altitude parachute extraction system.

Reliability

Because it has been designed from the ground up, the HMMV represents the latest state-of-the-art in RAM-D (Reliability, Availability, Maintainability and Durability). The Ultra Tracks have gone through extensive testing in the Arctic of Alaska and the Cascade Mountains in Washington. The addition of the Ultra Tracks to the HMMV makes it one of the lightest track units with the largest payload per tracked vehicle weight that is available which can be used both as a wheeled or tracked vehicle and is most cost effective.

In March, 1983, AM General was awarded a contract to manufacture the HMMV (a high mobility multipurpose wheeled vehicle).

After watching trial runs in 1985 at the Nevada Automotive Test Center operated by Mr. Hank Hodges, Imagineering, Inc. started doing preliminary work to mount the Ultra Tracks on the HMMV.

Imagineering, Inc. made a proposal to the Skunk Works (ADEA) at Fort Lewis, Washington to do testing of the Ultra Tracks mounted on a HMMV. Tests were concluded in 1988 after eight months.

Mobility

The HMMV's exceptional cross country mobility results from its 16" ground clearance. The ground clearance goes to 26" and the width to 8'0" increasing stability when the HMMV is equipped with Ultra Tracks. The gradeability is 60%; side slope is 40%, speed (level ground) is 30 mph, 60% grade at 6 mph and with a gross weight of 9200 pounds. The nominal ground pressure (no sinkage) is 2.11 psi. With 4" of sinkage, the ground pressure is 1.59 psi which allows the HMMV to be used in sand, mud, tundra and snow where other tire units cannot go. The changeover time is around two hours.

Survivability

The survivability of the vehicle in combat is enhanced by the low silhouette (only 69" with tires and 79" with Ultra Tracks). It can accelerate from 0–15 mph in 10 seconds, from 0–30 mph in 30 seconds and has a range of up to 150 miles.

The U.S. Army's Bv 206 Oversnow Vehicle

URBAN LUNDBERG
Hägglands
35414 Mound Road
Sterling Heights, Michigan 48310

BV 206 OPENING UP A NEW DIMENSION OF MOBILITY IN ALASKA'S DEFENSE LINE

Since 1969 when the M116 squad carrier was turned in, U.S. Army units in Alaska have had an urgent need for a helicopter transportable all terrain vehicle to carry the maneuver elements' existing load, crew served weapons, and ammunition during crosscountry movement, especially during winter-operation. Twelve different varieties of vehicles were considered as potential replacement for the M116, but none met the basic requirements of mobility.

During 1977–78, two candidate vehicles were identified; the Volvo Bv 202 and the Hagglunds Bv 206. In 1978 the two units participated in a feasibility test conducted by Cold Regions Test Center (CRTC) in Alaska.

The test clearly indicated that the Hagglunds vehicle was superior to the older Bv 202 and finally recommended to be procured for the units in Alaska.

In 1983 the Tank Automotive Command (TACOM) located in Detroit procured 264 vehicles from Hagglunds to be shipped to the 172nd Infantry Brigade in Alaska. The quantity of vehicles was later increased to 304, to include vehicles for the NATO Land Forces in Europe (25 to Germany and 15 to Italy). At the same time, 160 vehicles were bought by the Norwegian Army to be provided to the U.S. Marine corps as Preposition Vehicles in Norway.

During 1984–86, the unit in Alaska expanded from one Brigade to one Division, the 6th Infantry Division (Light), consisting of three Brigades. That change resulted in an increased need for Bv 206s, and during 1988–90 TACOM procured 770 additional vehicles to be distributed to U.S. Army, U.S. Air Force, U.S. Marine Corps, National Guard (NG), and NASA. The National Guard unit in Alaska is the primary NG user, but some vehicles will also be sent to NG units in North Dakota, Vermont, New Hampshire and Maine.

The key to Hagglunds success in marketing the Bv 206 is directly linked to the vehicle's mobility. It was like opening up a "new dimension of mobility" for the units in Alaska when the Bv 206 was introduced. They were pleasantly surprised to be able to use the vehicle during summer operation as well as winter operation and an availability factor of 96% was a complete new experience.

Getting an army where it has to be, when it has to be there, is no simple task, particularly in Alaska where roads are sparse and the terrain is often impassable.

As recently as six years ago, when helicopters couldn't fly, the deployment supporting artillery cross country was delayed; food, fuel and ammunition went undelivered; and casualty evacuation became slow and burdensome. Helicopters can be grounded up to 35 percent of the time during the winter—bad news for an infantry squad packing 3,000 pounds of cold weather gear, or an artillery firing team trying to push a howitzer through a mud bog or snowdrift.

The Bv 206 ushered in a new era in mobility for the arctic soldier, increasing the infantry's winter operational range from three miles per day to more than 20.

Designed for platoons operating in northern and mountainous regions, the Bv 206 has "laid track" in exercises throughout Alaska and accompanied 6th Infantry Division (Light) troops on virtually every major out-of-state exercise since 1986. When operating as a troop carrier, the front cab seats six soldiers and the rear cab has space for 11. Backpacks and other equipment can be loaded on the roof rack.

In the pre-Bv 206 era, cross country movement of Alaska's soldiers and supplies was possible only by aircraft or on foot. Resupplying units or towing howitzers with wheeled vehicles in the Alaskan interior was virtually impossible due to deep snow in the winter and nonexistent roads in the summer.

"If we didn't have Bv 206s we'd have to carry all of our equipment on our backs or on ahkios (sleds)," said CSM Sam Spears of the 1st Battalion (Airborne), 501st Infantry Regiment. "It would slow us down and make everything a lot harder."

In the six-plus years since becoming a part of the Army inventory, the Bv 206 has not only made life easier for the infantryman, it's redefined the way field artillery is employed in an arctic environment. The vehicle is the primary transport for fire support teams and survey parties, and is the prime mover of the 11th Field Artillery's big guns. In addition to carrying troops and equipment, evacuating injured soldiers and towing two 10-man ski patrols, the Bv 206 can pull light weapons such as the division's 105 mm howitzers.

"Our job would be difficult at best; in some cases it would be impossible without the Bv 206," said Lt. Col. Joseph Leigh Jr., commander of the battalion. "Because of its very light footprint, the Bv 206 can traverse snowdrifts with absolutely no problem...it's simple, even when overloaded with equipment, supplies, weapons, ammo, survival gear and a howitzer."

With a maximum road speed of 34 mph, the Bv 206 has a range of between 120 and 200 miles, depending on the terrain. That terrain can be deep snow, thick brush, forests, muskeg or mountains—the Bv 206 can climb grades of up to 70 percent. Even rivers, streams and lakes are no match for the Bv 206: the vehicle is designed for swimming operations.

In addition to infantry and field artillery units, the Bv 206 is used by medical companies here for casualty evacuation missions. And just like the ground pounder and the redleg, when you ask a medic what his job would be like without the vehicle, the words "next to impossible" are always part of his answer. "I'd hardly be able to perform my job without the Bv 206, especially in the winter," said Spec. Scott Sumpter, a medical NCO with Alpha Med., 706th Maintenance Battalion. "It would definitely cut our mission capabilities down to near nothing...it would be extremely rough."

Why is now this vehicle so fantastic? The secret lies in the design requirement once generated by the Swedish Army. How the Swedish Army uses the Bv 206 is explained by Geijer (1988).

LITERATURE CITED

Arctic Soldier, Vol # 15, Issue # 4.

Geijer, P. (1988) How.....The Swedish Army uses the All Terrain Carrier, Bv 206. Hägglands Vehicle AB, S-189182, Örnsköldsvik, Sweden.

The Flextrac MPV: A Novel Concept In A Personal All-Terrain Vehicle

MARK D. OSBORNE
Senior Research Engineer
Keweenaw Research Center
Michigan Technological University
Houghton, Michigan 49931

ABSTRACT

Personal vehicle mobility has entered a new age with the development of the Flextrac Multi-purpose Vehicle (MPV). Developed in Scandinavia, the Flextrac MPV utilizes a novel concept in vehicle mobility. Designed for one or two people, the Flextrac uses one single track, consisting of 36 flexible sections to propel and steer the vehicle through deep snow, sand and swamps. Because it does not have skis and slides as most current snowmobiles have today, it is capable of negotiating non-snow terrain. The track extends the entire length of the body and is considerably wider than snowmobile tracks, providing a light footprint and good flotation, even in soft snow or soils. The low ground pressure also contributes to less environmental damage than most vehicles. This vehicle was tested by the Keweenaw Research Center (KRC), a research agency of Michigan Technological University (MTU), over a wide variety of both summer and winter terrains, including deep powder snow, swamps, sand and swimming in a pond. Several performance tests were conducted to evaluate hill climbing capability, pulling capacity, acceleration, braking, towed motion resistance, turning radius and fuel consumption over a wide variety of terrains.

The design concepts of the Flextrac MPV's undercarriage along with its performance capabilities are discussed and presented in this paper.

This project was funded by the U.S. Army Tank-Automotive Command (TACOM) and the U.S. Army Cold Regions Research and Engineering Laboratory (CRREL).

INTRODUCTION

The Flextrac MPV, as shown in Figure 1, is a unique concept in all-terrain vehicle mobility. It was tested as a candidate for the U.S. Army Mobile Over Snow Transport (MOST) system by the Keweenaw Research Center (KRC), a research agency of Michigan Tech-nological University (MTU). The test program was funded by the U.S. Army Tank-Automotive Command (TACOM) through the U.S. Army Cold Regions Research and Engineering Laboratory (CRREL).

This paper is not to be construed as an official Department of the Army position. Mention of any trade names or manufacturers in this paper shall not be construed as an official endorsement or approval of

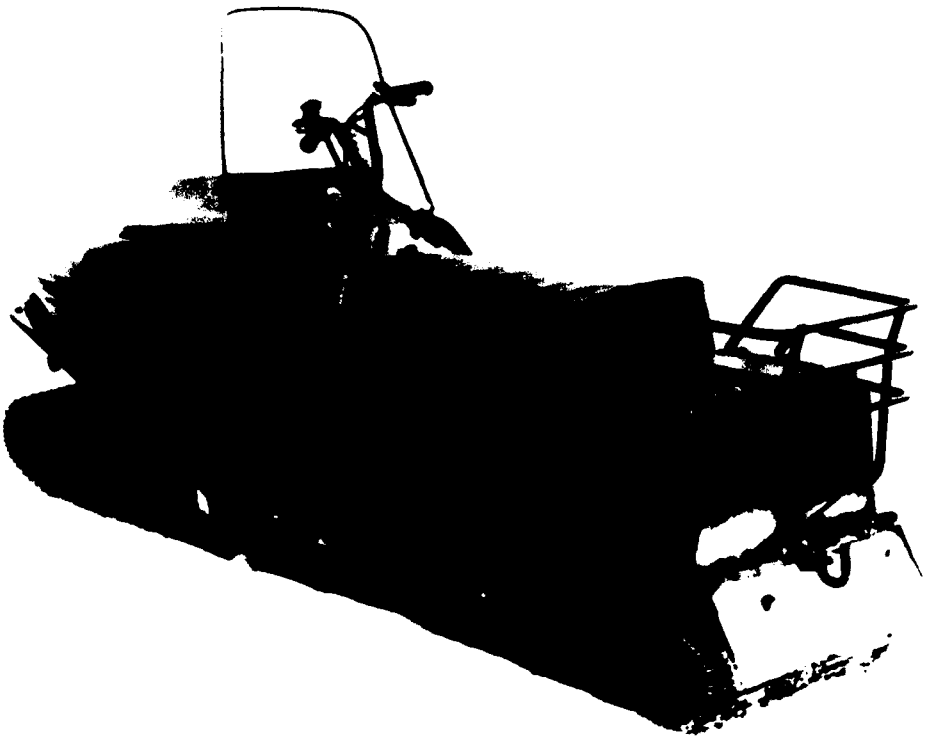

Figure 1. The Flextrac Multi-purpose Vehicle.

such products or companies by the U.S. Government. Any opinions expressed in this paper are solely those of the author and in no way reflect the opinions or endorsements of the U.S. Government or the U.S. Army.

The Keweenaw Research Center is located in Michigan's Upper Peninsula on the Keweenaw Peninsula which extends into Lake Superior. The effect of Lake Superior can be seen in the fairly moderate seasonal temperatures and large annual snowfall (200 inches). The combination of a varied climate and the Keweenaw's rugged terrain makes the area an ideal location for vehicle testing in all types of conditions. KRC has over ten years of vehicle mobility testing experience, mostly in winter conditions. The staff consists of mechanical and civil engineers along with technicians for vehicle instrumentation and computerized data collection. KRC is a complete engineering and test facility as components are designed and analyzed using finite element analysis, prototype components can be fabricated in KRC's machine shop and then tested in the laboratory and in the field on a vehicle. KRC has a vehicle test course spread out over 500 acres of leased land with several thousand acres of public land available for vehicle testing as well.

The Flextrac vehicles were tested in several types of snow conditions, on ice, in swamps, muskeg, sand, dirt, gravel, pavement, rough cross-country and in water. This paper reviews the unique design of the Flextrac and its performance capabilities.

BACKGROUND

The Flextrac vehicle has been in development for over 15 years. It was invented by a person in Finland who worked on the original concept for about ten years. Approximately five years ago Indevex AB, a company in Sweden purchased all patent rights for producing and marketing the vehicle. Indevex AB now has 48 patents on the Flextrac in the USA and several other countries. Indevex now markets the Flextrac MPV in Scandinavia through Yamaha and plans to start marketing in other parts of Europe and the USA in the near future. The Swedish Army and Royal British Marines have been using the Flextracs for over a year. The MPV is also being tested in France, Canada and the USSR.

Figure 2. MPV carrying two people and pulling a sled with 500 lbs. of load on a snow covered lake

FLEXTRAC MPV DESIGN FEATURES

The unique single track, no ski design allows the Flextrac MPV to traverse almost any type of terrain. It is designed as a work-horse type utility vehicle versus the common recreational snowmobile or wheeled all-terrain vehicles (ATV) now popular in the United States.

Figure 2 demonstrates that the Flextrac MPV is a one or two man vehicle capable of pulling a sled or wheeled trailer, depending on the terrain encountered. It is advertised to carry 400 pounds on the vehicle and over 800 pounds in a sled. During certain tests at KRC the Flextrac MPV carried two men on the vehicle and towed a sled with a failed snowmobile plus additional weight for a total sled load of over 1,000 pounds on a packed snowmobile trail.

The ground pressure is advertised at 0.36 psi in the unloaded condition and 0.51 psi at the rated load condition. Even though this vehicle weighs over 700 pounds in the unloaded state its relatively low ground pressure is a result of the single large track which is 23.6 inches wide and 184.25 inches long (total length). The large track area with aggressive track design allow the Flextrac MPV to traverse various terrains with minimal damage to the environment, which is becoming a greater concern these days. Shown in Figure 3 is the Flextrac's wide track.

The Flextrac MPV is powered by a Yamaha 340 cc air-cooled, single carburetor two cycle engine with oil injection. It develops approximately 32 hp. An air filter system has been designed for use in both winter and summer conditions. In the winter the system uses one paper element air filter and in dusty summer conditions two paper element filters are used to restrict dust ingestion. Power is transferred from the engine to the final drive through two common snowmobile clutches into a gear type transmission. The transmission has two forward speeds, low and high, as well as neutral and reverse. The gearing is set for low speed high torque applications. A double chain drive is used to transfer power from the transmission to the final drive sprocket, which drives the track. Figure 4 is a photograph of the engine and Figure 5 is a photograph of the chain drive and fuel tank in the Flextrac MPV.

The body portion (upper part) of the MPV has an externally filled gas tank, two storage areas for carrying tool kits or gear and hydraulic brakes. An electric start kit is also available as an option. Shown in Figure 6 are the storage areas of the MPV.

The body of the Flextrac MPV separates from the undercarriage through eight bolts for easy vehicle maintenance. The engine, transmission, and final drive unit are all mounted on an internal frame that is slid into the body through the front of the machine. If there ever is a need for major overhauls on the power train the com-

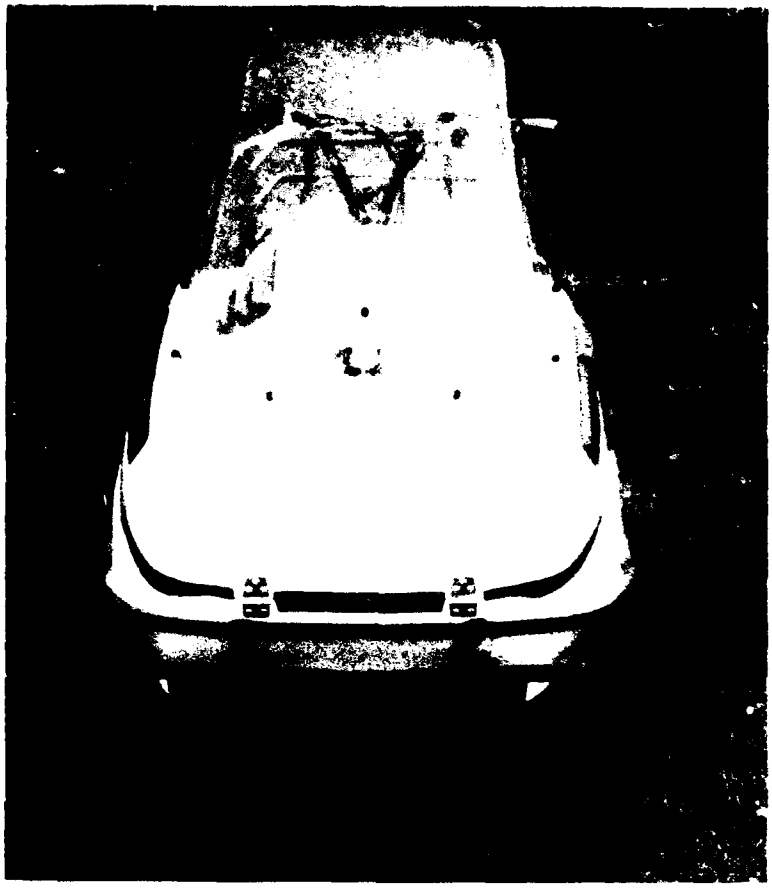

Figure 3. MPV's wide track.

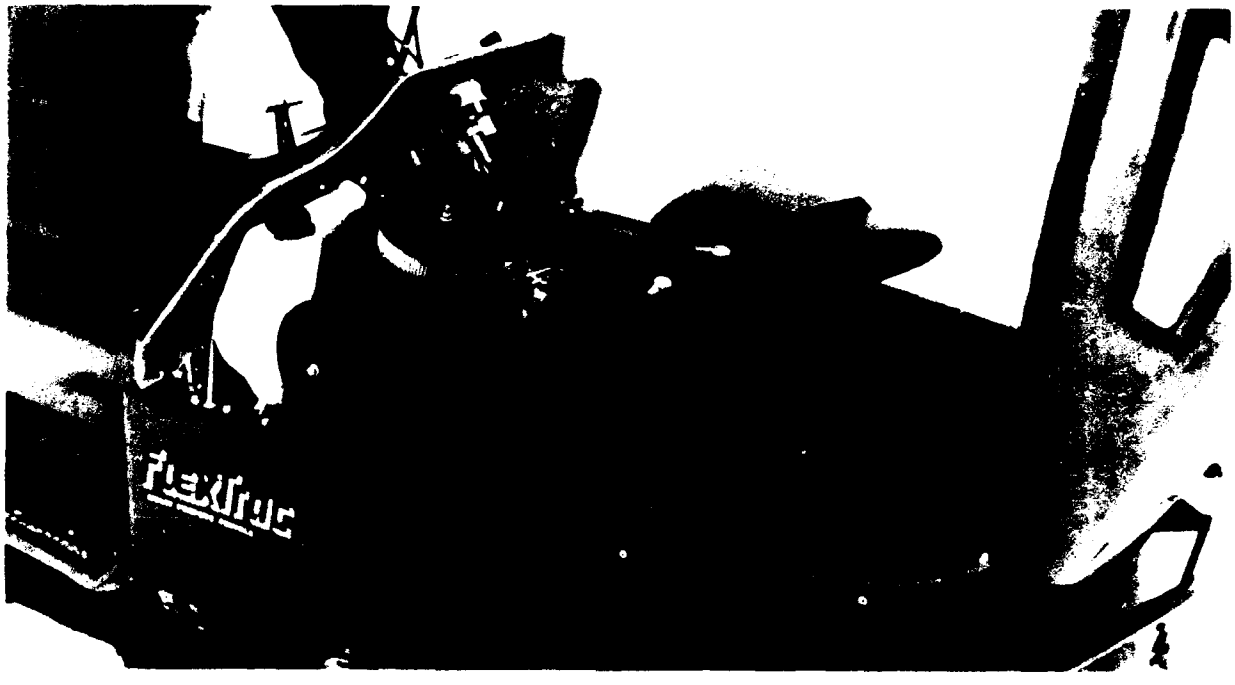

Figure 4. Flextrac's engine.

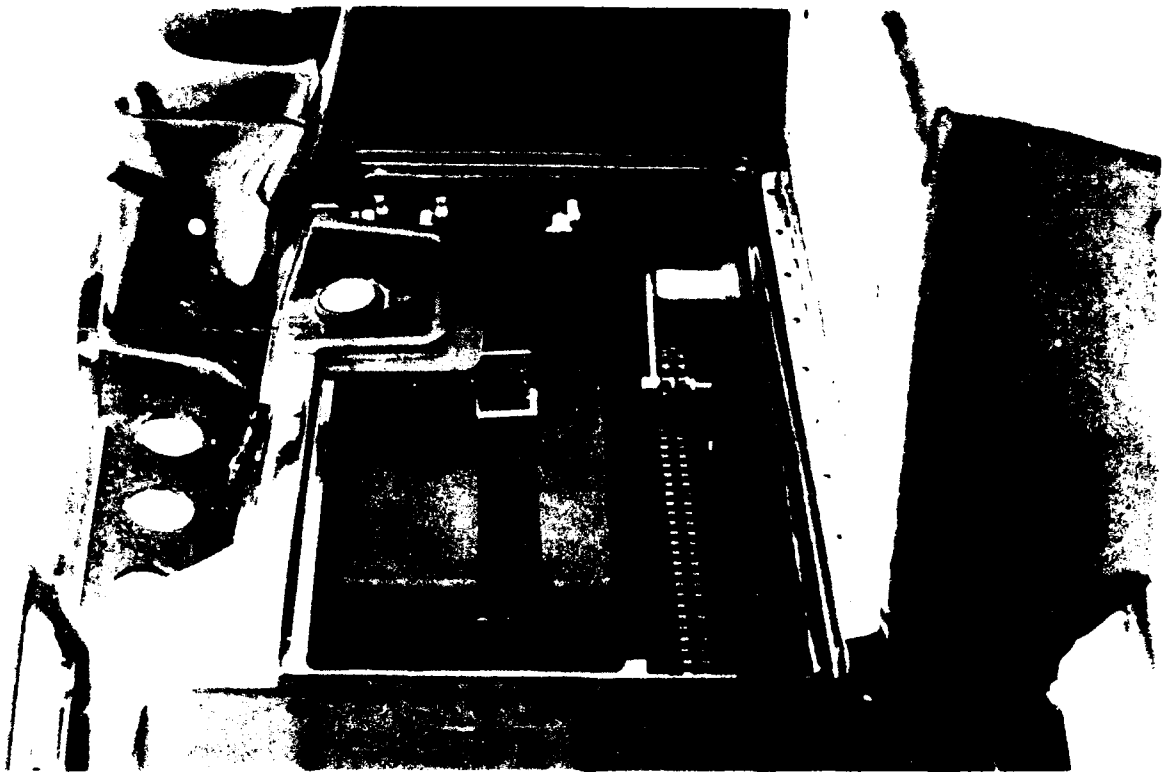

Figure 5. Chain drive system and fuel tank.

plete power train can be removed easily by sliding the internal frame out of the body. An external tow hitch is mounted on the rear of the vehicle through the body and to the internal frame. The concept of the internal frame is unique in that it is not found on most snowmobiles. It also has future possibilities that are not in production yet such as mounting a winch or small snowplow to the front of the vehicle. Some four wheel ATVs use snowplows and since the Flextrac MPV has superior traction as compared to the ATV, it could be an additional useful feature of the MPV.

Although the body or upper portion of the Flextrac MPV is different than most other vehicles, the undercarriage and track system is totally unique in concept and is the key to superior vehicle mobility. As mentioned before the undercarriage can be easily separated from the vehicle body. The undercarriage consists of a number of bogie wheel frames, track guide wheels, axles and suspension components.

The track is comprised of 36 individual sections linked together by steel pins. This is very similar in concept to a military tracked vehicle single pin track design. The track material is a composite type plastic that is produced by DOW. It is molded into final shape in Sweden using a specially designed mold. One of the most important factors in the Flextrac MPV's design is the fact that the track allows the vehicle to turn without the use of skis, which makes it a *multi-terrain* vehicle. The track allows this by its "fan" shaped design which allows expansion or contraction of each section. When turning to the right for example, the right side of the track at the front of the vehicle will contract while the left side of the same sections will expand. The track is guided around the undercarriage through the use of track lugs in the center areas of the track sections. This area is more rigid as the outer section of the track is the region of greatest flexibility.

The undercarriage has a tubular steel frame to which six bogie frames are mounted. The undercarriage frame bolts through the body to the internal steel frame inside the body. Each bogie frame has four rubber coated bogie wheels for support of the track system. The bogie frames are attached to the undercarriage frame through a combination of steel and composite spring plates which provide the only suspension on the current vehicle design. Guide wheels are mounted to the bogie frames and undercarriage frame to keep the track centered both on the upper and lower sides of the track. Large wheel-axle assemblies are located at the front and rear of the track loop to provide the correct radius for

Figure 6. Storage areas on the Flextrac MPV.

track motion around the undercarriage frame. Attached to the front of the undercarriage frame at a pivot point is the track steering mechanism. This unit contains guide wheels, bogie wheels, and a wheel-axle assembly but also pivots off of the main undercarriage frame. This pivoting action is controlled by a steering arm linkage which is activated by the handlebars when the driver steers the vehicle. By pivoting this front undercarriage unit, tension is applied to one side of the vehicle track while it is compressed on the opposite side. This allows an entire front one third of the track to turn on an angle while the rear two thirds stay straight. This allows the track to steer. The final drive sprocket drives the track from the rear of the vehicle. Track tension is adjusted by tightening or loosening a nut on a shaft in the front section of the undercarriage frame. This nut is attached to a steel rod with a coil spring around the shaft and the spring goes into a cylindrical tube. The steel rod is also attached to the front idler wheel-axle assembly. When the steel rod is extended, pressure is applied to the front of the track through the front axle assembly causing an increase in track tension. Correct track tension is necessary for proper track guidance and driving performance. Shown in Figure 7 is a side view of the track, bogie frames connected to the undercarriage frame through the composite spring system and the bracket used to attach the undercarriage to the body. Figure 8 shows the undercarriage separated from the track.

PERFORMANCE OF THE FLEXTRAC MPV

The Flextrac MPV is designed as a utility vehicle and not necessarily as a recreational vehicle. The vehicle is heavy with a stiff suspension. It is not exceptionally fast as it has a top speed of about 35 mph on the smoothest terrains. The gearing is low in both the low and high ranges. It has exceptional power and in reality most work can be done in the high range. It is feasible to assume that if different gear sizes were used the vehicle could still have plenty of low end power yet travel at speeds up to 50 mph, yet for most of the applications that the machine was designed, speed is not a requirement.

KRC tested the Flextrac in several types of snow and on ice. On ice the vehicle was somewhat difficult to control (as just about any vehicle is) as the hard plastic track does not penetrate the ice. It was tested in deep powder snow, on packed snow and on deep, wet snow.

Figure 8. Complete undercarriage assembly.

Figure 9. Flextrac traversing snow covered swamp

It was also tested on one of the most difficult terrains there is to traverse, a wet slushy snow with water underneath. The Flextrac MPV was able to traverse all of these types of terrains even while pulling a sled loaded with 300 lbs. of cargo. In deep powder snow the vehicle feels unstable and requires developing a technique for handling. The vehicle is not as unstable as it feels. As an experienced snowmobile driver I felt that the MPV was better at going through deep powder snow than a snowmobile. On a snowmobile the driver usually has to build up speed and momentum to keep moving because if he stops he has a difficult time getting started again. On the Flextrac MPV the driver can stop and start again without a problem. Pulling a sled with weight in it would be next to impossible for a snowmobile (except for a wide track) while the Flextrac has plenty of power to do this. The same can be said for deep, slushy, wet snow or snow with water underneath it. As for a comparison to a four wheel ATV, there was an instance at KRC where a Flextrac had to pull a four wheel drive ATV through two foot deep wet crystalline snow for about 300 yards because the ATV just did not have the ground clearance or low ground pressure to stay on top of the snowpack. The Flextrac MPV did not slip at all while pulling the ATV in the wet snow. On packed snow the snowmobile is faster and provides a smoother ride even while pulling a sled because of the more advanced suspension system available on snowmobiles today. Figures 9 and 10 show some of the snow and wet terrain conditions encountered by the MPV during testing.

On snow covered slopes a Flextrac is better than most snowmobiles at climbing the slopes. In one instance we stopped a Flextrac with a loaded sled half way up a 30 percent slope and were able to resume climbing with about 4-6 inches of snow on the slope. Stopping a snowmobile on the slope only allowed the vehicle to sink in when accelerating. When attempting to back down in reverse the skis became stuck in the snow and the snowmobile had to be lifted and turned around. The advantage of the Flextrac is that when reverse is used there are no skis to dig in and stop it. Usually when climbing a slope with a snowmobile the driver has to develop a lot of speed to be able to climb the slope but there are times when there is no room to attain enough speed to climb the slope. In Figure 11 the Flextrac MPV is shown climbing a steep snow covered slope.

Drawbar pull and towed motion resistance tests were conducted on snow as well as other terrains. The Flextrac MPV has a fairly high towed motion resistance as compared to most snowmobiles. This is in part due to the large surface area of the track, the design of the track and the guide wheel and bogie wheel system of the undercarriage. Along with the high motion resistance the Flextrac MPV also has a very high drawbar pull

Figure 10. Flextrac running on snow and water in late spring.

Figure 11. Flextrac climbing a snow covered slope.

Figure 12. Flextrac MPV negotiating a paved slope.

capability on snow covered terrains. It is about twice the drawbar pull of a common snowmobile. Speed and acceleration are slower on a Flextrac than on a common snowmobile but braking is better on the Flextrac. This is due mainly to the high motion resistance of the track on the Flextrac.

As a utility vehicle in snow covered terrains the Flextrac has better overall mobility as compared to a common snowmobile although the snowmobile is usually faster and provides a smoother ride for the user. The fact that sets the Flextrac apart from the snowmobile is that it is really an all-terrain vehicle such that when there is a minimal amount of snow on the ground the driver can keep moving without damaging the vehicle.

At KRC the Flextrac MPV was tested in all types of environments. In the spring the vehicles were taken on trails where they had to cross creeks and small rivers or parts of the trails with wet snow over one to two feet of water. This type of environment would have been difficult or impossible to cross with a snowmobile or four wheel ATV.

The Flextrac was also driven on pavement, sand, gravel, in swamps and in muskeg. On pavement, sand and gravel a four wheel ATV can travel faster. But a Flextrac can go more places than an ATV. In some of the conditions such as frozen, snow covered swamps in the early winter season it would have been difficult for the snowmobile or ATV to traverse but the light ground pressure of the Flextrac allowed it to stay on top of the weak strength terrain. One of the most impressive attributes of the Flextrac MPV was its ability to be ridden in muskeg. Muskeg is a floating mat of vegetation over water that can be almost any depth. Wheeled vehicles can not be driven in muskeg. It is very difficult to walk on muskeg. Most tracked vehicles are too heavy to drive in muskeg, even though they generally have low ground pressure and good flotation. Even the Flextrac MPV had a difficult time crossing muskeg as some deep holes would slow down the vehicle and some water would get on the drive belt causing slippage and a loss of power. But if a driver operated the Flextrac carefully through the muskeg it could be crossed which would be difficult to impossible for any other type of vehicle except for possibly an air cushion type of vehicle. Figure 12 shows the Flextrac MPV climbing a paved slope. Shown in Figures 13 and 14 is the Flextrac on sand and traversing a swamp water hole, respectively.

One other test was the swimming test in a shallow pond (2 to 5 feet deep). Figure 15 is a photograph of the Flextrac swimming in the shallow pond near KRC. The Flextrac SX was tested with only the driver and no additional weight. The Flextrac did swim and the driver was able to get off and get back on the Flextrac without it tipping while floating in the water. When weight was

Figure 13. Flextrac MPV traversing sand covered terrain.

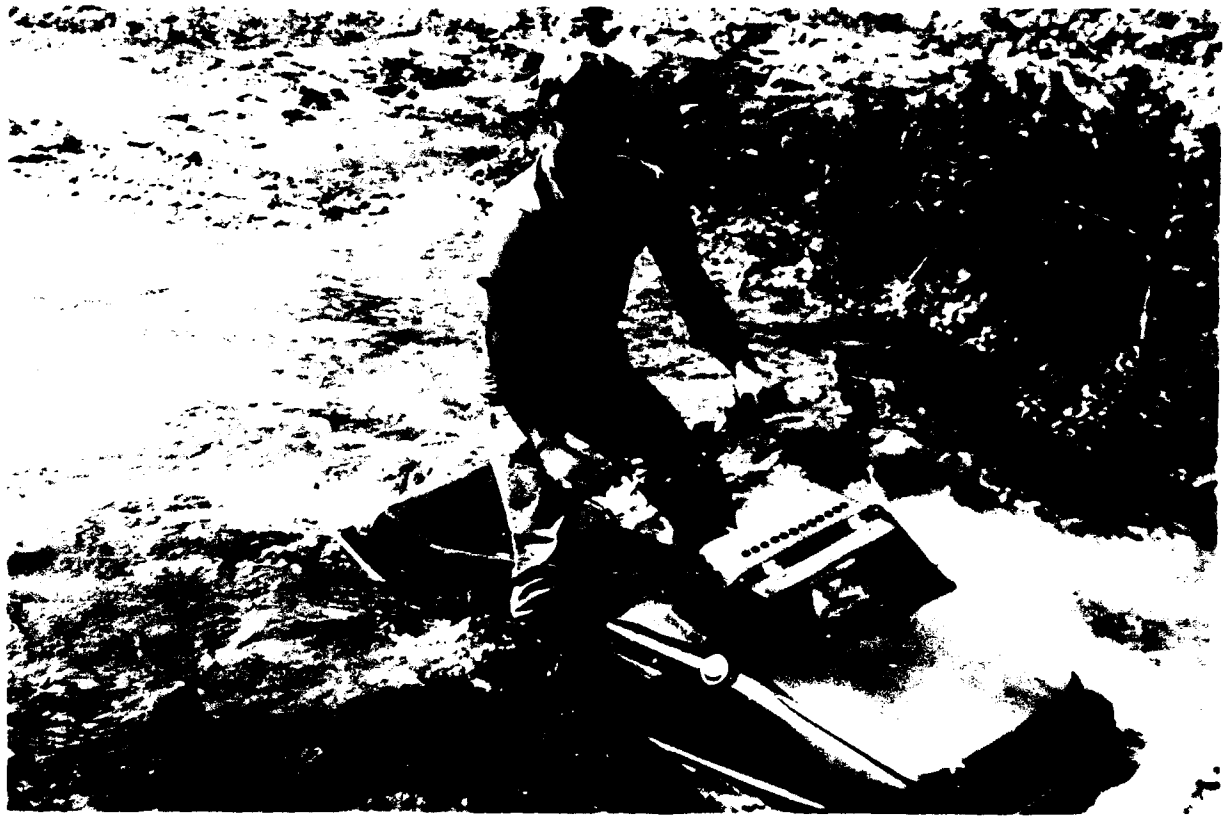

Figure 14. Flextrac MPV driving through a swamp mud hole.

Figure 15. Flextrac swimming in a pond.

added water did seep into some of the internal compartments and caused the air filter to become wet and the belt to slip. The operator has to be sure and seal all areas that may allow water into the internal compartments before going through a large body of water. Also, the freeboard area is very small and if a kit was designed properly it is possible that the vehicle would not sink as deeply into the water as it does at this time. What this demonstrates is that if a driver encounters an area where he has to cross a fairly deep small body of water it can be done with a Flextrac.

All vehicles usually have to go through a development stage to work out design problems. The early snowmobiles and ATVs had problems. Some of the early model snowmobiles were known for breaking down after only a day of riding. The current model snowmobiles and ATVs rarely breakdown. The same type of development process is occurring with the Flextrac. The early SX version had several reliability problems and problems with design that caused failures. The newer MPV has shown a tremendous improvement with reliability over the SX version. There are still some problems with the MPV but these are being resolved by the manufacturer and it is hoped that in the near future the reliability of the Flextrac will be as good as a snowmobile or ATV.

SUMMARY

The Flextrac MPV is truly a unique concept in personal vehicle mobility. The single all track drive system allows it to traverse almost any type of terrain imaginable. It has excellent hill climbing and pulling capability and is a true workhorse. Through engineering development the Flextrac may one day fill the gap between the snowmobile and the four wheel ATV.

REPORT DOCUMENTATION PAGE

Form Approved
OMB No. 0704-0188

1. AGENCY USE ONLY (Leave blank)	2. REPORT DATE	3. REPORT TYPE AND DATES COVERED
	July 1993	

4. TITLE AND SUBTITLE
First International Conference on Winter Vehicle Mobility
Santa Barbara, California, June 1991

5. FUNDING NUMBERS

6. AUTHORS
George L. Blaisdell, Editor

7. PERFORMING ORGANIZATION NAME(S) AND ADDRESS(ES)
U.S. Army Cold Regions Research and Engineering Laboratory
72 Lyme Road
Hanover, N.H. 03755-1290

8. PERFORMING ORGANIZATION REPORT NUMBER
Special Report 93-17

9. SPONSORING/MONITORING AGENCY NAME(S) AND ADDRESS(ES)

10. SPONSORING/MONITORING AGENCY REPORT NUMBER

11. SUPPLEMENTARY NOTES

12a. DISTRIBUTION/AVAILABILITY STATEMENT
Approved for public release; distribution is unlimited.

12b. DISTRIBUTION CODE

13. ABSTRACT (*Maximum 200 words*)

The First International Conference on Winter Vehicle Mobility was the first international meeting entirely devoted to the subject of vehicle travel in cold regions. The technical sessions focused on prediction and testing methods, general vehicle mobility, mobility enhancement, cold regions materials properties, and novel designs for winter mobility. This report includes 21 papers presented at the conference.

14. SUBJECT TERMS			15. NUMBER OF PAGES
Winter mobility Vehicles	Mobility research		224
			16. PRICE CODE

17. SECURITY CLASSIFICATION OF REPORT	18. SECURITY CLASSIFICATION OF THIS PAGE	19. SECURITY CLASSIFICATION OF ABSTRACT	20. LIMITATION OF ABSTRACT
UNCLASSIFIED	UNCLASSIFIED	UNCLASSIFIED	UL